Role of membrane attack complex in immunometabolism and inflammasome activation

Gisela Jimenez Duran

October 2022

Cardiff University

Infection & Immunity

School of Medicine

GlaxoSmithKline –Immunology Network

Medicines Research Centre – Stevenage

Role of complement membrane attack complex in immunometabolism and inflammasome activation

Gisela Jimenez Duran

PhD in Immunology

October 2022

ABSTRACT

The complement system, an ancient and critical part of innate immunity, has been recently involved in novel roles other than lysis to clear pathogens, implicating regulation of the innate immune response, as well as acting as an immunometabolic regulator. Complement has been shown to contribute to metabolic reprogramming of T-cells, synoviocytes as well as cells in the CNS, however, whether this is also the case for the terminal stage in the complement activation pathways, the membrane attack complex (MAC), is unclear. MAC is upregulated in diabetic and rheumatoid arthritis patients, contributing pathologically by increasing inflammation. Previous research has highlighted that a sublytic dose of MAC can initiate NLRP3 inflammasome activation via calcium influx and loss of mitochondrial membrane potential. This thesis shows that sublytic concentrations of MAC mediate a previously undescribed perturbation in cellular energy metabolism and mitochondrial dysfunction in human monocyte-derived macrophages. This is characterised by phenotypic skewing towards glycolysis and alterations of pyruvate metabolism, as well as loss of maximal mitochondrial respiratory response, fragmented mitochondrial morphology and depleted mitochondrial membrane potential, mediating mitochondrial reactive oxygen species production and NLRP3 inflammasome activation, gasdermin D formation and pro-inflammatory cytokine release. This novel link between sublytic MAC and immunometabolism elucidates a novel signalling cascade with metabolic alterations at its centre, having direct consequences for downstream inflammatory processes, and is important for development of novel therapeutics for areas where MAC may mediate disease.

TABLE OF CONTENTS

3. **CHAPTER 3: MAC DRIVES GLYCOLYSIS-DEPENDANT INFLAMMASOME ACTIVATION, REACTIVE OXYGEN SPECIES AND LACTATE PRODUCTION IN NAÏVE M-CSF DIFFERENTIATED HUMAN MONOCYTE-DERIVED MACROPHAGES (MDMs)**

4. **CHAPTER 4: COMPLEMENT MAC IS AN IMMUNOMETABOLIC REGULATOR OF NLRP3 ACTIVATION AND IL-18 SECRETION IN HUMAN MACROPHAGES**

COMMON ABBREVIATIONS

AD – alzheimer's disease

AMP - Adenosine monophosphate

ATP - Adenosine triphosphate

Ca2+ or iCa2+ - Calcium or intracellular calcium

CNS - Central nervous system

ECAR – Extracellular acidification rate

ETC – electron transport chain

GM-CSF – Granulocyte macrophage colony-stimulating factor

GSDMD - Gasdermin D

GPCR - G protein-coupled receptor

GLUT1 - Glucose transporter 1

HA – Heptelidic acid

LAT1 - L-type amino acid transporter 1

LPS – Lipopolysaccharide

MAC – Membrane attack complex

M-CSF - Macrophage colony-stimulating factor

MDM – Monocyte-derived macrophage

MS – multiple sclerosis

mTOR - Mechanistic target of rapamycin

mtROS – Mitochondrial ROS

NHS - Normal human serum

NLR - Nucleotide-binding domain and leucine-rich repeat receptor

OCR - Oxygen consumption rate

OXPHOS - Oxidative phosphorylation

PRRs - Pattern recognition receptors

RA – rheumatoid arthritis

RET – reverse electron transport chain

ROS - Reactive oxygen species

TCA cycle - Tricarboxylic acid cycle

2-DG – 2-deoxyglucose

ACKNOWLEDGEMENTS

PUBLICATIONS

First author

(2022) Sublytic membrane attack complex drives glycolysis and mitochondrial dysfunction with inflammatory consequences in human monocyte-derived macrophages, **Frontiers of Immunology**. (Jimenez-Duran, Kozole et al. 2022) https://www.frontiersin.org/articles/10.3389/fimmu.2022.918551/full

* Part of the data shown in chapters 4 and 5 of this thesis is covered in this publication.

(2021) Metabolic regulators of enigmatic inflammasomes in autoimmune diseases and crosstalk with innate immune receptors, **Immunology**. (Jimenez-Duran and Triantafilou 2021) https://doi.org/10.1111/imm.13326

(2020) Pharmacological validation of targets regulating CD14 during macrophage differentiation, **EBioMedicine**. (Jimenez-Duran, Luque-Martin et al. 2020) https://doi.org/10.1016/j.ebiom.2020.103039

Co-author

(2021) STING is essential for Human rhinovirus replication by triggering biogenesis of PI4P lipid enriched replication platforms and facilitating viral exit and transmission via autophagy, **Nature Communications**. (Triantafilou, Ramanjulu et al. 2022) https://www.nature.com/articles/s41467-022-28745-3

(2021) Neuronal TNF-α, not alpha-synuclein, drives neurodegeneration in the Ifnb−/− mouse model of Parkinson's disease dementia, **Annal of Neurology**. (Villanueva, Tresse et al. 2021) https://onlinelibrary.wiley.com/doi/10.1002/ana.26209

1. Chapter 1: Introduction

1.1 Innate Immunity and Pattern Recognition Receptors

Around 750 million years ago the innate immune system (IIS), a highly evolutionarily conserved component of immunity, first emerged. Although the IIS was first considered as a stopgap prior to activation of the adaptive immune system, research in the last few decades has revealed that it also has a variety of biological functions participating in maintenance of healthy tissue microenvironment and cell metabolism. Therefore, the IIS is able to act as a sensor of tissue damage and infection, leading to inflammation (Creagh and O'Neill 2006).

The primary function of the IIS is as a sense and warning system. The IIS cells and molecules are highly specialised to be the first line of defence against exogenous microbes and endogenous abnormal entities, such as injured tissue or apoptotic, infected or malignant cells. Recognition of these endogenous and exogenous entities (known as danger- or pathogen-associated molecular patterns, DAMPs or PAMPs) is done by the pattern-recognition receptors (PRR), which are secreted or expressed by a variety of immune cell types. Among the classic PRRs are the toll-like receptors (TLRs), the retinoic acid inducible gene 1 receptors, known as RIG-like receptors (RLRs), the Nod-like receptors (NLRs) and certain proteins of the complement system. This topic is covered in great detail by specific reviews such as (Köhl 2006).

The first family of PRRs to be discovered were the TLRs, which are membrane-bound glycoproteins that recognize viruses, bacteria, protozoa and fungi through leucine-rich repeats (LRRs). LRRs participate in ligand binding and autoregulation, located in the extracellular or luminal domain of the TLR. The NLRs consist of a group of intracellular microbial sensors that can recognise mainly bacteria, whereas the RLRs are more anti-viral. However, some NLRs have also been reported to sense viruses, such as NLRP3, which can be activated in response to M2 protein during influenza infection (Kanneganti 2010). Certain NLRs (NOD1 and NOD2) and TLRs can activate in similar ways a key transcription factor for immune and inflammatory gene expression, nuclear factor (NF)-κB. Again in a similar way, RLRs and anti-viral TLRs are able to detect viral nucleic acids and activate some family members of interferon-regulated factors (IRFs). Certain NLRs and RLRs can therefore activate several responses similarly to TLRs (Creagh and O'Neill 2006, Dowling and O'Neill 2012) .

Engagement and crosstalk between signalling pathways of the different PRR families has become apparent and ensures an efficient co-ordination of innate immune responses, leading to induction of protective functions to the cells that receive those signals and cell activation. It is known that interactions between NLRs, TLRs and RLRs can result in induction and maturation of the key proinflammatory cytokines IL-1β and IL-18 through the assembly and activation of NLR-containing multiprotein complexes, known as inflammasomes (Dowling and O'Neill 2012).

1.2 The Complement System

Complement was discovered in the late 19th century as a potent host defence mechanism in innate immunity. Complement research started in the 1890s with Buchner, Bordet et al. who first reported a 'heat-labile' factor in serum (referring to complement) capable of killing bacteria when being present with another 'heat-stable' factor (referring to an antibody) (Buchner 1891, Morgan 1990). Complement was defined by Ehrlich a few years later as "the activity of blood serum that completes the action of antibody" (Witebsky 1954, Kaufmann 2008). Research in recent decades has revealed that it also has a variety of biological functions participating in pathogenesis of disease (Ricklin, Reis et al. 2016).

Consisting of more than 50 distinct glycoproteins found on cell surface, plasma and intracellularly, the complement system is mainly organized in 1) Components, 2) Receptors, 3) Effector molecules and 4) Regulators, which interact in catalytic cascades (Dunkelberger and Song 2009, Ricklin and Lambris 2013). Most of the complement proteins are present as inactive precursors (zymogens) and are activated by proteolytic cleavage when complement recognises pathogens, apoptotic cells, immune complexes and damaged tissue. This recognition can be mediated by Immunoglobulin M and G antibodies producing activation of several complement proteins, which 'complement' the antibody functions (Walport 2001).

Complement plays an important role in complementing regulatory functions for several innate and adaptive immune cells, increasing antibody response and enhancing immunologic memory (Merle, Noe et al. 2015). Therefore, complement acts as a bridge between the innate and adaptive immune system in order to eliminate pathogens. Furthermore, complement mediates disposal of immune complexes and apoptotic cells (anti-inflammatory function), as well as tissue repair and regeneration. Complement acts as a host defence system against bacterial infection by evoking inflammatory responses such as chemotaxis, as well as opsonising and directly lysing bacteria (Walport 2001,

Ricklin, Hajishengallis et al. 2010). The relevance of Complement system in disease has increased in recent decades and relies in the ability of certain pathogens to evade complement and spread into the organism (Lambris, Ricklin et al. 2008). Identification of complement protein deficiencies originated by gene mutations are also believed to lead to a variety of clinical conditions, such as autoimmune diseases (Skattum, van Deuren et al. 2011).

The complement components are a group of plasma proteins (enzymatic and lectin proteins) which participate in complement activation. The enzymatic proteins are mainly C1-C9, factor B and D (Alper, Johnson et al. 1969, Murphy, Kraakman et al. 2016). The receptors are a group of membrane proteins (CR1-4, C1qR, C3aR and C5aR) which are mainly expressed on immune cells and interact with effector molecules generated through complement activation. Each of these effector molecules has a specific physiological function and refer to certain enzymatic components (C3, C4, C5) which have been cleaved into two molecules named 'a' and 'b' (e.g. C3a and C3b). C3a, C4a and C5a act as anaphylatoxins, inducing inflammatory response and chemotaxis of certain cells and increasing blood supply to the site where they are released. C3b and C4b act as opsonins, leading to phagocytosis (Gros, Milder et al. 2008, Murphy, Kraakman et al. 2016). These bind to the targeted bacterial cells and allow their recognition by macrophages, which contain receptors for C3b and C4b (Mevorach, Mascarenhas et al. 1998).
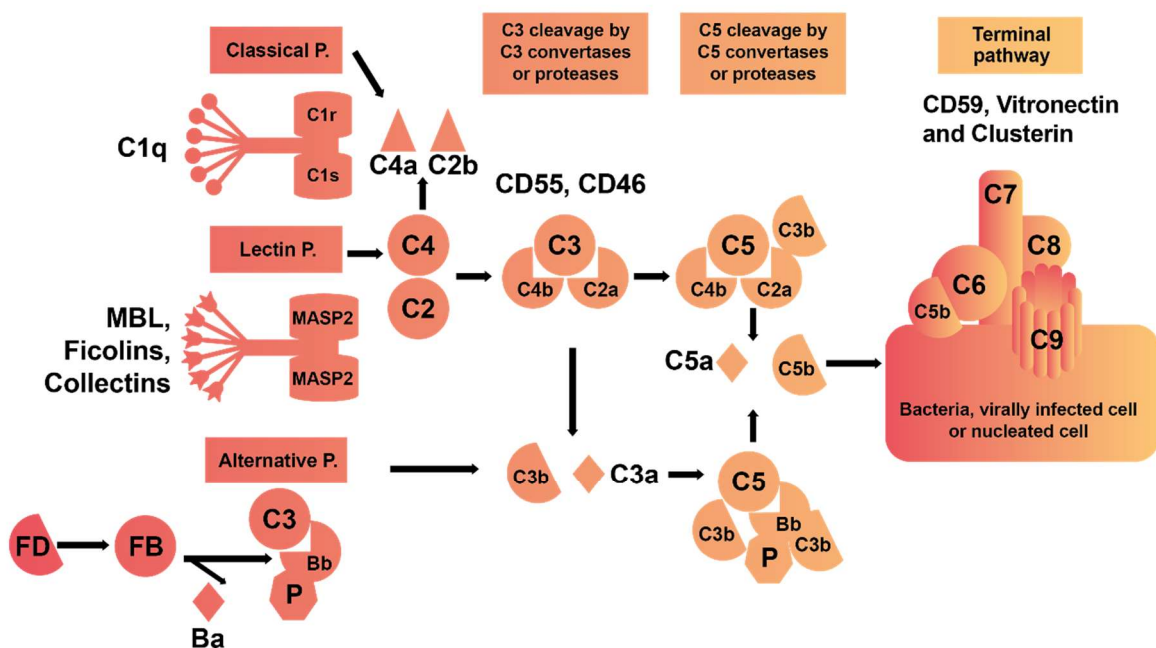
Figure 1. Classical, alternative and lectin complement pathways. Each of these pathways activate complement and generate a 'membrane-bound C3 convertase', which cleaves further C3 molecules, releasing C3a and subsequently forming the C5 convertase. The C5 convertase initiates the Terminal Pathway by cleaving C5 and releasing C5a. C5b binds to C6 and C7, resulting in the fluid phase C5b-7 complex. Ultimately, C8 and several monomers of C9 bind to C5b-7 complex creating a pore in the cell membrane of bacteria or virally infected cells, and eventually forming C5b-9, the membrane attack complex (MAC). FD: factor D, FB: factor B, P: properdin

Complement regulators are soluble and membrane proteins which involve many regulatory mechanisms to prevent host tissue damage caused by complement activation. The soluble regulators are mainly Factor I and H, and C4BP, and the membrane complement regulators are mainly CD46, CD55 and CD59 factors (which are expressed by most nucleated cells), as well as CR1. CD46 and CD55 mediate inactivation of C3b and C4b deposited on host cells, to prevent the formation of C3 and C5 convertases. CD59 is a membrane attack complex (MAC) regulator which binds to the cell surface on host cells, once C5b6-8 has been deposited on cells, CD59 prevents C9 from binding the complex and polymerizing, avoiding the formation of MAC (figure 1) (Davies and Lachmann 1993, Kim and Song 2006, Morgan 2016).

Most of the circulating complement proteins are synthesised in the liver. However, emerging research has reported that a variety of extra-hepatic organs, tissues and cells are also able to synthesise complement proteins. This local production can contribute to the circulating complement pool and allows an immediate access by immune cells, allowing complement to regulate immune cell function (Colten and Strunk 1993).

Activation occurs through 3 distinct pathways, the classical pathway (CP), lectin pathway (LP) and the alternative pathway (AP), each of them responding to different stimuli. The CP responds to immune-complexes formed in cell surfaces of pathogens by binding of the effector complement molecule C1q. The LP responds to Mannose Binding Lectins (MBL) bound to carbohydrates on the surface of pathogens. The AP is mainly activated through the spontaneous hydrolysis of C3, a process known as tick-over (Figure 1) (Murphy, Kraakman et al. 2016).

Each of these pathways activate complement and generate a 'membrane-bound C3 convertase', which cleaves further C3 molecules, releasing C3a and subsequently forming the C5 convertase. The C5 convertase initiates the Terminal Pathway by cleaving C5 and releasing C5a. C5b binds to C6 and C7, resulting in the fluid phase C5b-7 complex, which

is inserted into the cell membrane through a labile hydrophobic membrane binding site in the complex. However, the majority of C5b-7 complexes decay in the fluid phase due to hydrolysation of the membrane binding site and vitronectin, clusterin (binding fluid-phase inhibitors) and even C8. Ultimately, C8 and several monomers of C9 (up to 12 monomers) bind to C5b-7 complex creating a pore in the cell membrane and eventually forming C5b-9, the membrane attack complex (MAC) (Figure 1) (Podack and Tschopp 1984). The formation of multiple MACs on the surface of invading pathogens and non-nucleated cells results in cell lysis (Kim and Song 2006, Gros, Milder et al. 2008). In fact, it has been reported that deficiencies of MAC forming complement proteins predispose for Neisseria infections (Ram, Lewis et al. 2010).

1.2.1 The Membrane Attack Complex

MAC deposition on cells is regulated by several defence mechanisms, such as CD59 inhibitor, to avoid lysis by preventing MAC formation or by accelerating removal of MAC from the membrane (Morgan 2016). However, dysregulation and overactivation of the complement system can result into several MAC pores deposited on the cell membrane, causing influx of ions into the cell. Non-nucleated cells such as erythrocytes, which are metabolically inert, result in cell lysis. However, nucleated cells are more resistant due to high regulator expression and metabolic activity (contain ion pumps and can remove MAC lesions from the membrane by endocytosis or ectocytosis) (Morgan 1989).

Deposition of MAC pores at sublytic levels in nucleated cells has been reported to modulate cell function in several studies. It has been shown that sublytic MAC can trigger apoptosis, protein synthesis, proliferation, granule release and proinflammatory effects (Morgan 1992, MORGAN 2003, Takano, Elimam et al. 2013). Inflammatory effects due to sublytic MAC deposition have been reported in retinal epithelial cells, which showed release of IL-6 and IL-8 inflammatory cytokines (Lueck, Wasmuth et al. 2011), and in neutrophils and rat macrophages, which induced release of inflammatory mediators such as Prostaglandin E2 (Hänsch, Seitz et al. 1984, Morgan 1992). Sublytic MAC was also shown to induce inflammatory effects by triggering the NLRP3 inflammasome in murine dendritic cells (Laudisi, Spreafico et al. 2013) and in lung epithelial cells through increased intracellular Ca^2+ and subsequent depolarisation of the mitochondrial membrane potential (Figure 2) (Triantafilou, Hughes et al. 2013). In addition, studies have showed MAC internalisation via formation of an Akt+ NIK+ signalosome on Rab5+ endosomes, over endocytosis or blebbing, leading to MAC co-localisation with ASC and NLRP3 (Jane-wit,

Surovtseva et al. 2015, Xie, Qin et al. 2019) (Sims, Faioni et al. 1988, Beum, Lindorfer et al. 2008, Diaz-del-Olmo, Worboys et al. 2021).

Increased intracellular calcium ($[Ca^{2+}]i$) due to sublytic MAC has been shown to cause cell activation and intracellular signalling pathways, where increased $[Ca^{2+}]i$ binds to calmodulin, leading to downstream calmodulin-dependent kinases to execute events in the cell (Morgan 2016). Furthermore, signalling of MAC interacting with the Giα-subunit (G-protein-coupled receptor family member) has been shown to regulate cyclic AMP (cAMP) production when Ca^{2+} influx was prevented by intracellular Ca^{2+} chelation and/or removal of extracellular Ca^{2+}, therefore indicating the presence of Ca^{2+}-independent MAC signalling pathways in the cell (Niculescu, Rus et al. 1997). The interactions between MAC proteins and the Giα-subunit in the membrane remain unresolved (Figure 2).
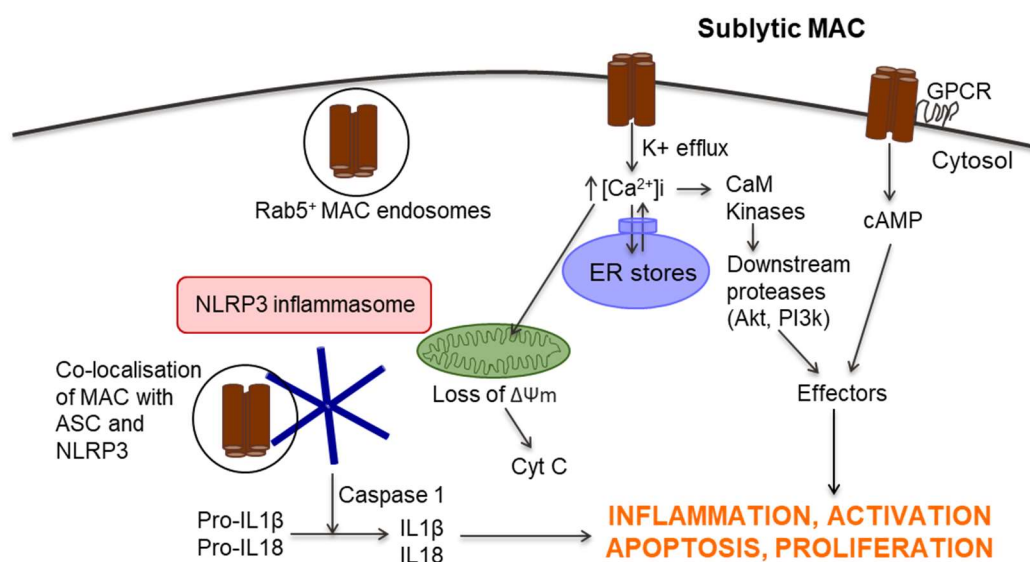
Figure 2. Downstream signalling of sublytic MAC stimulation. Increased intracellular calcium ($[Ca^{2+}]i$) due to sublytic MAC stimulation has been shown to cause cell activation and intracellular signalling pathways, where increased $[Ca^{2+}]i$ binds to calmodulin, leading to downstream calmodulin-dependent kinases to execute events in the cell. Signalling of MAC interacting with the Giα-subunit (G-protein-coupled receptor family member) has been shown to regulate cyclic AMP (cAMP) production. Sublytic MAC was also shown to induce inflammatory effects by triggering the NLRP3 inflammasome through increased intracellular Ca2+, loss of mitochondrial membrane potential and subsequent release of cytochrome C into the cytosol, causing apoptosis in lung epithelial cells. MAC has also been shown to internalise via formation of an Akt+ NIK+ signalosome on Rab5+ endosomes, and to co-localise with ASC and NLRP3. Overall, Sublytic MAC can trigger apoptosis, cell activation, proliferation and proinflammatory effects.

1.3 The Inflammasome

Formation of multiprotein complexes by members of the NLR protein family and HIN domain containing (PYHIN) family upon exposure to certain DAMPs and PAMPs are known as inflammasomes. Inflammasomes structure and function to integrate multiple signals from PRRs and other danger detectors to produce a targeted inflammatory response, has been conserved among vertebrates (Dowling and O'Neill 2012). NLR protein family include mainly Pyrin domains-containing protein 1 (NLRP1), NLRP3, NLRP6, NLR family CARD (caspase activation and recruitment) domain containing 4 (NLRC4), NAIP (neuronal apoptosis inhibitor protein), C2TA (class 2 transcription activator, of the MHC), and members of the PYHIN family include absence in melanoma 2 (AIM2), and IFN-γ inducible protein 16 (IFI16). NLRP3 inflammasome is the best characterised inflammasome in humans and mice up to date, and it is composed of NLRP3, also named NALP3, procaspase-1 and adaptor apoptosis speck protein (ASC) (Mevorach, Mascarenhas et al.) (Latz, Xiao et al. 2013, Guo, Callaway et al. 2015).

Canonical activation of the NLRP3 inflammasome involves sensing of lipopolysaccharide (LPS) or bacterial peptidoglycans by TLR4 or monosodium urate particles. Cytosolic NLRP3 is then released by HSP90 and SGT1 and binds to ASC through the pyrin domain, resulting in procaspase-1 binding to the ASC CARD domain and subsequent oligomerisation to form ASC speck complexes, which consist of several molecules of NLRP3, procaspase-1 and ASC. This leads to release of active p10 and p20 caspase-1. TLR4-independent sensing of LPS derived from bacteria is known as non-canonical NLRP3 inflammasome activation, which can occur through caspase- 4 and 5 (human), 11 (murine) and 8, with subsequent K+ efflux promoting the activation of canonical NLRP3 pathway and eventually leading to GSDMD cleavage, this pathway is therefore a non-canonical way to get to canonical NLRP3 activation pathway (Mayor, Martinon et al. 2007, Guo, Callaway et al. 2015) (Figure 3).
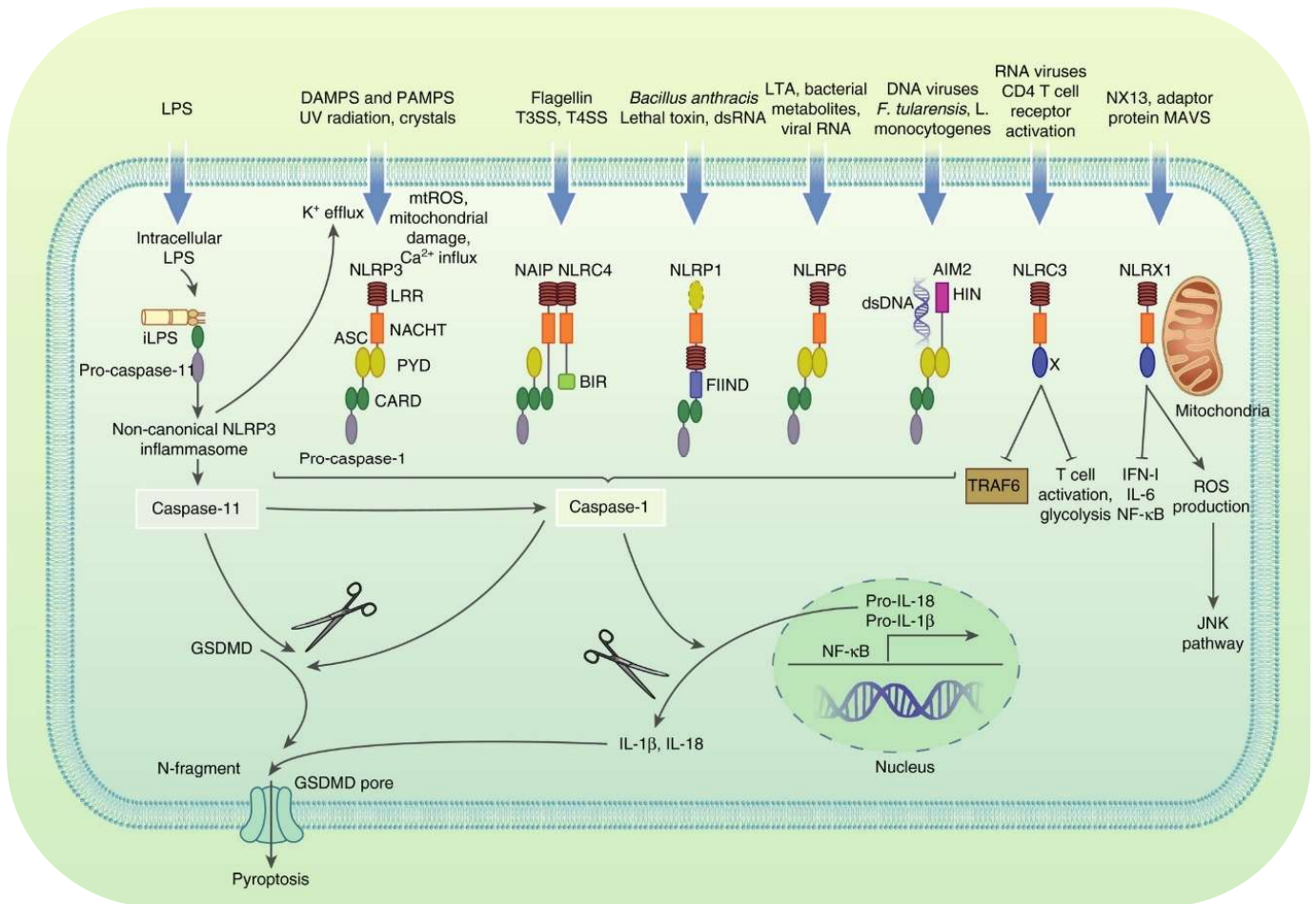
Figure 3. Canonical and non-canonical inflammasomes activation. Activating ligands and structure of canonical NLRP3, NLRC4, NLRP1 (human NLRP1 inflammasome contains PYD, mouse NLRP1 doesn't), NLRP6 and AIM2 inflammasomes, as well as non-canonical NLRP3 inflammasome, and NLRC3 and NLRX1, which are non-inflammasome forming NLRs. Canonical activation of inflammasomes: ASC oligomerisation into speck complexes, recruiting pro-caspase 1, causing self-cleavage and activation of caspase-1. Caspase-1 cleaves pro-IL-1β, pro-IL-18- and GSDMD. The resulting N-terminal fragment of GSDMD forms pores on the cell membrane and allows secretion of IL-1β and IL-18, leading to inflammation and pyroptosis. Non-canonical NLRP3 inflammasome activation: sensing of intracellular LPS by pro-caspase 11 leads to activation of caspase-11 and subsequent GSDMD cleavage, as well as K+ efflux promoting the activation of canonical NLRP3 pathway. In human cells this process occurs via caspase- 4 and 5 instead of caspase-11 (murine cells). Image done by Gisela jimenez-duran author of this thesis, obtained from her review (Jimenez-Duran and Triantafilou 2021) (open access article distributed under the terms of the Creative Commons CC BY license, which permits unrestricted use with proper citation).

NLRP3 inflammasome assembly through caspase-1 activation is highly regulated and 2 different danger signals are required for its activation (Figure 3). Signal 1 primes the inflammasome to enable Signal 2, which then leads to inflammasome activation. Signal 1 is initiated by activation of PRRS, including TLR4 and cytokine receptors, leading to nuclear translocation of nuclear factor κB (NF-kB) and subsequent upregulation and translation of NLRP3 and IL1β. Signal 2 can be triggered by DAMPs or PAMPs and consists of NLRP3 assembly and formation of ASC speck complexes, resulting in cleavage of procaspase-1 into active caspase-1, which cleaves proIL-1β, proIL-18 and gasdermin D (GSDMD) into matured IL-1β and IL-18. The resulting N-terminal fragment of GSDMD forms pores on the cell membrane and allows secretion of IL-1β and IL-18 pro-inflammatory cytokines, leading to inflammation and pyroptosis (Agostini, Martinon et al. 2004, Latz, Xiao et al. 2013). Exogenous signals for signal 2 are mainly microbial, viral and fungal products, UV radiation, crystals or accumulation of altered protein complexes, such as amyloid β in Alzheimer's disease. Endogenous signals include mainly ATP influx, reactive oxygen species (ROS), increased $[Ca^2+]i$. as a result of ion fluxes and subsequent mitochondrial damage, or changes in glucose and lipid metabolism (Figure 3). Interestingly, all endogenous signals involve metabolic changes such as increased glycolysis to support cell activation (Heneka, Kummer et al. 2013, Guo, Callaway et al. 2015). Interestingly, the main NLRs that have been linked with metabolic regulation include NLRP1, NLRP3, NLRP6, NLRP12, NLRC4, NAIP, non-inflammasome forming NLRs NLRC3, and NLRX1, and members of the PYHIN family include AIM2 (Jimenez-Duran and Triantafilou 2021) (Figure 3).

IL-1β is essential to combat pathogen infections. However, dysregulation of inflammasome activation has been reported to contribute to several autoimmune and metabolic diseases, as inflammasomes appear to be major sensors for cell metabolic activity and stress. Such diseases include rheumatoid arthritis (RA), type 2 diabetes, obesity, cancer, non-alcoholic fatty liver disease, among others (Kastbom, Verma et al. 2008, Pontillo, Brandao et al. 2010, Arbore and Kemper 2016).

1.4 Complement in the regulation and assembly of NLRP3 inflammasome

Certain complement receptors and regulators have recently been presented as critical signals for NLRP3 inflammasome activation, either linked with signals coming from RLR or TLR activation, or independently. The fact that increased $[Ca^{2+}]i$ and subsequent mitochondrial stress have been identified as endogenous signal 2 inflammasome activation triggers, led investigations to determine whether or not increased $[Ca^{2+}]i$ resulting from sublytic MAC deposition in nucleated cells could induce NLRP3 inflammasome activation. Sublytic MAC was shown to induce inflammatory effects by triggering the NLRP3 inflammasome resulting in IL-1β and IL-18 release in murine dendritic cells (Laudisi, Spreafico et al. 2013) and in lung epithelial cells, via increased intracellular $[Ca^{2+}]i$ through the MAC pore and release from ER stores, leading to mitochondrial damage and apoptosis (Figure 2 and 4) (Triantafilou, Hughes et al. 2013).

In vivo studies confirmed inflammasome activation by sublytic MAC, where plasma IL-1β and IL-18 was measured in mice treated with LPS. Mice deficient in C6, a critical component of the MAC complex, had significantly reduced plasma IL-1β and IL-18 levels (Morgan 2016). Before the inflammasome was discovered, the C3a anaphylatoxin was shown to induce IL-1β release in human monocytes (Haeffner-Cavaillon, Cavaillon et al. 1987). More recent investigations have shown that C3aR activation in human monocytes, human macrophages and dendritic cells results in signal 2 inflammasome activation. This process has been reported to occur in the presence of LPS and TLR4 activation through increased ATP efflux from the cytosol via an unknown channel and ERK1/2 phosphorylation. ATP efflux triggered by C3a has been reported to result in P2X7 activation (ATP receptor), which has been defined as a potent trigger for signal 2 inflammasome activation (Asgari, Le Friec et al. 2013) (Figure 4).

Furthermore, C5a anaphylatoxin has been shown to act as a trigger for signal 1 priming of the NLRP3 inflammasome. A study showed that cholesterol crystals can activate the classical and alternative complement pathways and that the resulting C5a generated, as well as TNF-α triggered priming of the inflammasome (Samstad, Niyonzima et al. 2014). C5a has been reported to trigger NF-κB activation and IL-18 secretion in retinal pigment epithelial cells, suggesting that signals mediated by C5aR activation regulate IL-1β transcription via NF-κB activation (Cao, Wang et al. 2016). Interestingly, C5a can also act as signal 2 for inflammasome activation. Studies in which inflammation was induced by uric acid crystals in monocytes as a model of gout disease have shown that C5aR1 triggers

priming and activation of the inflammasome through lysosomal damage and cathepsin B activity (An, Mehta et al. 2014). This role for C5a was confirmed by other studies using neutrophils in a mouse peritonitis model (Cumpelik, Ankli et al. 2015). Furthermore, C5a has also been shown to trigger signal 2 inflammasome activation via increased ROS production (Schroder, Zhou et al. 2010, Latz, Xiao et al. 2013) (Figure 4), which has been linked in many studies with anaphylatoxin receptor activation in neutrophils and granulocytes (Astier, Meiffren et al. 2006, Strainic, Liu et al. 2008). The CD46 complement regulator has been identified as a trigger of signal 1 inflammasome priming as it has been reported to induce NF-kB activation and upregulation of IL-β during TCR stimulation on human CD4+ T cells (Kolev, Dimeloe et al. 2015).
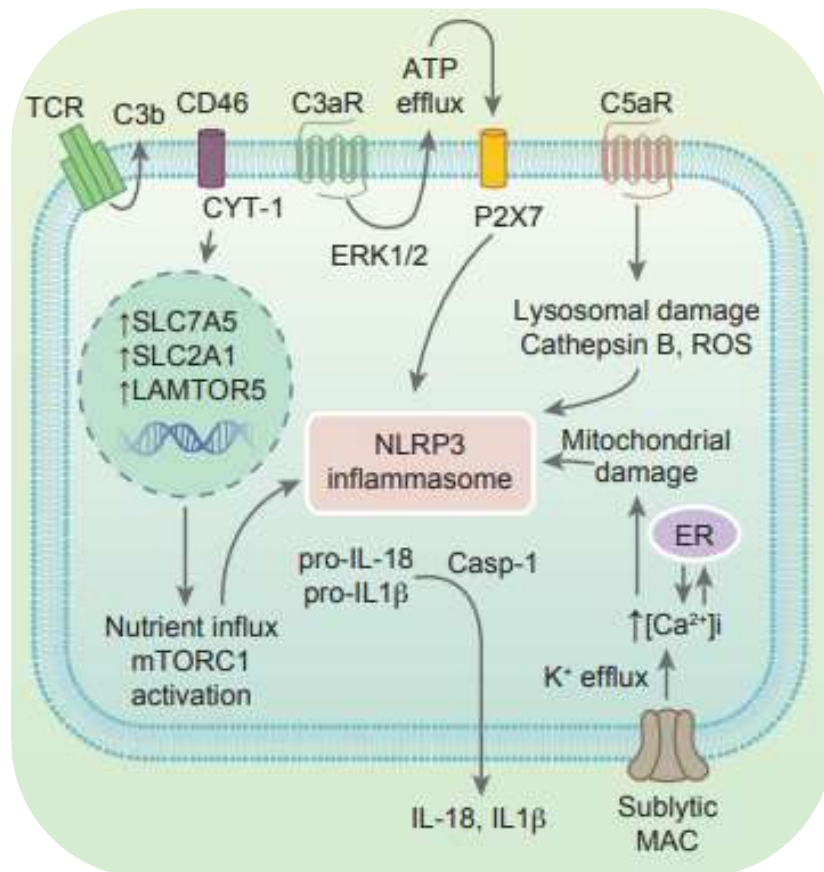
Figure 4. Complement-Metabolism-Inflammasome axis. Pro-inflammatory and cell signalling effects of C3aR, C5aR, CD46 and sublytic MAC, and cell metabolism effects of C3a and CD46. SLC7A5 and SLCA1 are the gene names for glucose and amino acid channels GLUT1 and LAT1, respectively. Image done by Gisela jimenez-duran author of this thesis, obtained from her review (Jimenez-Duran and Triantafilou 2021). "This is an open access article distributed under the terms of the Creative Commons CC BY license, which permits unrestricted use, distribution, and reproduction in any medium, provided the original work is properly cited."

1.5 The interplay between Complement, Inflammasome and Metabolism

In recent decades it has become apparent that the complement system and inflammasomes are not only pathogen sensors, but also systems that can recognize cell metabolic changes and induce reactive responses, for instance, to support cell activation or to maintain cell homeostasis. Activation of the NLRP3 inflammasome has been shown to be modulated by the metabolic state of a cell. Metabolic products can either induce or inhibit the inflammasome. For instance, increased AMP, which leads to inhibition of inflammasome activation by activating the nutrient sensor AMP-dependent protein kinase (AMPK), since AMPK causes a switch from glycolysis (and energy-consuming pathways linked to a high cellular activity) to OXPHOS, which is linked to anti-inflammatory, quiescent or contracting cell responses (De Nardo and Latz 2011). Monounsaturated fatty acids (through AMPK signalling) (Finucane, Lyons et al. 2015) and prostaglandin E2 (Sokolowska, Chen et al. 2015), among others, have also been shown to inhibit induction of the inflammasome.

On the other hand, glycolytic and Krebs cycle enzymes have been reported to induce NLRP3 inflammasome activation. The pyruvate kinase M2 glycolytic enzyme has been shown to induce NLRP3 inflammasome activation in macrophages stimulated with LPS, through hypoxia-inducible factor 1 (HIF-1α) regulation, which binds to the IL-1β promoter leading to maintained IL-1β production (Palsson-McDermott, Curtis et al. 2015). Furthermore, a study using human retinal tubular epithelial cells in diabetic nephropathy demonstrated that heightened glucose influx, heightened ATP production, and increased glycolysis resulted in priming and activation of the NLRP3 inflammasome (Chen, Zhang et al. 2013). These processes are known to be essential for cell effector functions, cell activation and proliferation.

Amino acid and lipid metabolism, and ROS production have also been shown to regulate the NLRP3 inflammasome. It is known that heightened mitochondrial activity, which is essential for cell effector functions, results in ROS production. A study showed that mitochondria colocalized with activated NLRP3 inflammasomes in THP-1 cells (human monocytic cell line) (Zhou, Yazdi et al. 2011), and it is known that mitochondrial activity results in increased ROS production, sustaining NLRP3 inflammasome activation (Schroder, Zhou et al. 2010). Furthermore, another study performed in macrophages demonstrated induction of NLRP3 inflammasome by the amino acid sensor mammalian

target of rapamycin complex 1 (mTORC1), which resulted in increased glycolysis (Moon, Hisata et al. 2015).

Evidence suggests therefore a role for the NLRP3 inflammasome as a major sensor of cellular metabolic reprogramming, where cells undergoing effector activities such as activation/proliferation produce metabolites that induce inflammasome activation, whereas contracting, quiescent or tolerogenic cells produce metabolites that inhibit inflammasome function. Furthermore, inflammasomes can also act as sensors of metabolic dysregulation at a systemic level, apart from intracellular metabolic imbalances (Schroder, Zhou et al. 2010). It has recently been found that complement can not only regulate metabolic changes at a systemic level (Phieler, Garcia-Martin et al. 2013), but also at an intracellular level. Autocrine complement activity can induce metabolic reprograming to drive cell activation through CD46 complement regulator co-stimulation in T cells (Kolev, Dimeloe et al. 2015).

In CD4^{+} T cells, CD46 is expressed in two different isoforms, based on their cytoplasmic tails, known as CYT-1 and CYT-2. CD46-CYT-1 is upregulated by TCR stimulation through autocrine C3b production, leading to increased expression of the amino acid and glucose channels LAT1 and GLUT1, which mediate nutrient influx into the cell required for T-cell activation. CD46-CYT-1 has also been shown to upregulate the late endosomal/lysosomal adaptor, MAPK and MTOR activator 5 (LAMTOR5), which drives mTORC1 activation leading to increased glycolysis. On the other side, CD46-CYT-2 is expressed in resting and contracting T-cells, where CD46-CYT-2 mediates a switch from glycolysis to OXPHOS metabolism (Kolev, Dimeloe et al. 2015, Arbore and Kemper 2016). Interestingly, CD46-CYT-1 signalling in activated CD4^{+}T cells upregulated IL-1β gene expression and triggered intracellular generation of C5a and activation of C5aR1, leading to increased ROS production and NLRP3 inflammasome activation by secretion of IL-1β as well as Th1 cell induction (Kolev, Dimeloe et al. 2015). Importantly, C3 and CD46 dysregulation in T cells is known to contribute to pathology in Th1-mediated autoimmune diseases (Astier, Meiffren et al. 2006, Cardone, Le Friec et al. 2010, Moreno-Navarrete and Fernández-Real 2019). (Figure 4).

Overall, complement has been shown to drive cellular metabolic reprograming in T cells, leading to induction or inhibition signals for NLRP3 priming and activation. Signals from C3a, C3b and C5a have been shown to induce transcription of NLRP3 and IL-1β (signal 1 inflammasome priming) by increased glycolysis and amino acid metabolism via CD46 and C5aR1, as well as triggering signal 2 inflammasome activation through increased ROS

production and mTORC1 mediated increased glycolysis via CD46, indicating the presence of a functional complement-metabolism-inflammasome axis (Arbore and Kemper 2016).

1.6 Glucose metabolism in macrophages and immunity

Macrophages are crucial immune cells with heterogeneous phenotypes, equipped with PRRs such as TLRs, and scavenger receptors allowing recognition of DAMPs or PAMPs and the removal of dying cells or pathogens via phagocytosis, contributing to tissue homeostasis. Macrophages are known to have different origins: fetal liver derived, embryonic yolk sac derived or bone marrow monocyte derived macrophages (MDMs) (Stremmel, Schuchert et al. 2018, Hume, Irvine et al. 2019). During inflammation, circulating monocytes are one of the first cells to migrate from the blood stream to the site of infection infiltrating into tissue, through chemokine and adhesion receptors, and differentiate into macrophages or dendritic cells. Macrophages have been classically accepted to polarise into the M1 proinflammatory phenotype or M2 anti-inflammatory phenotype, however, this classical view has been expanded by several recent studies (see (Murray 2017) for an overview). Macrophage phenotypes resemble a spectrum rather than two extreme phenotypes from highly proinflammatory to pro-fibrotic, pro-tumoral, anti-inflammatory, and many more (Martinez and Gordon 2014).

Typically, macrophages are known to differentiate from monocytes by macrophage colony-stimulating factor (M-CSF) or granulocyte macrophage colony-stimulating factor (GM-CSF). GM-CSF is a growth factor used for generation of classical in vitro models of pro-inflammatory macrophages prior to polarisation with, typically, LPS, and is known to prime macrophages for pro-inflammatory responses without directly tiggering polarisation (Fleetwood, Cook et al. 2005). GM-CSF has also been shown to dominate in pathogenic inflammatory conditions such as RA and MS, over M-CSF (McInnes, Buckley et al. 2016, Wicks and Roberts 2016). M-CSF is also a growth factor readily detected under homeostatic conditions and its receptor functions via several pathways including PI3K/Akt and MEK-ERK1/2 (Stanley and Chitu 2014), whereas GM-CSF is not detected systemically in tissues under homeostatic conditions unless induced by inflammatory situations, and its receptor activates the JAK2/STAT5 pathway (Michl, Ohlbaum et al. 1976, Newsholme, Curi et al. 1986, O'Neill and Hardie 2013, Mills, Kelly et al. 2016). Importantly, MDMs have been implicated in a variety of diseases with inflammatory scenarios leading to immune activation, such as RA, atherosclerosis, sepsis and systemic lupus erythematosus (Ma, Gao et al. 2019, Siouti and Andreakos 2019), as well as

diseases that encompass immune suppression, such as cancer or tolerance to bacteria (Cohen 2002, Fleetwood, Cook et al. 2005, Porta, Rimoldi et al. 2009, Katsiari, Liossis et al. 2010, Chinetti-Gbaguidi, Colin et al. 2015).

In macrophages, activation of the NLRP3 inflammasome and their pro- or anti-inflammatory phenotype can be modulated by enzymes mainly linked with glucose metabolism, which has been reported to activate NLRP3 by direct interaction (Dowling and O'Neill 2012, Galván-Peña and O'Neill 2014). Briefly, the glycolytic metabolic pathway starts with glucose uptake from the extracellular space, leading to intracellular glucose processing in the cytosol to eventually convert it into pyruvate as well as other products (Figure 5). In addition, the glycolysis pathway has a crucial role in providing biosynthetic intermediates for the synthesis of ribose for nucleotides, amino acids, fatty acids and NADH generated by the pentose phosphate pathway (PPP). Pyruvate can be converted into lactate and secreted to the extracellular space or enter the tricarboxylic acid (TCA) cycle (O'Neill, Kishton et al. 2016). Interestingly, limitations to pyruvate import to the TCA cycle by PDK4 regulation have been shown to shift glucose metabolism towards aerobic glycolysis and lactate production, and has been presented as a potential target for sepsis and inflammation (Park and Jeoung 2016) (Van den Bossche, Baardman et al. 2016). The TCA cycle, also named citric acid cycle or krebs cycle, takes place in the mitochondrial matrix and is used by most quiescent cell settings. It is known to be a common point for several nutrient inputs such as pyruvate from glycolysis or fatty acids which are converted into acetyl coenzyme A (acetyl-CoA) that joins the TCA cycle to generate citrate, to eventually generate two main products, NADH and $FADH_2$, which transfer electrons to the electron transport chain (ETC) to support oxidative phosphorylation (OXPHOS), also named mitochondrial respiration (Figure 5) (O'Neill, Kishton et al. 2016). The ETC consists of a series of proteins located in the inner mitochondrial membrane that are capable of transferring electrons in redox reactions, pumping protons across the membrane and eventually generating ATP in a highly efficient matter. Compared to glycolysis, OXPHOS is more efficient at generating ATP as it generates 36 ATP molecules from one molecule of glucose, whereas glycolysis generates 2 molecules of ATP from a single molecule of glucose. However, induction of enzymes of the glycolysis pathway, as well as the high rates of glycolysis that can provide essential biosynthetic intermediates for cell activation, allow a more rapid activation compared to OXPHOS, which requires mitochondrial biogenesis. Therefore, cells that need to rapidly generate ATP undergo a switch to glycolysis (O'Neill, Kishton et al. 2016).
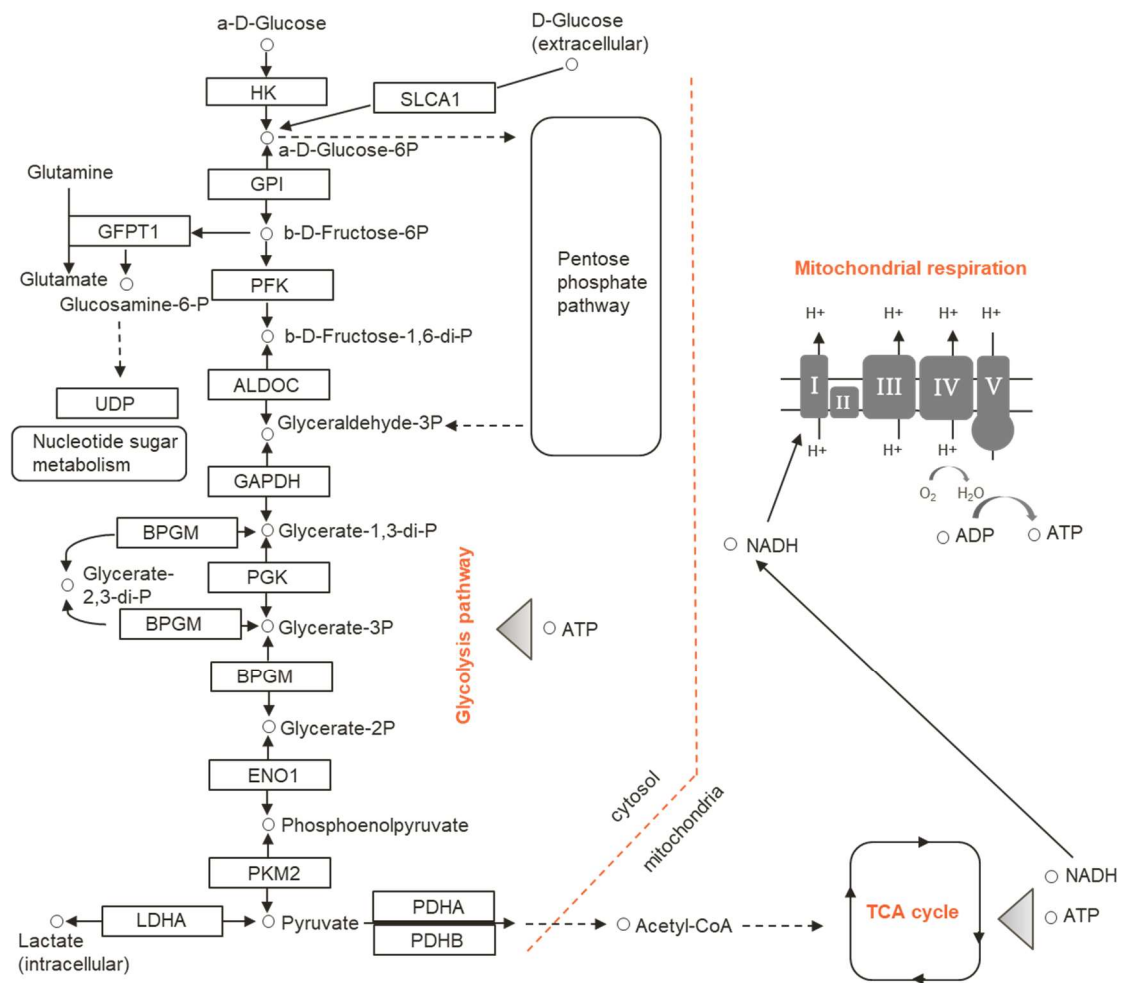
Figure 5. Schematic figure of glycolysis pathway, TCA cycle and mitochondrial respiration. Metabolites are represented as a circle and metabolic enzymes are represented as a square. Glycolysis pathway is represented with part of glutamine metabolism and nucleotide sugar metabolism on the left, and the pentose phosphate pathway on the right, representing parallel metabolic pathways of glycolysis, all happening in the cytosol. Located in the mitochondria are the TCA cycle and mitochondrial respiration, with the complexes I to V of the electron transport chain represented.

Increased glycolysis is known to be part of the bioenergetic profile of pro-inflammatory macrophages and the link between metabolism and inflammatory phenotypes of macrophages is well characterised (Kelly and O'neill 2015). Activated macrophages produce more ROS and switch to glycolysis, allowing rapid ATP production and providing biosynthetic intermediates to carry out its effector functions, whereas anti-inflammatory macrophages rely on oxidative metabolism (Mills, Kelly et al. 2016, O'Neill, Kishton et al. 2016). In addition, LPS induces hypoxia-inducible factor 1α (HIF1α) activation, which is a crucial transcription factor for the induction of several glycolytic enzymes (Tannahill, Curtis et al. 2013, Kelly and O'neill 2015, Mills, Kelly et al. 2016). Interestingly, GM-CSF differentiated MDMs have higher levels of mitochondrial respiration and aerobic glycolysis, as well as higher expression of genes encoding glycolytic enzymes compared to M-CSF MDMs (izquierdo et al 2015), providing energy to the cell needed to support pro-inflammatory functions.

In addition, the bioenergetic profile of human macrophages is known to differ from mouse macrophages in response to LPS. Pro-inflammatory LPS-treated mouse bone marrow-derived macrophages (BMDMs) undergo a metabolic switch to glycolysis, showing higher glycolysis and lower mitochondrial respiration values, as well as inability to respond to FCCP. Conversely, LPS-treated human MDMs show no clear changes in oxidative metabolism with a slight decrease in basal glycolysis (Mills, Kelly et al. 2016, Van den Bossche, Baardman et al. 2016). Interestingly, however, IFN-γ activated human macrophages, which support a classically activated macrophage phenotype, are known to undergo a rapid switch to aerobic glycolysis and repurposing of the mitochondria, including ROS production, allowing for HIF-1α and IL-1β production (Ivashkiv 2018). These IFN-γ-driven immunometabolic changes in human macrophages resemble the bioenergetic profile of pro-inflammatory LPS-treated mouse macrophages, and were reported to contribute to atherosclerosis in diabetic patients (Wang, Zhang et al. 2018). The LPS versus IFN-γ different responses in GM-CSF human macrophages were explained by a recent study that found that IFN-γ suppressed LPS-induced anti-inflammatory and metabolic components of the LPS response, such as IL-10 expression, and superinduced TNF expression supporting macrophage activation (Kang, Bachu et al. 2019).

1.7 Synopsis and aims of the study

Multiple lines of evidence have shown that a sublytic dose of MAC in nucleated cells, which can be resistant to lysis, can initiate several pro-inflammatory effectors such as interleukin-1β (IL-1β), IL-6 and prostaglandin E2 secretion (Morgan 1992, Lueck, Wasmuth et al. 2011, Morgan 2016). Studies in various cell types and in mice have elucidated that sublytic MAC initiates NLRP3 inflammasome activation, driving IL-1β and IL-18 release (Laudisi, Spreafico et al. 2013, Triantafilou, Hughes et al. 2013). The mechanism that mediates these changes, however, is not fully understood but calcium influx into the cytosol and mitochondria, leading to loss of mitochondrial membrane potential have been implicated (Triantafilou, Hughes et al. 2013), indicating a possible link to mitochondrial biology and metabolism. It has been demonstrated that the common point between most endogenous signals for signal 2 inflammasome activation, such as increased intracellular calcium and mitochondrial stress, is the involvement in metabolic changes such as increased glycolysis to support cell activation (Arbore and Kemper 2016). Furthermore, it is known that insertion of MAC into the lipid bilayer results in alteration of the membrane lipid composition, which may alter fatty acid and cholesterol metabolism (Elimam, Papillon et al. 2013). Interestingly, to date, there hasn't been any published studies looking at cellular metabolic changes triggered by MAC. Given that MAC is widely regarded as an inflammatory trigger and such stimuli have been implicated in modulation of immunometabolic response, the main hypothesis of this thesis is that sublytic levels of MAC deposition on human primary macrophages induce changes in cellular energy metabolism to modulate the pro-inflammatory events that have been reported. To address that, the following objectives have been stablished:

– Establish sublytic MAC stimulation conditions in primary macrophages by stimulating them with Normal Human Serum (NHS) as a source of complement, or with the purified complement components C5b6-9.

Determine changes in metabolic pathways triggered by sublytic MAC stimulation, focussing on glycolysis:

– Measure lactate production, as an initial readout for glycolysis, as well as glycolysis activation by Seahorse assays (real-time kinetics) and gene expression of glucose metabolism related genes in response to MAC stimulation.

– Measure whether MAC has an effect on ROS production, as switches to glycolysis are also linked to ROS bursts (Mills et al., 2016) , which can then control cell signalling and downstream effects which may control macrophage fate.

– Determine NLRP3 inflammasome activation in response to glycolysis and ROS inhibitors upon MAC stimulation.

– Measure mitochondrial dysfunction downstream of MAC by quantifying mitochondrial dynamics, mitochondrial membrane potential, as well as intracellular calcium fluxes.

– Metabolomics and proteomics analysis downstream of MAC stimulation. Biological experiments were performed at GSK Stevenage and resulting cell pellets were then analysed by colleagues in GSK UP. Raw data was generated and analysed by this author within GSK UK.

2. Chapter 2: Materials & Methods

2.1 Key resources table

REAGENT	SUPPLIER	IDENTIFIER
Antibodies		
Anti-human C7 monoclonal	Quidel	A221
Anti-human CD55 monoclonal	IBGRL	BRIC 216
anti-human CD59 monoclonal	IBGRL	BRIC 229
Purified anti-human HLA-A,B,C monoclonal	BioLegend	311402
IRDye® 800CW Donkey anti-Rabbit IgG Secondary Antibody	LI-COR	926-32213
IRDye® 680LT Donkey anti-Mouse IgG Secondary Antibody	LI-COR	926-68072
Rabbit Anti-Peroxiredoxin 3	Abcam	Ab73349
Rabbit cleaved Gasdermin D monoclonal (Asp275) (E7H9G)	Cell Signalling	36425
Mouse anti-β-actin monoclonal	Sigma	A2228
Anti-human C9 neoantigen monoclonal WU13-15	HyCult	HM2264
Rabbit anti-human ASC (AL177)	Adipogen	AG-25B-0006-C100
Donkey anti-Mouse IgG (H+L) Secondary Antibody, Alexa Fluor® 488 conjugate	Thermo-Fisher	A-21202
Donkey anti-rabbit IgG Secondary Antibody, Alexa Fluor® 546 conjugate	Thermo-Fisher	A10040
Biotinylated C5b-9	(Abcam, biotinylated in-house)	ab66768

Ruthenylated anti-C6	(Quidel, ruthenylated in-house)	A219

Chemicals, Peptides, and Recombinant Proteins

LPS Lipopolysaccharides from *E. coli* O55:B5	Sigma	L2880-10MG
Carbonyl cyanide 4-(trifluorome-thoxy)phenylhydrazone (FCCP)	Sigma	C2920-10mg
Nigericin	Invitroogen	TLRL-NIG
Rotenone	Sigma	R8875
Glycine	Sigma	50046
Methylmethanethiosulfonate (MMTS)	Sigma	208795
Sodium dodecyl sulfate (SDS)	Sigma	L3771
Sodium deoxycholate	Sigma	30970
MitoPQ, mitochondria-targeted redox cycler	Abcam	ab146819
MitoTracker™ Red CMXRos	Thermofisher	M7512
Fura-2 AM, Ca2+ selective fluorescent indicator	Abcam	ab120873
Human recombinant GM-CSF	R&D Systems	215-GM-010/CF
Ionomycin	Sigma	I3909
2-deoxyglucose	Sigma	D6134- 1G
Heptelidic Acid	Abcam	ab144269
MCC950	Sigma Life Science	CP-456773
Z-VAD-FMK	Sigma	V116-2MG
CellROX deep red reagent	Thermofisher	C10422
Menadione	Sigma	M5625-100G
phorbol 12-myristate 13-acetate (PMA)	Sigma	P1585
C5b6	CompTech	A122
C7	CompTech	A124
C8	CompTech	A125
C9	CompTech	A126
Normal human serum (NHS)	Generated	N/A

		in-house
C7-depleted NHS	Quidel	A503

Critical Commercial Assays

JC-10 Mitochondrial Membrane Potential Assay Kit – Microplate	Abcam	ab112134
Amplex Red Hydrogen Peroxide/Peroxidase Assay Kit	Invitrogen	A22188
Cell-TiterGlo kit	Promega	G7571
Calcein AM cell viability kit	Trevigen	4892-010-K
L-Lactate Assay Kit (Colorimetric/Fluorometric)	Abcam	Ab65330
Human total IL-18 Duoset ELISA	R&D Systems	DY318
Human total IL-1β Duoset ELISA	R&D Systems	DY319
XF Cell Mito Stress test kit	Agilent	103015-100
XF Cell glycolytic rate test kit	Agilent	103344-100

Software and Algorithms

GarphPad Prism	GraphPad Software	http://www.graphpad.com/scientificsoftware/prism/
Image J and Fiji	ImageJ	https://imagej.net/Welcome and https://imagej.net/Fiji
Zen Blue image analysis software	Zeiss	https://www.zeiss.com/microscopy/int/products/mi

		croscope-software/zen.html
Seahorse Wave Desktop Software	Agilent	https://www.agilent.com/en/product/cell-analysis/real-time-cell-metabolic-analysis/xf-software/seahorse-wave-desktop-software-740897
MetaboAnalyst	MetaboAnalyst	https://www.metaboanalyst.ca/
Perseus	MaxQuant	https://maxquant.net/perseus/
PANTHER classification system	GeneOntology, Unifying Biology	http://pantherdb.org/

Table 2.1 Key resources table

2.2 Primary monocyte isolation, differentiation and treatment

PBMCs were isolated from healthy human blood cones or whole blood from GSK's Blood Donation Unit (BDU) by gradient centrifugation for 20 min at room temperature (RT) at 300 g using accuspin tubes (Sigma) containing Ficoll –Paque plus (GE healthcare). After centrifugation, the Human peripheral blood mononuclear cells (PBMC) layer was collected and monocytes isolated using MACS CD14 MicroBeads (Miltenyi Biotech) according to supplier's protocol with an LS column (Miltenyi Biotech): PBMCs were re-suspended with 1 mL MACS buffer plus 100 µL CD14 MicroBeads for every 100 mL of blood for 15 min at 4°C. An LS column was placed on to a MACS magnet and a cell strainer was placed on top of the column. 3 mL of MACS buffer was added to the LS column. Once the buffer was eluted out, the samples containing PBMCs mixed with the CD14 microbeads were added to the column. CD14 negative cells were eluted out, and 3 wash steps (3 x 3 mL MACS buffer) were performed to

ensure optimal elution. The LS column was removed from the MACS magnet and placed on top of a 15mL Falcon tube. 5 mL MACS buffer was added to the LS column. The plunger from the cell strainer removed earlier was re-attached to the column and pushed down to elute the CD14+ cells.

Cell viability and concentration was determined using a Vi-CELL XR cell counter. Purified CD14+ monocytes were plated at relevant cell concentration for experiment (100,000 cells/well in 96-well plates and 96XF seahorse plates (Agilent), 1 million cells/well in 24-well plates, unless indicated otherwise) and treated with growth factor M-CSF (150 ng/ml) or GM-CSF (5 ng/ml) (R&D Systems) and cultured in RMPI-1640 (Life Technologies) with 10 % FCS (for M-CSF differentiation) or 5% FCS (for GM-CSFs) and 2 mM L-glutamine for 6 days, at 37 °C, 5% CO_2 to allow differentiation. All human biological samples were sourced ethically, and their research use was in accord with the terms of the informed consents under an IRB/EC approved protocol.

On day 6, cells were visually observed to ensure suitability and washed once with treatment media RPMI-1640 with 2mM L-Glutamine and sensitised to complement attack by adding 7 µg/ml of anti-CD55, anti-CD59 and anti-HLA antibodies for 50 min at 37 °C, 5% CO_2. Antibody-sensitised cells were exposed to normal human serum (NHS) (pooled from 10 donors, generated in-house), 25 µg/ml of anti-C7 antibody with NHS (previously incubated for 30 min, on ice) or C7-depleted NHS (Quidel) as a negative controls for MAC formation, heat-inactivated NHS (NHS pre-incubation at 56°C for 30 min) as a negative control for complement activation, or non-sensitised cells with NHS alone at 37 °C, 5% CO_2 for the indicated amount of time. Antibody concentrations were based on information from supplier's protocols and expertise from previous experiments in Triantafilou's lab in macrophages. Subtlytic doses of MAC were characterised as the NHS concentration causing <20% cell death as measured using viability assays described below (Campbell, Daw et al. 1979, Reid, Cooke et al. 2012). Alternatively, MAC attack was induced using human purified proteins C5b6-9 only for the extracellular hydrogen peroxide assay in this thesis. Cells were washed once with treatment media RPMI-1640 with 2mM L-Glutamine and incubated with anti-CD59 for 50 min at 37 °C, 5% CO_2. Antibody-sensitised cells were exposed to purified protein C5b6 for 10 min at room temperature, followed by addition of purified C7 for 15 min at 37 °C, 5% CO2. C8 and C9 were then added sequentially and left at 37 °C, 5% CO2 for the indicated amount of time. C7, C8 and C9 were added in a molar excess to the C5b6 concentration. Manufacturer for all purified proteins was Comptech.

<u>In-house NHS preparation</u>: Due to the large number of donors, blood was donated periodically for approximately 1 hour. The blood was therefore collected in the lab in the on-site blood donation unit in order to prevent disruption to RT incubation. This allowed blood from each donor to be handled as consistently as possible, thereby minimising the risk of activating and consuming complement in some samples but not others. 30 ml whole blood without anti-coagulant was collected from 10 donors into S-Monovette Zgel serum separation tubes (Sarstedt) (7.5 ml per tube, 4 tubes per donor). The tubes were inverted 10 times and incubated at RT for 20 min to induce clotting. After 20 minutes, the tubes were incubated on ice for at least 10 min. This contracted the clot and slowed any Complement activity. After blood from the final donor was collected, it was inverted and placed on ice. The samples were then transferred to a Biosafety Cabinet and processed together following the 10 minute incubation for the final blood samples. The tubes were centrifuged, 2000 g, 10 minutes, 4 °C. The serum was separated from the blood and layed above the gel layer. The serum from each tube was transferred into a sterile 150 ml Sterilin container (Sterilin) and aliquoted into 1ml cryovials (Nunc), snap-frozen on dry ice and stored at 80°C for use.

2.3 Viability assays

Cell viability was measured by two different assays to assess the cell viability post MAC stimulation, as sensitised cells were exposed to a titration of NHS or C5b6-9. The CellTiter-Glo assay (Promega), which quantifies intracellular ATP as an indicator of viability by luminescence, and the non-metabolic Calcein AM assay (Thermofisher), which measures fluorescence staining of intracellular calcein of attached live cells, a hydrophilic compound that is well-retained in the cytosol, were used. Both assays were performed according to supplier's protocols. After stimulation, MDMs were washed HBSS before CellTiter-Glo or calcein AM addition. For CellTiter-Glo assay, HBSS and reaction mix were added to wells in a 1:1 ratio and incubated for 10 min at RT covered from light before transferring half of the volume from each well into a new 96-well black microplate with clear bottom and reading luminescence in a plate reader. For Calcein AM assay, a 24-well black plate with clear bottom was used for cell stimulations. 2 μM of calcein AM was added to cells diluted in calcein AM DW buffer and incubated for 20 min at 37 °C before fluorescence reading at ex/em 490/520 nm in a plate reader. Raw data obtained from fluorescence (Calcein AM) and luminescence (CellTiter-Glo) readings, which were proportional to the number of viable cells, were normalised to untreated positive control as 100% cell survival.

2.4 MAC deposition assay

MAC deposition on cell lysates was measured by terminal complement complex (TCC) MSD (protocol generated in-house at GSK by the assay development team). After MAC stimulation, cells were washed twice with PBS and lysed with RIPA buffer (Sigma) for 20 min on ice. The biotinylated C5b-9 (Abcam, biotinylated in-house) capture antibody was added to a MSD GOLD 96-Well Streptavidin Sector plate for 1 h and washed three times with 0.05% Tween in PBS. All incubations were done at RT with shaking. Samples and standard curve (using human purified sC5b-9 for standards) were then added and left for 1 hr, followed by addition of ruthenylated anti-C6 (Quidel, ruthenylated in-house) detection antibody for 2 hrs. The plate was washed three times followed by addition of 2X Read buffer T (Mesoscale), and measured using MSD Sector 6000 Plate Reader (Mesoscale).

2.5 Cytokine detection

MDMs were at concentration of 1 million cells/well in 24-well plates or 130,000 cells/well in 96-well plates and treated accordingly for the required period of time. Macrophage supernatants were collected, diluted as required and assayed for the presence and quantification of IL-1β and IL-18 using commercial Duoset human ELISA kits (Applied Biosystems), according to the supplier's protocol. The capture antibody was added to a 96-well transparent microplate in PBS over night at RT and washed three times with wash buffer (0.05% Tween in PBS). All incubations were done at RT with shaking. Plates were blocked with reagent diluent (1% BSA in PBS) for 1 hour and washed three times with wash buffer. Samples and standard curves, using recombinant human total IL-1β or IL-18 for standards, were then added and incubated for 2 h, washed three times with wash buffer and followed by addition of the detection antibody for 2 h. Plates were then washed three times with wash buffer followed by addition of Streptavidin-HRP B and incubation for 20 min at RT avoiding direct light. Plates were washed three times again with wash buffer followed by addition of substrate solution (prepared as a 1:1 mixture with color reagent A and B) and incubation for 20 min at RT avoiding direct light. Stop solution was finally added, plates were gently tapped and absorbance was measured in a microplate reader at 450 mn and 540 nm. Readings at 540 nm were subtracted from readings at 450 nm, correcting

for optical imperfections in the plate. Raw data was extrapolated from the standard curve to IL-1β or IL-18 concentration.

2.6 Peroxiredoxin assay and Western Blotting

MDMs were plated at a concentration of 1 million cells/well in 24-well plates and treated with sublytic MAC, anti-C7 + MAC or 5 μM MitoPQ for 1 hour. After cell incubation the media was removed, and cells incubated in 300 μL of media containing 80 mM methylmethanethiosulfonate (MMTS) for 10 min at RT. Then cells were washed in HBSS and lysed with 150 μL RIPA lysing buffer (50 mM Tris, pH (8.0), 150 mM NaCl 1% (v/v) Triton-X100 (Tx100), 0.1% (w/v) SDS, 0.5% (w/v) sodium deoxycholate), supplemented with 1:100 Protease Inhibitor Cocktail (Sigma), phenylmethanesulfonyl fluoride (0.1 mM)) and MMTS (80 mM). Lysates were centrifuged in Eppendorf tubes (13,000 x g for 10 min at 4°C), cell debris was removed and samples were diluted in NuPAGE® LDS Sample Buffer (4X), boiled at 90°C for 5 min and run in a 4-12% BisTris SDS-PAGE electrophoresis gel at 160V constant. After the run, proteins in the gel were transferred onto nitrocellulose membranes using the iBlot device for 7 min. After the transfer, nonspecific sites on the membranes were blocked with Odyssey® Blocking Buffer for 1 hour on rotary at RT. Afterwards, membranes were incubated overnight at 4°C with primary antibodies (goat anti-human IL-1β (1:1000), rabbit anti-Prx3 (1:500), rabbit anti-gasdermin D (1:500) and mouse anti-β-actin (1:5000)). Membranes were washed 5 x 5 min in TBS-Tween (0.1 %) before incubation with secondary antibodies for 1 h at RT (IRDye® 800CW donkey anti-goat (1:10000) or IRDye® 800CW donkey anti-rabbit (1:7000) and IRDye® 680CW donkey anti-mouse (LI-COR) (1:10000)). Membranes were covered from light, washed as above, followed by a 30 min wash in MQ-PBS, 0.1% Tween20 before visualisation on Odyssey CLX. Western blot bands were quantified by measuring densitometry on Image J or ImageStudioLite. Bands for GSDMD were corrected against density of β-actin before comparison to UT or LPS-nigericin control. Prx dimerization was calculated by; % dimer = (SI dimer / ((SI dimer + SI monomer)) x 100) % where SI= signal intensity Dimer was expressed relative to untreated control. Cell lysates for peroxiredoxin assay were generated by incubation of treated cells in 80 mM methylmethanethiosulfonate (MMTS) for 10 min at RT before HBSS wash and lysis in buffer (50 mM Tris, pH (8.0), 150 mM NaCl 1% (v/v) Triton-X100, 0.1% (w/v) SDS, 0.5% (w/v) sodium deoxycholate), supplemented with 1:100 Protease Inhibitor Cocktail (Sigma), phenylmethanesulfonyl fluoride (0.1 mM)) and MMTS (80 mM)).

2.7 Lactate measurement

MDMs were at concentration of 1 million cells/well in 24-well plates and treated accordingly for the required period of time. Macrophage supernatants were then collected, diluted accordingly and assayed for lactate measurement using the Fluorometric L-Lactate Assay Kit (Abcam), according to the supplier's protocol. The reaction mix was prepared using 47.6 uL of lactate assay buffer, 0.4 uL of lactate probe and 2 uL of enzyme mix for a total of 50 uL per reaction. Supernatants from samples and standard curve were mixed with the reaction mix in 1:1 ratio and incubated at room temperature for 30 min protected from light. Fluorescence was measured by microplate reader with Ex/Em at 535/587 nm. Raw data was extrapolated from the standard curve to lactate concentration and plotted as such.

2.8 Real-time qPCR

Total RNA was extracted using QIAshredder Columns (Qiagen) and the RNeasy Mini kit (Qiagen), according to the supplier's protocol. Purity and concentration of RNA was assessed using Nanodrop2000 UV-visible spectrophotometer by 260:230 and 260:280 nm absorbance ratios as recommended by the manufacturer's instructions. Cut-off of 1.95 for 260:280 nm ratio was used. cDNA was generated using 30-200 ng/µl total RNA by a RT-PCR using the High Capacity cDNA Reverse transcription kit (Applied Biosystems), according to the supplier's protocol:

	Step 1	Step 2	Step 3	Step 4
Temperature (°C)	25	37	85	4
Time (min)	10	120	5	

Table 2.2 Reverse transcription thermal cycling program

Quantitative PCR was run using SYBRGreen Mastermix (Applied Biosystems) on a QuantStudio 7 Flex System (Applied Biosystems) as described in the tables below. Final concentration for Applied Biosystems and Qiagen primers was 900 nM and 100 nM for primer-BLASTprimers.

Component	Volume/reaction (µl)
Fast SYBR™ Green Master Mix (2X)	2.5
Primers (20X)	0.25
Nuclease-free H_2O	0.25
Total Master mix per Reaction	3.0

Table 2.3 Master mix volume per reaction

Stage	Step	Temperature (°C)	Duration	Cycles
Hold	1	95	20 secs	
PCR	1	95	1 sec	40
	2	60	20 secs	
Melt Curve	1	95	15 secs	Continuous
	2	60	60 secs	
	3 (dissociation)	95	15 secs	

Table 2.4 Program for the thermal-cycling conditions

Details for primers from Applied Biosystems were as follows: SLC7A5, Hs01001189m1; SLC2A1, Hs00892681m1; LAMTOR5, Hs00246261m1; IL-1β, Hs01555410m1; HIF-1α, Hs00153153_m1; PFKFB3, Hs00998698_m1. Details for primers from Qiagen were as follows: PDK2, QT00038262; PDK4, QT00003325; PDPR, PPH17807A-200; PDHB PPH13220A-200.

Gene expression was normalised to housekeeping genes UBB, Hs00430290_m1; B2M, Hs00187842m1, TBP, Hs00427620_m1 (Applied Biosystems) or:

Forward: GAGCACAGAGCCTCGCCTTT Ex1-2 Reverse: TCATCATCCATGGTGAGCTGG Ex1-2	B-ACTIN	Primer-BLAST
Forward: TGGACAGGACTGAACGTCTTG ex2-3 Reverse: CCAGCAGGTCAGCAAAGAATTTA ex2-3	HTRP	Primer-BLAST
Forward: CCCGAAACGCCGAATATAATCC ex spanning Reverse: AATCAGTGCCGTGGTTCGTG ex spanning	TBP	Primer-BLAST

Table 2.5 Primer-BLAST primer details

Data analysis was performed using the Delta Delta Ct method: gene target C_T (C_Tg) values were normalized against the average of the housekeeping genes C_T (C_Th) following the formula: $\Delta C_T = C_T g - C_T h$. All ΔC_T values were then normalized against the average ΔC_T value of unstimulated control samples ($\Delta C_T u$) with the formula: $\Delta\Delta C_T = \Delta C_T - \Delta C_T u$. Final gene expression values were plotted as relative quantification (Rq) and calculated by converting the $\Delta\Delta C_T$ values from log to linear scale with the formula: gene expression = $2^{-\Delta\Delta CT}$. The average value was calculated between duplicates.

2.9 ROS production assays: intracellular ROS and extracellular hydrogen peroxide

For the IncuCyte assay, cells were incubated with 1 µM CellROX green reagent (Thermofisher) for 20 min at 37°C, and plates were introduced to the FLR IncuCyte (fluorescence reading, real time live cell imaging system kept at 37°C) for a first reading. Cells were sensitised with anti-CD55, CD59 and HLA antibodies and stimulated with a sublytic dose of NHS or with controls HI-NHS, C7-depleted NHS, NHS only or with Menadione (positive control for ROS production) at 20 µM (previously

determined from a concentration-response curve as part of an optimisation test shown in this thesis). Plates were incubated within the IncuCyte set up and 4 readings per well (mean fluorescence intensity (MFI) and 10X image) were performed over time in intervals of 20 min, for 24 hours at ex/em 485/520 nm using the 10X objctive. MFI and cell confluency readings done by the FLR IncuCyte were exported. MFI values were plotted as a percentage relative to positive control menadione-treated cells.

For the CellROX plate reader assay, cells were treated as required including 20 µM menadione as a positive control for intracellular ROS. After treatment, cells were washed twice with HBSS and incubated with 5 µM CellROX™ Deep Red Reagent (Thermofisher) for 20 min at 37°C, 5% CO2. Plates were then washed twice with HBSS and fluorescence was measured in a plate reader at ex/em 640/665 nm. Raw data obtained from fluorescence readings were normalised to untreated cells (0%) and to the positive control Menadione (100%).

For the Amplex red assay (Thermofisher), which measured extracellular hydrogen peroxide, cells were treated as required including 20 nM of PMA as a positive control using the Krebs–Ringer phosphate buffer (145 mM NaCl, 5.7 mM sodium phosphate, 4.86 mM KCl, 0.54 mM CaCl2, 1.22 mM MgSO4, 5.5 mM glucose, pH 7.35). Supernatants were collected and transferred in 96-well black plates with clear bottom. A hydrogen peroxide standard curve was prepared and all samples were mixed with 100 µM Amplex® Red reagent and 0.2 U/mL horseradish peroxidase (HRP) working solution at 1:1 dilution. The plate was incubated for 30 min protected from light. Fluorescence was measured in a plate reader with ex/em 530–560/590 nm. Raw data was extrapolated from the standard curve to hydrogen peroxide concentration in nM.

2.10 Seahorse assays

The XF24 or XF96 Seahorse assay (Agilent) was used to determine the bioenergetic profile of M- or GM- macrophages. Macrophages were plated at relevant cell concentration for experiment and incubated to differentiate as above in CellTak (20 µg/ml) coated 24XF or 96XF seahorse plates. Prior to treatment, cells were washed twice with assay media XF RPMI medium, pH 7.4 (Agilent) supplemented with 2 mM L-glutamine, 25 mM glucose and 1 mM pyruvate (Agilent), or for glycolytic stress test (XF24), supplemented with 2 mM L-glutamine (Agilent). Cells were treated as required in assay media and during the 50 min incubation of antibody sensitisation with or without 5 mM Glycine, plates were left in a CO_2-free incubator. Cells were then

exposed to NHS for the required period of time and inserted into the Seahorse analyser. For the mitochondrial stress test, Oxygen consumption rate (OCR) and extracellular acidification rate (ECAR) were recorded to assess the mitochondrial respiratory activity and glycolytic activity, respectively. After four measurements under basal conditions, cells were treated sequentially with 1 μM oligomycin, 1.2 μM carbonyl cyanide p-(trifluoromethoxy) phenylhydrazone (FCCP), and 1 μM antimycin A plus 1 μM rotenone (all Agilent supplied). For the Glycolytic Rate Test, Glycolytic proton efflux rate (GlycoPER), PER and OCR were measured. After four measurements under basal conditions, cells were treated sequentially with 1 μM antimycin A plus 1 μM rotenone and 50 mM 2-DG. For the Glycolytic Stress Test (XF24), ECAR and OCR were measured. After four measurements under basal conditions, cells were treated sequentially with 25 mM Glucose, 1 μM oligomycin and 55 mM 2-DG. Data from all conditions were normalised using a post-run BCA assay, which was used following supplier's protocol. Technical replicates per condition per donor were averaged. All parameters were calculated using Wave 2.6.1.

2.11 Intracellular calcium assay

Intracellular Ca^{2+} of MDMs was measured by monitoring of Fura-2 AM (Abcam) at $Ex_{340/390}/Em_{505}$. MDMs at 100,000 cells/well in 96-well black microplates with clear bottom (Greiner) or at 900,000 cells/well in 27 mm Nunc glass bottom dishes (Thermofisher), for plate reader or confocal microscopy measurements, respectively, were pre-incubated with 3 μM Fura-2 reagent for 20 min in assay buffer (HBSS with 20 mM HEPES for plate reader, or HBSS with 5mM glucose, 20 mM HEPES for imaging), washed twice in assay buffer and stimulated as required. Fluorescence quantification by plate reader measured the dual excitation ratio at 340/380 nm, allowing an accurate measurement of intracellular Ca^{2+}. Ratios were normalised to untreated control as 100%. Alternatively, select conditions were visualised by a Zeiss LSM880 confocal microscope system equipped with a Zeiss Plan-Apochromat 63x/1.4 N. 63X images were taken for each condition. The excitation maxima of the dye is known to shift from 363 nm to 335 nm upon binding of the dye to Ca^{2+}. Excitation wavelength was set at 380 nm, indicating that a decrease in green fluorescence signal was indicative of Ca^{2+} increase. Alternatively, in a separate experiment, excitation wavelength was set at 380 nm, indicating increase in Fura-2 green signal upon increase in intracellular Ca^2.

2.12 Mitochondrial dynamics

MDMs were plated at 900,000 cells/well in 27 mm Nunc glass bottom dishes (Thermofisher). Prior to treatment, cells were washed twice with imaging media (HBSS containing 5 mM glucose, 20 mM HEPES and 1% BSA) and stained with 500 nM MitoTracker Red CMXRos for 15 min. Cells were washed twice and visualised on a Zeiss LSM880 confocal microscope prior to imaging. Cells were stimulated with sublytic MAC, anti-C7 + MAC or 5 µM ionomycin for 15 min in imaging media without BSA, and data capture occured on the above system with a Zeiss Plan-Apochromat 20x or 63x objective. For 20X, 9 images were taken for each condition and donor (3 x 3 tile), for 63X, 5 images per condition and donor were taken. Mitochondrial dynamics were quantified, using 4 cells per condition per donor for the analysis, with the thresholds Yen and Yuang in the semi-automated analysis macro tool MiNA, used with Fiji/ImageJ software (Valente, Maddalena et al. 2017). The mitochondrial branch length mean values and the mitochondrial footprint values were exported, averaged, and used as a measure for mitochondrial network morphology.

2.13 Mitochondrial membrane potential assay

MDMs were plated at 100,000 cells/well in 96-well black microplates with clear bottom (Greiner) and washed in assay media (HBSS with 20 mM HEPES). Cells were then stimulated with sublytic MAC, anti-C7 control, as well as positive controls 5 µM ionomycin, 1.2 µM FCCP or 1 µM rotenone for 30 min. Mitochondrial membrane potential was measured using the JC-10 Mitochondrial Membrane Potential Assay Kit – Microplate (Abcam), according to the supplier's protocol. Fluorescence intensities were quantified using a plate reader at Ex/Em = 490/520 and 540/590 nm for ratio analysis. Ratios were normalised to untreated control as 100%. An increase in 520/590 nm ratio indicates a drop in mitochondrial membrane potential, as JC-10 is capable of selectively entering mitochondria, reversibly changing its colour from green (emission of JC-10 monomeric form at 520 nm) to orange (emission of J-aggregate form at 590 nm) as membrane potentials increase.

2.14 ASC and MAC staining and confocal microscopy

80,000 monocytes per well were left to differentiate in Lab-tek culture slides (Life Technologies). After MAC treatment and LPS plus Nigericin as a positive control for ASC-Specks, cells were washed twice in PBS, prior to fixation with 10% formalin solution (Sigma) for 15 min. Subsequently the cells were washed in PBS with BSA (0.02 % w/v) and NaN_3 (0.02%) NaN_3 twice and were left in 200 µL of this buffer for labelling with the appropriate primary antibody. Cells were labelled with antibodies for ASC (Anti-ASC rabbit anti-human (AL177), Adipogen) and/or MAC (anti-C9 neoantigen, WU13-15, HyCult) (1/100 dilution) for 1h at RT. Subsequently, the cells were washed three times using PBS/0.02% BSA/0.02% NaN_3 and labelled with the appropriate secondary antibody (1/500 dilution) for 1 hour at RT in order to visualise the receptors of interest. The nucleus of the cells was labelled by adding 1 µl of TOPRO-3 to each well and incubating for 5 min prior to washing the cells three times using PBS/0.02% BSA/0.02% $NaN_3.$ Cells were imaged on a Carl Zeiss, Inc. LSM710 ELYRA P1 confocal microscope using a 1.4 NA 63x Zeiss objective. The images were analysed using Zen Blue image analysis software (Carl Zeiss, Inc.). The data presented are a representative image from at least 20 cells taken from three different replicates. All 20 cells displayed similar results across all three replicates. In order to quantify the degree of co-localisation, Costes' approach was used (Bolte and Cordelieres, 2006), allowing the calculation of Pearson's correlation coefficient R(obs). Values greater than 0.5 are considered significant co-localisation. Costes' approach, Pearson's correlation coefficients and P values were calculated using MBF ImageJ with JACoP (http:// macbiophotonics.ca/).

2.15 Gene expression from RNA seq data from GSK's MDMs Omics Viewer

Unstimulated MDMs differentiated with GM-CSF or M-CSF for 5 days were washed and snap frozen for RNA extraction. Total RNA was extracted using QIAshredder Columns (Qiagen) and the RNeasy Mini kit (Qiagen), according to the supplier's protocol. Cell stimulation and RNA extraction was performed by GSK colleague Claire Cattermole. The generated RNA was shipped for RNA sequencing and analysis by GeneWiz. Analysed data was plotted into Spotfire by GSK colleague Darren Gormley as part of one of the 3 studies that form the 'Monocyte Derived Macrophage (MDM) Omics Viewer', an internally generated omics data sets for gene lookup; allowing users to interrogate expression and differential expression with-in experiment and across

experiments. Genes of interest were searched by the author of this thesis and a screenshot of the graphs from spotfire MDM Omics viewer (GSK internal tool) was used for generating the figure 19.

2.16 Metabolomics analysis

MDMs at 1 million cells/well in 24-well plates were sensitized to complement as above and treated with a sublytic dose of NHS or left untreated for 4 hours. Following treatment, supernatants were removed, the MDMs rinsed with fresh assay media RPMI-1640 with 2mM L-Glutamine, and snap frozen at -80°C.

Metabolomics experiments were designed, prepared and stimulated by Gisela Jimenez-duran (thesis author) and sent to GSK's MST-MedDesign, Discovery Analytical department in Upper Providence, US, where samples were run for metabolomics analysis. Data was re-analysed and graphs were generated by Gisela Jimenez-Duran, help from one of the members from the metabolomics team was provided for volcano plot and heat map generation.

For metabolite exaction, 75% 9:1 MeOH:CHCl$_3$ was added directly to wells containing frozen cells (-80 °C). Cells from four technical replicates for each donor and sample type (NHS treated and untreated) were scraped from their respective wells, combined into Covaris adaptive focused acoustic tubes (for a total of 4 million cells per sample), and disrupted using a 2 minute lysis method on a Covaris S220 Focused Ulrasonicator (Peak Power - 200, Duty Factor - 10, Cycle/Burst - 200). Lysed samples were centrifuged at 5000 x g for 15 minutes at room temperature. Supernatant was split into two equal fractions and set on a Speedvac concentrator to dryness. Samples were reconstituted in either 3:1 MeCN:H2O or H2O+0.1% formic acid for analysis by LC-MS/MS with hydrophilic interaction (HILIC) or reverse phase chromatography respectively.

All data was acquired with a Thermo-Fisher Scientific Ultimate 3000 Liquid Chromatograph coupled to a Q-Exactive Oritrap Mass Spectrometer with Heated Electrospray Ionization Source. For HILIC LC-MS/MS analysis, samples were analysed in positive and negative ion mode using a Phenomenex Luna NH2 analytical column (100 mm x 2 mm, 3 μm) held at room temperature with 10 minute linear gradient (A - 5% MeCN/20mM NH$_4$CH$_2$CO$_2$/20mM NH$_4$OH; B - MeCN) from 95 to 0 % MeCN followed by 5 minute hold at a flow rate of 0.400 mL/min. For reverse phase LC-MS/MS analysis, samples were analysed in positive ion mode only using a Waters

Acquity BEH C18 analytical column (100 mm x 2.1 mm, 1.7 μm) held at 40ºC with 4 minute linear gradient (A - H2O + 0.1% formic acid; B - MeOH + 0.1% formic acid) from 0.5 to 70% MeOH, ramp to 98% MeOH @4.5 minutes, hold 98% to 5.4 minutes at a flow rate of 0.350 mL/min.

Mass spectrometric analysis was performed using data dependent acquisition. Full scan spectra were acquired at a scan range of 61 to 915 m/z at a resolution of 70,000 with an automatic gain control (AGC) of 1e6 ions and maximum injection time of 200 ms. Top 7 data dependent acquisition was employed with priority placed on a custom inclusion list built for known metabolite features. The custom inclusion list was derived from the analysis of neat standards part of the Mass Spectrometry Metabolite Library (IROA Technologies). Precursor ions were isolated with a quadrupole mass window of 1.2 m/z and HCD fragmentation performed with stepped collision energy of 20, 30, and 45 V. MS/MS spectra were acquired at a resolution of 17,500 with an AGC target of 3e3 ions and a maximum injection time of 200 ms.

Raw data was aligned, integrated, and grouped using Thermo Compound Discoverer v3.1.0.305.   Deuterated L-Tryptophan, L-Phenylalanine, and Caffeine internal standards added to sample reconstitution solvents were used for data normalization. Peak annotation was based on the same database used to build the custom inclusion list for known metabolite features, and included retention time, m/z, and MS/MS data for > 500 primary metabolites. Peaks not annotated using the custom database were searched against m/z Cloud as an alternative approach to peak annotation. Statistical and pathway enrichment analysis, as well as data representation was performed using MetaboAnalyst 5.0 (Xia and Wishart 2010, Pang, Chong et al. 2021). Significance between untreated and NHS conditions was done by unpaired student's t-test, fold change and p value cut off were +/- 0.5 and 0.05, respectively. For individual graphs plotted in graphpad PRISM, statistical significance between untreated and NHS conditions was assessed by unpaired student's t-test with Welch's correction for unequal SDs.

2.17 Proteomics analysis

MDMs at 1 million cells/well in 24-well plates were washed in assay media (RPMI-1640 with 2mM L-Glutamine) and treated with sublytic MAC, anti-C7 control or left untreated with assay media for 4 hours. MDMs were washed in assay media and snap frozen at -80°C.

Proteomics experiments were designed, prepared and stimulated by Gisela Jimenez-duran (thesis author) and sent to GSK's MST-MedDesign, Discovery Analytical department in Upper Providence, US, where samples were run for proteomics analysis. Data was re-analysed and graphs were generated by the author of this thesis, help from one of the members from the proteomics team was provided for heat maps generation.

Cells were lysed in the culture plates using a PreOmics kit and scraped into tubes. Protein quantitation was performed using a Pierce Rapid Gold BCA assay kit. (Thermo Scientific). Samples were reduced, alkylated, digested with trypsin/lys C and then labelled using 10-plex tandem mass tag (TMT) reagents (Thermo Fisher). Samples were combined to yield two TMT10 labelled sets, each containing one internal reference scaling (IRS) channel. The IRS sample is made by combining equal aliquots of all 18 samples and allows for normalization across the TMT sets (Plubell, Wilmarth et al. 2017). Labelling efficiency and mixing ratios were tested by injecting a small amount of each TMT pool on a QExactive Orbitrap mass spectrometer (Thermo-Fisher Scientific). The two TMT-labelled pools were fractionated using hydrophilic interaction chromatography (HILIC) manual spin columns (Nest Group, Inc) into 4 fractions. The 4 fractions were dried under vacuum centrifugation and resuspended in 0.1% (v/v) TFA in HPLC grade water.

Each fraction was separated by nanoflow HPLC (Easy nLC 1000, Thermo-Fisher Scientific) using a C18 PepMap trap column (2cm x 175μm ID, PepMap C18, 3μm particles, 100 Å pore size) and a 25 cm EasySpray column (PepMap 25cm x 75μm ID, C18, 2 μm particle size, 100 Å pore size) with a linear gradient (2-28% MeCN, 0.1% FA) over 240 minutes at 300 nL/min. Mass spectrometric analysis was performed on a QExactive Orbitrap mass spectrometer (Thermo-Fisher Scientific) operated in positive ionisation mode with data dependent acquisition. Full scan spectra were acquired at a scan range of 400 to 2000 m/z at a resolution of 70,000, with an automatic gain control (AGC) of 1e6 ions and a maximum injection time of 200 ms. The 10 most intense precursor ions were isolated with a quadrupole mass filter of 2.0 m/z and collision induced dissociation (CID) fragmentation was performed with a stepped collision energy of 24, 27, 30 V. MS/MS spectra were acquired at a resolution of 35,000 with an AGC target of 5e4 ions and a maximum injection time of 200 ms.

Protein identification for the total TMT labelled data set was performed using MaxQuant 1.6.10.0. The reporter ion MS2 type set as TMT10plex; trypsin/P set as the enzyme; fixed modification PreOmics iST-NHS (C); variable modification Oxidation

(M); maximum 2 missed cleavages. Searches were conducted using the human Uniprot database. Quantification of proteins uses razor peptides with a minimum count of 2. Contaminants and reverse hits were removed from the data sets prior to analyses. The data were normalised within and across the TMT sets prior to statistical analyses (Plubell, Wilmarth et al. 2017). A total of 2885 proteins were identified of which 1982 were quantified.

Statistical analyses were performed using Perseus (version 1.6.15.0) (Tyanova, Temu et al. 2016). Perseus was used for generation of hierarchical clustering of normalized protein intensities (z-score) for significantly regulated proteins (ANOVA permutation=based FDR <0.05) and for the one-way ANOVA, FDR corrected, with post-hoc Tukey's test (p<0.05 significant for both MAC vs untreated and MAC vs AC7) significant proteins from which a list of MAC regulated proteins was generated and used for supplementary tables, panel of proteins of interest (mainly mitochondrial proteins) and GO statistical enrichment testing for GO biological processes provided by PANTHER classification system online software, using ID lists with associated expression value z-scores, which provided up-regulated and down-regulated pathways by MAC.

2.18 STATISTICAL ANALYSIS AND DATA AVAILABILITY

Statistical analysis

Data represent the mean ± SEM. Differences between groups are analysed using an unpaired student's t-test with Welch's correction for unequal SDs or 1-way ANOVA with post-hoc Tukey's test as required, using GraphPad Prism 7 software, unless indicated otherwise. $*p < 0.05$, $**p < 0.01$, $***p < 0.001$, $****p<0.0001$. For all experiments n = number of separate donors unless stated otherwise.

Data availability
The mass spectrometry proteomics data have been deposited to the ProteomeXchange Consortium via the PRIDE (Perez-Riverol, Csordas et al. 2019) partner repository with the dataset identifier PXD027316. The metabolomics dataset is available on Metabolomics Workbench under the Project ID PR001213 and Study ID ST001922.

3. Chapter 3: Sublytic MAC drives glycolysis-dependant inflammasome activation, reactive oxygen species and lactate production in naïve M-CSF human monocyte-derived macrophages

Emerging evidence has shown that the complement system and inflammasomes are not only pathogen sensors of innate immunity, but also systems that can recognize changes in cell metabolism and induce reactive responses, for instance, to support cell activation. Improper regulation of complement, however, can cause chronic inflammation and has been associated with autoimmune and metabolic diseases, such as RA, osteoarthritis (OA) and type II diabetes among others. A variety of studies found MAC to be increased in target organs of diabetic complications or in synovial tissue and fluid of RA patients, contributing to pathology and driving inflammation (Wang, Rozelle et al. 2011, Banda, Hyatt et al. 2012, Holers and Banda 2018, Shim, Begum et al. 2020).

MAC was initially described as a membrane pore forming complex capable of lysing bacteria, but multiple lines of evidence have shown that a sublytic dose of MAC in nucleated cells, which can be resistant to lysis, can initiate several signalling events, including pro-inflammatory effectors such as interleukin-1β (IL-1β), IL-6 and prostaglandin E2 secretion (Morgan 1992, Lueck, Wasmuth et al. 2011, Morgan 2016). Studies in lung epithelial or dendritic cells, as well as C6-deficient mice, have elucidated that sublytic MAC initiates NLRP3 inflammasome activation, driving IL-1β and IL-18 release (Laudisi, Spreafico et al. 2013, Triantafilou, Hughes et al. 2013). The mechanism that mediates these changes is not fully understood but calcium influx and loss of mitochondrial membrane potential have been implicated (Triantafilou, Hughes et al. 2013), indicating a possible link to mitochondrial biology and metabolism. Emerging evidence has linked complement with cell metabolism where C3a, C3b and C5a were reported to shift the metabolic profile of immune cells to support pro-inflammatory functions (Arbore and Kemper 2016). Moreover, complement regulator CD46, C3aR, C5aR1 signalling were reported required for NLRP3 priming and CD4^{+} T cell function (Kolev, Dimeloe et al. 2015, Arbore and Kemper 2016, Yan, Freiwald et al. 2021), and autocrine C5aR1 signalling is known to enhance intracellular ROS and trigger IL-1β signalling in T-cells (Revu, Wu et al. 2018, West, Kolev et al. 2018), indicating the existence of a complement-metabolism-inflammasome axis. In addition, a recent study showed that C3 metabolic reprogramming and drives inflammatory priming of synovial fibroblasts (Friscic, Bottcher et al. 2021). Other recent studies showed that complement acts as a global immunometabolic regulator, especially in the brain (McDonald, McCombe et al. 2020, Kunz and Kemper 2021)

supporting the involvement of complement in immunometabolism. Interestingly, glycolytic metabolites as well as MAC have been found to be upregulated in samples from RA patients in clinical studies (Neumann, Barnum et al. 2002, Romero, Fert-Bober et al. 2013, Narasimhan, Coras et al. 2018). Several complement have therefore been shown to regulate immunometabolism, however, whether MAC is involved in this complement-metabolism-inflammasome axis is still unknown.

In macrophages, activation of the NLRP3 inflammasome and their pro- or anti-inflammatory phenotype can be modulated by enzymes mainly linked with glucose metabolism, which has been reported to activate NLRP3 by direct interaction. Activated macrophages produce more ROS and switch to glycolysis, allowing rapid ATP production and providing biosynthetic intermediates to carry out its effector functions, whereas anti-inflammatory macrophages rely on oxidative metabolism (Mills, Kelly et al. 2016, O'Neill, Kishton et al. 2016). These observations have mainly used lipopolysaccharide (LPS) to induce inflammation, however, endogenous triggers of immunometabolic changes and inflammation, such as complement, have more relevance in sterile inflammation scenarios. In addition, macrophages have been widely implicated in the pathogenesis of several autoimmune diseases such as RA (Ma, Gao et al. 2019, Siouti and Andreakos 2019). Given that MAC is regarded as an inflammatory trigger and inflammatory stimuli such as LPS have been implicated in modulation of immunometabolic response, this chapter investigated the effect of sublytic MAC in naïve M-CSF human MDMs from the perspective of metabolic control of inflammation.

3.1 Determination of NHS concentration needed for sublytic MAC formation and MAC deposition in M-CSF MDMs

As a model of assessing complement-based MAC-driven attack, induction of sublytic MAC on cells is well documented (Morgan and Campbell 1985, Laudisi, Spreafico et al. 2013, Triantafilou, Hughes et al. 2013, Lusthaus, Mazkereth et al. 2018). Here, we used the methods highlighted in Figure 6A to induce sublytic MAC in human naïve M-CSF differentiated MDMs using monoclonal anti-CD55, CD59 complement regulators and HLA antibodies ('Abs.') to sensitise cells to complement, and normal human serum (NHS) as a source of complement. The cell survival assays ATP-dependent CellTitre-Glo and ATP-independent calcein stain, were used to ensure assay validity during modulations of metabolic function (Figure 6B). The resultant concentration-dependant lysis curves were comparable between assays. CellTiter-Glo assay was then selected for an NHS titration experiment. Addition of NHS to MDMs resulted in a partial loss in viability as concentration of NHS increased, which was blocked by addition of the terminal pathway complement protein C7-blocking antibody, referred to anti-C7 throughout (Figure 6C). To assess the effect of sublytic MAC, concentrations of NHS that resulted in 80 % viability were used, as has been used in other studies to replicate sublytic MAC concentrations (Campbell, Daw et al. 1979, Reid, Cooke et al. 2012). A lysis curve was performed before every experiment in this thesis to account for batch variation and or cell differentiation/donor variation. In addition to measuring viability MAC deposition on MDMs was confirmed by quantitative measurement of C5b6-9 presence by a Meso Scale Discovery (MSD) based assay (Figure 6D), highlighting the suitability of this model to study MAC effects in MDMs. NHS. M-CSF macrophage-like morphology (elongated cells) was confirmed by cell imaging with an EVOS microscope (Figure 6E).
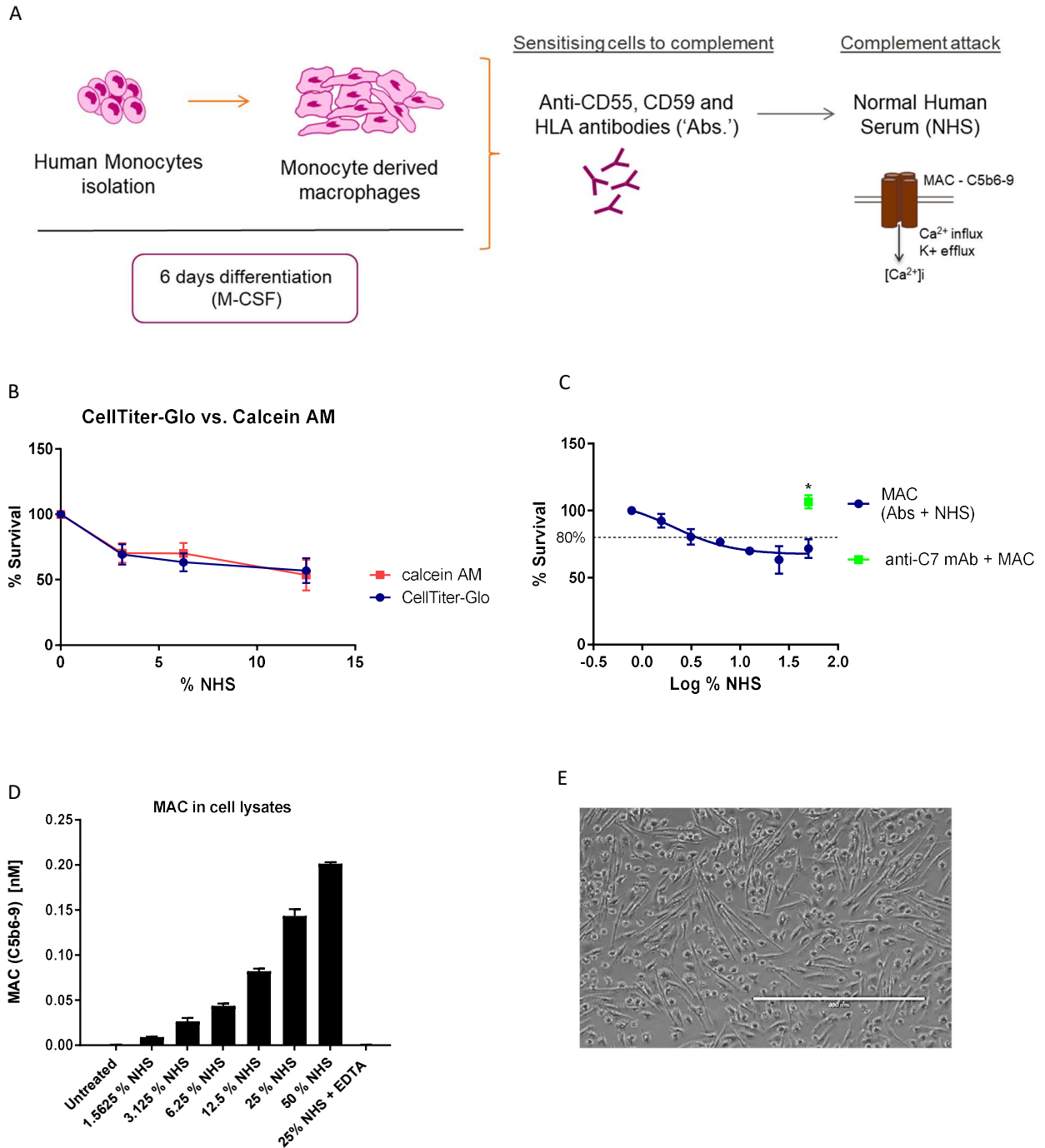
Figure 6. MAC deposition and lytic effect on MDMs.
(A) Schematic of sublytic MAC stimulation of MDMs using NHS. (B,C,D) MDMs treated with antibodies (anti-CD55, CD59, HLA) and increasing concentrations of NHS as in (A) for 1 hour before viability measurement by (B) CellTiter-Glo and Calcein AM assay comparison (n=3), (C) CellTitre-Glo assay (n=6) and (D) TCC MSD measuring C5b-9 (MAC) deposition in cell lysates (n=3). Negative controls were performed by addition of anti-C7 antibody (C) and EDTA to stop complement activation (D). Error bars represent +/- S.E.M. Statistical significance in C was determined by unpaired student's T-test with Welch's correction for unequal SDs. (E) M-CSF macrophages morphology (10X, scale bar 400 μm, EVOS microscope).

3.2 Sublytic MAC triggers inflammasome gene expression and activation

To determine whether sublytic MAC triggers NLRP3 inflammasome priming and activation, gene expression of NLRP3 and Caspase 1 was assessed by qPCR (Figure 7A), as well as protein expression of pro-IL1β by Western Blot (Figure 7B) and secretion of IL-1β (Figure 7C) and IL-18 (Figure 7D) by ELISA from primary macrophages.

Sublytic MAC formation triggered upregulation of NLRP3 (3-fold increase) and Caspase 1 (5-fold increase) at 2 and 4 hours post-stimulation (Figure 7A). Pro-IL1β protein expression was increased at 4 and 6 hours post-stimulation (Figure 7B) and the release of IL-1β and IL-18 occurred between 2 and 6 hours post-stimulation (Figure 7C and D).

Cells were also incubated with the anti-complement regulators and HLA antibodies only (Abs. only), NHS only, the 'Abs.' in combination with HI-NHS and with NHS which had been depleted for C7 (C7-depl. NHS) controls, with the aim to verify that sublytic MAC was the trigger of the upregulation, protein expression and cytokine secretion observed (Figure 7). It was shown that in the presence of these controls, there was negligible upregulation of Caspase 1 compared to stimulation conditions (Figure 7A) and no pro-IL1β protein expression, except on the C7-depleted NHS control (Figure 7B), suggesting that other complement components might induce signal 1 inflammasome priming, as shown previously (An, Mehta et al. 2014). Furthermore, cells treated with all previously mentioned controls showed a significantly lower IL-1β and IL-18 cytokine release compared to stimulation conditions (Figure 7C and D). Therefore, the data demonstrated that inflammasome activation can be triggered by sublytic MAC formation in primary macrophages.
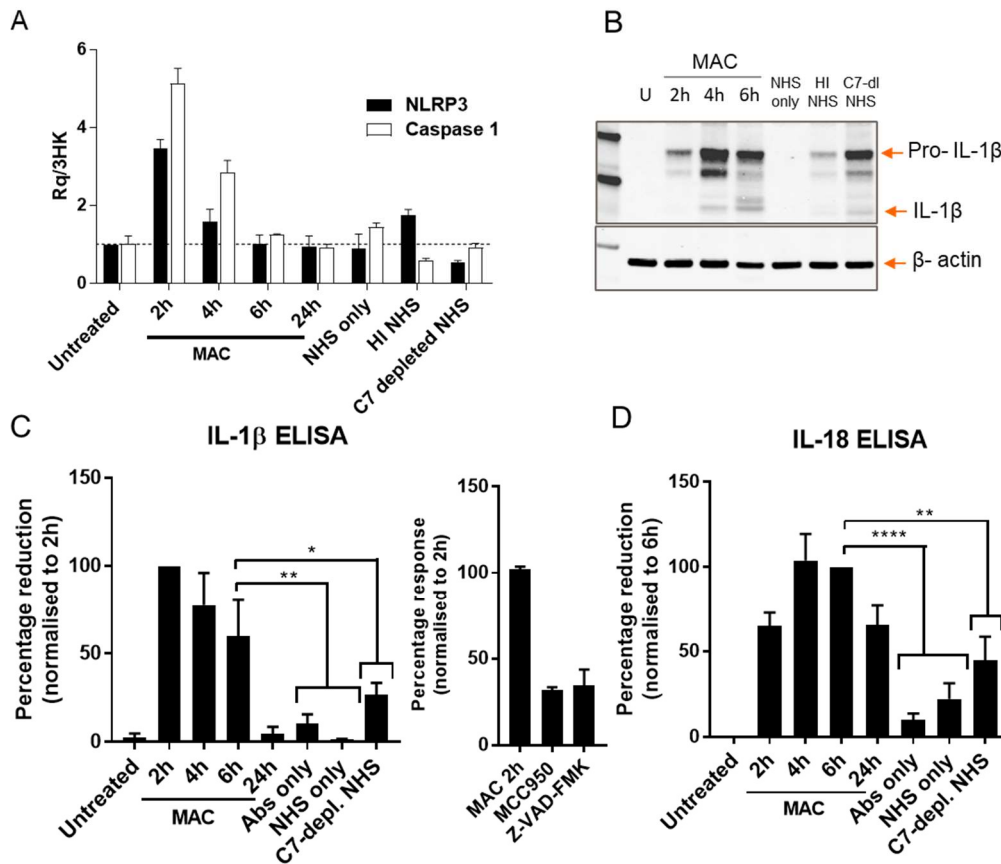
Figure 7. MAC drives NLRP3 inflammasome activation. M-CSF differentiated MDMs pre-treated with 'Abs.' (Anti-CD55, CD59 and HLA antibodies) and incubated with 3.5% NHS (as sublytic MAC concentration), indicated as 'MAC' or with controls Abs only, 3.5 % NHS only, 3.5% heat inactivated NHS (HI NHS) or 3.5% C7 depleted NHS (C7-depl. NHS) for 2, 4, 6 and 24 hours. (A) Gene expression of NLRP3 and Caspase 1. Gene expression was normalised to housekeeping genes β-actin, HPRT and TBP. ΔΔCt is relative to unstimulated cells (n=3). (B) Cell extracts were analysed for the presence of pro-IL1β and IL1β by Western blot (n=3). (C-D) Supernatants were collected and analysed for IL1β and IL-18 by ELISAs. MCC950 (1 μM) and Z-VAD-FMK (20 μM) inhibitors were pre-treated for 1 hour (n=3). All data showing significant difference are n=3 (One-Way ANOVA test). **** is $P < 0.0001$, *** is $P < 0.001$, ** is $P < 0.01$ and * is $P < 0.05$. Error bars are +/- standard error of mean (S.E.M).

3.3 Sublytic MAC drives lactate production and glycolysis-dependant inflammasome activation

It has been reported that inflammatory macrophages use glycolysis, among other metabolic pathways i.e. fatty acid synthesis and amino acid metabolism, to proliferate and

support the production of pro-inflammatory cytokines, such as IL-1β and IL-18 resulting from NLRP3 inflammasome activation (O'Neill et al. 2016). In order to elucidate the MAC–inflammasome interactions in relation to intracellular metabolic changes, focussing on glycolysis, modulation of glycolysis pathway was performed using 2- desoxy-D-glucose (2-DG) and Heptelidic acid (HA) inhibitors, and inflammasome activation was assessed. 2-DG and HA are glycolytic inhibitors of hexokinase and glyceraldehyde 3-phosphate dehydrogenase (GAPDH), respectively.

Cells were pre-incubated with 2-DG or HA inhibitors and treated with sensitising antibodies anti- CD55, CD59 and HLA and a sublytic MAC dose of NHS at several time points (Figure 5). Inflammasome priming was determined by NLRP3 and Caspase 1 gene expression by qPCR, and pro-IL1β protein expression by Western Blot (Figure 8A/B). 2-DG and HA inhibitor caused a downregulation of NLRP3 expression and 2-DG caused a 2-fold decrease of Caspase 1 expression compared to stimulation conditions without the inhibitor (Figure 8A). Protein expression of pro-IL1β was abolished in cells incubated with 2-DG and HA at 4 hours post- MAC stimulation, and decreased at 6 hours post-stimulation (Figure 8B). Inflammasome activation was assessed by measuring IL-1β and IL-18 release by ELISA (Figure 8C/D). Pre-incubated cells with 2-DG and HA showed a significant reduction of IL-1β and IL-18 secretion compared to stimulated cells in the absence of inhibitors. In addition, pre-incubation of cells with 2-DG or HA prior to sublytic MAC treatment didn't affect cell survival (Figure 8E).

In response to the sensitivity of MAC-dependent inflammasome activation to glycolytic inhibitors, the role of glycolysis upon MAC stimulation was next assessed. To confirm glycolytic upregulation, we used lactate as a proxy of glycolysis. Measurement of lactate production was performed on sensitised cells stimulated with a sublytic dose of MAC for 2, 4, 6 and 24 hours (Figure 8F). Sublytic MAC triggered an increase of lactate production over time up to 24 h, as the values were significantly higher to all controls tested: sensitising antibodies (Abs. only) alone and in combination with HI NHS and C7-depleted NHS, and NHS only at 6 hours. Overall, the data demonstrated that inhibition of glycolysis by 2-DG and HA resulted in a reduction of MAC-mediated inflammasome priming and subsequent activation, as well as an increased lactate production driven by MAC, indicating an involvement of the glycolysis pathway as part of the downstream signalling of MAC which may have a role in the NLRP3 activation pathway.
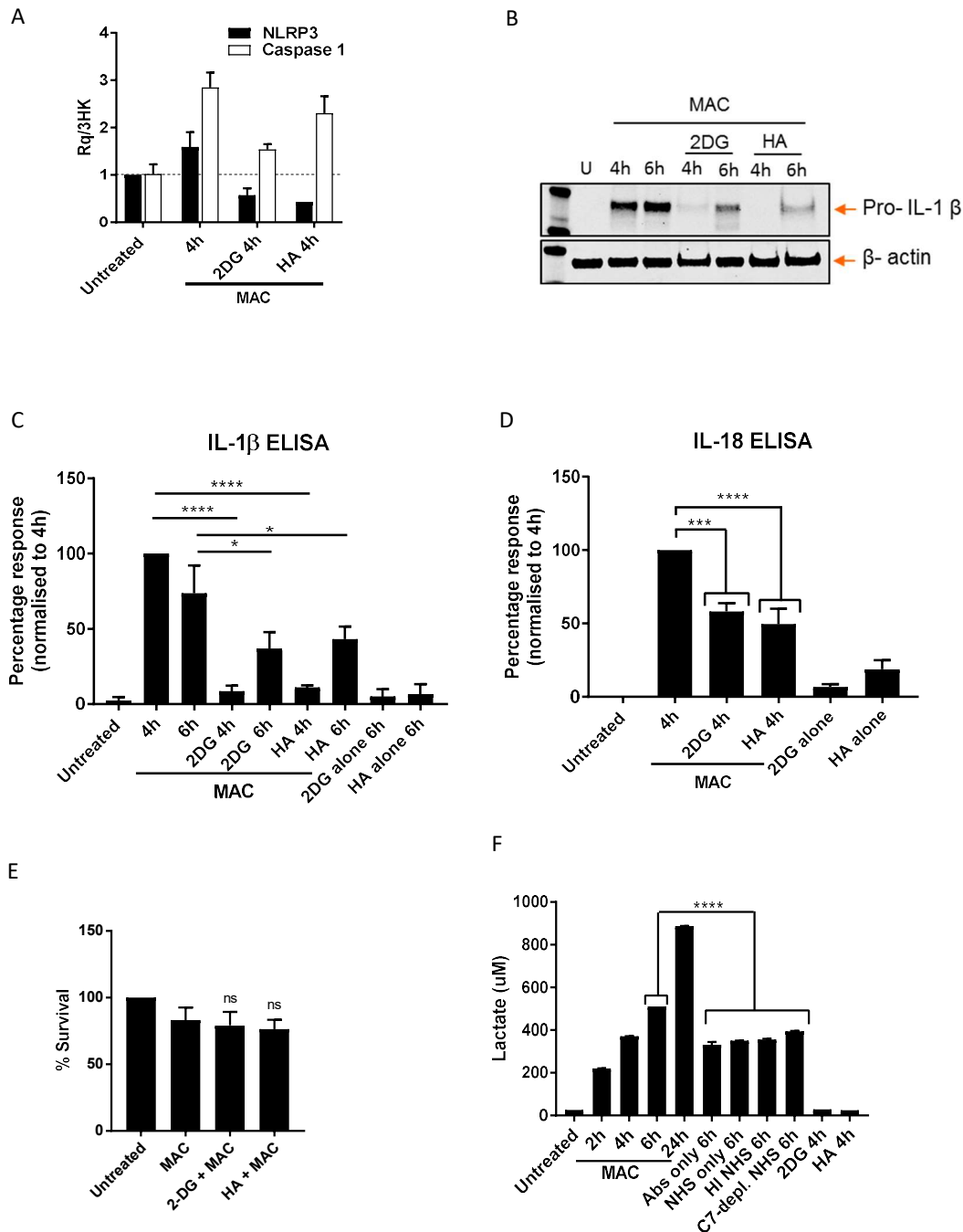
Figure 8. Investigating glycolysis in inflammasome activation downstream of MAC. M-CSF primary macrophages pre-incubated with glycolytic inhibitors 2- desoxy-D-glucose (2-DG), at 5 mM for 2 hours and Heptedilic acid (HA) at 10 µM for 1 hour. Cells in the presence and absence of inhibitors were stimulated with 'Abs.' (Anti-CD55, CD59 and HLA antibodies) and incubated with 3.5% NHS (as sublytic MAC concentration), indicated as 'MAC', for 4 or 6 hours. (A) Gene expression of NLRP3 and Caspase 1 (n=3). Gene expression was normalised to housekeeping genes β-actin, HPRT and TBP. Inhibition of glycolysis causes a reduction of NLRP3 and Caspase 1 upregulation in response to sublytic MAC stimulation. (B) Cell extracts were analysed for the presence of pro-IL1β by Western blot (n=3). (C, D) Supernatants were collected and analysed for IL1β and IL-18 by ELISAs. Inhibition of glycolysis causes a significant reduction of IL1β and IL-18 secretion. (E) CellTiter-Glo assay to determine cell viability in the presence of 2-DG and HA

inhibitors in M-CSF macrophages incubated for 2 hours and 1 hour respectively, and stimulated with MAC (Abs + NHS) for 24 hours. (n=3) (F) Lactate production was measured in response to sublytic MAC stimulation overtime. All data showing significant difference are n=3 (One-Way ANOVA test). Error bars are +/- standard error of mean.

3.4 MAC induces upregulation of genes involved in glycolytic and amino acid metabolism

With the aim to address whether sublytic MAC triggers any intracellular metabolic changes in glycolysis and amino acid (AA) metabolism at a gene expression level, as it was shown in CD4+ T cells downstream of C3b interaction with the complement regulator CD46 (Kolev, Dimeloe et al. 2015), primary macrophages were pre-incubated with 2-DG and HA inhibitors and/or sensitised and then stimulated with sublytic MAC for 2, 4, 6 and 24 hours (Figure 9). Interestingly, gene expression of SLC2A1 (gene for glucose transporter, GLUT1), SLC7A5 (amino acid channel, LAT1) and LAMTOR5, which drives mTROC1 activation causing increased glycolysis, were upregulated by 3-fold increase between 2 and 4 hours post MAC stimulation (Figure 9A), whereas sensitised cells incubated with either HI NHS or C7-depleted NHS, or cells with NHS only had reduced to no upregulation of these genes compared to cells with stimulation conditions at 4 hours.

Sensitised and MAC stimulated cells in the presence of 2-DG and HA glycolytic inhibitors showed no upregulation of the glucose channel GLUT1 gene and LAMTOR5. Interestingly, whereas 2-DG had no effect on LAT1 expression, HA blocked the upregulation of LAT1 caused by sublytic MAC (Figure 9B), suggesting that GAPDH is involved in the regulation of LAT1. The data showed that glycolysis and AA metabolic genes are upregulated as a result of sublytic MAC formation.
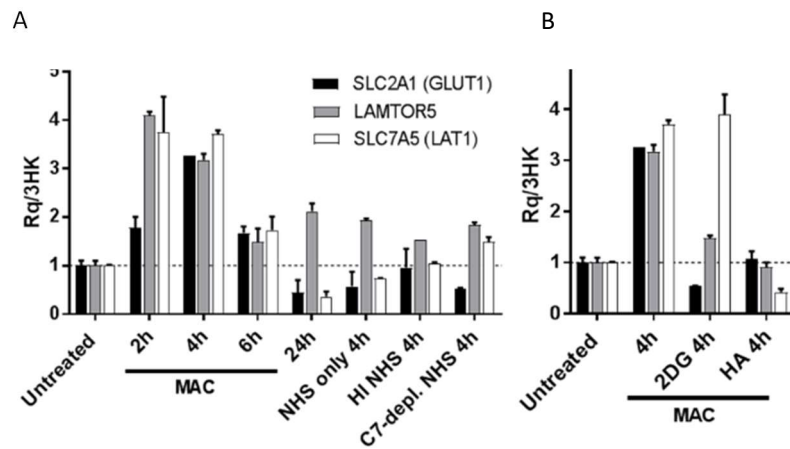
Figure 9. Sublytic MAC triggers lactate release and upregulation of glycolysis and amino acid metabolic genes. Cells in absence (A) and presence (B) of inhibitors incubated with Abs. and stimulated with NHS (as sublytic MAC concentration) over time. (B) Glycolytic inhibitors 2- deoxy-D-glucose (2-DG), at 5 mM, preincubated for 2 h and Heptelidic acid (HA) at 10 μM for 1 h. Gene expression of SLC2A1, SLC7A5 and LAMTOR5 (n=3). Gene expression was normalised to housekeeping genes β-actin, HPRT and TBP. ΔΔCt is relative to unstimulated cells.

3.5 Intracellular ROS production is triggered by MAC stimulation

LPS activated macrophages have been reported to undergo a switch to glycolysis with subsequent alteration of the mitochondrial membrane potential and an increase in mitochondrial ROS, by a proposed mechanism named reverse electron transport-ROS (RET-ROS), and that these changes are required to induce an inflammatory response (Mills, Kelly et al. 2016). In addition, sublytic MAC was shown to trigger an increase in intracellular calcium ($[Ca2+]i$) with subsequent mitochondrial Ca2+ uptake (Triantafilou, Hughes et al. 2013), and in a separate study, mitochondrial Ca2+ uptake was shown to increase in ROS production (Feissner, Skalska et al. 2009). Given the above observations showing that MAC supports glycolysis by increased lactate and upregulation of glycolysis promoting genes, and that glycolysis is needed to support inflammasome activation (Figure 8, 9), it was hypothesised that MAC would trigger ROS production in macrophages, which has yet to be determined.

In order to address intracellular ROS production, cells were pre-incubated with CellROX dye for 20 minutes, sensitised and stimulated with sublytic MAC. ROS production was quantified by mean fluorescence intensity on an FLR IncuCyte during a time course of 15 hours (Figure 10). Sensitised cells stimulated with MAC showed an increase in ROS production between 1 and 4 hours up to 100% (Figure 10A), as normalised to menadione treated cells, a positive control for ROS production which concentration was previously optimised using the same assay (Figure 10C). A concentration of 20 uM of Menadione was selected for the CellROX assay with MDMs, showing clear green fluorescence indicative of increased intracellular ROS in a representative image (Figure 10B). Sensitised cells incubated with either C5- or C7-depleted NHS had lower ROS production levels than MAC stimulated cells. These are higher than the UT control, suggesting some components of the NHS that are not C5 and/or C7 can contribute to phenotype but together additively MAC drives higher ROS. Therefore, it was shown that sensitised cells stimulated with sublytic doses of MAC can trigger an increase in intracellular ROS production.
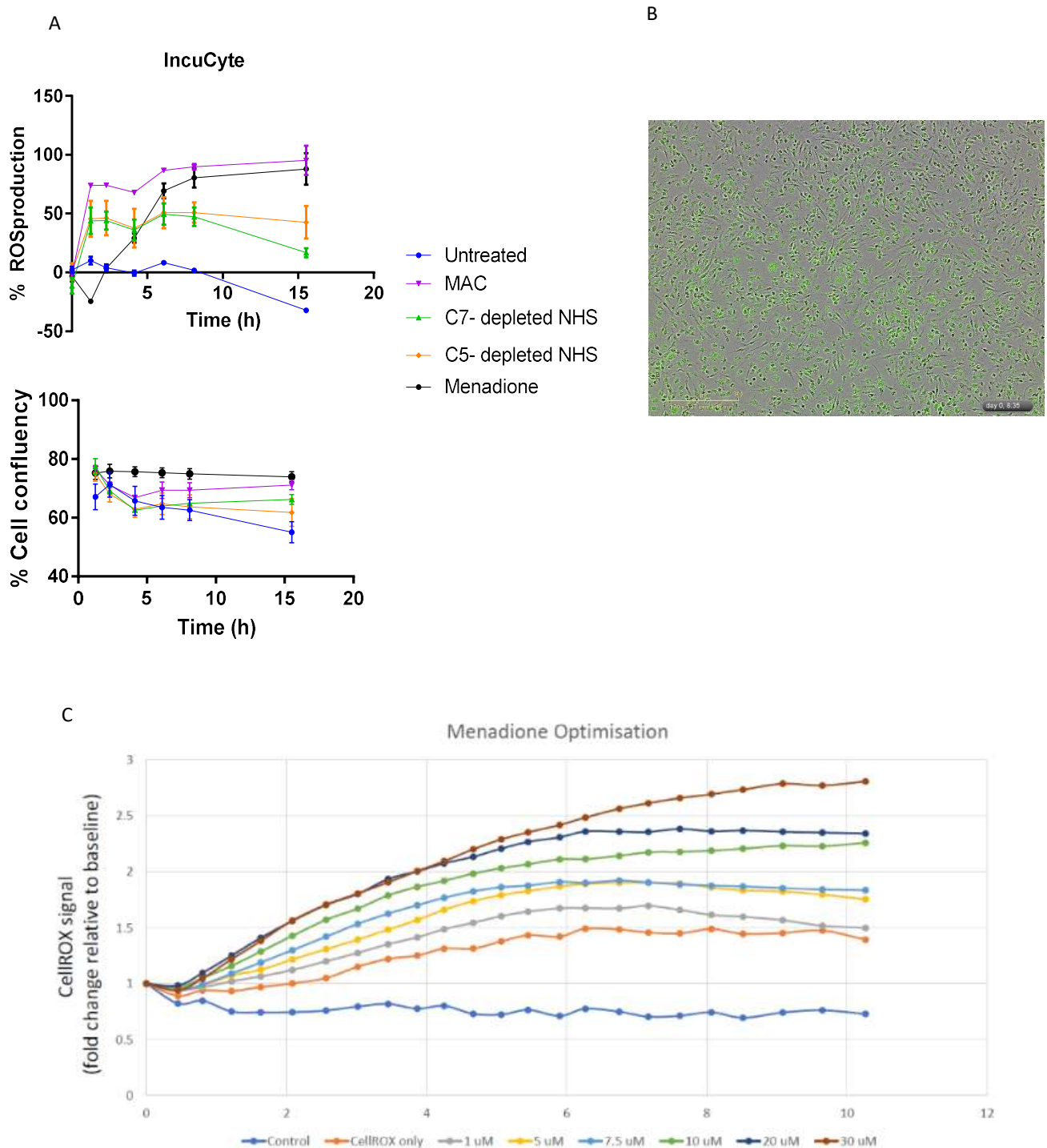
Figure 10. NHS stimulation triggers ROS production. (A, C) ROS production and (A) cell confluency measured overtime using FLR IncuCyte. (A-C) MDMs were pre-treated with ROS fluorescent dye CellROX green reagent for 20 min (n=3). (A) sensitised with Abs. and stimulated with a subytic dose of MAC, or with controls C5- and C7- depleted NHS or 20 µM Menadione as a positive control for ROS production, which was previously optimised in (C). (B) 20 µM Menadione-treated MDMs showing green fluorescence from CellROX dye (10X, FLR IncuCyte microscope). (A) Raw data is expressed as a percentage relative to positive control menadione-treated cells. n= 3.

3.6 Optimisation of extracellular ROS assay to measure hydrogen peroxide production

The CellROX assay shown above measures general ROS production intracellularly. To further assess specific ROS production triggered by MAC, measurement of hydrogen peroxide extracellularly was assessed and optimised in MDMs using the Amplex red assay. A concentration-response curve with ascending concentrations of NHS was performed in RPMI with 2 mM L-glutamine, usually used for MDM stimulations, or in amplex red assay buffer Krebs–Ringer phosphate (KRPG), to test complement activation and cell lysis in this buffer. Cell viability was assessed after 1 hour with CellTiter-Glo assay and cells in KRPG buffer showed a slight increase in cell lysis compared to RPMI media (Figure 11A), indicating higher complement activity and confirming the suitability of this buffer to assess MAC attack.

The Amplex red assay was then performed by testing kinetic measurement of MDMs left untreated, with sensitising antibodies (anti-CD55, CD59, HLA) or assay background control without cells for 1 hour (Figure 11B). The resulting fluorescence values which measured hydrogen peroxide production were increased notably over time, whereas the background control only showed a slight increase. Antibody-sensitised cells showed no added background compared to cells left untreated. For simplicity, Amplex red assay was then performed as endpoint assay. Before testing MAC stimulation, the assay was optimised testing controls PMA, LPS, rotenone or menadione for 30 min, 1 or 2 hours, adding the Amplex red reagent to the cells during the time course as suggested by the manufacturer's protocol (Figure 11C) or adding the reagent at the end of the time course and transferring supernatants into a new plate before reading fluorescence (Figure 11D). Fluorescence signal was more stable in Figure 11D, adding the reagent after the time course, where PMA signal increased over time, whereas in Figure 11C the signal was decreased after 2 hours. Positive controls PMA and Menadione showed the highest fluorescence signals of hydrogen peroxide after 30 min, however, while PMA increased over time, menadione signal decreased significantly after 2 hours. Optimal use of the amplex red assay was stablished at 200 nM PMA as positive control and assay reagent to be added post stimulation time.

Finally, to test whether addition of NHS for MAC attack caused any interference with the assay, increasing concentrations of hydrogen peroxide with and without a fixed sublytic MAC dose of NHS were added to wells without cells (Figure 11E). While the hydrogen peroxide (H_2O_2) curve showed increased MFI values in proportion to its concentration, all the curve points of hydrogen peroxide plus NHS had no increase in MFI, indicating that

certain components in the NHS (potentially catalase) are responsible for the degradation of hydrogen peroxide. In conclusion, measurement of extracellular hydrogen peroxide levels was proposed to be executed by stimulating sensitised MDMs with purified MAC proteins C5b6-9 instead of NHS, as a more robust system to induce sublytic MAC and avoid assay interference.
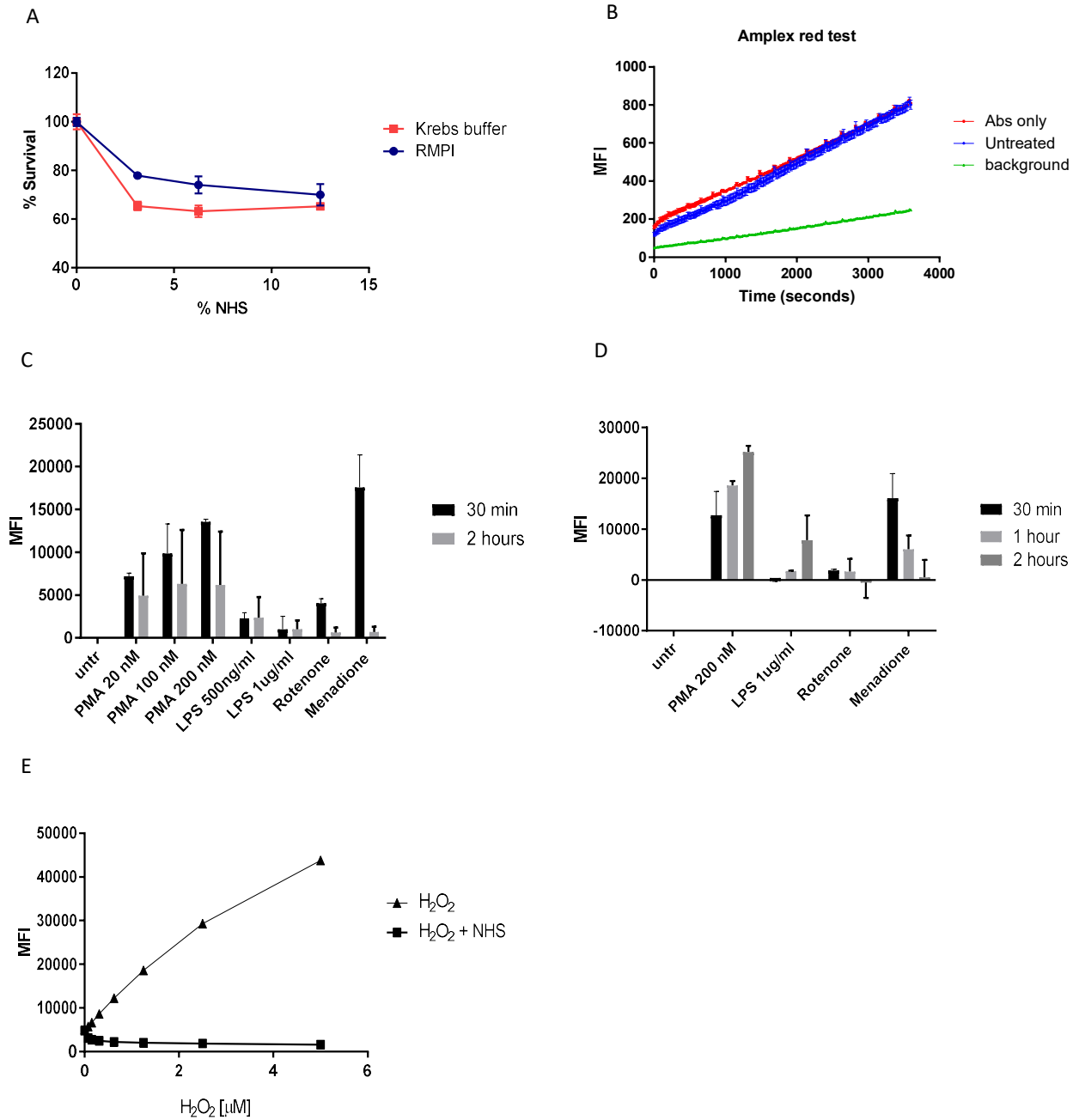
Figure 11. Optimisation of amplex red assay for hydrogen peroxide measurement. (A) MDMs sensitised with antibodies (anti-CD55, CD59, HLA) and increasing concentrations of NHS for 1 hour before viability measurement by CellTiter-Glo in RMPI with 2 mM L-glutamine or amplex red assay buffer Krebs–Ringer phosphate (KRPG) (n=3). (B) Amplex red assay (kinetic measurement) of MDMs sensitised with antibodies (anti-CD55, CD59, HLA) or assay background control without cells (n=3). (C-D) amplex red assay testing controls PMA (20, 100 or 200 nM), LPS (500 ng/ml or 1 µg/ml), rotenone (2 µM) or menadione (20 µM) for 30 min, 1 or 2 h, (C) keeping the Amplex Red reagent during the time course or (D) adding the reagent at the end of the time course. (D) Mean fluorescence intensity of standard curve of hydrogen peroxide or standard curve of hydrogen peroxide plus NHS (n=3).

64

3.7 Assembly of C5b6-9 purified complement components triggers IL-1β release

In order to establish a system to induce MAC deposition on the surface of MDMs without the presence of NHS, cells were sensitised with anti-CD59, the complement regulator for MAC, and subsequently treated with purified complement proteins C5b6 for 10 minutes, C7 for 15 minutes and finally C8 and C9 for 2 hours, building the MAC pore into the membrane.

A concentration-response curve with ascending concentrations of C5b6, each with a molar excess of C7, C8 and C9 was performed in order to establish a sublytic MAC concentration (Figure 12A). Cell viability was assessed with CellTiter-Glo assay and sublytic doses of MAC corresponded to 2.5 µg/ml of C5b6 (80% cell survival) and 5 µg/ml of C7, C8 and C9. In order to confirm MAC deposition in the cells, increasing concentrations of C5b6-9 complex were added and showed a concentration-dependant response in MAC deposition measured by TCC MSD (Figure 12B).

Once the sublytic MAC dose was determined, IL-1β was measured by ELISA as a proxy for inflammasome activation (Figure 12C). Sensitised cells were incubated with C5a to allow signal 1 inflammasome priming and treated with C5b6-9 purified components for 4, 6, 8 and 18 hours. IL-1β secretion occurred 18 hours post-stimulation indicating inflammasome activation. Sensitised cells incubated only with C5a, C7, C8, C9 or C5b6-9 without C5a incubation showed negligible levels of IL-1β secretion, indicating that sublytic MAC deposition using purified components C5b6-9 in combination to C5a triggers inflammasome activation.
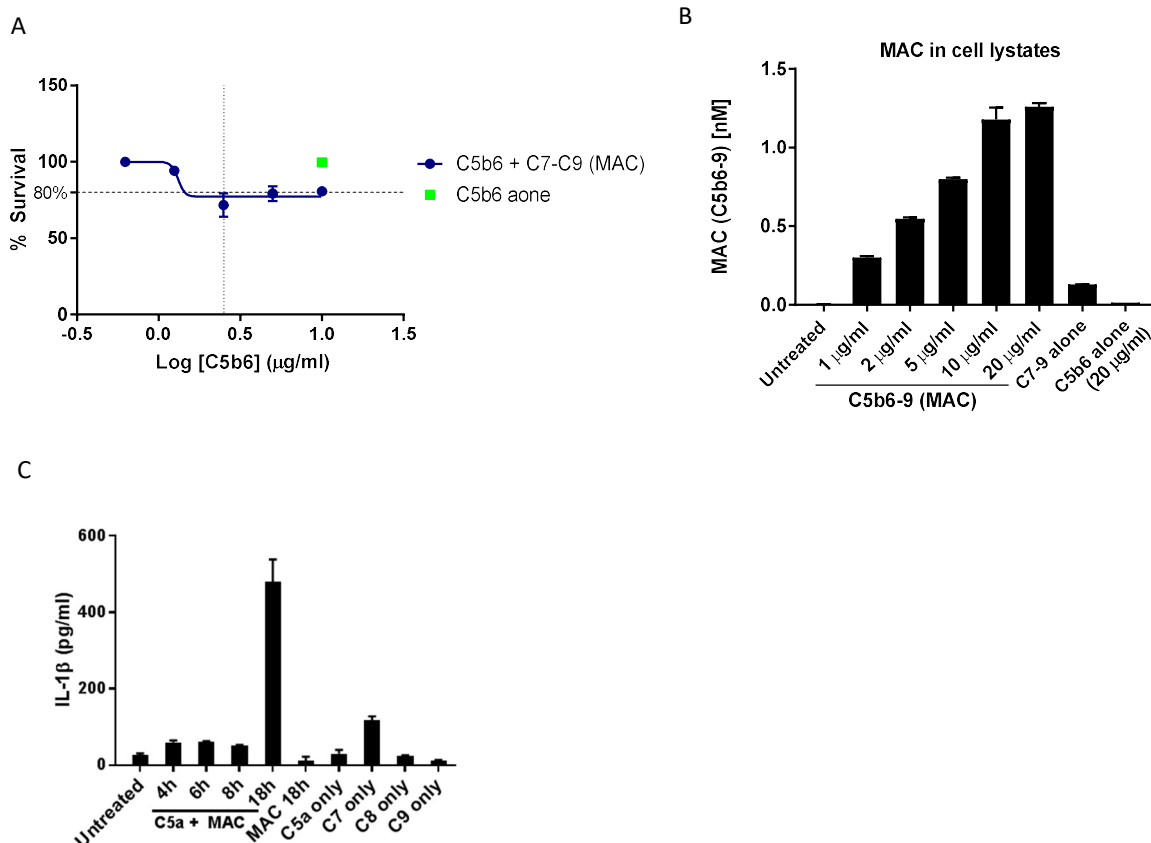
Figure 12. Sublytic concentrations of C5b6-9 complex triggers IL-1β production. (A) Cell Titer-Glo assay of MDMs pre-treated with anti-CD59 and C5a and exposed to titrated dose of C5b6 (1.75 – 10 µg/ml), with C7-C9 in molar excess. Sublytic doses of MAC are 2.5 µg/ml of C5b6 (80% cell survival) (n=3). (B) TCC MSD for MAC deposition from cell lysates, cell treated with increasing concentrations of C5b6-9 complex for 1 h (n=3). (C) IL1β ELISA of cells pre-treated with C5a and anti-CD59, and incubated with sublytic concentration of MAC or controls C7-9 only for 4, 6, 8 or 18 h (n=3).

3.8 Extracellular hydrogen peroxide production and intracellular ROS is triggered by MAC stimulation

In order to address ROS production, MDMs were sensitised and exposed to MAC attack over a period of time, intracellular ROS and released hydrogen peroxide were measured using CellROX or Amplex red kit, respectively.

Measurement of extracellular hydrogen peroxide levels was done by stimulating sensitised cells with the purified components C5b6-9 due to NHS interference with the assay (Figure 11E). Sublytic MAC attack was performed using the C5b6-9 purified components from 30 min to 4 hours (Figure 13A). Results showed an increase in hydrogen peroxide between 30 min and 3 hours, peaking at 3 hours after stimulation. In conclusion, it was shown that sensitised cells stimulated with sublytic doses of NHS or C5b6-9 trigger an acute increase

in intracellular ROS production within 30 min, and release of hydrogen peroxide peaking after 3 hours of stimulation.

ROS production was quantified by mean fluorescence intensity over a time course of 24 hours and using a plate reader instead of the IncuCyte for higher suitability. Sensitised cells stimulated with a sublytic MAC dose of NHS showed an acute increase in intracellular ROS production between 30 min and 3 hours (peaking at 30 min), from 30% to 40%, as normalised to menadione treated cells (Figure 13B). Sensitised cells incubated with anti-C7 mAb plus NHS and untreated cells had baseline levels of ROS production over time up to 24 hours. Viability of cells under sublytic MAC doses of NHS for 24 hours was maintained at 80% survival (Figure 13C).
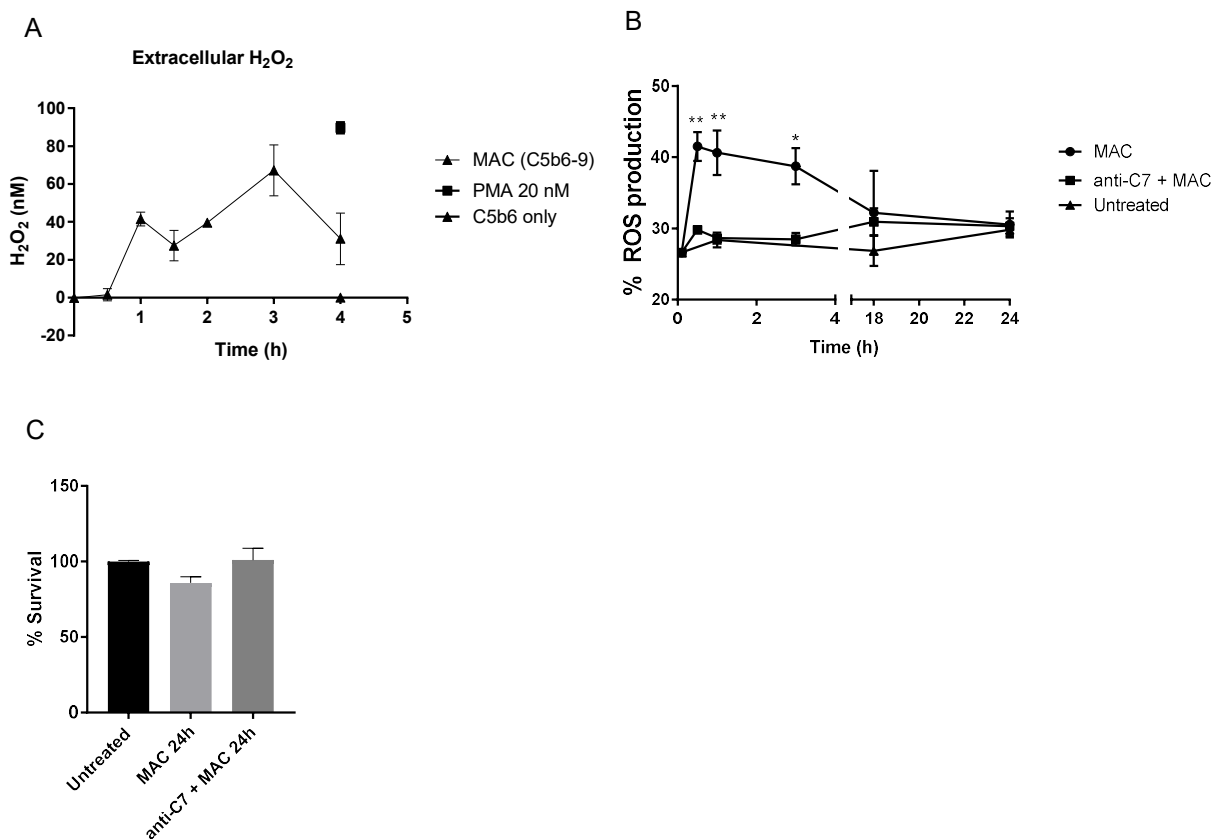
Figure 13. Intracellular ROS and Hydrogen peroxide production triggered by MAC pore formation. (B) Hydrogen peroxide production measured with Amplex red kit over time by MFI. Macrophages stimulated with MAC (C5b6-9 purified components or with controls C5b6 only or PMA at 20 nM (positive control for hydrogen peroxide generation) (n=3). (B) ROS production measured overtime by mean fluorescence intensity (MFI). Primary macrophages stimulated with Abs. and NHS (sublytic MAC concentration), or with controls anti-C7 mAb + MAC (NHS) or Menadione (positive control for ROS production). Raw data is relative to Menadione (n=3). (C) CellTiter-Glo assay. Cells were stimulated with Abs. (anti-CD55, CD59, HLA) and NHS at a sublytic MAC concentration, or with control anti-C7 mAb with MAC (NHS) for 24 hours (n=3).

3.9 Sublytic MAC deposition using 24-well XF Seahorse plates

Seahorse XF assays by Agilent have been established as the gold standard assay to quantify mitochondrial dysfunction and bioenergetics in cells, by measuring glycolytic activity as extracellular acidification rate (ECAR) and mitochondrial respiration as oxygen consumption rate (OCR), with a variety of assays to stress cells and measure certain metabolic parameters that describe their metabolic potential (Meyer, Lamont et al. 2021) (Agilent).

The observations above showing MAC supporting glycolysis and ROS production led to investigate further the metabolic changes of MDMs caused by MAC. Thus, in order to perform Seahorse experiments and determine that glycolysis activation is triggered by sublytic MAC, optimal cell density with or without Cell-Tak was tested using seahorse plates, which have conical bottom wells and therefore have a different surface compared to standard flat bottom plates. Cell-Tak acts as a cell and tissue adhesive, cells without coating appeared to be concentrated at the edge of the wells (leaving the centre of the well with almost no cells) which is sub-optimal for seahorse measurement (Figure 14A). The results showed that optimal macrophage differentiation in seahorse plates need cell-tak coating and optimal cell density was 325,000 cells per well (Figure 14B).

Images of 3 different cell densities were then taken with EVOS microscope and cells at each density were sensitised with anti- CD55, CD59 and HLA antibodies and stimulated with ascending concentrations of NHS. The experiment was run in parallel with standard flat bottom plates (regularly used in previous experiments) and cell viability was assessed with CellTiter-Glo assay in order to compare the assay between plate types (Figure 15). An optimal cell density of 250,000 cells per well was determined by cell imaging and according to cell survival assay results. The sublytic MAC dose giving 80% survival was about 3% NHS with 250,000 cells per well in seahorse plate and 500,000 cells per well in standard plate. The data showed that NHS stimulations showed comparable amounts of sublytic MAC deposition between standard and 24XF seahorse plates and that Seahorse experiments can be performed under these conditions with 250,000-325,000 cells per well.

A   **Cell Tak**   **Without Cell Tak**

Centre of the well – 325,000 cells per well
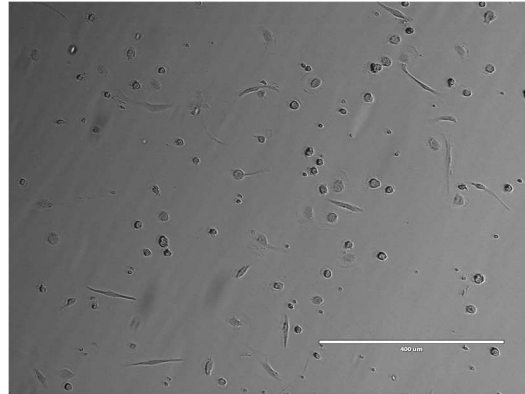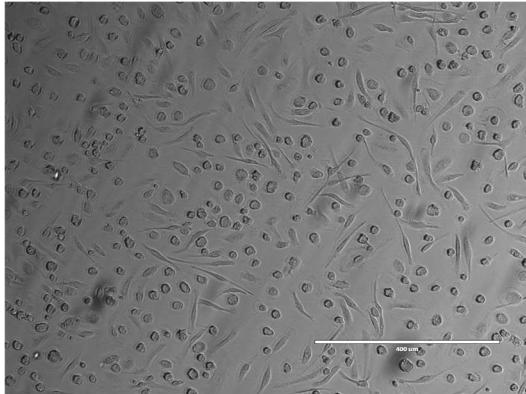
Edge of the well – 325,000 cells per well
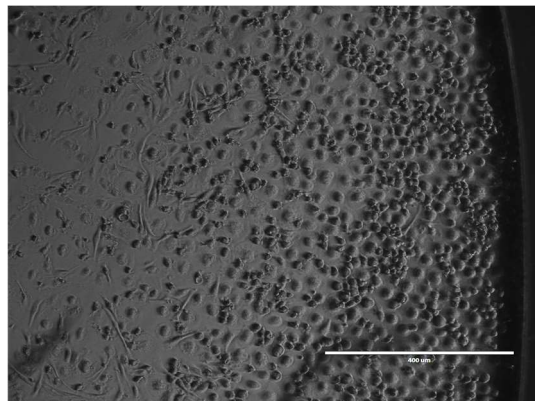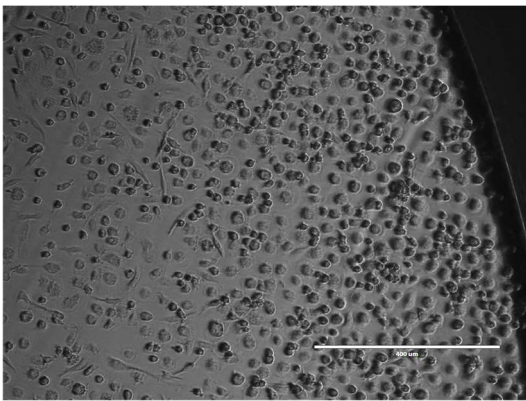
B   Cell Tak   Without Cell Tak
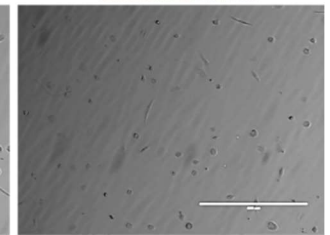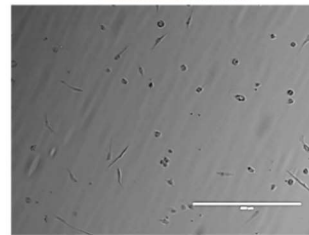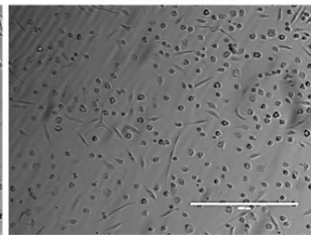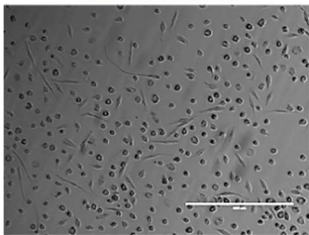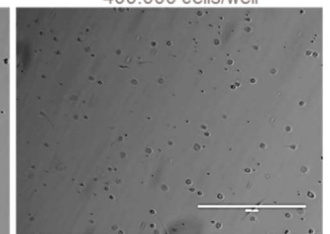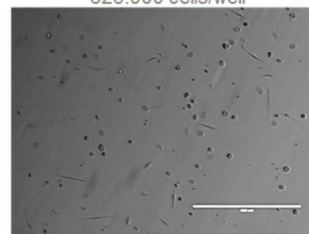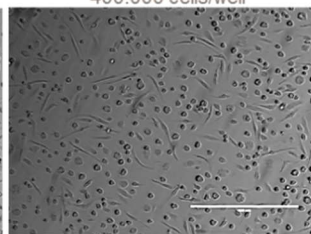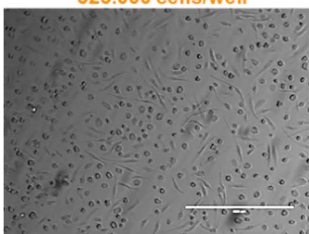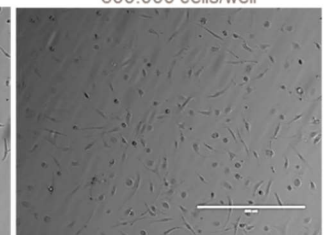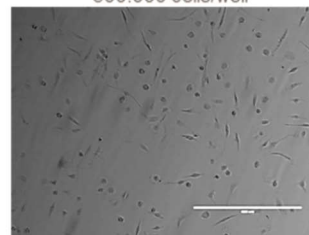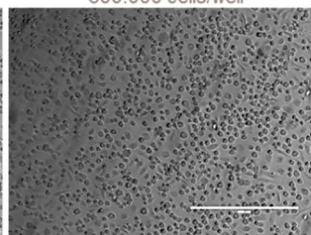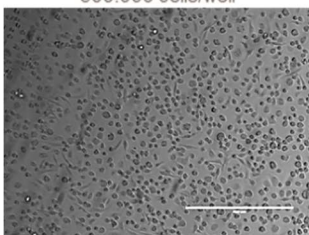
Figure 14. Cell number and coating optimisation for 24XF Seahorse plates. (A, B) Different cell densities in the presence or absence of Cell-Tak were tested in 24XF seahorse plates to determine the optimal conditions of primary macrophages. Optimal cell density set at 325.000 cells per well. Representative images from 1 donor, total n=3. (10X, scale bars 400 μm).
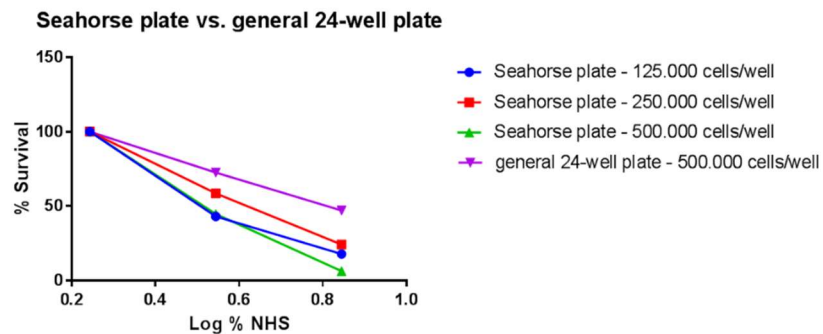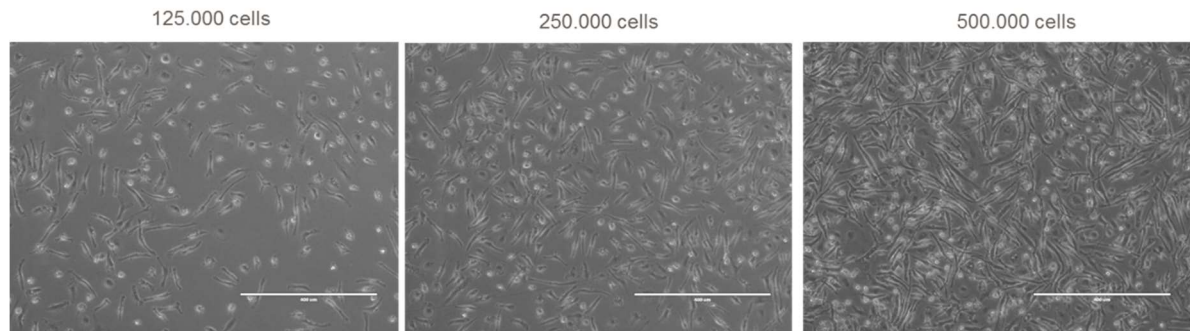
Figure 15. Optimal cell density of 250,000 cells per well for Seahorse plates. MDMs plated at 125,000, 250,000 and 500,000 cells/well and images were taken with EVOS microscope (10X) (representative images from 1 donor, total n=3). Cells in Seahorse plates and standard plate were sensitised with anti-CD55, CD59 and HLA antibodies and stimulated with ascending concentrations of NHS. CellTiter-Glo assay was performed to determine cell viability (n=3). Sublytic doses of MAC were stablished as 80% survival (10X, scale bars 400 μm).

3.10 MAC triggers an acute increase in glycolytic rate and oxygen consumption rate in GM-CSF macrophages by 24XF Seahorse measurement

With the aim to further explore changes in glucose metabolism triggered by sublytic MAC, seahorse assays were performed. Supporting literature indicates that GM-CSF macrophages have higher glycolytic capacity and higher ECAR and OCR baseline levels than M-CSF macrophages (Izquierdo et al., 2015). Therefore, human monocytes were differentiated also differentiated with GM-CSF, as well as M-CSF, as usual. Firstly, with the aim to define the sublytic MAC dose of NHS on GM-CSF macrophages, cells were sensitised (anti-CD55, CD59 and HLA) and stimulated with increasing concentrations of NHS. Cell viability was measured by CellTiter-Glo assay and the sublytic dose of MAC was stablished as 80% survival (corresponding to 9% NHS) (Figure 16A).

Sensitised GM-CSF macrophages were then stimulated with sublytic MAC (9% NHS) for 1 hour. ECAR (Merle, Noe et al.) and OCR were measured by 24XF Seahorse assay, using the standard glycolytic stress test (Figure 16B). Cells treated with MAC showed a 2-fold increase in ECAR levels (measurement of glycolytic rate) before and after addition of glucose, compared to untreated and control samples. Glycolytic capacity, measured by the increase of ECAR after addition of Oligomycin, was also slightly higher in MAC treated cells compared to controls. OCR levels (measurement of mitochondrial respiration) were at least 2-fold increased in MAC treated samples compared to controls, indicating that MAC drives metabolic reprogramming of GM-CSF macrophages by shifting cells into higher glycolytic and mitochondrial function, potentially with the aim to provide more energy to the cell for its pro-inflammatory function. These findings were intriguing and led to the development of a robust and reproducible assay in more donors. M-CSF macrophages were also stimulated with sublytic MAC for 1 hour, ECAR/OCR values were measured in 24XF Seahorse using the standard glycolytic stress test, but no increase in ECAR nor OCR was observed in MAC treated samples or any other controls (Supplementary Figure 1).
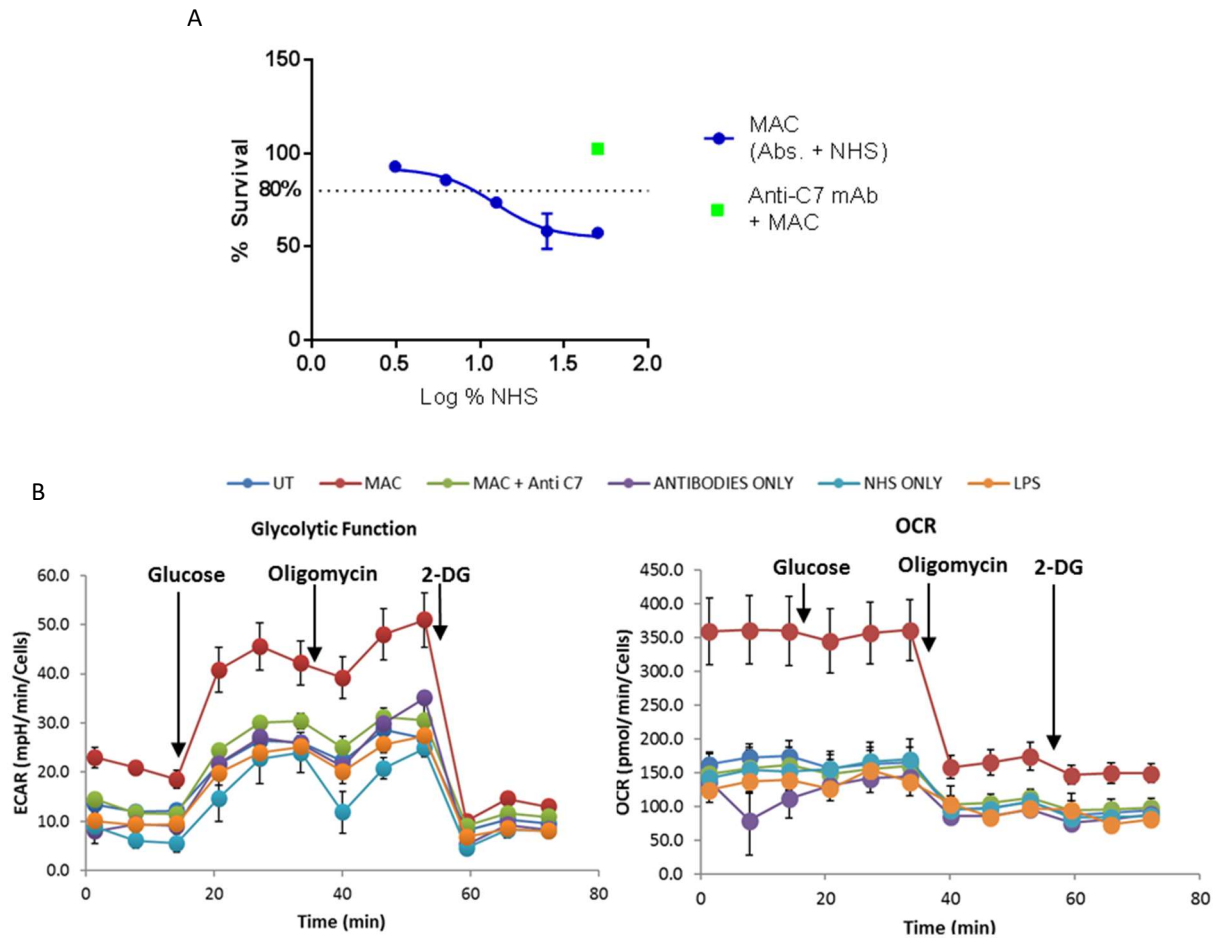
Figure 16. MAC attack, lactate production and Seahorse assays in GM-CSF macrophages.
(A) Cell viability (Cell Titer-Glo) of increasing concentrations of NHS or anti-C7 control with MAC to determine sublytic MAC concentration in GM-CSF macrophages. (n=3) (B) Seahorse experiments: glycolytic rate (ECAR) and oxygen consumption rate (OCR) were measured with standard glycolytic stress test (n=1).

3.11 Optimisation of cell number and assay to measure metabolism of M and GM-CSF differentiated MDMs on a 96-well Seahorse

With the aim to explore changes in metabolism triggered by MAC and have a higher throughput than 24-well plates, cell density and the MAC assay were optimised on the 96XF Seahorse plates (Figures 17, 18). Six different cell densities of M- and GM-CSF MDMs differentiated with (Figure 17C-H) or without (Figure 17A, B) Cell-Tak (Figure 18) were sensitised and stimulated with increasing concentrations of NHS for 1 hour to define the sublytic MAC dose for 96XF plates (Figure 17A-D). Cell viability was measured by CellTiter-Glo assay and the sublytic dose of MAC was stablished as 80% survival, corresponding to 11% and 3.5% NHS for most cell densities of GM- and M-CSF MDMs with Cell-Tak, respectively. OCR was measured on unstimulated GM- and M-CSF macrophages by 96XF Seahorse assay using the standard mitochondrial stress test (Figure 17E, F). Results showed that GM-CSF macrophages were more metabolically active than M-CSFs as they responded much better to FCCP (1.2 uM), as well as higher baseline values. M-CSF macrophages showed no increase between baseline OCR levels and FCCP treatment, and error bars (S.E.M) were much higher than GM-CSFs, suggesting rates were meaured outside of the operating capacity of the machine. The optimal cell density to perform the MAC assay in 96XF Seahorse was 90.000 cells per well, based on MAC assay (cell viability) and Seahorse results (Figure 17A-F)

- Cell-Tak

A

GM-CSF

B

M-CSF

+ Cell-Tak

C

GM-CSF

D

M-CSF

E

GM-CSF

F

M-CSF

G

GM-CSF

H
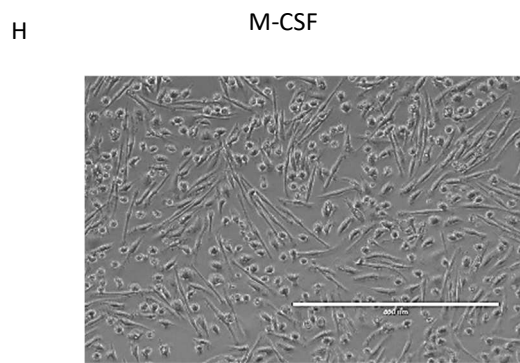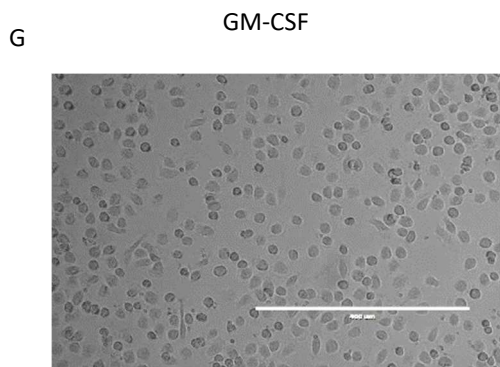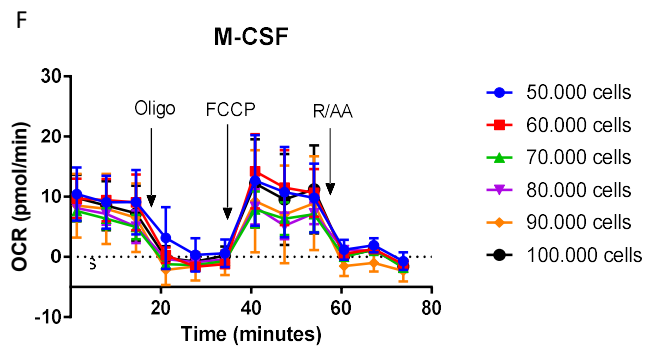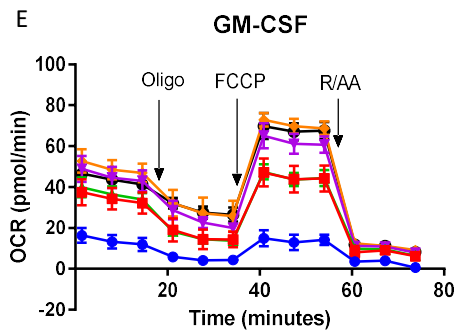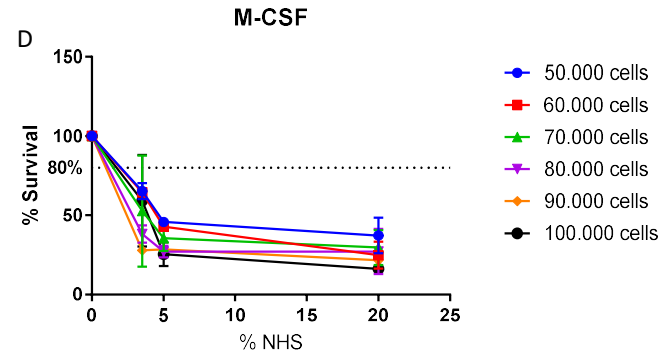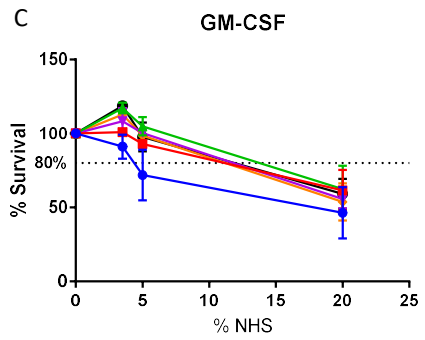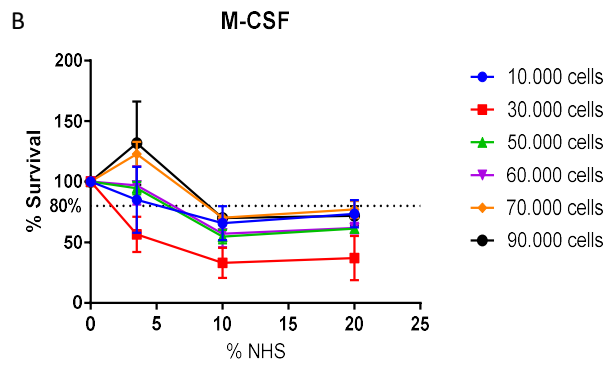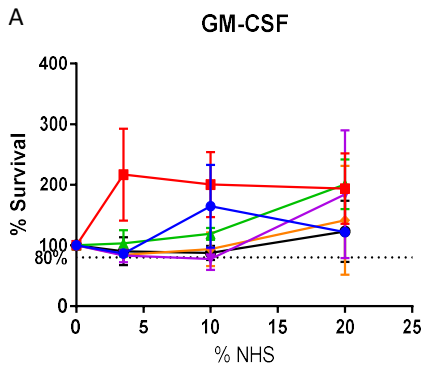
M-CSF

Figure 17. Cell number and MAC assay optimisation on 96 XF Seahorse. GM-CSF (A, C, E) and M-CSF (B, D, F) MDMs were differentiated with (C, D) or without (A, B) Cell-Tak coated 96XF seahorse plates at 6 different cell densities. (A-D) Cells were stimulated with MAC (anti-CD55, CD59 and HLA antibodies sensitisation and NHS at sublytic dose) for 1 hour and cell viability was measured by CellTiter-Glo assay (n=3). (E, F) Oxygen consumption rate (OCR) was measured under the Mitochondrial Stress Test in XF96 Seahorse (n=3). (G, H) Images taken with EVOS microscope at 10X (scale bar 400 μm) of GM-CSF and M-CSF macrophages at an optimal cell density of 90.000 cells per well in a XF96 seahorse plate (n=3) (representative image from 1 donor).

M-CSF MDMs in 96 XF Seahorse plates

Cell-Tak   **No Cell-Tak**

10.000 cells/well	30.000 cells/well	10.000 cells/well	30.000 cells/well
50.000 cells/well	60.000 cells/well	50.000 cells/well	60.000 cells/well
70.000 cells/well	90.000 cells/well	70.000 cells/well	90.000 cells/well

GM-CSF MDMs in 96 XF Seahorse plates

Cell-Tak   **No Cell-Tak**

10.000 cells/well	30.000 cells/well	10.000 cells/well	30.000 cells/well
50.000 cells/well	60.000 cells/well	50.000 cells/well	60.000 cells/well
70.000 cells/well	90.000 cells/well	70.000 cells/well	90.000 cells/well

Figure 18. Coating optimisation for Seahorse plates. Optimised cell density (90,000 cells/well) in the presence or absence of Cell-Tak were tested in seahorse plates to determine the optimal conditions of M- or GM-CSF differentiated MDMs. 10X images taken with EVOS microscope (scale bar 400 μm), representative from 1 donor.

3.12 Expression of complement regulators and HLA does not vary between M- and GM-CSF differentiated MDMs

CD55 complement regulator's decay-accelerating activity mediates inactivation of C3b and C4b to prevent the formation of C3 (C3bBb and C4bC2a) and C5 convertases (C3bBbC3b and C4bC2aC3b) (Noris and Remuzzi 2013). CD59 prevents C9 from binding the partially formed MAC complex C5b6-8 and polymerizing, avoiding the formation of MAC (Davies and Lachmann 1993, Kim and Song 2006, Morgan 2016). HLA antibodies are known to induce complement activation via Fc-dependent functions and binding to C1q, which once fixed cleaves C2 and C4 (Duquesnoy, Marrari et al. 2013, Rijkers, Schmidt et al. 2019). In addition, HLA antibodies are defined as complement-fixing based on clinically relevant tests such as the complement-dependent cytotoxicity test, and are often used in *in vitro* complement stimulation scenarios (Saito, Yamakawa et al. 2014). Given the use of GM-CSF macrophages for seahorse and further metabolic assays, expression of complement regulators CD55, CD59 and HLA-A, B and C, as well as other relevant complement proteins and receptors, was checked using RNA seq data (generated by colleagues at GSK) comparing expression of these proteins between untreated GM-CSF and M-CSF differentiated MDMs. Results showed that there was no significant difference in expression of these complement regulators and HLA between these two cell types (Figure 19A). Only complement receptor C3aR1 and C5aR1 had significantly higher expression in M-CSF MDMs versus GM-CSFs (Figure 19B). The lack of notable differences between the two cell types in expression of the regulators and their linked complement proteins, as well as HLA, indicated that the same concentration of antibodies against CD55, CD59 and HLA used to sensitise cells to MAC attack can be used in future experiments for GM-CSF MDMs as it was in M-CSF MDMs (Figure 6).
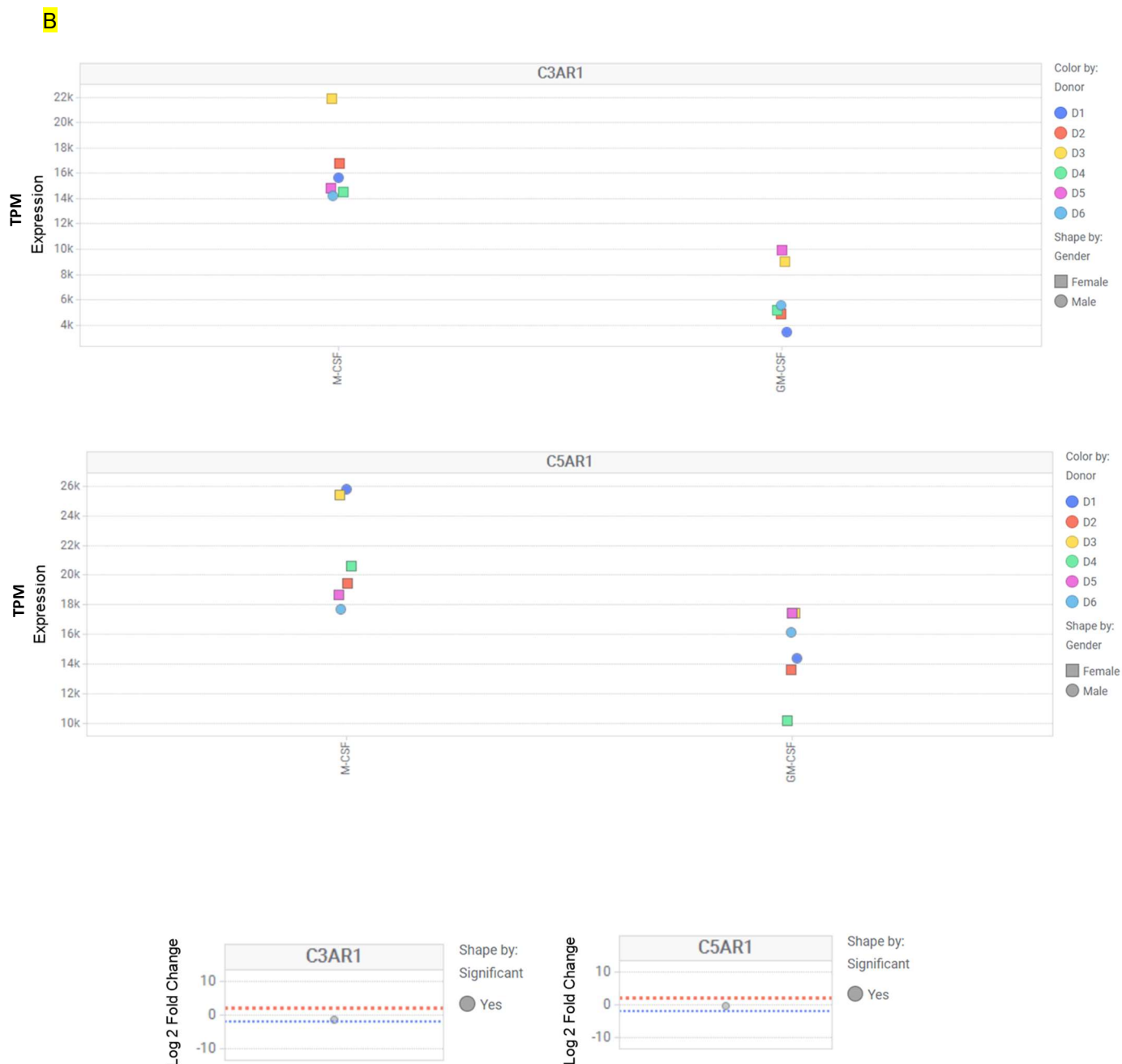
Figure 19. Gene expression from RNA seq analysis of complement proteins between GM- and M-CSF differentiated MDMs shows no clear differences. TPM (Transcripts per million) expression data of a variety of complement regulators, complement proteins and complement receptors from RNA seq data comparing expression between untreated GM-CSF and M-CSF differentiated MDMs for 5 days (n=6). Gene expression is represented in axis of the graphs either as Log 2-fold change or as TPM (transcripts per million) normalised expression. Data analysis generated and exported using Spotfire. RNA seq experiments were performed by colleagues in GSK UK, data was exported and interpreted by this author using Spotfire.

3.13 Discussion

Deposition of MAC pores at sublytic levels in nucleated cells has been shown to induce a wide range of effects in several cell types, such as apoptosis, protein synthesis, proliferation, granule release, proinflammatory effects, etc. (Morgan 1992, MORGAN 2003, Elimam, Papillon et al. 2013, Takano, Elimam et al. 2013). Inflammatory effects due to sublytic MAC deposition have been reported in mesangial cells and microglia (Yang, Yang et al. 2014, Zhang, Li et al. 2014), retinal epithelial cells, which showed release of IL-6 and IL8 inflammatory cytokines (Lueck, Wasmuth et al. 2011), and in neutrophils and rat macrophages, which induced release of inflammatory mediators such as Prostaglandin E2 (Hänsch, Seitz et al. 1984, Morgan 1992). Sublytic MAC was also shown to induce inflammatory effects by triggering the NLRP3 inflammasome in murine dendritic cells (Laudisi, Spreafico et al. 2013) and in lung epithelial cells through increased intracellular Ca2+ and mitochondrial damage (Triantafilou, Hughes et al. 2013). Activation of the NLRP3 inflammasome has been shown to be modulated by the metabolic state of a cell. Metabolic products can either induce or inhibit the inflammasome, such as increased AMP, which leads to inhibition of inflammasome activation by activating the nutrient sensor AMP-dependent protein kinase (AMPK), since AMPK causes a switch from glycolysis (and energy-consuming pathways linked to a high cellular activity) to OXPHOS, which is linked to anti-inflammatory, quiescent or contracting cell responses (De Nardo and Latz 2011). Moreover, the complement system has been shown to induce metabolic reprogramming in Th1 cells through co-stimulation of CD46, leading to an increase in nutrient influx and glycolysis activation, and subsequent induction of NLRP3 (Kolev, Dimeloe et al. 2015). Therefore, inflammasomes are major sensors for cell metabolic activity, and dysregulation of the NLRP3 inflammasome and complement system contributes to a variety of metabolic pathologies and diseases, including cancer and type 2 diabetes, among others (Arbore and Kemper 2016).

Considering this, the main hypothesis of the study is that sublytic levels of MAC deposited in primary macrophages induce changes in metabolic activity to support the pro-inflammatory events that have been reported. To date, this study shows for the first time that there are interactions between the MAC- inflammasome axis with intracellular metabolic pathways, focussed here on glycolysis, leading to NLRP3 inflammasome activation with release of IL-1β and IL-18. The data demonstrates that inflammasome activation triggered by sublytic MAC relies on glycolysis, and shows sublytic MAC as a trigger of glycolysis and ROS production.

In order to address the effects caused by sublytic MAC deposition in primary macrophages, a sublytic MAC concentration was established. Two different viability assays (metabolic and non-metabolic) were assessed to determine the validity of the results, which showed comparable viability values at the same NHS concentrations, confirming a robust sublytic MAC dose of NHS. A sublytic MAC dose of 3.5 % NHS determined in this study is broadly in agreement with a previous study in which lung epithelial cells were stimulated with ascending concentrations of NHS and a sublytic MAC concentration of 5 %NHS was determined (Triantafilou, Hughes et al. 2013). Alternatively, when MAC attack was applied using purified components, a sublytic MAC dose of 2.5 ug/ml of C5b6 and 5 ug/ml of C7, C8 and C9 was defined. These concentrations were in a similar range to studies performed in monocyte derived DC or human primary microglia, where C5b6 was also added first, followed by C7-9 proteins at a higher concentration (Chen, Yang et al. 2007) (Yang, Yang et al. 2014). Moreover, MAC deposition in macrophages stimulated with either NHS or purified components C5b6-9 was confirmed by MSD and concentration of MAC was quantified. One published study confirmed by ELISA MAC deposition in a human bone osteosarcoma cell line, but concentration of MAC was not quantified (Jeon, Han et al. 2018). At the time of writing, this thesis shows the first evidence of the concentration of MAC present in macrophages as a result of C5b6-9 or NHS stimulation.

In order to demonstrate that primary macrophages can induce the NLRP3 inflammasome as a result of sublytic MAC deposition, sensitised cells were stimulated with 3.5% NHS over a time course. The M-CSF-differentiated primary macrophages elongated morphology was confirmed by cell imaging and was in agreement with several studies (Akagawa 2002, Karlsson, Cowley et al. 2008). Gene expression of NLRP3 and Caspase 1, protein expression of pro-IL-1β and secretion of IL-1β and IL-18 were increased at 2 hours post-NHS stimulation, indicating a rapid assembly and activation of NLRP3 inflammasome. Upregulation of NLRP3 and protein expression of pro- IL-1β are priming signals of the inflammasome (signal 1), and secretion of mature IL-1β and IL-18 indicate inflammasome activation (signal 2).

Interestingly, maximal increase of pro-IL-1β protein expression occurred 4 hours post-stimulation. However, the lower intensity of the pro-IL-1β band and the absence of a mature IL-1β band at 2 hours, might suggest that inflammasome priming and activation has already occurred, with pro-IL-1β being cleaved and mature IL-1β secreted into the extracellular medium.

Furthermore, cells incubated with the controls: anti-complement regulators and HLA antibodies only (Abs. only), NHS only, the 'Abs.' in combination with HI-NHS and with C7 depleted NHS, indicated that inflammasome activation can be triggered only by sublytic MAC formation in primary macrophages. This result is in agreement with a previous study (Triantafilou, Hughes et al. 2013), which showed that sublytic MAC triggers NLRP3 activation in lung epithelial cells. However, the C7-depleted NHS control showed pro-IL-1β protein expression suggesting that other complement components than MAC might induce signal 1, which is in agreement with evidence demonstrating that C5a binding to C5aR1 acts as a priming signal 1 during the uptake of DAMPs, and sustains inflammasome activation via cathepsin B release and increased lysosomal damage in monocytes (An, Mehta et al. 2014).

Once a sublytic MAC dose and its capacity to induce the NLRP3 inflammasome in primary macrophages was established, modulation of glycolysis pathway was performed (using 2DG and HA inhibitors) in order to elucidate the MAC-inflammasome interactions in relation to intracellular metabolic changes (specifically glycolysis). It has been reported that inflammatory macrophages use glycolysis, among other metabolic pathways i.e. fatty acid synthesis and amino acid metabolism, to proliferate and support the production of inflammatory cytokines, such as IL-1β and IL-18 resulting from NLRP3 inflammasome activation (O'Neill, Kishton et al. 2016). For instance, it has been shown that increased AMP leads to inhibition of inflammasome activation by causing a switch from glycolysis to OXPHOS metabolism in the cell (De Nardo and Latz 2011). Most of these studies have been performed in cells stimulated with LPS but the metabolic changes that might be triggered in response to complement and in particular to MAC pore formation remain unknown.

Results shown in Figure 7 are in agreement with (O'Neill, Kishton et al. 2016) and (De Nardo and Latz 2011), and demonstrated that inhibition of glycolysis by 2DG and HA resulted in inhibition of MAC-mediated inflammasome priming and activation. These data showed that downstream of MAC, glycolysis is required to support the production of inflammatory cytokines IL-1β and IL18 by the inflammasome.

In Figure 7B, incubation of 2-DG and HA at 6 hours shows a partial inhibition of the inflammasome priming and activation compared to 4 hours, where a complete inhibition is observed. This could be explained by compensatory metabolic pathways being increased in order to allow inflammasome activation and release of inflammatory cytokines, such as fatty acid synthesis and amino acid metabolism, according to (O'Neill, Kishton et al. 2016).

In order to determine whether sublytic MAC triggers macrophage metabolic reprogramming to a glycolytic state which supports inflammasome activation, lactate production (a proxy for lactate dehydrogenase activity, a key enzyme in glycolysis) was assessed. An increase of lactate production over time up to 24 hours was observed in response to sublytic MAC. Overall, the data shown in Figure 8 demonstrated that an increase in glycolysis occurs as a result of sublytic MAC deposition in primary macrophages, which is necessary for inflammasome activation leading to secretion of inflammatory cytokines IL-1β and IL-18 (Figure 7).

With the aim of further exploring changes in metabolic pathways triggered by sublytic MAC at a gene expression level, qPCR was performed. Upregulation of genes for glucose and amino acid channels GLUT1 and LAT1, and LAMTOR5 (drives mTROC1 activation causing increased glycolysis) was observed in response to sublytic MAC deposition. Interestingly, genes for these 3 proteins have been reported to be upregulated in response to CD46 co-stimulation with C3b in Th1 cells, leading to an increase in nutrient influx and glycolysis activation, and subsequent induction of NLRP3 inflammasome (Kolev, Dimeloe et al. 2015). This suggests a role for the complement system in cellular metabolic reprogramming linked to inflammasome activation, indicating the existence of a complement-inflammasome-metabolism axis where, according to our data, MAC seems to be involved. Interestingly, 2-DG and HA blocked the upregulation of the glycolysis related genes as expected, but HA also blocked the upregulation of SLC7A5, suggesting that GAPDH might be involved in the regulation of LAT1, as glycolysis is a central metabolic pathway that generates precursors for the synthesis of amino acids and fatty acids (Kalhan and Hanson 2012).

Taken into consideration the involvement of sublytic MAC in glycolysis activation observed in this study, it was proposed to investigate whether these observations were relevant in the following functional assays: measurement of ROS production and Seahorse experiments to further investigate glycolysis activation by measurement of extracellular acidification rate (Merle, Noe et al.) and determination of mitochondrial respiration (oxygen consumption rate (OCR).

Evidence has been presented showing that sublytic MAC triggers an increase in intracellular calcium ([Ca2+]i) and subsequent mitochondrial Ca2+ uptake, causing alteration of mitochondrial membrane potential and cytochrome C efflux to the cytosol, leading to apoptosis (Triantafilou, Hughes et al. 2013). Interestingly, it has also been reported that mitochondrial Ca2+ uptake results in ROS production (Feissner, Skalska et al. 2009). Furthermore, it has recently been reported that LPS-activated macrophages

showed a switch to glycolysis and subsequent alteration of the mitochondrial membrane potential, triggering an increase of Reverse Electron Transport-ROS (RET-ROS), and that those changes were required to induce an inflammatory response (Mills, Kelly et al. 2016). Taken into consideration these findings and our results showing sublytic MAC as a trigger of glycolysis to support inflammasome activation, it was hypothesised that sublytic MAC results in ROS bursts, which might be linked to the activation of inflammasomes, as C5aR1 has already been shown to activate NLRP3 via increase in ROS production (Arbore and Kemper 2016). Fluorescence readings showed that sublytic MAC concentrations of NHS caused an acute increase in intracellular ROS production peaking at 30 min after MAC stimulation, and extracellular hydrogen peroxide from 1 hour up to 3 hours after C5b6-9 stimulation. ROS production has been shown to be increased by C5b6-9 stimulation in leukocytes, mesangial cells, GECs, and proximal tubular epithelial cells (Takano, Elimam et al. 2013). In glomeruli from rats with anti-Thy1 nephritis, it was shown enhanced production of hydrogen peroxide, superoxide, and hydroxyl radicals downstream of MAC (Takano, Elimam et al. 2013), and in rat mesangial cells sublytic MAC stimulation triggered superoxide production within 30 min stimulation and extracellular hydrogen peroxide within an hour (Adler, Baker et al. 1986), which is in agreement with the hydrogen peroxide production data shown in this study.

It has been shown that human macrophage metabolism assessed in MDMs can differ from mouse bone marrow-derived macrophages (BMMs) metabolism. Pro-inflammatory mouse macrophages have been reported to undergo a metabolic shift from OXPHOS to glycolysis, showing higher ECAR and lower OCR values than naïve M-CSF differentiated BMMs by Seahorse assay (Mills, Kelly et al. 2016) (Van den Bossche, Baardman et al. 2016). However, pro-inflammatory human MDMs differentiated with GM-CSF have been shown to have both higher ECAR and OCR values than M-CSF macrophages (Izquierdo, Cuevas et al. 2015), indicating that these cells rely on glycolysis and also mitochondrial respiration to carry their pro-inflammatory effector functions. In addition, human M-CSF macrophages had minimal glycolytic capacity after addition of oligomycin as measured by Seahorse (glycolytic stress test) (Izquierdo, Cuevas et al. 2015).

Considering the above findings, primary macrophages differentiated with GM-CSF as well as with M-CSF and stimulated with a sublytic dose of NHS were analysed by 24XF seahorse after optimising plate coating conditions and cell density. Increased levels of ECAR and OCR triggered by MAC stimulation were observed being 2-fold higher than all controls, indicating that the increase was caused only by MAC signalling. LPS was added as a control to see whether it had an effect in ECAR or OCR, as it has been shown that

LPS increases ECAR levels in BMMs (Mills, Kelly et al. 2016), but no effects were observed. Possibly due to differences in mouse and human macrophages metabolism or due to the time of LPS stimulation (1 hour). To date, this piece of data has been demonstrated for the first time in this study, it hasn't been published in any other cell type and proposes a novel role of MAC as a potential regulator of immunometabolism.

In order to define the sublytic MAC dose of NHS for GM-CSF macrophages, a lysis curve stimulating cells with a titration of NHS had been previously tested. Sublytic dose of MAC was defined as 9% NHS. Interestingly, this concentration was 3-fold higher compared to M-CSF macrophages (3.5% NHS). It was argued that this was possibly due to the presence of higher concentrations of the complement regulators CD59 and/or CD55 in GM-CSF pro-inflammatory macrophages, however, Figure 19 showed this was not the case and therefore the reason for this difference remains unknown. The amount of lactate production was assessed over-time in GM-CSF macrophages as well, which peaked at 24 hours post-stimulation coinciding with the M-CSFs, but the concentration of lactate was 3-fold higher than the M-CSFs. This result was in line with the observed increase in ECAR downstream of MAC in GM-CSF macrophages, whereas no ECAR increase was observed in M-CSF macrophages downstream of MAC stimulation (Supplementary Figure 1).

96XF seahorse results in this study are in line with a published study showing GM-CSF macrophages being more metabolically active than M-CSFs, with higher mitochondrial respiration (OCR) values (Izquierdo, Cuevas et al. 2015). In this study, M-CSF macrophages had minimal OCR basal rate values. M-CSF MDMs were well below the standard operating parameters for the Seahorse and so are not ideal models for understanding MAC-mediated metabolic changes. Also, GM-CSF macrophages responded much better to FCCP than M-CSFs, which was also in line with the publication (Izquierdo, Cuevas et al. 2015), although the OCR values were significantly lower in the results shown here. Possibly due to a difference in cell density and XF24 Seahorse in the paper versus XF96 here. Figure 17 showed compatibility to establish sublytic densities of MAC when using the 96 XF Seahorse plates, a sublytic MAC dose was defined in all the cell densities tested.

Overall, this study demonstrates that sublytic MAC concentrations in naïve MDMs are able to trigger NLRP3 inflammasome activation, an activation that relies on glycolysis, and presents sublytic MAC as a trigger of glycolysis and ROS production, suggesting potential metabolic reprogramming that mediates proinflammatory effects. However, real-time glycolysis measurement post MAC stimulation didn't show changes in glycolysis, but findings in GM-CSF MDMs showing to be more metabolically active than M-CSFs and a

glycolytic increase post MAC stimulation suggest further seahorse experiments in GM-CSF MDMs are needed chapter to confirm and further explore the glycolytic and mitochondrial changes observed in this chapter.

4. Chapter 4: Complement MAC is an immunometabolic regulator of NLRP3 activation and IL-18 secretion in GM-CSF human macrophages

GM-CSF is a growth factor widely known to prime macrophages for proinflammatory responses after stimulation, without directly tiggering polarization, and has been found to dominate over homeostatic M-CSF levels in pathogenic inflammatory conditions, such as rheumatoid arthritis and multiple sclerosis (Wicks and Roberts 2016). GM-CSF MDMs have been found to have higher oxygen consumption rate and aerobic glycolysis, as well as higher gene expression of glycolytic enzymes compared to M-CSF MDMs (izquierdo et al 2015). In addition, increased glycolysis is known to be part of the bioenergetic profile of pro-inflammatory macrophages and the link between metabolism and inflammatory phenotypes of macrophages is well characterised (Michl, Ohlbaum et al. 1976, Newsholme, Curi et al. 1986, O'Neill and Hardie 2013, Mills, Kelly et al. 2016).

Experimental observations in M-CSF MDMs as covered in the previous chapter (3) pointed towards MAC being a trigger of glycolysis via lactate increase and gene expression, as well as ROS production and glycolysis-dependant NLRP3 inflammasome activation, suggesting potential metabolic reprogramming that mediates proinflammatory effects downstream of MAC. However, real-time glycolysis measurement post MAC stimulation didn't show any increase, possibly due to lower than optimal detection in Seahorse. GM-CSF MDMs were shown to be more metabolically active than M-CSFs at a basal level and, an early observation that needed further probing, showed increased levels of glycolysis and mitochondrial respiration post MAC stimulation. Thus, a high-throughput and more sensitive Seahorse technology was employed in this chapter to confirm and assess the effect of sublytic MAC in immunometabolic response of disease-relevant *in vitro* macrophages.

In addition, recent studies connecting complement to mitochondria and energy metabolism, in the regulation of early psychosis, diabetes or age-related macular degeneration (Armento, Honisch et al. 2020, Goetzl, Srihari et al. 2020, Kopylov, Papysheva et al. 2020) suggest the relevance of a complement-mitochondrial axis with new potential therapeutic targets. The mechanisms by which MAC has been described to activate NLRP3 inflammasome in lung epithelial cells implicate release of Ca2+ from the endoplasmic reticulum stores, subsequent increase in intracellular Ca2+ and transport of Ca2+ to the inner mitochondrial membrane via the MCU, causing overload and

depolarization of the mitochondrial membrane (Triantafilou, Hughes et al. 2013), which can be a sign of bioenergetic stress. Furthermore, LPS-activated BMDMs have been reported to switch to glycolysis with subsequent alteration of the mitochondrial membrane potential, triggering an increase in mitochondrial ROS, which is required to induce an inflammatory response (Mills, Kelly et al. 2016). Chapter 3 results in M-CSF macrophages showed MAC as a driver of ROS production, but whether this is also the case for GM-CSF MDMs and whether it is of mitochondrial origin, or if there are further mitochondrial dysfunction implications such as mitochondrial Ca2+ overload, depolarisation of the membrane or even altered mitochondrial networks it is still unknown. Thus, experiments were performed in GM-CSF MDMs to evaluate mitochondrial dysfunction by looking at mitochondrial Ca2+ and dynamics, as well as mitochondrial ROS and subsequent NLRP3 inflammasome activation as a result of sublytic MAC stimulation.

4.1 GM-CSF MDMs are susceptible to sublytic-MAC deposition

As model of assessing complement-based MAC-driven attack, induction of sublytic MAC on cells is well documented (Morgan and Campbell 1985, Laudisi, Spreafico et al. 2013, Triantafilou, Hughes et al. 2013, Lusthaus, Mazkereth et al. 2018). Here, the methods highlighted in Figure 20A were used to induce sublytic MAC in GM-CSF differentiated MDMs using NHS. CellTiter-Glo (luciferase-based, metabolic assay) and Calcein AM (fluorescence-based, non-metabolic assay) viability assays were run in parallel to assess the validity and robustness of the assays (Figure 20B). The resultant concentration-dependant lysis curves were comparable between assays. CellTiter-Glo assay was then selected for an NHS titration experiment. Addition of NHS (Figure 20C) to MDMs resulted in a partial loss in viability as concentration of NHS increased, which was blocked by addition of C7-blocking antibody (Figure 20C). To assess the effect of sublytic MAC, concentrations of NHS (Figure 20C) that resulted in 80 % viability were used (Campbell, Daw et al. 1979, Reid, Cooke et al. 2012). In addition to measuring viability, terminal complement components and C9 were quantitatively measured (Figure 20D) and visually observed (Fiure 20E) on MDMs after sublytic MAC deposition, both methods highlighting the suitability of the anti-C7 control. In addition, sublytic levels of MAC were maintained over both 4 and 24 hours with maintenance of viability between 70% and 80% (Figure 20F, G). Together these results indicated a suitable model to methodically assess metabolic regulation of inflammatory phenotypes of MDMs by sublytic MAC.

A

Human Monocytes isolation → Monocyte derived macrophages

6 days differentiation (GM-CSF)

Sensitising cells to complement

Anti-CD55, CD59 and HLA antibodies ('Abs.')

Complement attack

Normal Human Serum (NHS)

MAC - C5b6-9
Ca²⁺ influx
K+ efflux
[Ca²⁺]i

B

Calcein AM vs. CTG viability assays

- MAC Calcein AM
- MAC CTG
- aC7 mAb+ MAC Calcein AM
- aC7 mAb+ MAC CTG
- Abs only Calcein AM
- Abs only CTG

x-axis: Log [% NHS]
y-axis: % Survival

C

x-axis: Log [% NHS]
y-axis: % Survival

- MAC (Abs. + NHS)
- aC7 mAb + MAC

***

D

y-axis: MAC (C5b6-9) [nM]
x-axis: Untreated, 1.56 % NHS, 3.12 % NHS, 6.25 % NHS, 12.5 % NHS, 25 % NHS, aC7 mAb + 25 % NHS, 25 % NHS + EDTA

** **

E

anti-C9 | TOPRO
Untreated

anti-C9 | TOPRO
MAC

anti-C9 | TOPRO
aC7 + MAC

F

x-axis: Log [% NHS]
y-axis: % Survival

- NHS titration 1h
- NHS titration 4h
- NHS titration 24h
- aC7 + MAC 4h
- aC7 + MAC 24h

G

y-axis: % Survival
x-axis: Untreated, MAC 1h, MAC 4h, MAC 24h

Figure 20. MAC deposition and lytic effect on GM-CSF MDMs. (A) Schematic of sublytic MAC stimulation of MDMs using NHS. (B,C,D) MDMs treated with antibodies (anti-CD55, CD59, HLA) and increasing concentrations of NHS for 1 hour before viability measurement by CellTitreGlo (B, C) and Calcein AM assay (B) terminal complement component MSD (cell lysates) (D) or immunocytochemistry (63X, scale bars 10 µm) (E) against C9 protein (green) and TOPRO for nuclear stain (blue). Sublytic doses of MAC were defined as 80% cell survival. Sublytic dose of NHS was used to stimulate cells in (E). Negative controls were performed by addition of anti-C7 antibody (B-E) and EDTA (D). (F) CellTiter-Glo assay in MDMs upon antibodies (anti-CD55, CD59, HLA) sensitisation and stimulation with increasing concentrations of NHS for 1, 4 and 24 hours. (G) Sublytic levels of NHS at 1 hour (corresponding to 80% survival), 4 and 24 hours (corresponding to 70-80% survival). B; n=3, C; n=6, D; n=3, F, G; n=3 +/-S.E.M, E; n=3 and representative image shown. (C, D) Unpaired t-test was used for statistical analysis.

4.2 Sublytic MAC stimulation drives glycolysis and mitochondrial dysfunction in human MDMs

The link between metabolism and inflammatory phenotypes of macrophages is well characterised (Michl, Ohlbaum et al. 1976, Newsholme, Curi et al. 1986, O'Neill and Hardie 2013, Mills, Kelly et al. 2016). We hypothesised that sublytic MAC stimulation of MDMs would drive metabolic changes that may impact on downstream inflammatory processes. Early observations of MDMs stimulated with sublytic MAC indicated a clear colorimetric alteration of the cell culture media, indicative of pH change (data not shown). We therefore tested and confirmed the increasing presence of extracellular lactate over time in sensitised MDMs stimulated with sublytic MAC, peaking at 24 hours (Figure 21A). Sensitised cells incubated with anti-C7 mAb plus NHS had baseline levels of lactate production after 24 hours of stimulation, indicating that the increase in lactate was caused by MAC.

To gain further insight into the metabolic alterations and source and kinetics of this glycolytic accumulation in response to sublytic MAC in MDMs, Seahorse XF Extracellular Flux Analysis was utilised (Figure 21). Optimised cell densities of MDMs at 100.000 cells/well (Figure 17) were stimulated with sublytic MAC and were metabolically explored using the Glycolytic Rate Test (Figure 21B, D) or the Mitochondrial Stress Test (Figure 21C, E). MDMs treated with sublytic MAC exhibited immediate increases in Glycolytic Proton Efflux Rate, a proxy for glycolytic metabolism (GlycoPER; Figure 21B) as observed in the increased basal and compensatory glycolysis (Figure 21D), but no change in basal oxygen consumption rate (OCR) and a complete collapse of spare respiratory capacity and mitochondrial maximum respiration, contributing to a shift in glycolysis as measured by the MitoOCR/GlycoPER ratio (Figure 21D), as well as other altered metabolic parameters (Figure 21D, E). These alterations in metabolic phenotype were MAC-

dependent, as well as anti-C7 sensitive, and did not happen in the negative control NHS only (human serum added to cells that have not been sensitised to MAC with the regulatory antibodies).
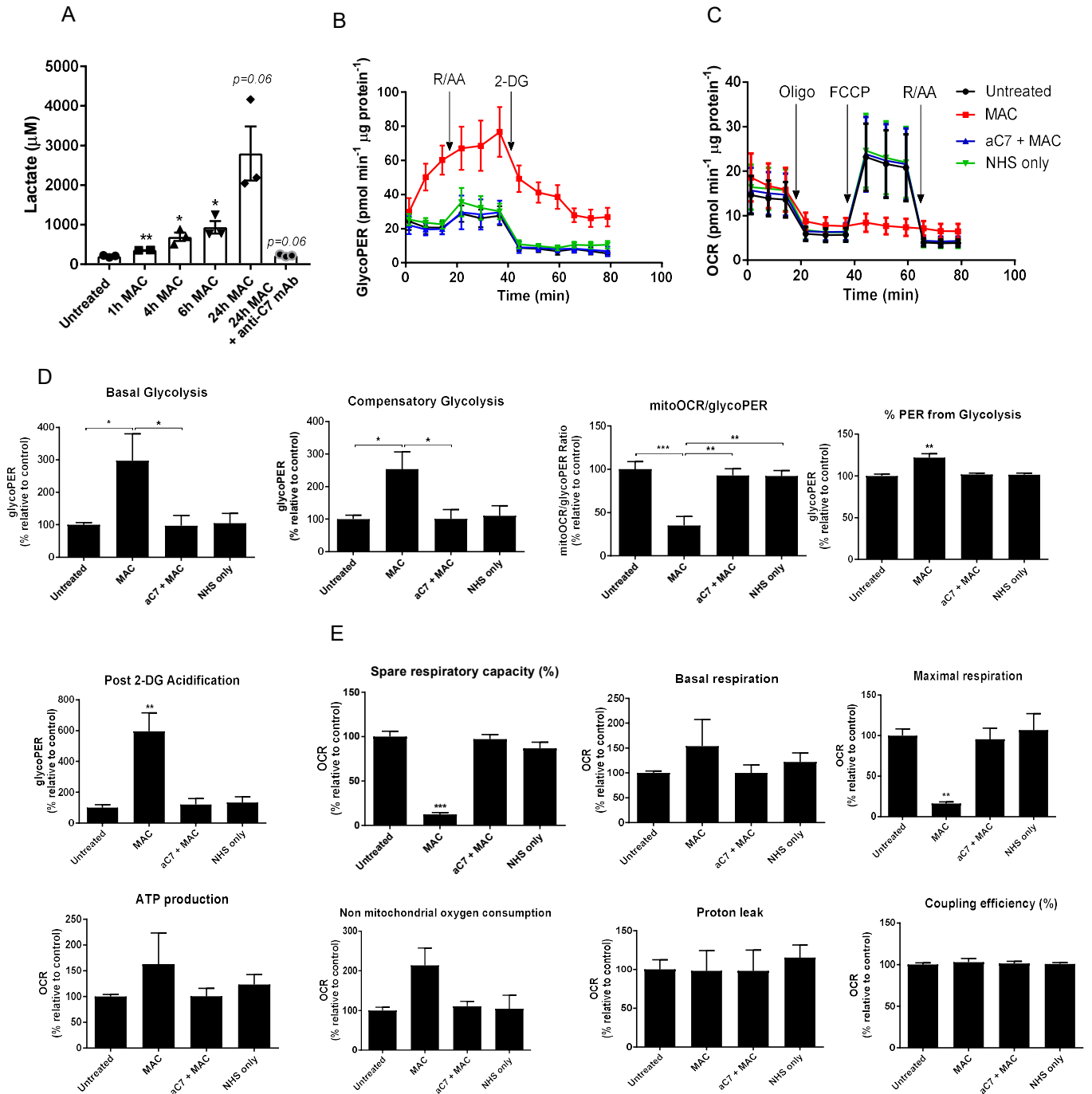
Figure 21. lactate production and Seahorse assays in GM-CSF macrophages. (A) Lactate production overtime with MAC (Abs. + sublytic NHS) or anti-C7 control (n=3). (B-H) MDMs stimulated for 1 hour with sublytic MAC, anti-C7 control or NHS only. before Glycolytic rate test (B, D) and Mitochondrial stress test (C, E). Kinetic data and calculated parameters in bar graphs are presented (n=5). Statistically significant data was assessed by (A) Unpaired t test or (B-H) a 1-way ANOVA with post-hoc Tukeys test. Error bars represent +/- S.E.M

Furthermore, glycine, which protects against cell lysis caused by MAC-deposition (Figure 22A), was pre-incubated with MAC and showed no changes to the MAC-induced phenotype (Figure 22B-E), demonstrating that these events were not mediated by the small percentage of cell death caused by sublytic MAC. In addition, the MAC-driven changes in phenotype also happened at 4 and 24 hours post- sublytic MAC stimulation (Figure 23 and 24). Interestingly, MAC-treated cells across all time points showed maintained basal rate and response to oligomycin, indicating that MAC wasn't driving complete respiratory inhibition or mitochondrial collapse, which would behave as the cells pre-incubated with rotenone/antimycin A (Figure 23 and 24). However, after 24 hours of MAC stimulation, some observations of metabolic failure occurred by decreased proton leak values, suggesting that after a longer time with MAC treatment, irreversible changes in metabolic function could occur in cells, potentially leading to cellular dysfunction (Figure 24).
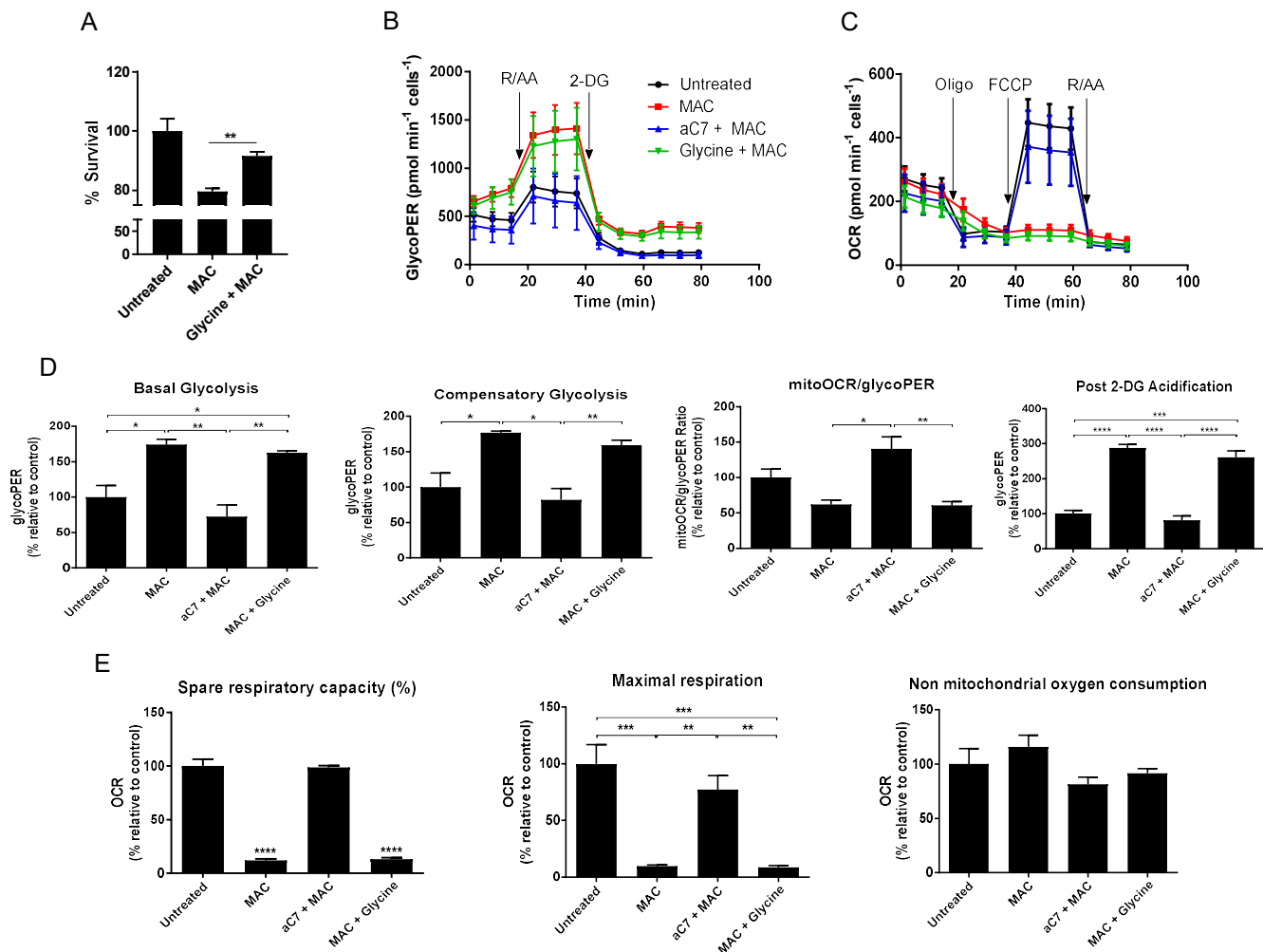
Figure 22. Seahorse assays with Glycine in GM-CSF macrophages. (A) MDMs were incubated with 5 mM glycine prior to sublytic MAC stimulation for 4 hours and cell viability was measured by CellTitre-Glo (n=3). Parameters from the seahorse Glycolytic rate test (B) and the Mito stress test (C) (n=4). (C,D,E) MDMs stimulated for 1 hour with MAC, anti-C7 control or pre-incubated 5 mM glycine before Glycolytic rate test (B, D) and Mitochondrial stress test (C, E). Kinetic data and calculated parameters in bar graphs are presented (n=4). Statistically significant data was assessed by (A) Unpaired t test or (B-E) a 1-way ANOVA with post-hoc Tukeys test. Error bars represent +/- S.E.M.
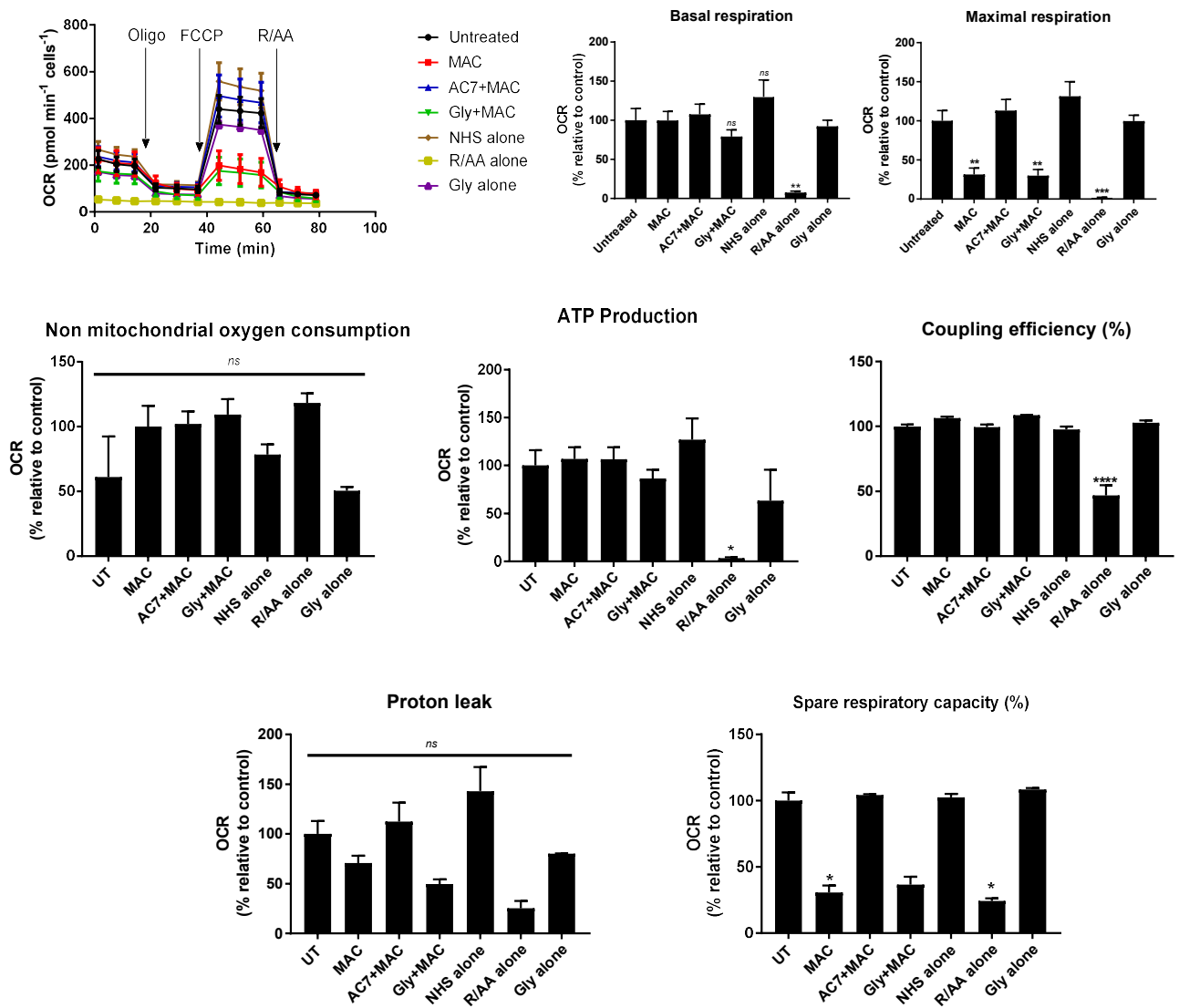
Figure 23. Seahorse assays at 4 hours. 4-hour stimulation of MDMs with indicated stimulations before mitochondrial stress test. Kinetic data and calculated parameters in bar graphs are presented. Statistical significance between MAC or Glycine + MAC and the rest of control groups (UT, anti-C7 + MAC, Gly alone, NHS alone), as well as UT vs. R/AA alone, was assessed by 1-way ANOVA with post-hoc Tukey's test. Error bars represent +/- S.E.M (n=3).
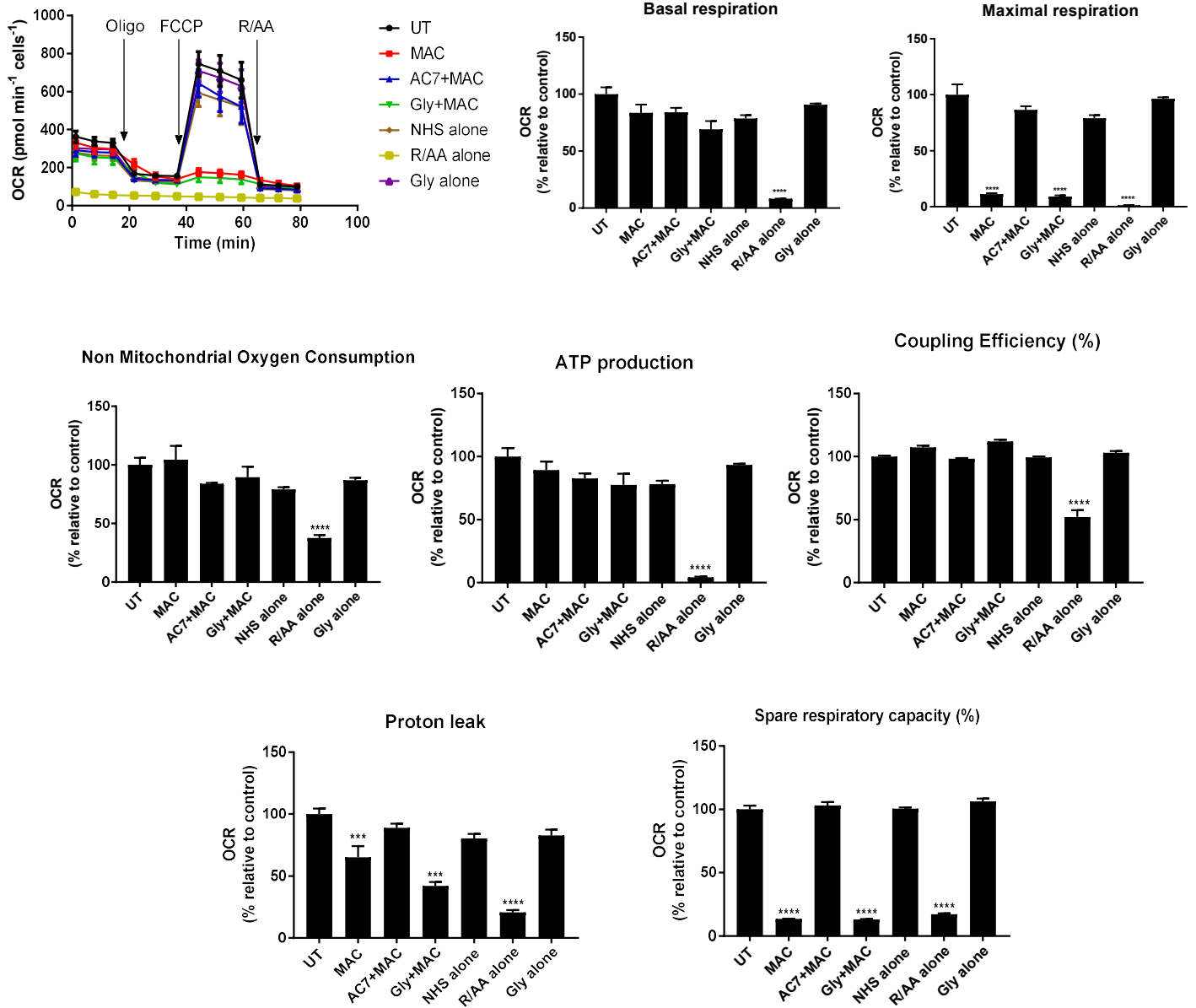
Figure 24. Seahorse assays at 24 hours. 24-hour stimulation of MDMs with indicated stimulations before mitochondrial stress test. Kinetic data and calculated parameters in bar graphs are presented. Statistical significance between MAC or Glycine + MAC and the rest of control groups (UT, anti-C7 + MAC, Gly alone, NHS alone), as well as UT vs. R/AA alone, was assessed by 1-way ANOVA with post-hoc Tukey's test. Error bars represent +/- S.E.M. (n=3)

4.3 Sublytic MAC stimulation drives an increase in mitochondrial calcium

As sublytic MAC caused the diversion of metabolic flux towards glycolysis and an inability to respond to FCCP and thus a collapse of maximal respiratory capacity, features of mitochondrial physiology that determine immunometabolic response post MAC stimulation were next investigated (Rambold and Pearce 2018, Mills and O'Neill 2019).

Ca^{2+} influx is the first detectable event upon MAC deposition, leading to increased cytosolic Ca^{2+} concentration (Morgan and Campbell 1985, Morgan, Luzio et al. 1986) and further transport of Ca^{2+} to the inner mitochondrial membrane via the mitochondrial calcium uniporter (MCU), causing overload and depolarization of the membrane in human epithelial cells (Triantafilou, Hughes et al. 2013). Ca^{2+} flux was therefore tested in MDMs upon sublytic MAC stimulation to observe and confirm the increase in cytosolic Ca^{2+} described above. Intracellular Ca^{2+} was detected using Fura-2 dye in MDMs. Firstly, to test suitability of this dye in MDMs, live confocal microscopy was used in cells stimulated with the ionophore ionomycin for 15 min, acting as a positive control for increased intracellular Ca^{2+}, as observed by a clear decrease in Fura-2 green signal (Figure 25A). A signal decrease was indicative of Ca^{2+} increase as excitation wavelength was set at 380 nm (see methods section 2.11 for further details). In addition, mitochondria of MDMs were also stained in red with Mitotracker CMXRos prior to ionomycin addition, causing clear mitochondrial fragmentation due to the downstream induction of cell death. In a separate experiment also using live confocal microscopy in MDMs (Figure 25B), cells were stained with red Mitotracker CMXRos and Fura-2 (excitation wavelength set at 340 nm this time - increase in Fura-2 green signal upon increase in intracellular Ca^{2+}) and stimulated with sensitising antibodies or left untreated for 1 hour. Addition of sensitising antibodies didn't cause any increase in intracellular Ca^{2+} or change in mitochondrial networks compared to untreated cells, as expected. MDMs were then sensitised and stimulated with sublytic MAC, anti-C7 or NHS alone controls or glycine plus MAC for 1 hour, and intracellular Ca^{2+} was measured by Fura-2 fluorescence plate reader quantification (Figure 25C) or selected conditions stained with Fura-2 (green, set at 340 nm) and Mitotracker CMXRos (red) by confocal microscopy, in order to get a representative image (Figure 25D). As expected, intracellular Ca^{2+} was increased upon sublytic MAC stimulation (Figure 25C, D), with co-localisation between the mitochondrial stain and Fura-2, indicative of mitochondrial Ca^{2+} increase. In addition, glycine plus MAC condition was not able to rescue the MAC-induced phenotypes, indicating these events were not mediated by the presence of dying cells in the external environment.

A

MitoTracker | Fura-2 at 380nm (decrease in signal upon increase in [Ca2+]i) | Merged

Baseline

+ Ionomycin

B

Before 'Abs' | After 'Abs'

C

Intracellular Ca2+

Ratio (340/380) % of control

UT | MAC | aC7 + MAC | Glycine + MAC | NHS only

D

UT | MAC | anti-C7 + MAC
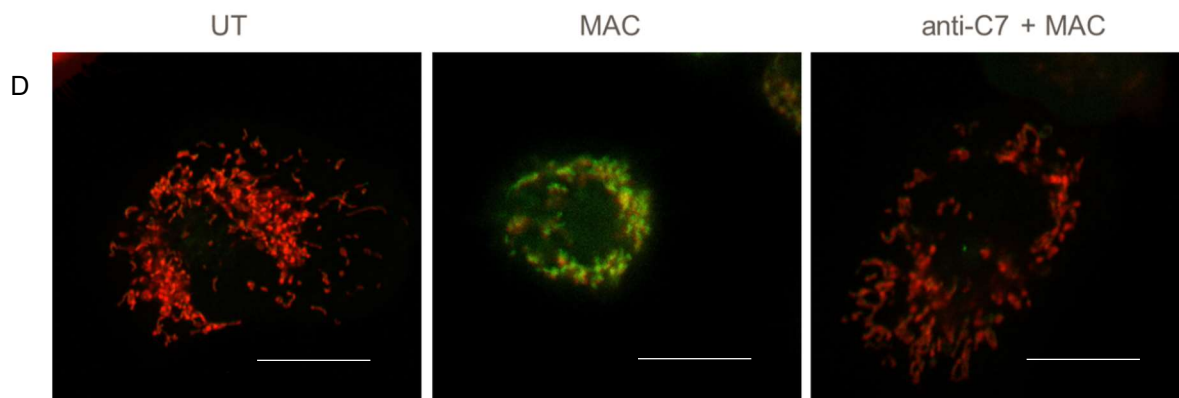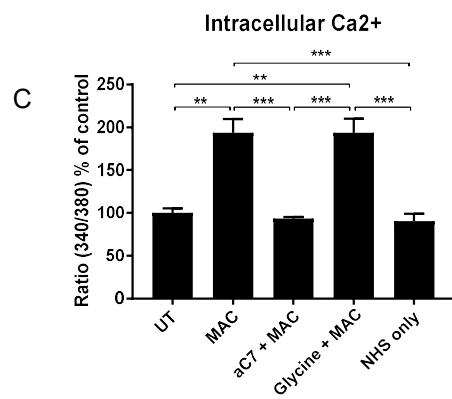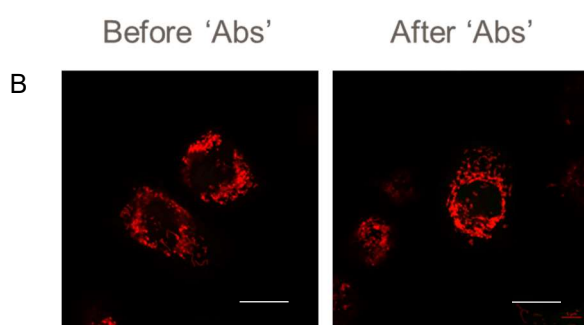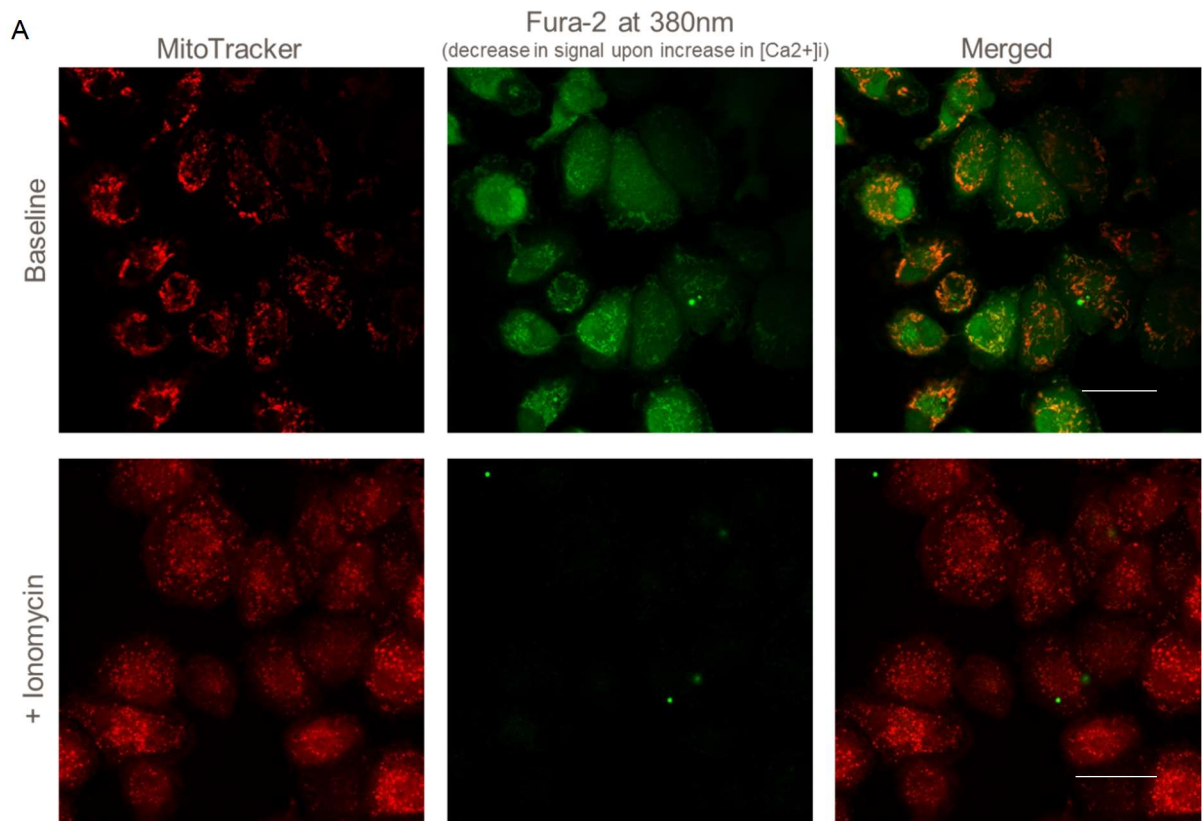
Figure 25. Intracellular calcium measurement and mitochondrial co-localisation after MAC treatment. (A, B, D) MDMs were stained with Fura-2 and mitochondrial stain 500 nM MitoTracker Red CMXRos for 15 min before treatment with (A) 5 µM ionomycin for 15 min (Fura-2 set at Ex 380 nm) (20X, scale bars 10 µm), or (B, D) sensitising antibodies alone or with MAC, anti-C7 control and untreated for 1 h (63X, scale bars 10 µm), measured by confocal microscopy (Fura-2 set at Ex 340 nm – increase in signal upon increase in calcium). (A, B, D) n=3 representative images shown. (C) Intracellular calcium of MDMs measured by monitoring of Fura-2 signal (340/380 nm ratio) after incubation with MAC, anti-C7 control, 5 mM glycine plus MAC, untreated and NHS only for 1 h by plate reader (n=3).

4.4 Sublytic MAC induces disruption of mitochondrial networks and collapse of mitochondrial membrane potential

As calcium flux can influence mitochondrial morphology and therefore mitochondrial biology and function (Williams, Boyman et al. 2013), and considering the seahorse results observed above showing inability of mitochondria to respond to FCCP, it was hypothesised that mitochondrial biology was significantly altered post MAC addition. One way to assess global mitochondrial stress is to look at mitochondrial dynamics and membrane potential, therefore these were assessed after MAC stimulation.

Live cell imaging of MDMs in imaging dishes stained with Mitotracker Red CMXRos to stain mitochondria showed no mitochondrial fragmentation in negative controls untreated or complement-sensitised cells without MAC stimulation (Figure 26), nor to anti-C7 plus MAC control cells (Figure 27A). However, addition of sublytic MAC during 1 hour (lysis curve in imagine dishes was tested in Supplementary Figure 2), and FCCP or ionomycin for 15 min, both used as a positive control for mitochondrial fragmentation (Hom, Gewandter et al. 2007), caused clear fragmentation of the mitochondrial network (Figure 26 and 27A). To confirm these effects, mitochondrial morphology was quantified from the images taken during live cell imaging. Mitochondrial fragmentation was assessed according to the mitochondrial branch length mean values, as well as mitochondrial footprint (area or volume of the image occupied by signal) as an additional measurement (Figure 27B, C), and exported from the semi-automated macro tool MiNA (Valente, Maddalena et al. 2017). Sublytic MAC and ionomycin treated cells showed shorter branches and therefore more fragmented mitochondria, indicating a MAC-driven disruption of mitochondrial dynamics. Yen (Yen J.C. 1995) (Figure 27B) and Huang (Huang 1995) (Figure 27C) thresholds were the most appropriate thresholds for this particular analysis, showing high adaptability to detect different length of branches; however, Yen threshold was selected as the most optimal than Huang threshold, which tended to unify separate branches into longer

ones, especially for conditions such as MAC or ionomycin inducing mitochondrial fragmentation.
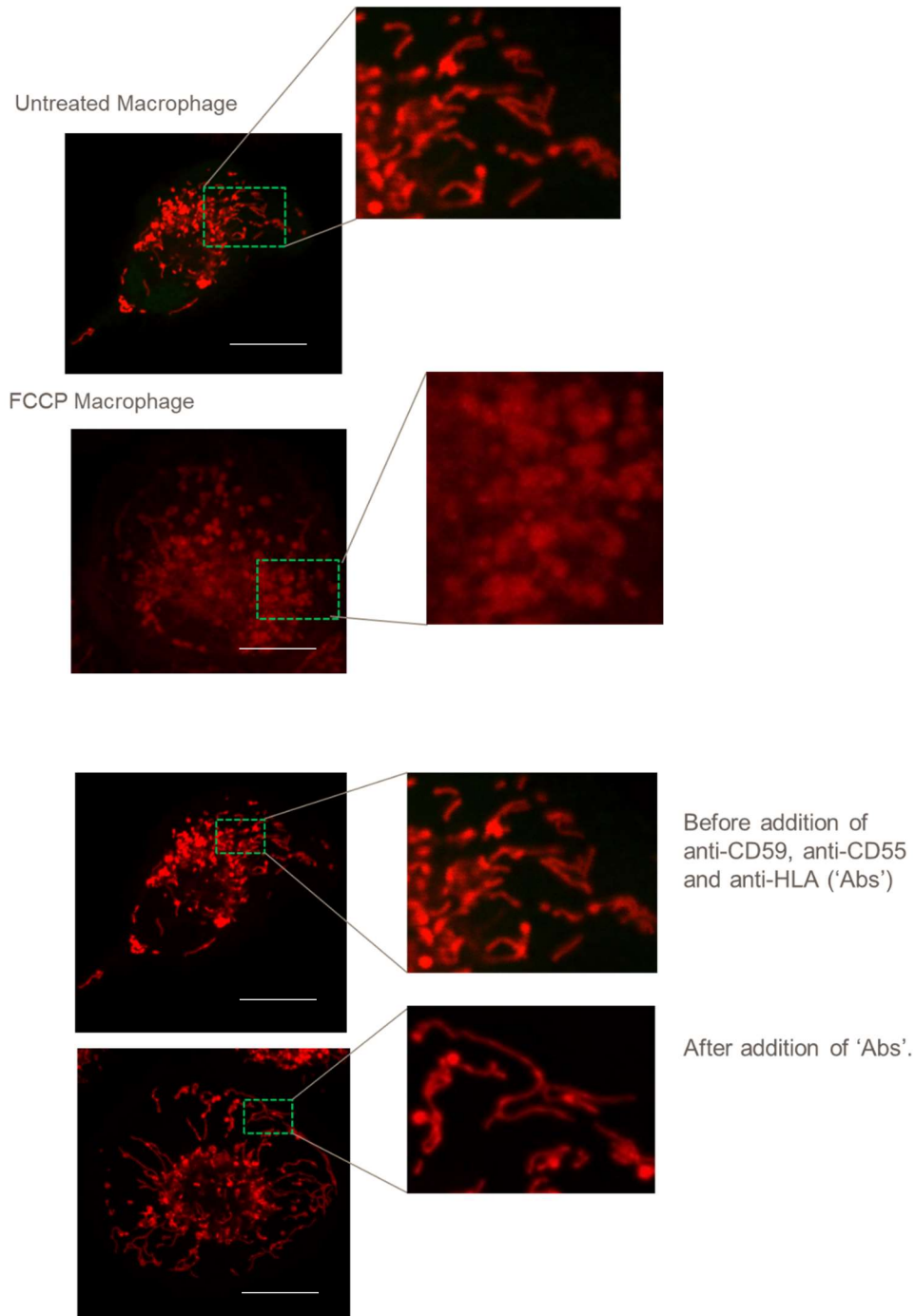
Figure 26. Optimisation of controls for mitochondrial dynamics measurement. (A) MDMs were stained with 500 nM MitoTracker Red CMXRos for 15 min before 1.2 µM FCCP stimulation for 15 min or complement sensitising antibodies for 50 min and imaged (63X, scale bars 10 µm) (n=4 independent donors; representative image shown).

In addition, mitochondrial membrane potential was measured by fluorescence quantification of MDMs stained with JC-10 dye. Sublytic MAC stimulation for 30 min induced a collapse of membrane potential as indicated by an increase of the 520/590 nm emission ratio and therefore predominant green monomeric forms, compared to untreated cells and anti-C7 control (Figure 27D). A variety of compounds including ionomycin, FCCP, the mitochondrial complex I inhibitor rotenone, and FCCP plus rotenone, which are known to induce mitochondrial depolarisation (Dispersyn, Nuydens et al. 1999, Abramov and Duchen 2003, Tada-Oikawa, Hiraku et al. 2003), were used as positive controls. FCCP and FCCP plus rotenone induced a significant drop in membrane potential. Overall, these results support previous findings in other cell types with regards to calcium flux and membrane potential (Triantafilou, Hughes et al. 2013) as well as providing novel evidence that mitochondrial morphology is directly altered as a result of MAC stimulation.

.

A

Untreated MAC anti-C7 + MAC Ionomycin

B

Yen threshold

Branch length mean (μm)

Yen threshold

Mitochondrial footprint (μm2)

C

Huang threshold

Branch length mean (μm)

Huang threshold

Mitochondrial fooprint (μm2)

D

JC-10

Ratio (520/590) % of control
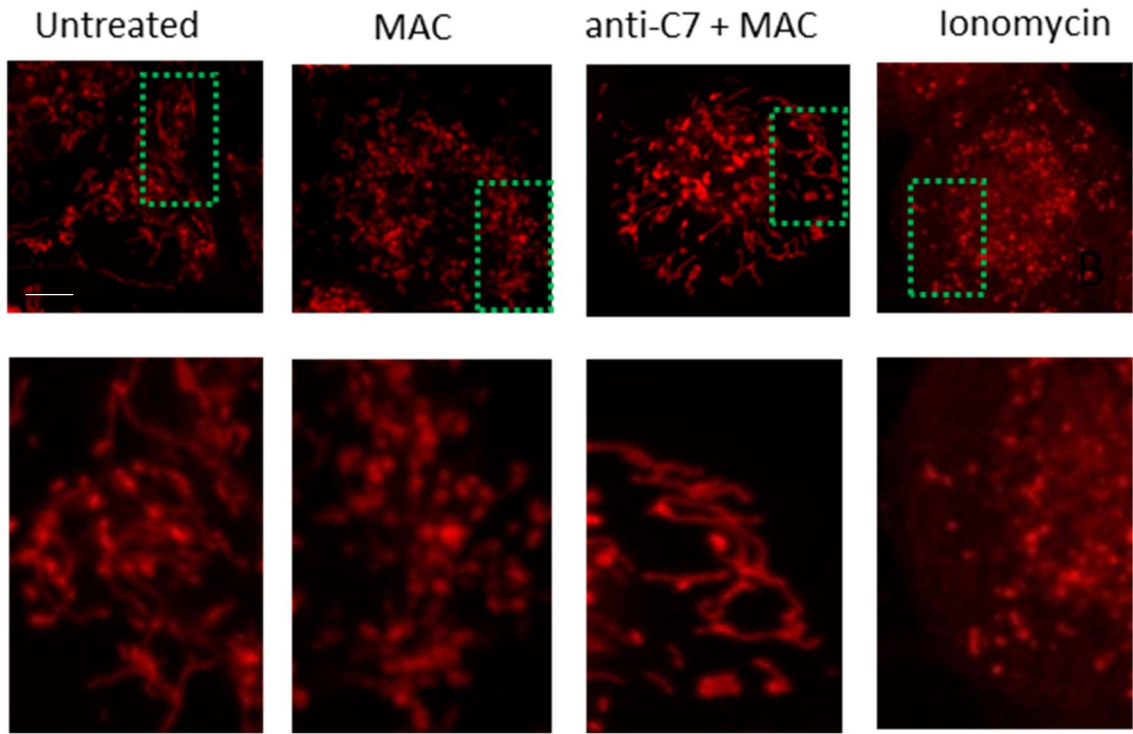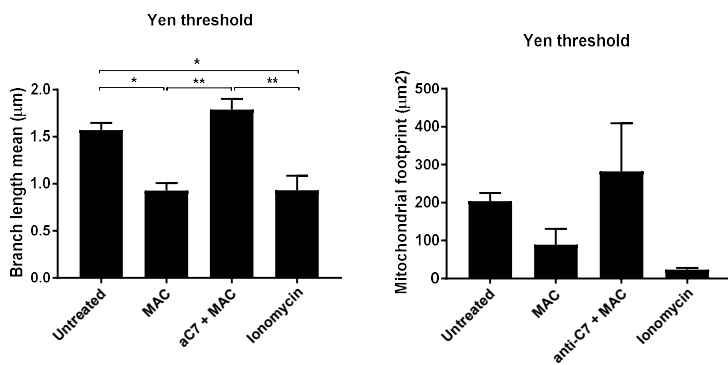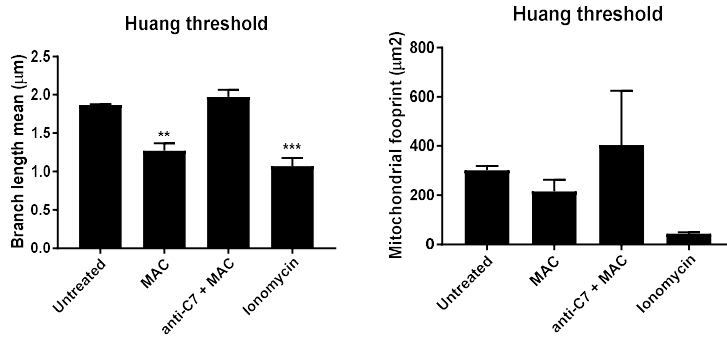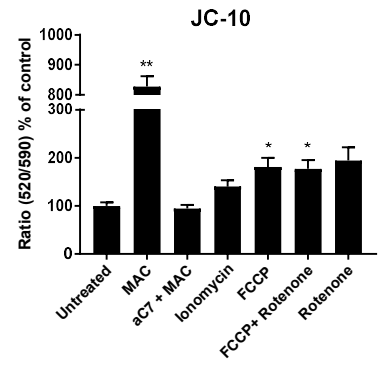
Figure 27. MAC drives disruption of mitochondrial dynamics and membrane potential. (A) MDM were stained with 500 nM MitoTracker Red CMXRos for 15 min before MAC stimulation +/- anti-C7 or 5 µM ionomycin and imaged (n=4 independent donors; representative image shown) (63X, scale bars 5 µm). (B, C) Quantification of mitochondrial network morphology, expressed as mitochondrial branch length mean or mitochondrial foodprint, from stimulations described in (A) were quantified from confocal microscopy images using MiNa Fiji/ImageJ software using Yen (B) or Huang (C) thresholds (n=4 cells per condition per donor analysed). (D) MDMs were stimulated for 1 h with MAC (+/- anti-C7), 5 µM ionomycin, 1.2 µM FCCP or 0.5 µM rotenone and membrane potential measured by JC-10 assay and normalised to untreated cells (n=3). Statistical analysis performed was assessed by 1-way ANOVA with post-hoc Tukey's test. Error bars represent +/- S.E.M.

4.5 Sublytic MAC drives ROS production

LPS activated BMDMs have been shown to switch to glycolysis with subsequent alteration of the mitochondrial membrane potential, triggering an increase in RET-ROS, and that these changes are required to induce an inflammatory response (Mills et al., 2016). Furthermore, two independent studies showed that sublytic MAC triggers an increase in intracellular calcium ($[Ca^{2+}]i$) and subsequent mitochondrial Ca^{2+} uptake (Triantafilou et al., 2013), and that mitochondrial Ca^{2+} uptake results in ROS production (Feissner, Skalska et al. 2009), suggesting a possible link between MAC and ROS. In this chapter, it has been shown that sublytic MAC triggers an increase in glycolysis and increased mitochondrial Ca^{2+}, but whether MAC and these subsequent changes, triggers an increase in ROS production in MDMs has not been elucidated. In addition, as mitochondrial dysfunction seems to be subsequent to sublytic MAC stimulation, it was postulated that this imbalance coupled with metabolic shifts would drive mitochondrial ROS, consequently activating innate immune signalling.

In response to MAC stimulation, general intracellular ROS as measured by CellROX staining was enhanced (Figure 28A), as was dimerisation of mitochondrial peroxiredoxin 3 (Prx3) measured by western blot and quantified by densiometry analysis (Figure 28B, C). Prx3 oxidation is known to degrade hydrogen peroxide (H_2O_2) within mitochondria via reversible oxidation of its active site cysteines (Cox, Winterbourn et al. 2010), indicating localized mitochondrial generation of ROS. MDMs were stimulated with sublytic MAC, with or without the anti-C7 antibody, or the mitochondria-specific ROS generator MitoParaquat (MitoPQ) (Robb, Gawel et al. 2015). The samples were resolved by non-reduced SDS-PAGE, where reduced Prx3 resolve as monomers and oxidized Prx3 as dimers (Figure 28B). Untreated and anti-C7 controls only showed partial dimerization, as is expected,

whereas sublytic MAC and MitoPQ showed a clear increase of the dimerized Prx3, indicative of mitochondrial oxidation due to possible increased ROS production.

ROS, and in particulary hydrogen peroxide, can exit the cell and influence localised inflammatory environments. To test whether the MAC-induced ROS was indeed moving outside of the MDMs in this scenario, hydrogen peroxide was tested. Indeed, an increase in hydrogen peroxide in the extracellular medium of MDMs stimulated with C5b6-9, the purified components of the MAC, was observed (Figure 28F). Purified components were used due to reactivity of the NHS with the hydrogen peroxide assay (Figure 11E) and these were confirmed to induce sublytic stimulation in both viability and MAC deposition assays (Figure 28D, E). The increase in hydrogen peroxide driven by C5b6-9 was sensitive to removal of terminal components C7-9, indicative of a MAC-sensitive response. We hypothesised that due to the mitochondrial dysfunction observed in the above figures, as well as mitochondrially-located Prx3 dimerisation, that the ROS production would be driven from the mitochondria itself. Upon addition of the mitochondrial complex I inhibitor, rotenone, ROS production was reduced to undetectable levels (Figure 28G), confirming this hypothesis. There was also a slight decrease in hydrogen peroxide detected from cells incubated with the glycolysis inhibitor, 2-DG. In addition, this production of hydrogen peroxide was not a result of dying cells associated with sublytic MAC, as shown in the addition of glycine. Finally, cell viability was measured at 3 hours post stimulation with C5b6-9 purified components (Figure 28H, I), still showing sublytic MAC levels (70-80% survival), ≥ 50% survival for rotenone and 2-DG inhibitors, and a complete protective effect in cells treated with Glycine plus MAC. Overall, Given the rotenone sensitivity and MAC-mediated dimerisation of Prx3, we showed that sublytic MAC drives mitochondrial dysfunction and mitochondrial ROS production.
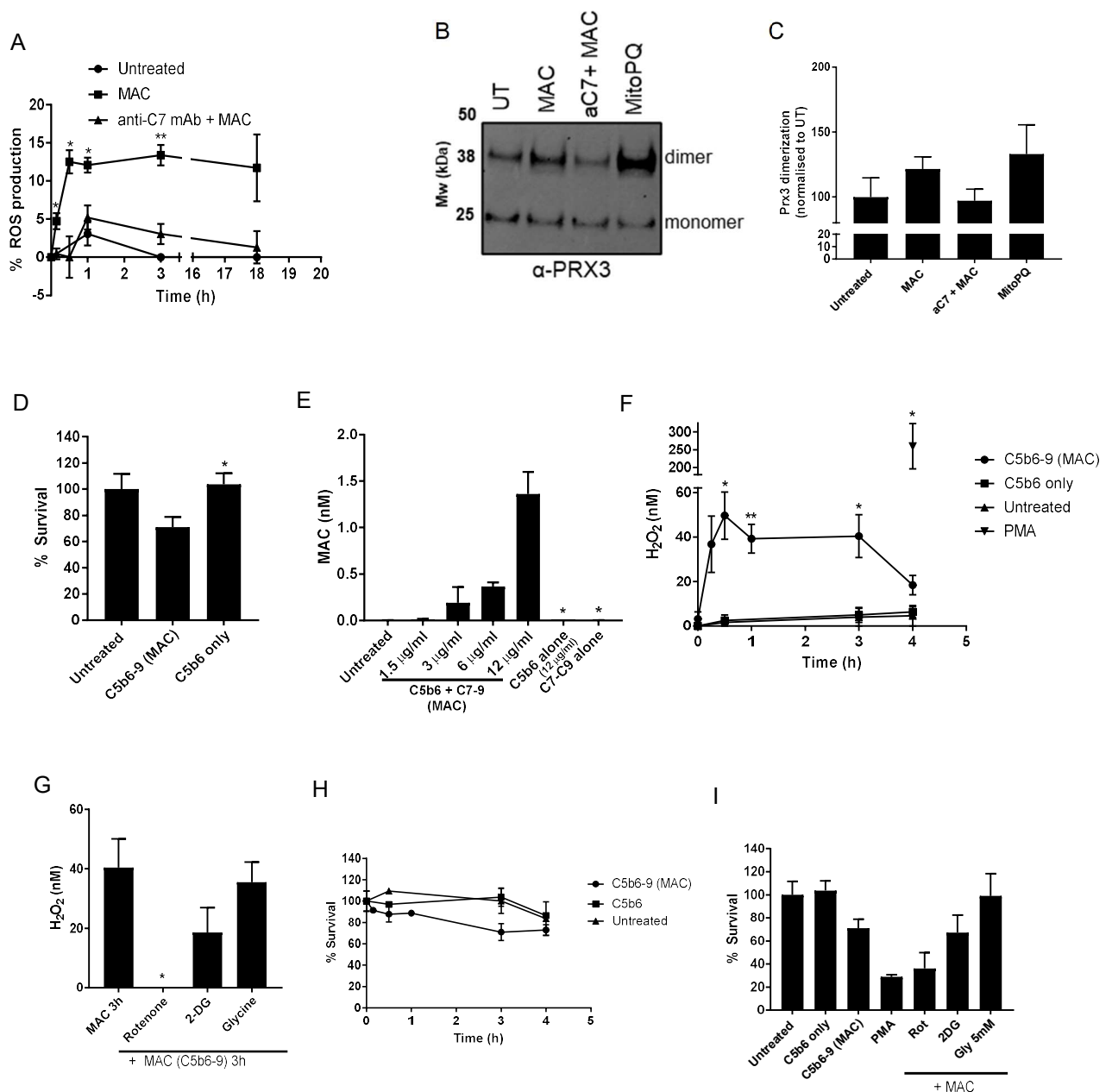
Figure 28. Intracellular ROS and hydrogen peroxide production triggered by MAC pore formation (A) Intracellular ROS production measured over time by mean fluorescence intensity using CellROX. MDMs were stimulated with MAC (+/- anti-C7) and normalised to 30 µM menadione treatment as positive control (n=3). (B) MDMs were incubated with MAC (+/- anti-C7) or 5 µM MitoPQ for 3 hours and Prx3 dimerization measured by Western blot (n=3; representative blot shown). (C) WB quantification from panel B, Prx3 dimerization measured by Image J and normalised to untreated (n=3). (D, E) Cells sensitised with neutralising anti-CD59 antibody and stimulated with purified components of MAC. (D) 6 µg/ml of C5b6 for 50 min plus one molar excess of C7, C8 and C9 for 1 hour, viability was measured by CellTiter-Glo (n=4). (E) MAC deposition after MDMs treated with anti-CD59 and increasing concentrations of C5b6 plus fixed concentrations of C7-C9 purified complement proteins, for 1 hour, measured by TCC MSD in cell lysates. Negative controls were performed by addition of C5b6 alone or C7-C9 alone (n=3). (F-I) MDMs stimulated with MAC (anti-CD59 plus C5b6-9 purified components (6 µg/ml C5b6 plus 12 µg/ml C7-C9) (+/- 50 min pre-incubation with rotenone (0.5 µM), 2-DG (5 mM) or Glycine (5 mM)) or with 6 µg/ml

C5b6 only or 200 nM PMA only controls (n=4). (F, G) H_2O_2 production measurement by Amplex red assay, (H, I) cell survival by CellTitreGlo assay from the H_2O_2 assay in F and G. Statistically significant data between MAC and control groups was assessed by unpaired student's t-test with Welch's correction for unequal SDs. Significance comparisons in (D) are to MAC, in (E) to 12 µg/ml C5b6 plus C7-C9, in (A) and (F) to respective time point of anti-C7 control and in (G) to MAC treatment. Error bars represent mean +/- S.E.M.

4.6 MAC promotes a late upregulation of glycolysis promoting genes and inhibition of pyruvate dehydrogenase complex by upregulation of PDK4

To investigate the mechanism of how sublytic MAC results in a switch towards glycolysis and adapts to dysregulation of mitochondrial metabolism, a panel of key genes relevant in metabolic reprogramming of inflammatory macrophages was assessed (data not shown). From this, the expression profiles of a number of these genes were further investigated (Figure 29, Supplementary Figure 3). MDMs were treated with sublytic MAC, anti-C7 control and LPS for 24 hours. Sublytic MAC triggered upregulation of pyruvate dehydrogenase kinase 4 (PDK4), known to inhibit pyruvate dehydrogenase (PDH) and linked with mitochondrial dysfunction (Park and Jeoung 2016) (Figure 29A). Expression of kinases PDK2 and PDK4, pyruvate dehydrogenase regulatory subunit (PDPR), which negatively regulates PDH by decreasing PDP activity as described in the schematic panel of Figure 29A, as well as pyruvate dehydrogenase E1 subunit beta (PDHB), was assessed post MAC stimulation after 1, 4 and 24 hours (Supplementary Figure 3), however, no changes in gene expression were observed except in PDK4 post 24 hours stimulation (Figure 29A).

In addition, upon sublytic MAC stimulation, the genes hypoxia inducible factor alpha (HIF1α), 6-phosphofructo-2-kinase/fructose-2,6-biphosphatase 3 (PFKPB3) and IL-1β, which have been linked with heightened glycolysis (Kelly and O'neill 2015, O'Neill, Kishton et al. 2016), showed a strong upregulation (Figure 29B). LPS, known to upregulate glycolytic genes in macrophages (Ramond, Jamet et al. 2019), upregulated HIF1α, PFKPB3 and IL-1β at the same or lower level than sublytic MAC, whereas it downregulated PDK4 by approximately 5-fold. The positive control for PDK4, a PDK4 agonist known to inhibit PDH, showed a clear PDK4 upregulation. Overall, it is clear that these key enzymes in regulating glycolysis response and pyruvate metabolism are upregulated in response to sublytic MAC deposition, further supporting the previous findings showing MAC as a trigger of immunometabolic alterations in macrophages.
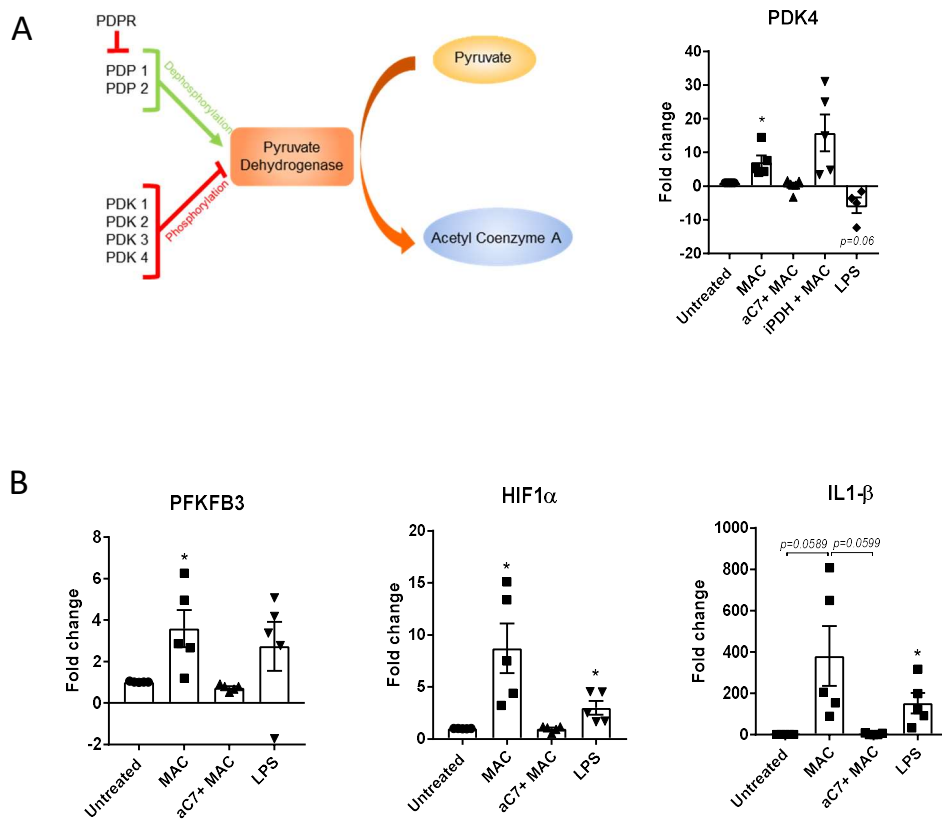
Figure 29. Sublytic MAC triggers upregulation of glycolysis metabolic genes. MDMs treated with MAC, anti-C7 plus MAC control or 100 ng/mL LPS for 24 hours. (A, B) Schematic figure of PDH regulation. Gene expression of PDK4 (containing PDK4 agonist which inhibits PDH (iPDH) plus MAC as a positive control for PDK4 expression) as well as HIF-1a, IL-1B and PFKFB3 (n=5). Gene expression was normalised to housekeeping genes β-actin, HPRT and TBP. ΔΔCt is relative to unstimulated cells. Statistically significant data between MAC and control groups or LPS and untreated was assessed by unpaired student's t-test with Welch's correction for unequal SDs. Error bars represent mean +/- S.E.M.

4.7 Sublytic MAC mediated perturbations drive subsequent NLRP3 inflammasome activation

The link between ROS production and inflammasome activation, namely NLRP3, is well documented (Tschopp and Schroder 2010). In addition, data so far suggested that MAC can modulate alterations in the bioenergetics of MDMs promoting glycolysis, which is a fast and responsive means of energy production fuelling a pro-inflammatory cytokine response.

Inflammasome activation and production of cytokine has been shown to be a consequence of such metabolic alterations in the cell, as well as of ROS production. Therefore, to investigate whether sublytic MAC was able to induce NLRP3 inflammasome activation, the production of IL-18, a constitutively present cytokine that is cleaved into its active form by caspase-1 upon activation by NLRP3, was assessed.

Sublytic MAC in MDMs was able to generate a time-dependent inflammatory response in the form of IL-18 production. Antibodies or NHS alone present in our model system did not contribute to this phenotype, which was anti-C7 sensitive, indicating a MAC dependant response (Figure 30A). In addition, the results showed an anti-C7 sensitive activation of GSDMD (Figure 30B), indicative of active pyroptotic machinery, as well as ASC speck formation (Figure 30C) downstream of sublytic MAC stimulation. To further explore the signals contributing to a commitment to an inflammatory response in MDMs undergoing sublytic MAC stimulation, IL-18 production was probed post-stimulation in the presence of a panel of inhibitors of various stages of the hypothesised signalling pathway (Figure 30D, E). Levels of IL-18 were reduced by addition of the NLRP3-inhibitor MCC950 and the caspase 1 inhibitor, Z-VAD-FMK, highlighting a canonical NLRP3-driven inflammasome response. Additionally, 2-DG and heptalidic acid, inhibitors of glycolysis, significantly reduced IL-18 production (Figure 30D).

To test whether the mitochondrial-ROS was responsible for NLRP3 activation and consequential IL-18 release, superoxide production site specific inhibitors of NADH-ubiquinone oxidoreductase, S1QE1.1, and cytochrome bc1 complex, S3QEL 2 were utilised (Orr et al. 2015)(Brand, Goncalves et al. 2016). These inhibitors block the superoxide production sites of complex I and III, respectively, without altering oxidative phosphorylation. Interestingly, both of these inhibitors blocked sublytic MAC mediated IL-18 production (Figure 30E). In addition, rotenone, also reduced IL-18 levels, although not significantly ($p=0.069$) (Figure 30D).

At this stage, it was suspected that formation of GSDMD pores may be contributing to the mitochondrial dysfunction observed in Figure 21 and 27. To address this, NLRP3 inhibitor MCC950 was used to block production of GSDMD pores (figure 30F). Using mitochondrial membrane potential as a read-out of mitochondrial dysfunction, pre-incubation of MCC950 showed no effect on the collapse of the mitochondrial membrane potential, leaving any cellular perturbations to occur upstream and independent of NLRP3 activation and resulting GSDMD formation. Together, these results indicate that downstream of MAC stimulation, glycolysis as well as mitochondrially-driven ROS that emanates from mitochondrial dysfunction, are responsible for activating the NLRP3 inflammasome, which in turn can drive production of pro-inflammatory cytokine production, such as IL-18, providing novel evidence that MAC can alter metabolic phenotype and mitochondrial behaviour to increase pro-inflammatory output.

A

B

C

D

E

F

108
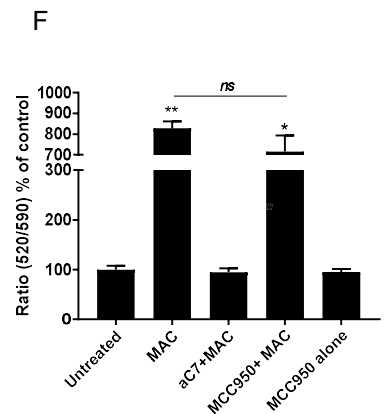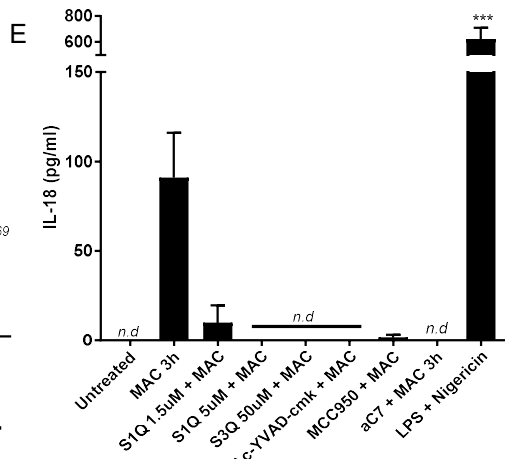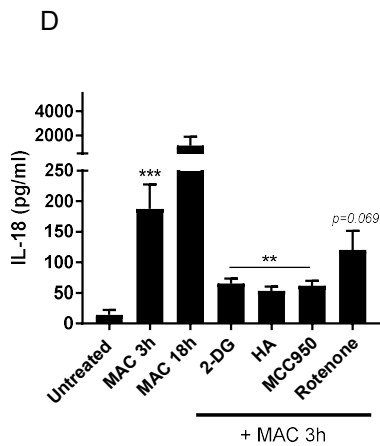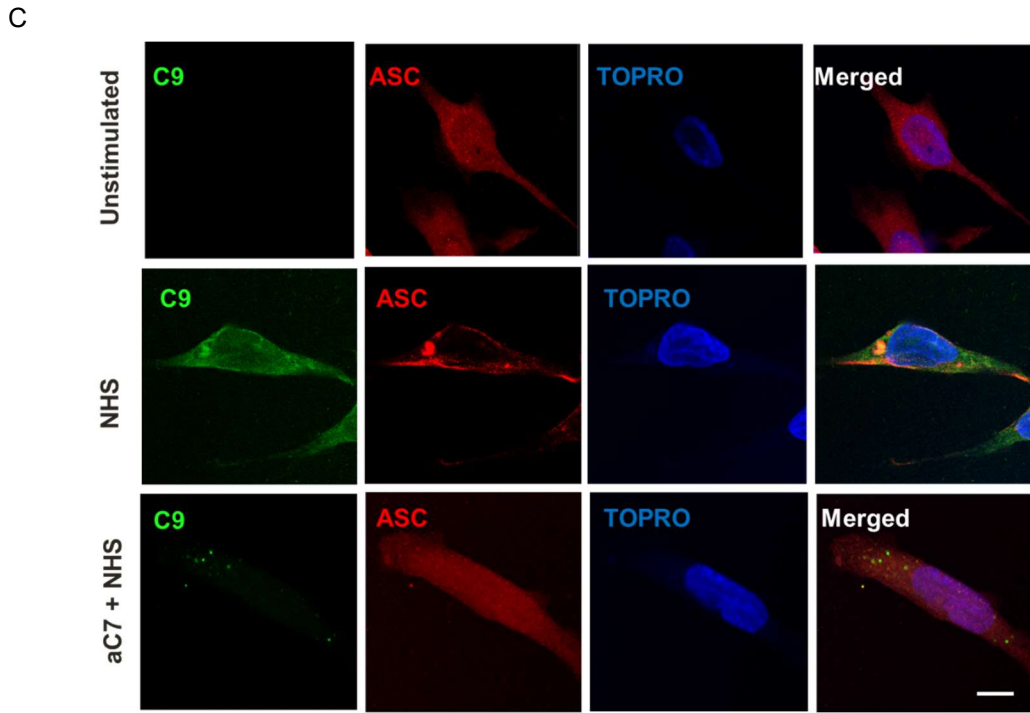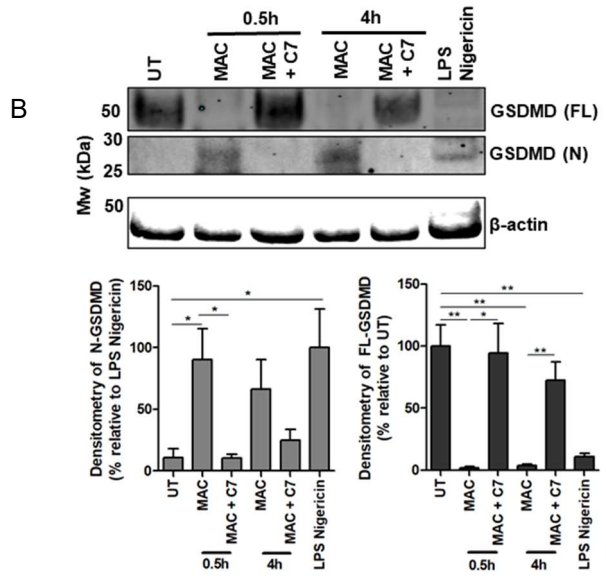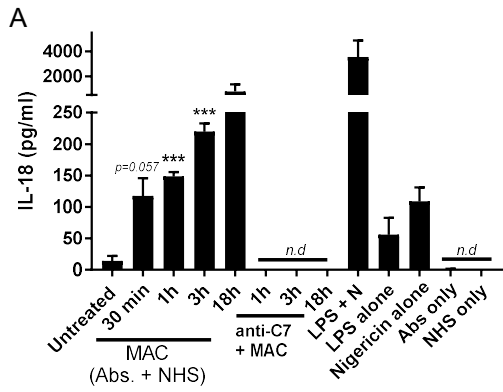
Figure 30. Sublytic MAC drives NLRP3 inflammasome activation. (A) IL-18 production detected by ELISA in supernatants of MDMs in 1 million cells per condition (24-well plates) stimulated with MAC or controls for select time points: antibodies only (Anti-CD55, CD59 and HLA), NHS only (just NHS without pre-incubation with antibodies), anti-C7 plus MAC or positive control LPS (100 ng/mL for 3h) followed by nigericin (5 μM for 1 h). (n=3). (B) Full length and cleavage of GSDMD as assessed by western blot in MDMs treated with MAC or MAC+ anti-C7 for 30 min or 4 hours, as well as LPS-nigericin (3h LPS (100 ng/mL) + 1h nigericin (10 μM)). Representative blot image is present alongside densitometry analysis of all 3 donors using UT/LPS-nigericin controls as relative comparisons (n=3). (C) Immunofluorescence staining against C9 or ASC in cells treated with MAC or anti-C7 control for 3 hours. Representative images from 1 donor (63X, scale bar 5μm) (total, n=3). (D) IL-18 production from MDMs supernatants in 1 million cells per condition (24-well plates) (same 3 donors from panel A which contains additional positive and negative controls) stimulated with MAC for 3 hours with pre-incubated inhibitors 2-DG (5mM for 2 h), HA (10 μM, 50 min), and rotenone (0.5 μM, 50 min) (n=3). (E) IL-18 ELISA of supernatants from MDMs in 130k cells per condition (96-well plates) stimulated with MAC for 3 hours with additional inhibitors MCC950 (1 μM), Ac-YVAD-CMK (10 μM), S1QE1.1 and S3QEL as indicated. Positive control was LPS (100 ng/mL for 3h) followed by nigericin (5 μM for 1 h). (F) Membrane potential by JC-10 of MDMs after 1h treatment with MAC or controls with MCC950 (1 μM) to block NLRP3 activation (n=3). Statistical analysis performed on (A,B,D-F) was assessed by unpaired student's t-test with Welch's correction for unequal SDs. Error bars represent ± S.E.M.

4.8 Discussion

Complement-mediated cell damage, and subcellular signalling downstream of sublytic MAC, has been implicated in many autoimmune diseases. Mechanisms that underlie pro-inflammatory signalling upon sublytic MAC stimulation have focussed on calcium flux with subsequent mitochondrial calcium overload and mitochondrial membrane potential collapse in epithelial cells (Triantafilou, Hughes et al. 2013), but no metabolic link has yet been made. Given these observations are relevant for mitochondrial biology and the results observed in chapter 3 showing GM-CSF MDMs being more metabolically active than M-CSFs, as well as GM-CSFs showing increased levels of real-time measured glycolysis post MAC stimulation, it was hypothesised that sublytic MAC stimulation of GM-CSF MDMs would drive an immunometabolic response that could modulate pro-inflammatory response, similar to other immune stimuli in macrophages. This study provides a critical and novel insight into how sublytic MAC can drive metabolic rewiring and mitochondrial dysfunction that actively contributes to the production of mitochondrial ROS, which consequently activates an NLRP3-driven inflammatory response.

Given the link to calcium imbalance and mitochondrial membrane potential collapse, this study sought to confirm that mitochondrial dysfunction and metabolic rewiring may have a role to play in activating inflammatory phenotypes in macrophages. To date, there has only been links between sublytic MAC and arachidonic acid metabolism and in phospholipid hydrolysis with no strong bridge with mitochondrial biology. Changes in glucose metabolism, particularly a shift towards glycolysis and away from oxidative phosphorylation, as well as inability to respond to FCCP, is inherently linked with a pro-inflammatory phenotype in LPS-stimulated macrophages due to increased levels of mtROS and succinate build up (Mills, Kelly et al. 2016). First, lactate build up was observed in the supernatants of GM-CSF MDMs stimulated with sublytic MAC. Interestingly, the concentration of lactate was 3-fold higher after 24 hours stimulation (Figure 21A) compared to M-CSF macrophages (Figure 8F), indicating that GM-CSF macrophages are indeed more glycolytic than M-CSFs in response to MAC attack and also at baseline levels., Using Seahorse technology, a shift towards glycolysis and away from oxidative phosphorylation was confirmed, typical of a pro-inflammatory macrophage. Furthermore, a MAC-driven mitochondrial dysfunction where cells were unable to respond to FCCP was also observed. These changes in glucose metabolism driven by MAC align with the metabolic signature of LPS-treated macrophages and with human tumour cells undergoing the Warburg effect, which describes a shift in metabolism towards glycolysis and away from oxidative phosphorylation, allowing rapid cell activation (Migneco, Whitaker-Menezes

et al. 2010, Potter, Newport et al. 2016). Basal OCR levels before FCCP injection remained unchanged at all time points after sublytic MAC stimulation, suggesting these changes weren't caused by damage of the mitochondrial membrane itself.

This metabolic shift away from mitochondrial metabolism instigated an investigation into the physiology of the mitochondria upon stimulation with sublytic MAC. As with other cell types, the mitochondrial membrane potential was seen to be reduced likely due to the calcium influx to the cell. As with other studies in macrophages, it was hypothesised this calcium influx and membrane potential collapse may lead to mitochondrial dysfunction which could contribute to cellular inflammatory phenotype. The results showed a fragmentation of mitochondrial morphology (Figure 27), reduction in membrane potential (Figure 27) and calcium influx, which co-localised with mitochondria (Figure 25). These findings are in agreement with evidence reporting increased [Ca2+]i upon sublytic MAC stimulation and depolarization of the mitochondrial membrane in epithelial cells (Triantafilou, Hughes et al. 2013). Further experiments were conducted to investigate if the MAC-driven mitochondrial imbalance coupled with metabolic shifts would drive mitochondrial ROS production. Interestingly, a previous study showed that LPS-activated BMDMs switch to glycolysis with subsequent alteration of the mitochondrial membrane potential, triggering an increase of Reverse Electron Transport-ROS (RET-ROS), which is required to induce an inflammatory response (Mills, Kelly et al. 2016). These findings align with the data in this study, confirming that sublytic MAC drives mitochondrial ROS production in MDMs, as indicated by oxidation of mitochondrially located Prx3, which was first monitored as a proxy for mitochondrial ROS production, and the increase in intracellular ROS and extracellular H_2O_2, which was rotenone-sensitive and partially dependant on glycolysis. In rat mesangial cells, sublytic MAC stimulation triggered superoxide production within 30 min stimulation and extracellular hydrogen peroxide within an hour (Adler, Baker et al. 1986), which is in line with the ROS data presented here. Together, these results clearly implicate the mitochondria in the response to sublytic MAC and suggest a mitochondria-location of the ROS source, which increases as a result of the mitochondrial dysfunction driven by MAC.

The fact that sublytic MAC drives glycolysis and a possible dysregulation in oxidative metabolism led to further exploration of the mechanisms involved in such process. A targeted panel of key genes relevant in metabolic reprogramming of inflammatory macrophages showed upregulation upon sublytic MAC treatment: HIF1α, PFKFB3, IL-1B and PDK4. HIF1α not only promotes glycolysis but also induces the expression of pro-inflammatory cytokines genes such as IL1-β, which is known to be part of the priming signal of NLRP3 inflammasome (O'Neill, Kishton et al. 2016). HIF1α drives an increase of

the glycolytic flux by promoting the expression of key enzymes such as phosphofructokinase 2 (PFK2). PFKFB3 encodes for PFK2 and has the dominant rate of kinase/phosphatase activity out of the four isoforms, promoting the catalysis from fructose-6-phosphate into fructose 2,6-bisphosphate and sustaining high rates of glycolysis. Interestingly, PFKFB3 is upregulated in numerous cancers and has been associated with the Warburg effect (Shi, Pan et al. 2017). The upregulation observed in PDK4, which inhibits pyruvate dehydrogenase enzyme (PDH), indicates a MAC-driven PDH inhibition which could lead to the mitochondrial dysfunction observed here, causing reduction of cytosolic pyruvate uptake into the TCA cycle and subsequent build-up of lactate. The MAC-driven reduction in maximal respiration post-FCCP injection observed in this study may be explained by this switch away from pyruvate delivery to the mitochondria. PDK4 has been presented as a target for treatment against inflammation and sepsis, where PDH inhibition leads to reduced mitochondrial activity and shifts glucose metabolism towards lactate production (Park and Jeoung 2016). The downregulation of PDK4 observed here in LPS-treated MDMs suggests activation of PDH and is in agreement with the bioenergetic profile described in LPS-treated MDMs, where glycolysis is slightly decreased and OXPHOS is not affected (Bossche, Baardman et al. 2016).

The NLRP3 inflammasome is known to integrate signals derived from ROS, glycolysis, amino acid and lipid metabolism (Arbore and Kemper 2016, O'Neill, Kishton et al. 2016). To determine whether the metabolic changes triggered by MAC drive inflammasome activation, cytokine release was measured post MAC stimulation. NLRP3 activation led to release of IL-18 but not IL-1β (Figure 30). However, the presence of ASC specks, GSDMD cleavage and reduced IL-18 levels in MCC950 and Z-VAD-FMK treated cells confirm NLRP3 inflammasome activation downstream of MAC stimulation. The absence of secreted IL-1β (Supplementary Figure 4) may be attributed to the lack of treatment with a commonly defined inflammasome priming signal such as LPS. Although complement stimulation with C5a has been shown to act as a priming signal for NLRP3 activation (Samstad, Niyonzima et al. 2014, Cao, Wang et al. 2016), it may not be sufficient to activate the signalling cascade required for IL-1β secretion, whereas IL-18 is not limited in this way (Gritsenko, Yu et al. 2020). Additionally, glycolysis inhibitors as well as rotenone, reduced the IL-18 production post MAC stimulation, highlighting the need for glycolytic contribution to inflammasome activation. The specific superoxide-production site inhibitors of complex I and III, S1QE1.1 and S3QEL 2 also inhibited IL-18 production, showing the requirement of mitochondrial ROS to activate NLRP3, linking together the observed mitochondrial dysfunction and consequential inflammatory response. Rotenone, however, only reduced IL-18 partially. This could be attributed to the fact that S1QE1.1 is more

potent and functionally different than rotenone, which inhibits forward electron transport (FET) more strongly than RET, and the opposite happens with S1QEL1 (Brand, Wong et al. 2016). Interestingly, ASC oligomerization co-localised with MAC staining (Figure 30), which is aligned with existing studies showing MAC internalisation and co-localisation with ASC and NLRP3 (Jane-wit, Surovtseva et al. 2015, Xie, Qin et al. 2019) (Diaz-del-Olmo, Worboys et al. 2021). It is possible that a threshold of MAC activation is what drives internalisation over endocytosis or blebbing, leading to different downstream effects (Sims, Faioni et al. 1988, Beum, Lindorfer et al. 2008). Overall, the inflammasome data in this study aligns with previous studies showing sublytic MAC driving NLRP3 inflammasome activation in epithelial cells and dendritic cells, as well as in mice deficient in C6, a critical component of the MAC complex, which had significantly reduced plasma IL-1β and IL-18 levels (Laudisi, Spreafico et al. 2013, Triantafilou, Hughes et al. 2013).

5. Chapter 5: Proteomics and metabolomics analysis of MAC stimulated GM-CSF MDMs

Several multi-omics studies including proteomics and/or metabolomics analysis have uncovered links between the complement system and a variety of diseases such as systemic lupus erythematosus or endometriosis, where complement was linked to the coagulation cascade in both diseases, as well as obesity (Oberbach, Blüher et al. 2011, Liang, Xie et al. 2018, Anastasiu, Moga et al. 2020). Interestingly, combined proteomic and metabolomic profiling of serum from healthy lean and obese individuals showed links between the complement C3 and C3b proteins and obesity, identifying novel makers of body fat mass changes (Oberbach, Blüher et al. 2011). However, there has been no studies to date exploring metabolomics or proteomics analysis downstream of MAC stimulation. Data in chapter 4 demonstrates a novel involvement of MAC in the complement-metabolism-inflammasome axis. Thus, this study sought to expand and investigate further the mechanisms that contribute to the immunometabolic changes driven by MAC that were uncovered in chapter 4, where, at the time of writing, MAC is presented for the first time as a driver of metabolic reprogramming. In summary, such process is characterised by increased lactate production and real-time glycolysis enhancement and away from OXPHOS, with a clear development of mitochondrial dysfunction with increased mitochondrial calcium, subsequent depolarisation of the mitochondrial membrane potential and disrupted mitochondrial dynamics, causing inability of cells to respond to FCCP, possibly due to the observed diversion of pyruvate away from the TCA cycle, and finally resulting in mtROS production and NLRP3 activation. To explore the mechanisms behind some of these shifts we opted for a multi-omics approach based on targeted metabolomics and proteomic cellular profiling. Intracellular targeted metabolomics analysis was performed in this study to assess key metabolites altered by sublytic MAC stimulation in GM-CSF MDMs. In addition to targeted metabolomics, exploratory proteomics analysis was also utilised in this study to gain further insight into translatable mechanistic effects in response to sublytic MAC. Both metabolomics and proteomics biological experiments were performed at GSK Stevenage by the thesis author and resulting cell pellets/supernatants were then analysed by colleagues in GSK Upper Providence, US. Raw data was generated and analysed by this author and colleagues within GSK UK.

5.1 Preparation of six donors for metabolomics and proteomics analysis post sublytic MAC stimulation

To prepare MDMs for metabolomics and proteomics analysis post sublytic MAC stimulation, a total of six biological replicates were used with two donors of blood prepared per day, over three separate days. On day 6 of differentiation, GM-CSF MDMs were subjected to to 4 hours of sublytic complement stimulation (see schematic in Figure 20A) at a donor-specific pre-defined dose of MAC that corresponded to 80 % viability, obtained from lysis curves using increasing doses of NHS for each donor (Figure 31A). Interestingly, the sublytic dose of MAC was more similar between the pair of donors that were prepared on the same day (donors 1-2, 3-4 and 5-6) compared to donors prepared on different days. In order to confirm donor susceptibility to MAC attack and to check that the stimulations were successful in all conditions after the 4 hours stimulation, MAC deposition was quantified in cell lysates by TCC MSD (Figure 31B). The results showed MAC deposition in MAC and MAC pre-incubated with 2-DG conditions, and no levels of MAC in negative controls untreated and anti-C7 plus MAC conditions, as expected. Cell morphology typical of GM-CSF macrophages was also confirmed in all donors by cell imaging (Figure 31C).

A

B

TCC MSD
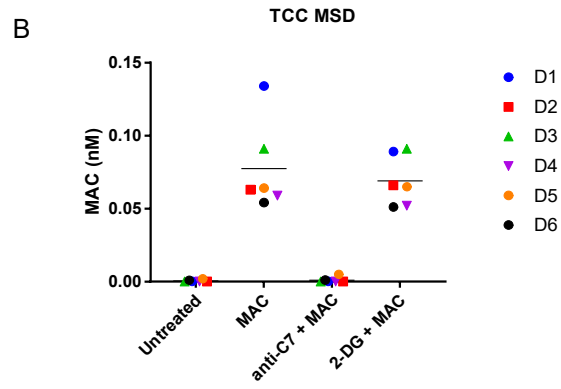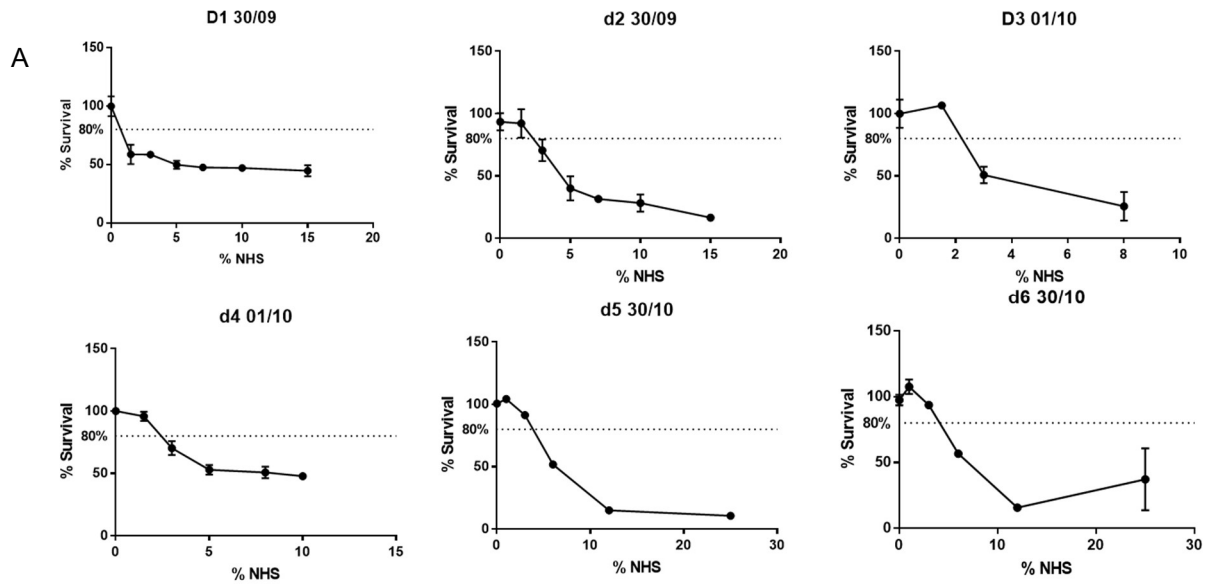
C
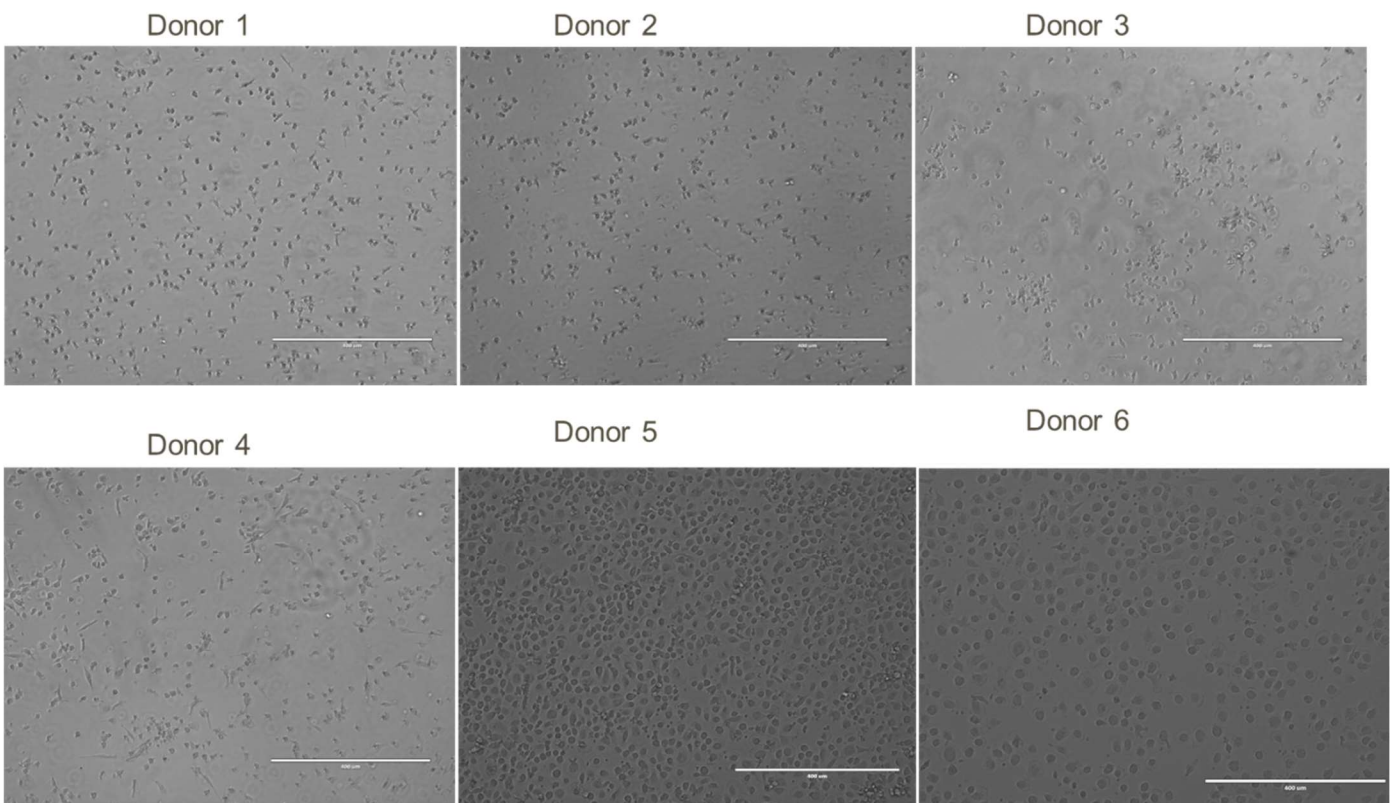
Figure 31. Sublytic MAC confirmation in MDMs from six donors for metabolomics and proteomics analysis (A) CellTiterGlo assay, lysis curves from six donors of MDMs stimulated with increasing doses of NHS. Percentage NHS corresponding to 80% survival for each donor was used for the 4 hours experiment for each donor (n=6). (B) MAC deposition in nanomolar of cell lysates of MDMs, measured by TCC MSD. Conditions used were MAC and 2-DG plus MAC, and negative controls untreated and anti-C7 plus MAC. 'D' means donor (n=6). (C) MDMs were imaged using EVOS microscope (10X, scale bar 400 µm)) (n=6). Error bars represent ± S.E.M.

5.2 Metabolite and protein intensities vary greatly within same treatment from donor to donor

After the 4 hours stimulation of 6 donors of MDMs with sublytic MAC, anti-C7 control or metabolic control 2-DG plus MAC, cells were lifted using cell-dissociation buffer and counted. Although the minimum number of needed cells for metabolomics and proteomics analysis was scaled up 4X for the experiments, a large number of cells was lost during this process, resulting in sub-optimal numbers for analysis. Cell lysates were sent for analysis, however, metabolomics results showed that metabolite intensities varied greatly within the same treatment from donor to donor and it was difficult to use donors in classical sense of replicates. This was observed in the principal component analysis (Figure 32A) and Hierarchal Clustering (Figure 32B) where metabolite intensities of all conditions coloured by donor are represented. The red circles show a big difference in distribution of metabolite intensities for the same untreated condition between donors. In addition, the principal component analysis resulting from proteomics analysis (Figure 33) showed a large separation between two sets of donor pairs, donors 3 & 4 and 5 & 6. Donors 1 & 2 were excluded from the analysis due to low cell count. Donors 5 & 6 showed to be significantly biologically different from each other with clear separation occurring at the donor level instead of at treatment level. However, for donors 3 & 4 the four treatment conditions could be clearly separated from each other with no donor specific effect, as it would be expected. Unfortunately, two donors were not enough replicates to obtain any significant data from the analysis. Overall, given the significant differences between donors, which were too big to be treated as replicates for the analysis of both metabolomics and proteomics, it was concluded that the stimulation experiment prior to these analyses should be repeated to decrease donor variability and improve the quality of the analyses.

A

B

118
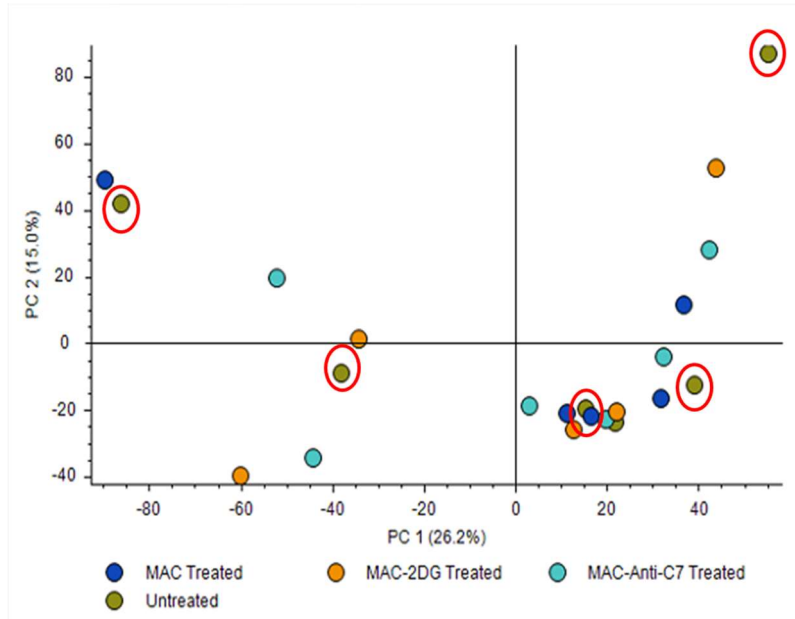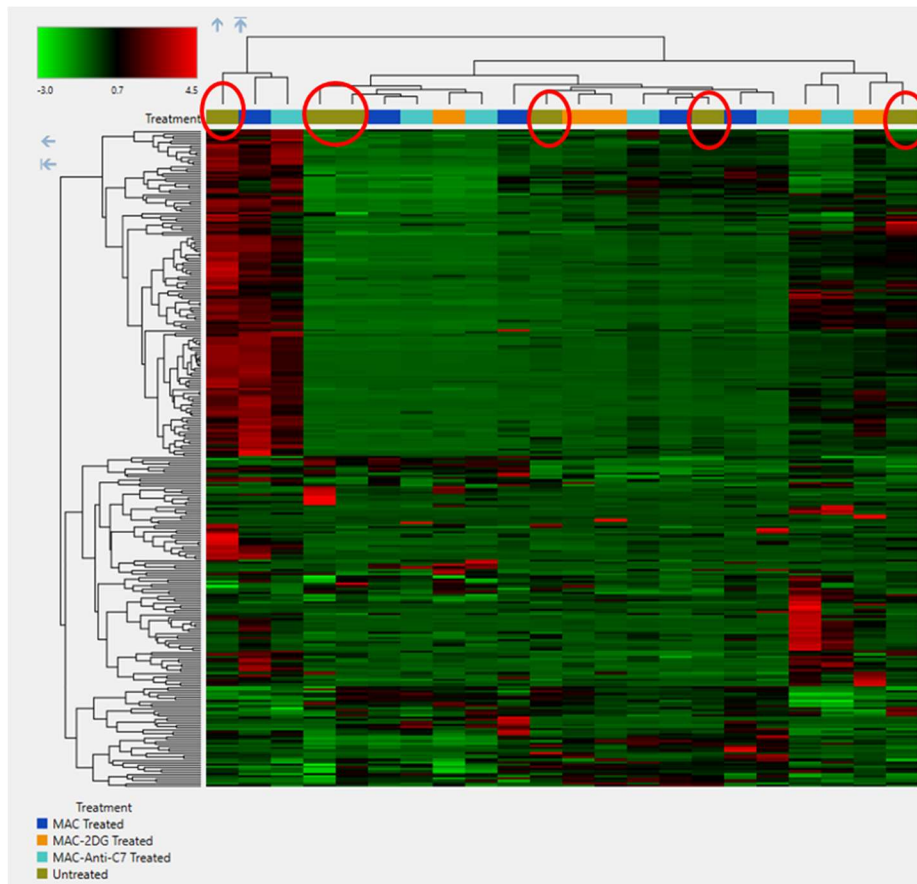
Figure 32. Principal component analysis and Hierarchal Clustering of metabolite intensities show high variability within the same treatment from donor to donor. Six donors of MDMs stimulated for 4 hours with MAC and 2-DG plus MAC, or negative controls untreated and anti-C7 plus MAC were utilised for metabolomics analysis. Initial distribution of metabolite intensities was represented by (A) Principal component analysis and (B) hierarchal clustering, both showing metabolite intensities of all conditions coloured by treatment (n=6). Red circles show distribution of metabolite intensities for the same untreated condition between donors
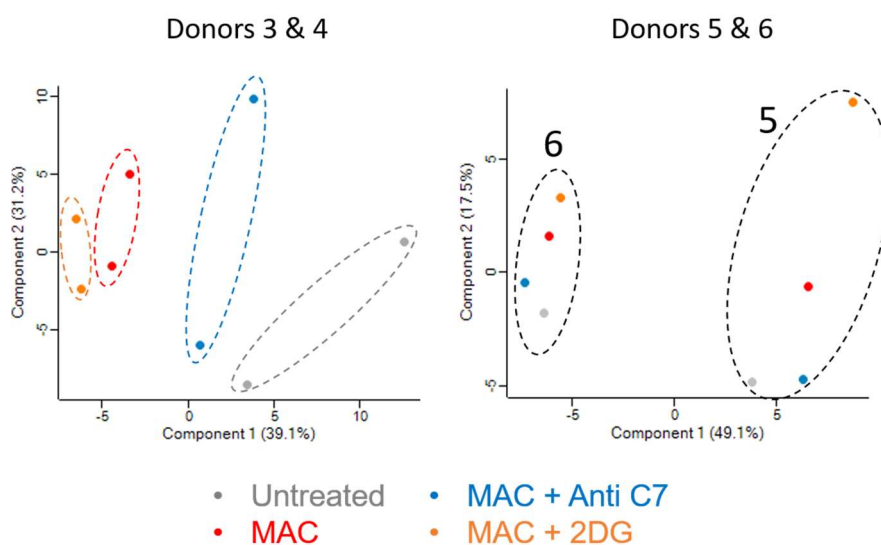
Figure 33. Principal component analysis protein intensities show high variability within the same treatment from donor to donor. Six donors of MDMs stimulated for 4 hours with MAC and 2-DG plus MAC, or negative controls untreated and anti-C7 plus MAC were utilised for metabolomics analysis. Initial distribution of protein intensities was represented by Principal component analysis. Red circles show distribution of protein intensities for the same untreated condition between donors.

5.3 Optimised sample collection for multi-omics analysis

To determine more reliable results from the targeted metabolomics and proteomics analysis post sublytic MAC stimulation, six donors of MDMs were prepared and differentiated all on the same day, to avoid excessive donor to donor variability observed above, caused by cell preparation done on different days (Figures 32 and 33). To determine a sublytic dose of complement, concentration-dependant lysis curves were initially performed to extract concentrations of NHS that resulted in 80 % viability (Figure 34A). In addition, MAC was quantitatively measured to confirm donor susceptibility to sublytic MAC treatment, using TCC MSD as in Figure 31B, post 4-hour stimulation experiment (Figure 34B). As all six donors were stimulated simultaneously on the same day and the number of treatments was reduced for metabolomics analysis to untreated and a sublytic dose of complement using NHS, whereas for proteomics analysis was untreated, sublytic MAC and anti-C7 control. In addition, after the 4-hour stimulation cells were left in the wells and snap frozen at -80 C instead of lifted and counted, to avoid cell loss.
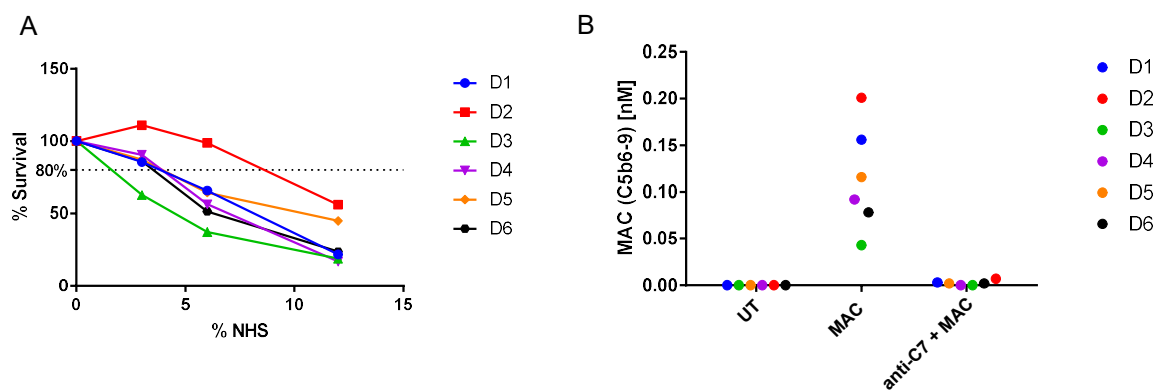
Figure 34. Sublytic MAC confirmation in MDMs from six donors for metabolomics and proteomics analysis prepared on same day (A) CellTiterGlo assay, lysis curves from six donors of MDMs stimulated with increasing doses of NHS. Percentage NHS corresponding to 80% survival for each donor was used for the 4 hours experiment for each donor (n=6). (B) MAC deposition in nanomolar of cell lysates of MDMs, measured by TCC MSD. Conditions used were MAC and untreated. 'D' means donor (n=6).

5.4 Targeted metabolomics in sublytic complement stimulated MDMs shows regulated features enriched in aerobic glycolysis and other glucose related pathways

The resulting targeted metabolomics analysis uncovered 26 upregulated and 62 downregulated features, as shown in the volcano plot and heat map (Figure 35 and 36), with clear separation between complement and untreated conditions and less donor variability than the first round of stimulations for metabolomics analysis (Figure 32). With a focus on changes in glucose metabolism driven by sublytic complement, a significant decrease in early glycolysis (glucose, fructose-6-phosphate) and parallel glucose metabolic pathway intermediates (nucleotide sugar metabolism; uridine 5'-diphosphate) was observed (Figure 37). However, results also showed a significant increase in later glycolysis pathway (3-phosphoglycerate; phosphoenolpyruvate) and decreased intracellular lactate (suggesting increased lactate export, as supported in Figure 21A), highlighting a shift towards aerobic metabolism and a clear involvement of the glycolysis pathway. In addition, a large increase in oxidized glutathione indicated potential oxidative stress, and a clear drop of glutarylcarnitine suggested disruption in mitochondrial fatty acid oxidation, as observed in depletions in fructose-6-phosphate with increased 3-phosphoglycerate, suggestive of increased flux through the pentose-phosphate pathways.
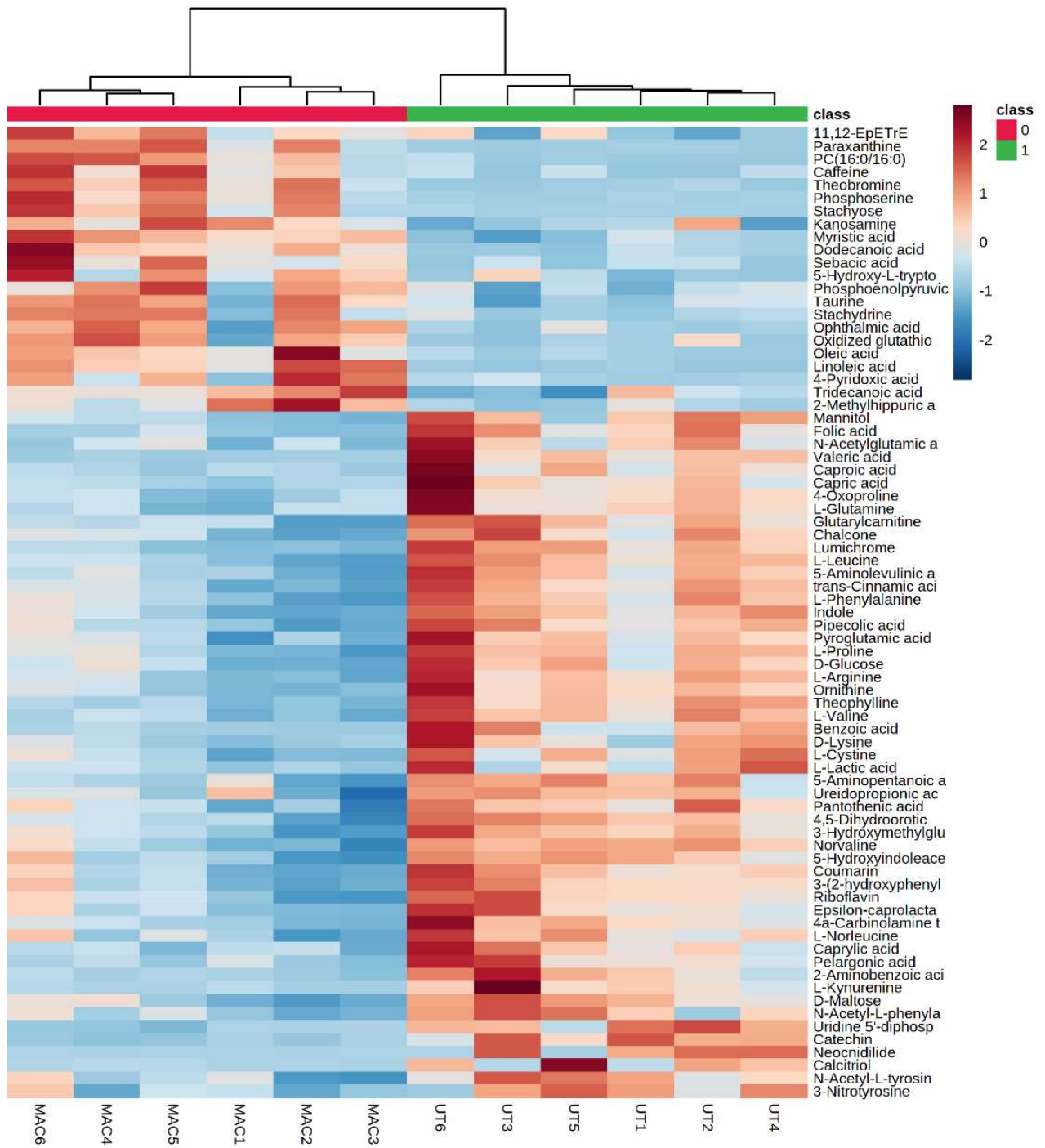
Figure 35. Heat map resulting from targeted metabolomics analysis comparing NHS (named as 0 here, red colour in figure legend) between Untreated (named as 1 here, green colour in figure legend) conditions for each donor (e.g. Untreated 1-6 referring to each donor labelled). n=6
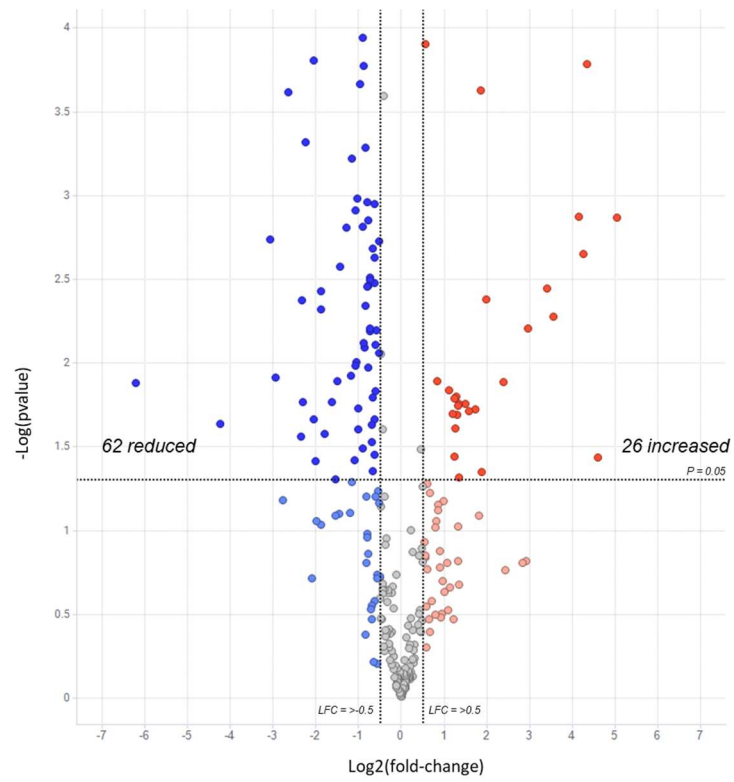
Figure 36. Volcano plot of target metabolomics between untreated and NHS conditions using fold change LFC +/- 0.5 and p value cut-off as 0.05 (n=6).
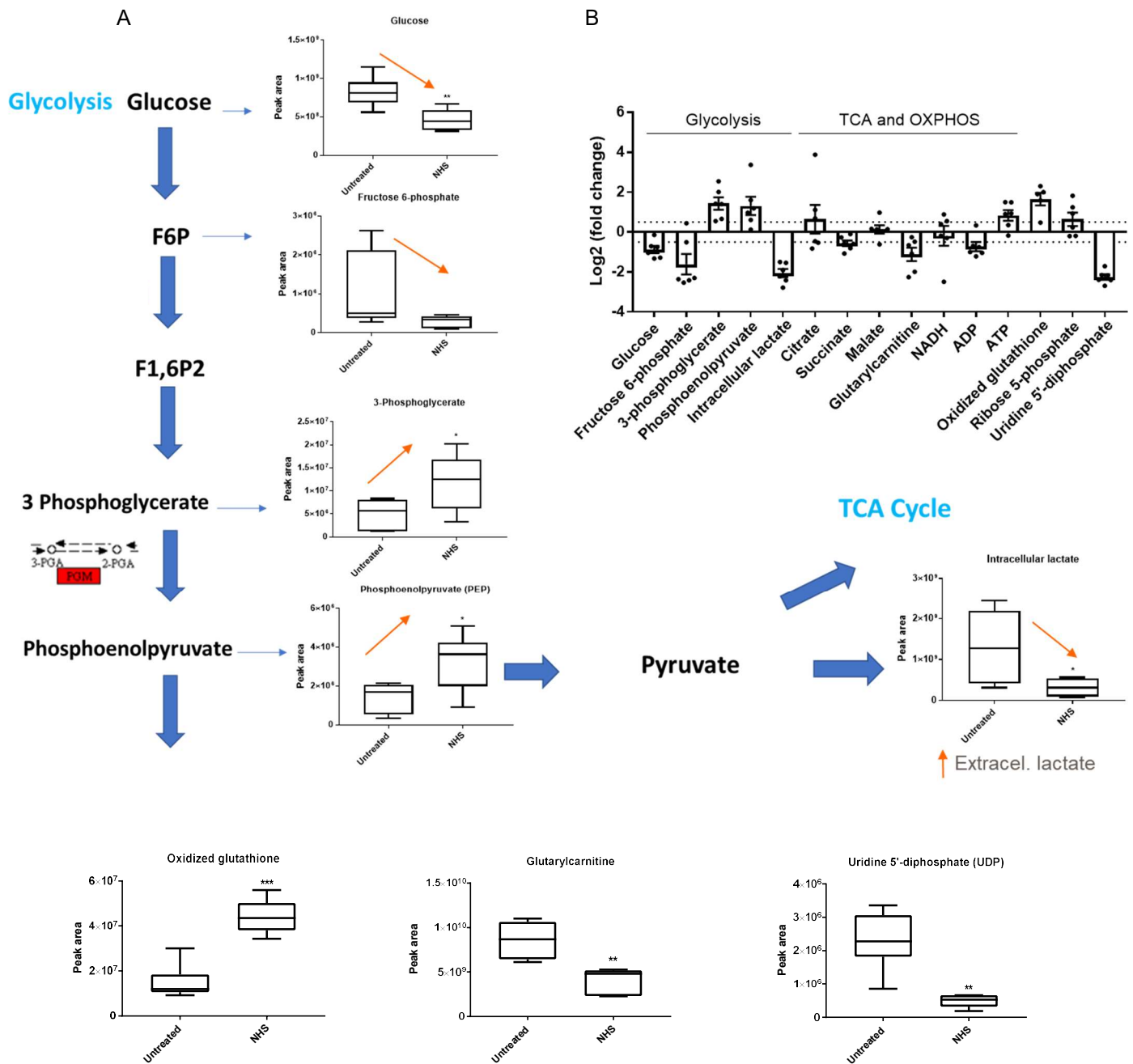
Figure 37. Targeted metabolomics in sublytic complement stimulated MDMs shows regulated features enriched in aerobic glycolysis and other glucose related pathways. Fold change of selected metabolites of glucose metabolic pathways between untreated and NHS conditions (n=6). Raw values of peak area from selected metabolites were plotted in individual graphs (n=6). Statistical significance between untreated and NHS conditions was assessed by unpaired student's t-test with Welch's correction for unequal SDs. Error bars represent +/- S.E.M. Whiskers represent min to max.

5.5 Differentially regulated metabolites induced by sublytic complement stimulation are involved in glycolysis and gluconeogenesis pathways

Based on the list of up- and downregulated metabolites resulting from the analysis, *in silico* enrichment analysis was used to clarify molecular and biological functions of the regulated metabolites, and the pathways they are involved in (Xia and Wishart 2010, Pang, Chong et al. 2021) (Figure 38). Glycolysis and gluconeogenesis and other glucose-mediated pathways, such as Warburg effect or nucleotide sugars metabolism, were captured in the upregulated portion of the altered metabolome. Mitochondrially associated pathways such as fatty acid oxidation were in the top of the list of the downregulated pathways. In addition, a large shift in caffeine metabolism between NHS-treated cells versus untreated was observed in the upregulated pathways, however, this is likely an artefact of adding non diet-controlled NHS to cells. Overall, the targeted metabolomics analysis implicated an increased use of glucose and late glycolytic intermediates, with possible effects in parallel glucose metabolic pathways such as nucleotide sugar metabolism and the pentose phosphate pathway.

A   Upregulated pathways

- Log p-value

126
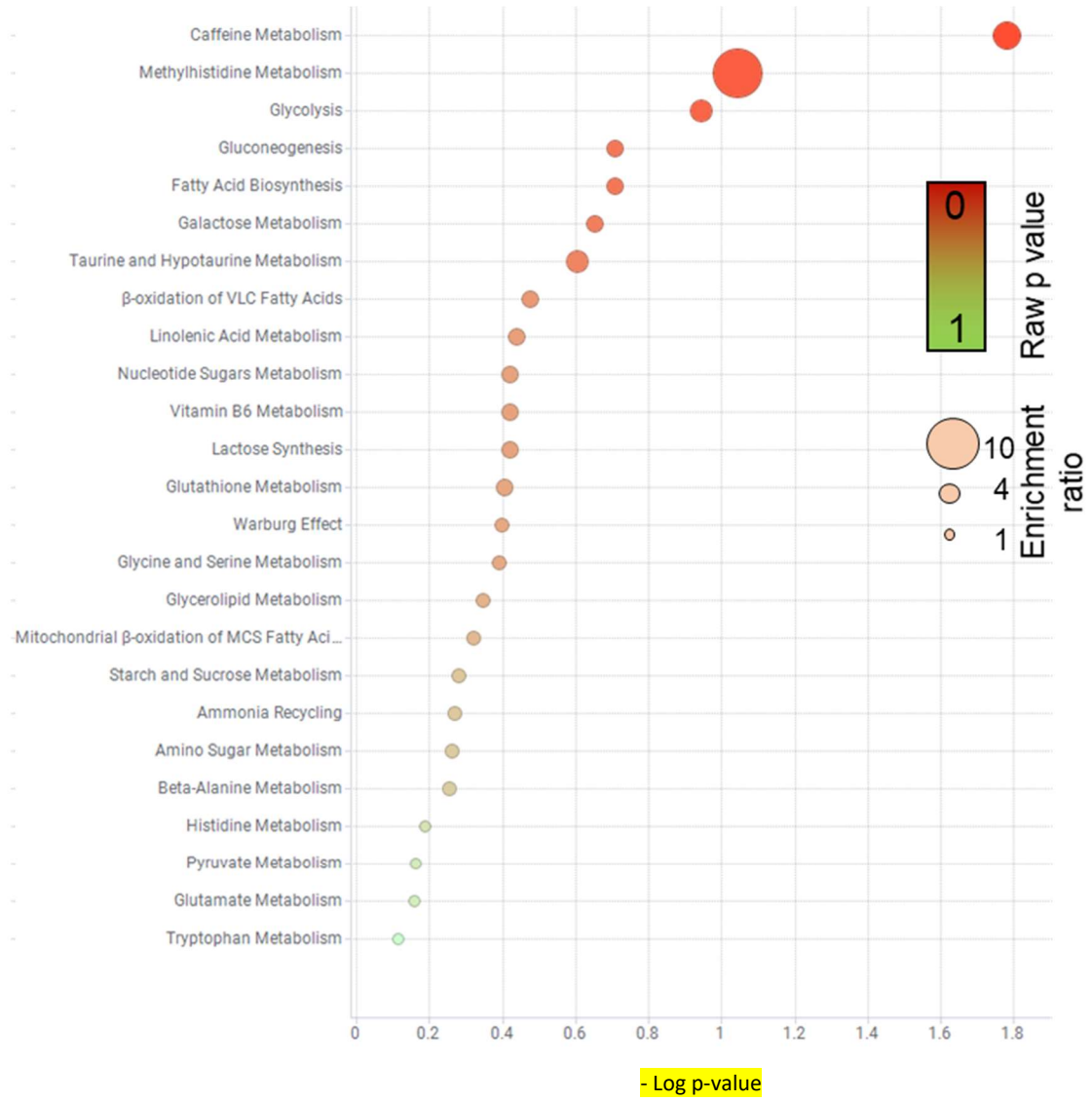
B

Downregulated pathways
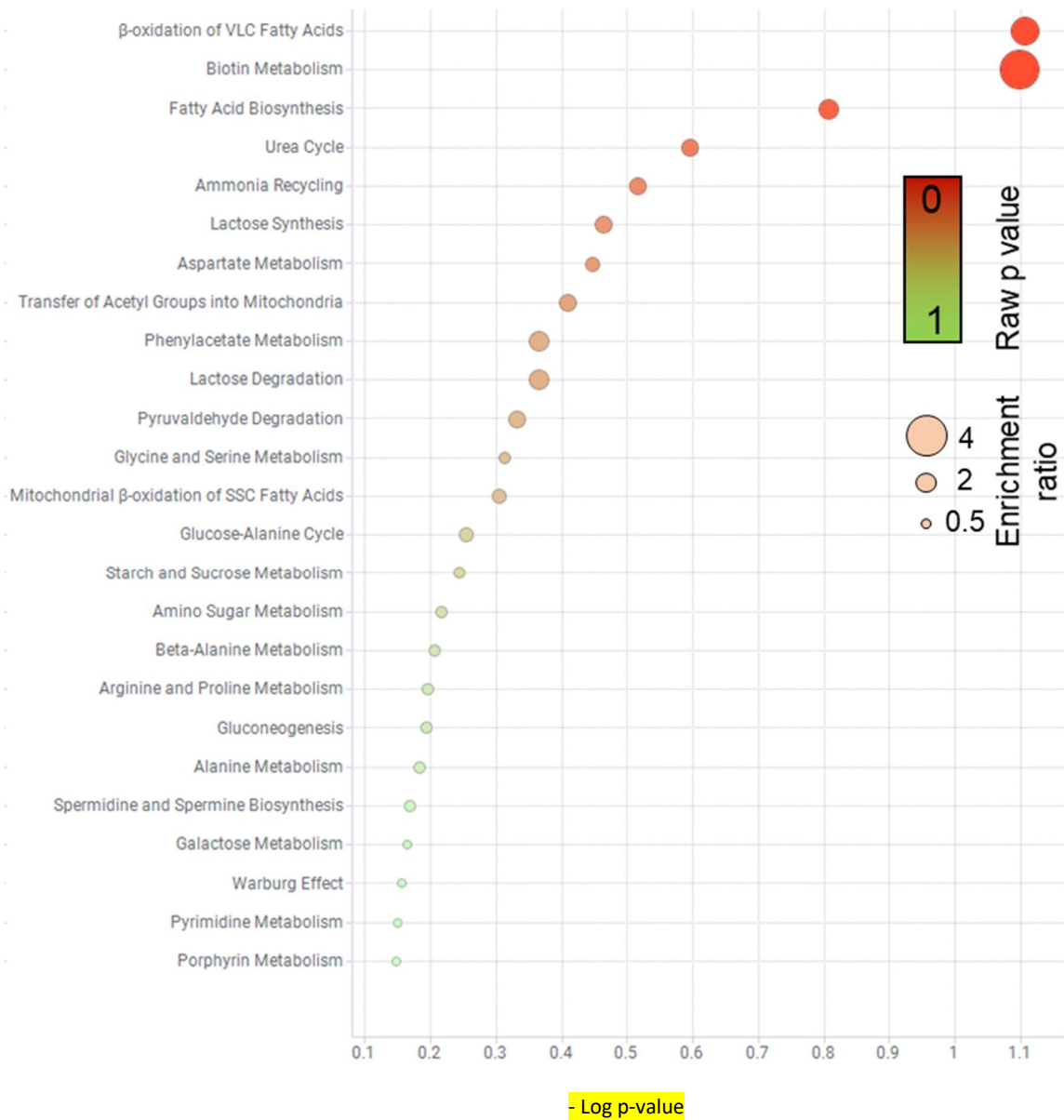
Figure 38. pathway enrichment analysis of upregulated and downregulated metabolites. Enrichment pathway analysis using p value and enrichment ratio to rate the most upregulated (A) and downregulated (B) metabolic pathways comparing NHS treated MDMs vs Untreated control. n=6

127

5.6 Proteomics analysis in sublytic MAC stimulated MDMs shows 462 significantly regulated proteins defined into three clusters

Given the afore-mentioned novel metabolic reprogramming driven by MAC, mtROS production and downstream NLRP3 inflammasome pathway shown in chapter 4, as well as the changes in glucose metabolism and mitochondria from the targeted metabolomics analysis described above, proteomics analysis of MDMs in response to sublytic MAC were performed to gain further mechanistic insight into the proteins that are altered during these changes.

The analysis showed 462 significantly regulated proteins by sublytic MAC after a 4-hour stimulation, based on hierarchical clustering of normalized protein intensities (z-score) (Figure 40A, Appendix B - Supplementary tables 1 and 2) and on a one-way ANOVA comparing MAC to both untreated and anti-C7 plus MAC control groups. Protein intensities normalised to IRS showed a clear treatment separation for all donors and low donor-to-donor variability as observed in the principal component analysis (Figure 39A), with untreated and anti-C7 controls being more similar compared to MAC treatment, which had an extremely strong phenotype from donor 3 that was excluded. Volcano plots showed a similar number of regulated proteins when comparing MAC to both untreated and anti-C7 control groups, with a minority of regulated proteins when comparing untreated to anti-C7, highlighting the return to the untreated baseline when anti-C7 was pre-incubated with MAC (Figure 39B). From the heatmap analysis, protein intensities were defined into three defined clusters based on their response to MAC treatment compared to control groups (Figure 40B). The largest cluster, cluster 2, showed a clear downregulation of protein intensities in response to MAC treatment compared to both control groups untreated and anti-C7, whereas cluster 3 showed the same results with opposite directionality for MAC treatment, where protein intensities showed a MAC-dependent upregulation. Cluster 1 showed a minority of proteins that were downregulated by both MAC and anti-C7 treatments compared to untreated, possibly due to other complement proteins apart from MAC causing an effect.
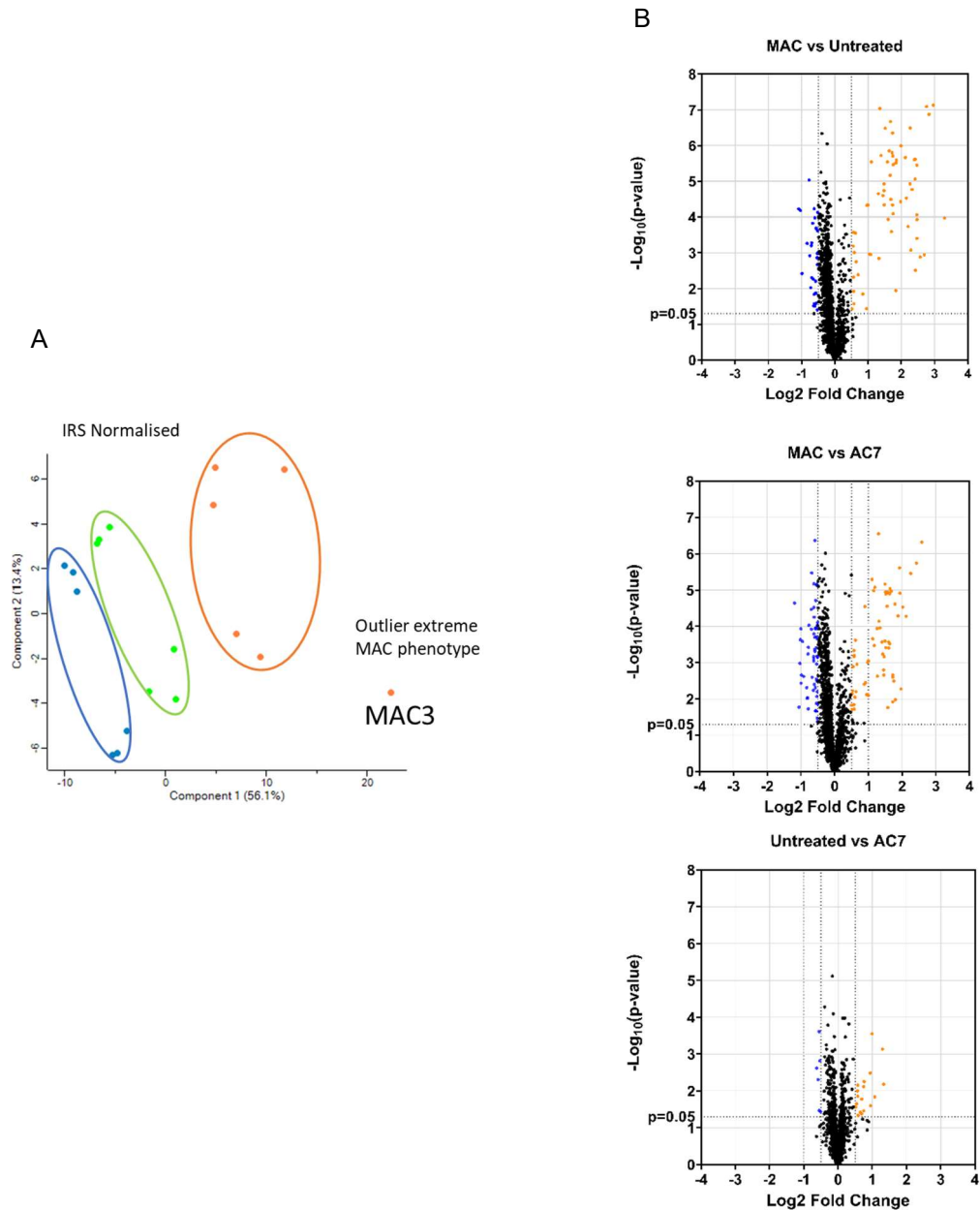
Figure 39. Principal component analysis and volcano plots from proteomics analysis show a clear treatment separation for all donors, low donor-to-donor variability and recovery to the untreated phenotype with anti-C7 control. MDMs treated with sublytic MAC, anti-C7 or untreated controls for 4 hours (n=6 independent donors). (A) Principal component analysis graph from IRS normalised protein intensities (see methods) showing untreated (blue), anti-C7 (green) and MAC (orange) treatments from all six donors. MAC treatment from donor 3 is marked as an outlier due to an extremely strong phenotype and was excluded. (B) Volcano plots representing all proteins from the analysis using a Log 2 fold change at 0.5 and unpaired t-test p<0.05.
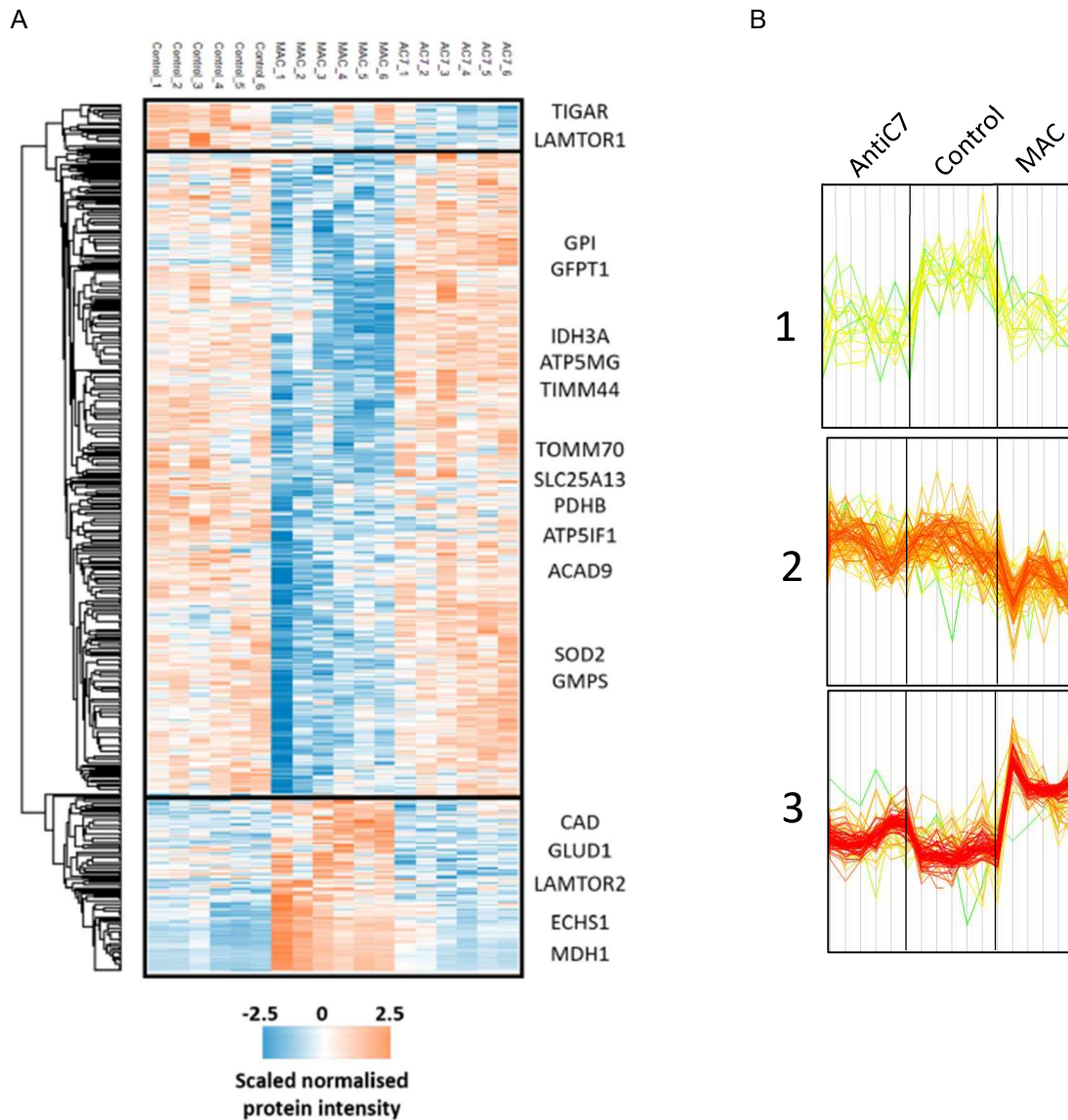
Figure 40. Proteomics analysis in sublytic MAC stimulated MDMs shows 462 significantly regulated proteins defined into three clusters. MDMs treated with sublytic MAC, anti-C7 or untreated controls for 4 hours (n=6). (A) Hierarchical clustering of normalized protein intensities (z-score) for significantly regulated proteins (ANOVA permutation, FDR based <0.05) (N= 462 regulated proteins). Mitochondrial proteins of interest are highlighted in their corresponding cluster. (B) Expression profiles of proteins in three selected clusters corresponding to (A) showing distinct behaviours: 1) downregulation in MAC stimulated and anti-C7 stimulated samples; 2) downregulation in MAC treated samples and rescue to UT baseline with anti-C7; and 3) downregulation in MAC treated samples and recovery with anti-C7.

5.7 Analysis of proteomic alterations caused by sublytic MAC highlights enhanced aerobic glycolysis and mitochondrial dysfunction by altered pyruvate and TCA metabolism, mitochondrial respiration and other altered metabolic pathways

Due to the large size of the analysis, a list of significantly regulated proteins by sublytic MAC focusing on glucose metabolism and mitochondrial function was extracted (Figure 41). Interestingly, key regulated proteins involved in the early stages of glycolysis (GFTP1 and GPI) and inhibition of pyruvate dehydrogenase were observed by downregulation of PDHB, suggesting aberrant preferential activation of glycolysis and consequential disruption of the TCA cycle (Yonashiro, Eguchi et al. 2018). These observations were supported by longer term upregulation of PDK4 gene expression by MAC (Figure 29), as well as PFKFB3, HIF1α and IL-1β, which have been involved in supporting long-term metabolic alterations in macrophages (Park and Jeoung 2016) (Kelly and O'neill 2015, O'Neill, Kishton et al. 2016).

A possible diversion towards parallel glucose metabolic pathways such as glutamine and glutamate metabolism was also observed, specially by regulation of GFPT1, GLUD1, GMPS and CAD. In glycolytic cancer cells, glutamine metabolism has been involved in feeding carbon source to TCA cycle intermediates, which then act as biosynthetic precursors (DeBerardinis, Mancuso et al. 2007, Tong, Zhao et al. 2009). Here, key regulated proteins involved in TCA cycle and mitochondrial respiration included IDH3, ATP5GM, ATP5IF1, MDH1 and ACAD9. Furthermore, regulation of SOD2 – a key regulator of mitochondrial superoxide, indicated changes in mtROS. Regulation of TIMM44 and SLC25A13 indicated involvement in mitochondrial import of metabolites. MAC also showed regulation of LAMTOR 1/2, also involved in metabolite transport and mTORC1 activation, which is known to promote glycolysis and subsequent NLRP3 inflammasome activation in macrophages (Moon, Hisata et al. 2015). In addition, a marked regulation of ESCH1 indicated involvement in the mitochondrial fatty acid beta-oxidation pathway, which was also regulated in metabolomics analysis (Figure 38). Overall, these results pointed out the translatable mechanistic effects in MDMs caused by MAC stimulation and confirmed the involvement of glycolysis and mitochondrial dysfunction pathways, characterised by altered pyruvate metabolism and other altered mitochondrial pathways.
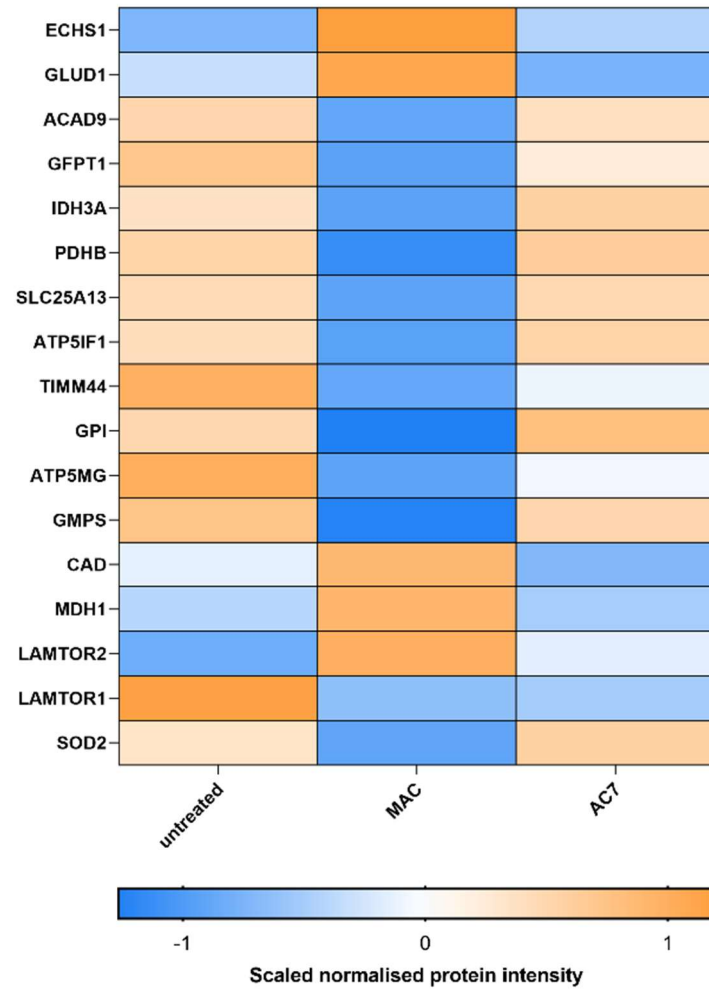
Figure 41. Hierarchical clustering of normalized protein intensities (z-score) for significantly regulated metabolic proteins of interest, which were identified as described in the main text and methods section. MDMs treated with sublytic MAC, anti-C7 or untreated controls for 4 hours (n=6). Statistical analysis performed was one-way ANOVA, FDR corrected, with post-hoc Tukey's test p<0.05 significant for both Untreated vs MAC and MAC vs AC7 (N= 17 regulated proteins).
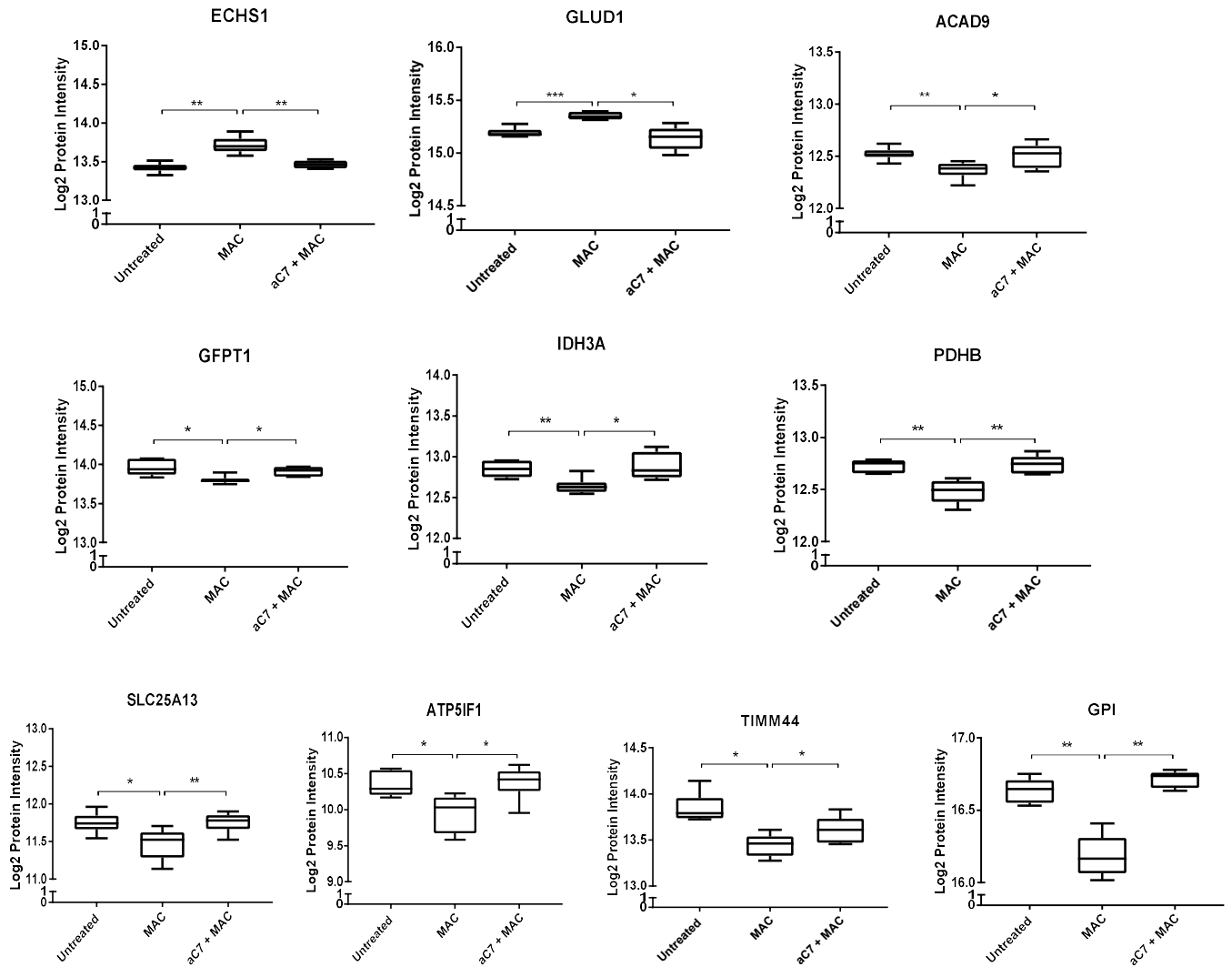
Figure 42. Fold change of significantly regulated metabolic proteins of interest represented in individual graphs. MDMs treated with sublytic MAC, anti-C7 or untreated controls for 4 hours (n=6). Statistical analysis performed was one-way ANOVA, FDR corrected, with post-hoc Tukey's test p<0.05 significant for both Untreated vs MAC and MAC vs AC7 (n=6). Whiskers represent min to max.

Based on the list of all up- and downregulated proteins by MAC resulting from the analysis (Appendix B, supplementary tables 1 and 2), gene ontology enrichment analysis was used (Ashburner, Ball et al. 2000, Mi, Muruganujan et al. 2019, 2021) to clarify molecular and biological functions of the regulated proteins, and the pathways they are involved in (Figure 43). Regulation of protein and macromolecular metabolic processes, as well as defence response were captured in the upregulated portion of the altered proteins by MAC, while molecule metabolic process, generation of precursor metabolites and energy, and response to external stimulus were part of the top downregulated pathways. Changes in caffeine metabolism enzymes at a proteomic level were not observed. These results clearly indicated the relevance and involvement of metabolic pathways regulated by sublytic MAC stimulation.

A

B
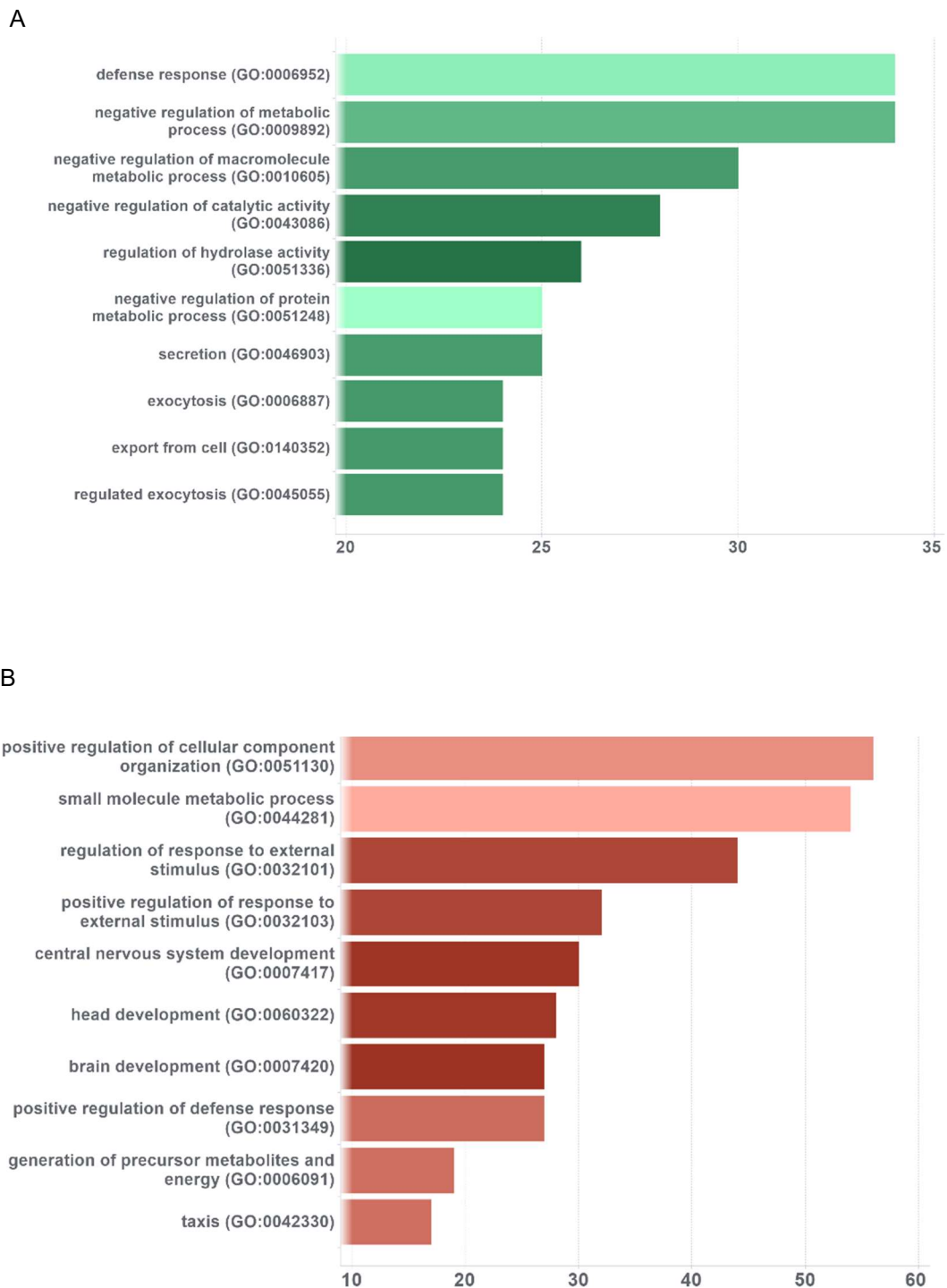
Figure 43. Pathway enrichment analysis of upregulated and downregulated proteins.
Top 10 list of MAC up and downregulated pathways from proteomics data using statistical enrichment test for GO biological processes analysis (A) (N= 99 upregulated proteins) (B) (N= 363 downregulated proteins). See methods section.

5.8 Top overall significantly regulated proteins by sublytic MAC included apolipoproteins, host complement proteins and proteins linked to elevated cytosolic calcium and metabolic pathways

In order to have a broader interpretation of the proteomics analysis with a focus on other pathways than metabolic and mitochondrial changes, a selection of significantly regulated proteins by sublytic MAC showing the largest changes in Log2 protein intensities, were plotted in individual graphs (Figure 44). Results showed a strong regulation of apolipoproteins (APOA1//2/4, APOC3, apolipoprotein A-IV), known to interact with the MAC complex and which have been implicated in Alzheimer's disease, attenuating classical complement activation (Kim, Basak et al. 2009, Yin, Ackermann et al. 2019). Host complement proteins that are likely to be involved with the MAC activation pathways also showed a strong upregulation by MAC (CFB, C4BPA, C3, C4a, C1R, CFH and C6). In addition, other relevant proteins linked to complement regulation (vitronectin, serum amyloid P-component and 2,5 phosphodiesterase 12) also showed to be upregulated by MAC.

Protein interaction analysis of the proteins significantly regulated upon MAC treatment was explored by constructing a protein interaction network diagram with the STRING database, named Functional STRING networks (Figure 45), to reveal numerous interacting links of biological relevance between the regulated proteins. The top network shows nodes size based on p-value (larger nodes = lower p-value) while the bottom network shows nodes colour based on Log2 Fold change. Several regulated proteins coincided between the two networks, being the largest and most significant regulated proteins by sublytic MAC stimulation. The main regulated proteins showing biological connection, with their respective nodes being connected, were mainly involved in the response to elevated platelet cytosolic Ca2+ pathway (CLU, SERPING1, SERPIND1). Other highly regulated proteins, although not showing biological connection between them, also showed involvement in elevated platelet cytosolic Ca2+ pathway (AHSG, ITIH4), as well as glucose metabolism (PPBP, AHSG) and metabolism of proteins (ITIH2). Interestingly, highly regulated proteins also included UBR2, involved in NLRP1 inflammasome activation (Xu, Shi et al. 2019), and SERPING1, the C1 inhibitor which inhibits activated C1r and C1s of the first complement component and thus regulates complement activation (Ponard, Gaboriaud et al. 2020). Finally, another highly regulated protein by MAC, HP, is known to be linked to diabetic nephropathy (Conway, Savage et al. 2007), where MAC deposition contributes to pathology (Flyvbjerg 2017).
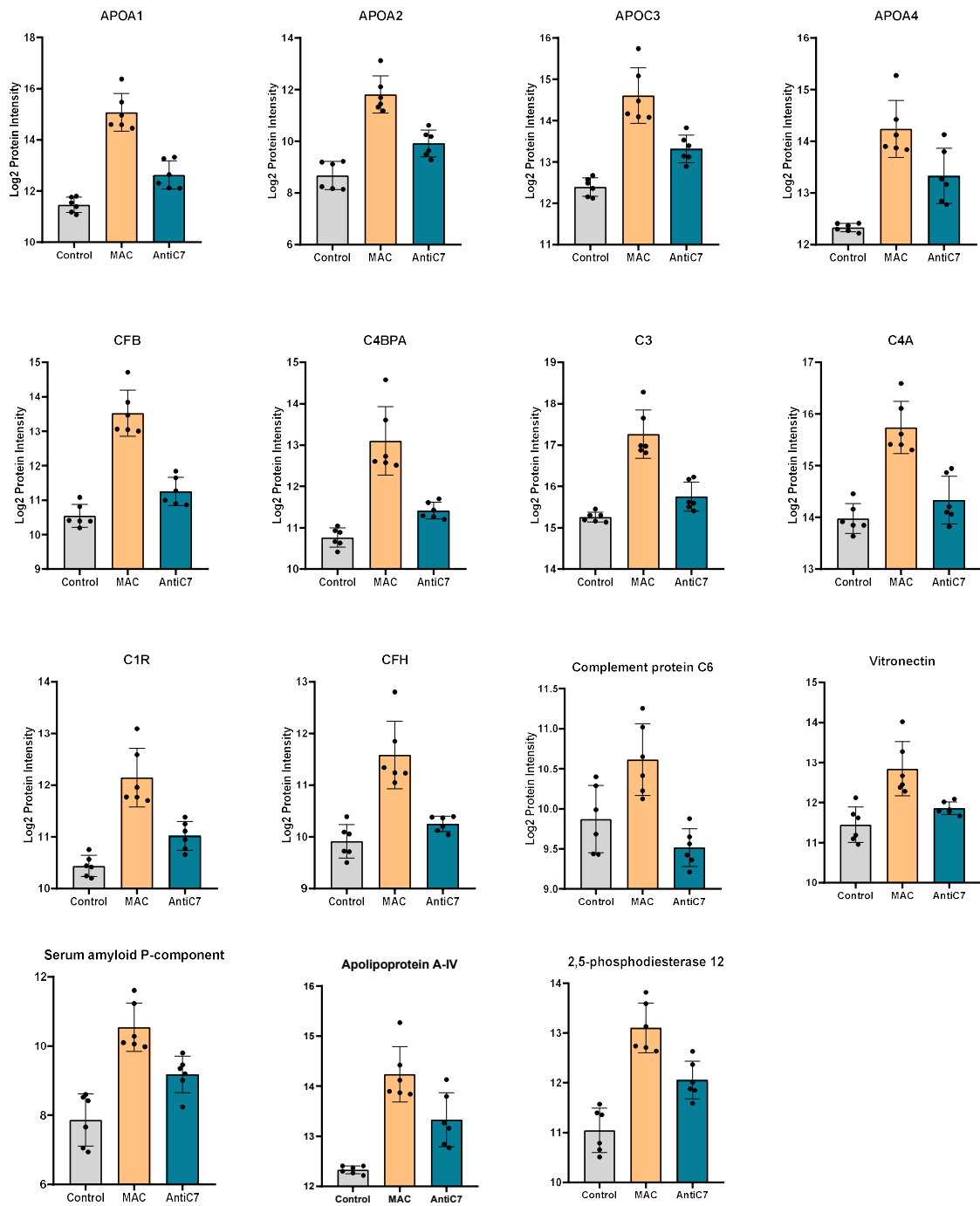
Figure 44. Selection of top overall significantly regulated proteins by sublytic MAC. MDMs treated with sublytic MAC, anti-C7 or untreated controls for 4 hours (n=6). Fold change of protein intensities of selected top overall significantly regulated proteins by MAC. Statistical analysis performed was one-way ANOVA, FDR corrected, with post-hoc Tukey's test $p<0.05$ significant for both Untreated vs MAC and MAC vs AC7.
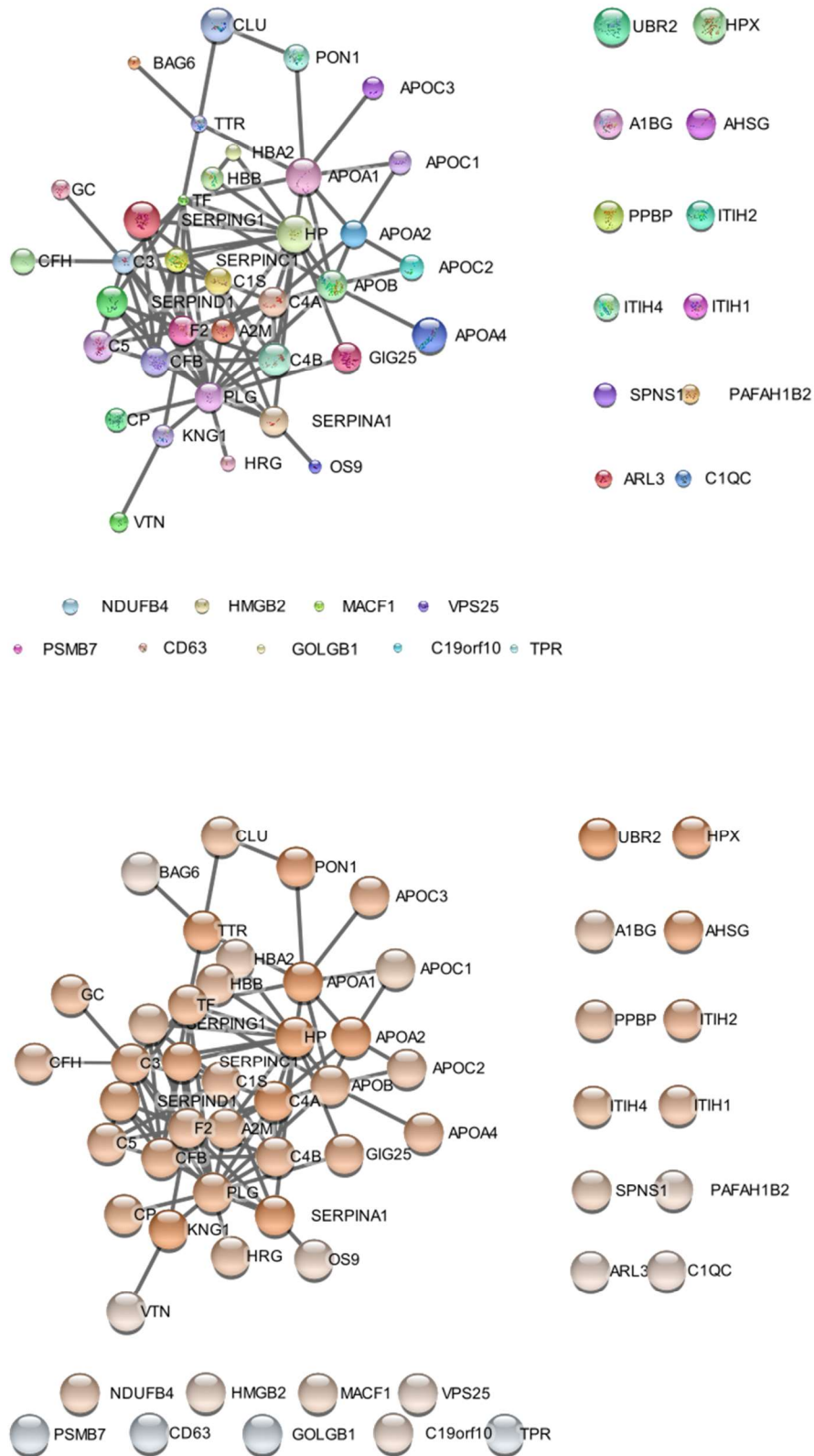
Figure 45. Functional STRING networks of all proteins from proteomics analysis significantly regulated upon MAC treatment created through stringAPP in Cytoscape. Permutation based FDR<0.05. Top network: nodes are sized based on p-value, larger nodes = lower p-value. Bottom network: Nodes are coloured based on Log2 Fold change (-2.5 - 2.5). n=6.

Overall, metabolomics and proteomics analysis have provided crucial insight on the mechanistic effects upon sublytic MAC stimulation (Figure 46), confirming a shift towards aerobic glycolysis with an increase of the late-stage glycolysis intermediates and subsequent lactate production, as well as giving insight into the mitochondrial dysfunction pathways. These were characterised by inhibition of pyruvate dehydrogenase complex, a possible diversion towards parallel glucose metabolic pathways, such as glutamate metabolism by increased GLUD1, and a resulting altered regulation of the TCA cycle by regulation of relevant proteins such as IDH3, which in turn affected mitochondrial respiration by alteration of proteins such as ATP5IF1, leading to mtROS production. These data were aligned with previous data in GM-CSF MDMs from chapter 4 showing sublytic MAC driving calcium influx and increased glycolysis characterised by extracellular lactate production, mitochondrial dysfunction characterised by collapsed mitochondrial respiration, fragmented mitochondrial morphology and increased mitochondrial ROS production. Finally, this increase in glycolysis and mtROS activated the NLRP3 inflammasome with caspase 1 activation, subsequent IL-18 and GSDMD cleavage, providing signalling for active pro-inflammatory cytokine. Longer term changes in gene expression also included increases in key pathways associated with pro-inflammation and glycolysis (Figure 46).
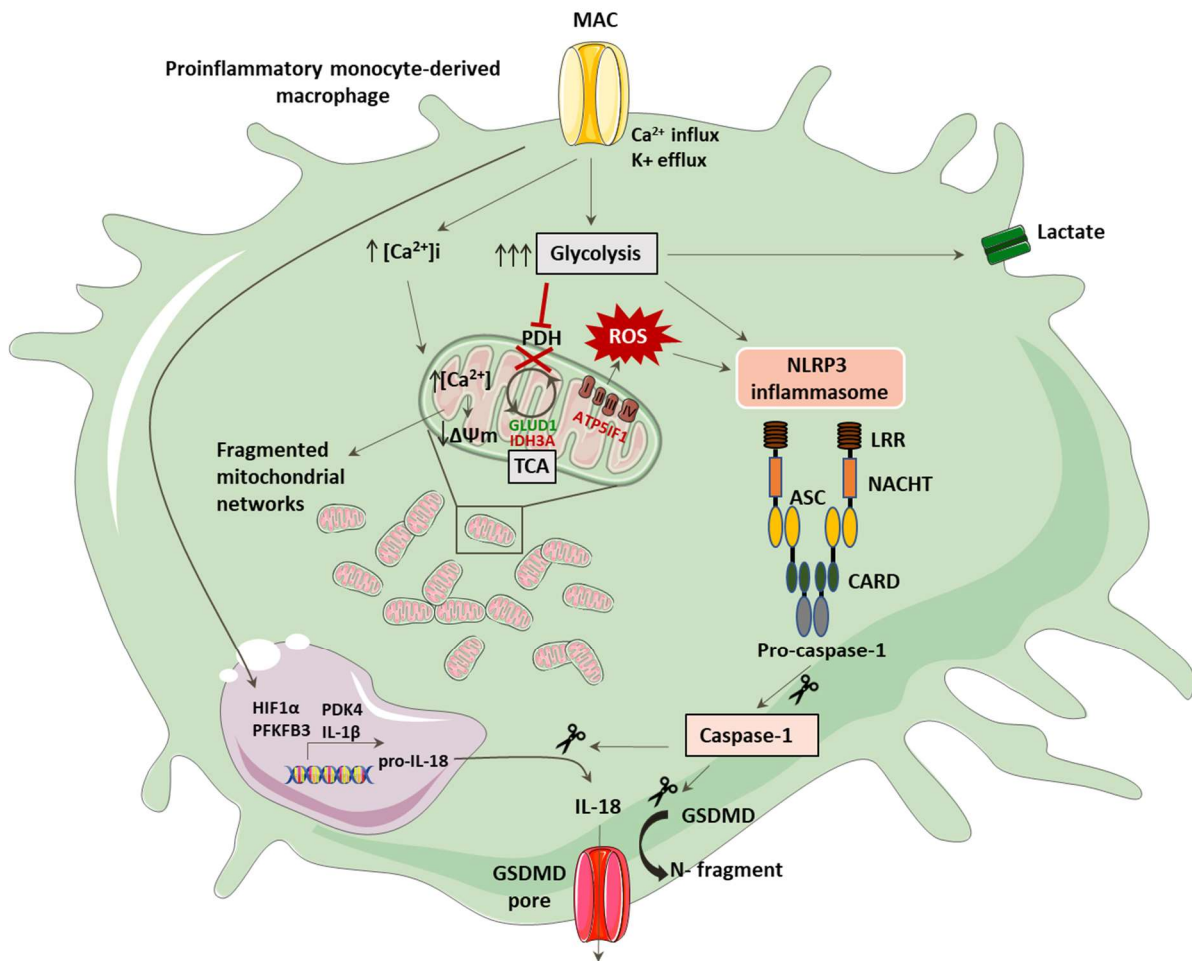
Figure 46 Schematic of sublytic MAC signalling in MDMs. MAC binding drives ion flux, increased cytosolic calcium and glycolysis characterised by increased extracellular lactate. MAC stimulation also drives mitochondrial dysfunction characterised by increased mitochondrial calcium, depolarisation of the mitochondrial membrane potential, fragmented mitochondrial morphology, as well as inhibition of pyruvate dehydrogenase (PDH) and therefore altered regulation of the TCA cycle (as seen by altered regulation of proteins such as GLUD1 and IDH3A), with subsequent collapse of mitochondrial respiration and increased mitochondrial ROS production. This activates NLRP3 which in turn mediates caspase 1 activation with subsequent IL-18 and GSDMD cleavage, leading to release of pro-inflammatory IL-18 cytokine. Longer term changes also include increases in key pathways associated with pro-inflammation and glycolysis.

5.9 Discussion

This study aimed to investigate the translatable mechanistic effects involved in the immunometabolic changes driven by sublytic MAC in MDMs by metabolomics and proteomics analysis, expanding on the functional data provided in chapter 4. As a reminder, both metabolomics and proteomics experiments were performed locally in GSK Stevenage, UK and sent to collaborators in GSK Upper Providence, US, where lysates were run and raw data was generated and sent back for analysis. Initial experiments to generate samples for proteomics and metabolomics analysis resulted in significant cell loss due to attempted lifting of MDMs from plates post stimulations, as well as significant donor-to-donor variability within the same treatment due to donor preparation on separate days, making it difficult to use donors in classical sense of replicates. Therefore, a second round of experiments was performed avoiding lifting of MDMs and preparing all six donors and stimulations on the same day. Such optimisation was crucial to reduce unwanted donor-to-donor variability and results showed a clear treatment separation for all donors. Metabolomics treatment conditions were reduced to untreated and sublytic complement, where MDMs were stimulated with a sublytic dose of NHS, whereas proteomics was performed with three treatment conditions including untreated, MAC and anti-C7 control, showing a significant number of proteins regulated specifically by sublytic MAC. The lack of anti-C7 control in metabolomics analysis was a caveat of this study and limited metabolomics results to general complement effects. Future studies should add an anti-C7 control to confirm the metabolomics results of this study as MAC-dependant effects either on a global metabolomic level or to probe metabolite networks of interest.

Both the targeted metabolomics and proteomics analysis supported a general shift to aerobic glycolysis and gave insight into the mitochondrial dysfunction observed above. Particularly, with the increase of the late-stage glycolysis intermediates with subsequent decrease of intracellular lactate, which supported the gradual increase of extracellular lactate observed in chapter 4 (Figure 21A). The downregulation of PDHB, together with the afore-mentioned increased gene expression of PDK4, indicate inhibition of pyruvate dehydrogenase complex, supporting aberrant preferential activation of glycolysis (Yonashiro, Eguchi et al. 2018) (Van den Bossche, Baardman et al. 2016). A downregulation of metabolites and proteins in the early stage of glycolysis indicated a possible diversion towards parallel glucose metabolic pathways, such as glutamine, glutamate and nucleotide sugar metabolism by regulation of key metabolites and proteins GFPT1, GLUD1, L-Glutamine and UDP. This pointed towards a possible compensation mechanism for the limited mitochondrial delivery of pyruvate, as glutamine and glutamate metabolism are known to feed carbon source to the TCA cycle in glycolytic cancer cells,

leading to subsequent efflux of substrates for use in biosynthetic pathways (DeBerardinis, Mancuso et al. 2007, Tong, Zhao et al. 2009). Accordingly, key proteins of the TCA cycle and respiratory chain were also regulated by MAC and were likely involved in the molecular mechanism driving mitochondrial dysfunction. For instance, regulation of ATP5IF1, which limits ATP depletion upon loss of mitochondrial membrane potential below a threshold, inhibiting OXPHOS and mediating a shift to enhanced aerobic glycolysis (Campanella, Parker et al. 2009, Weissert, Rieger et al. 2021). Proteomics and metabolomics data also supported our mtROS production data by downregulation of SOD 2, as well as increased oxidized glutathione.

Interestingly, a study using transcriptomics, proteomics, and metabolomics analysis to assess metabolic features that are critical for macrophage activation (Bordbar, Mo et al. 2012), defined five metabolic objective functions associated with general macrophage function and activation, among which were energy (ATP) generation and redox maintenance (NADH), as macrophages require high glycolytic activity to generate ATP and NADH for essential functional purposes. In addition, the study evaluated the suppressive effects of tryptophan uptake to identify intracellular reaction changes linked to metabolites with suppressive properties. Their results showed that macrophages entered a ketogenic-like state during increased tryptophan uptake, resulting in increased production of reduced gluthathione and decreased pyruvate dehydrogenase activity, a switch characteristic of a ketogenic state (Wang and De Vivo 2018). These findings were aligned with data showed in this study, where macrophages have inhibition of pyruvate dehydrogenase, suggesting a possible mechanism where MAC drives MDMs into a ketogenic state, having increased tryptophan uptake, which would be an interesting route of investigation for future studies. Interestingly, another study showed that fasting individuals in ketosis are known to have decreased inflammation (Garai, Lóránd et al. 2005).

Proteomics analysis also showed a strong regulation of apolipoproteins, which have been implicated in Alzheimer's disease (AD), attenuating classical complement activation (Bordbar, Mo et al. 2012) by high-affinity binding to the initiating C1q protein. In addition, another study showed enhanced binding of apolipoproteins A-I and A-II to human endothelial cells exposed to activated complement. Interestingly, complement activation through C9 polymers expressed binding sites for apoA-I and -A-II (Hamilton, Zhao et al. 1993), suggesting a specific role for MAC in these interactions and a possible more direct involvement with AD. ApoE, with human alleles being ApoE2, ApoE3, and ApoE4, is known to carry cholesterol and other lipids in the blood, and the presence of ApoE4 is known to increase the risk of AD (Liu, Zhao et al. 2017, Yin, Ackermann et al. 2019).

In addition, host complement proteins that are likely to be involved with the MAC activation pathways (CFB, C4BPA, C3, C4a, C1R, CFH and C6) and other relevant proteins linked to complement regulation such as serum amyloid P-component (SAP) were also upregulated by MAC in the proteomics analysis. Interestingly, SAP regulates complement activation also by interacting with C1q, as well as members of the ficolin family and the complement regulator C4-binding protein (C4BP) (Doni, Parente et al. 2021), activating complement and interacting with Fcγ receptors. In addition, one of the top upregulated proteins by MAC, SERPING1, is known to be the C1 inhibitor which inhibits activated C1r and C1s of C (Ponard, Gaboriaud et al. 2020), and thus regulates complement activation. These results elucidate novel strong links between MAC and other complement proteins such as C1, via apolipoproteins, SAP and SERPING1 in MDMs.

Functional protein networks of proteomics analysis also identified novel strong connections between MAC and the top upregulated proteins from the analysis. These proteins were mainly involved in the response to elevated platelet cytosolic Ca2+ pathway (CLU, SERPING1, SERPIND1, AHSG and ITIH4), indicating possible involvement in the mechanism of increased mitochondrial Ca2+ driven by MAC observed in this thesis (see chapter 4). Interestingly, top regulated proteins by sublytic MAC also included proteins relevant in glucose metabolism (PPBP, AHSG) and metabolism of proteins (ITIH2), which is in synergy with the above observations. UBR2, another highly regulated protein from the analysis, is known to be involved in NLRP1 inflammasome activation (Xu, Shi et al. 2019), indicating a possible involvement of other inflammasomes other than NLRP3 to be activated by MAC, which to date remains to be explored. Finally, another highly regulated protein by MAC, HP, is known to be linked to diabetic nephropathy (Conway, Savage et al. 2007), where MAC deposition was found to be increased and plays an important role in disease progression (Flyvbjerg 2017, Liu, Li et al. 2017, Koopman, Van Essen et al. 2021).

Overall, the proteomics and metabolomics analysis performed in this study show synergy in their findings and support the overall conclusions of this thesis whilst also providing novel ground for exploring potential drivers of MAC-mediated metabolic reprogramming and potential biomarker opportunities in MAC-mediated disease. Future studies should look at the specific relative contribution of MAC-mediated immunometabolically altered macrophages in disease and whether interventions focused on pathways discussed above improve disease outcomes in these models.

6. Chapter 6: Conclusion

Initially, this project set out to investigate the metabolic mechanisms driven by MAC that support or modulate inflammasome activation in MDMs, and to investigate the regulation of these metabolic and inflammasome changes in Alzheimer's disease (AD). However, what we set out to do in context of complement-neuroimmunology angle was not possible due to the COVID-19 pandemic, causing restrictions in working spheres where we had to limit our focus to the work covered here and specific COVID-related work that is not disclosed in this thesis. In addition, part of the data shown in chapters 4 and 5 has recently been published in Frontiers of Immunology by the author of this thesis (Jimenez-Duran, Kozole et al. 2022).

The role of complement, not only as an anti-microbial detection system, but as a modulator of other immune pathways, metabolic pathways and inflammasome, as well as its relevance in multiple autoimmune conditions, led to a new appreciation of complement as an immunometabolic regulator that is able to function intra- as well as extracellularly (Michailidou, Jongejan et al. 2018, Lage, Wong et al. 2020, Xie, Jane-Wit et al. 2020). The discovery of intracellular complement, specifically C3a generation and downstream signalling in CD46, C3b and C3aR causing metabolic regulation (by glycolysis/OXPHOS changes) of inflammasome activation in T-cells, brought attention to a complement-metabolism-inflammasome axis (Arbore and Kemper 2016). Studies in synovial fibroblasts and cells of the CNS followed on this concept by showing that other complement components such as C3 and C1q can also shift the metabolic profile of these cells (Benoit and Tenner 2011, Friščić, Böttcher et al. 2021). However, whether MAC was involved in this axis was unknown. The role of host-derived endogenous regulators of immunometabolism is still not as well studied compared to exogenous stimuli (PAMPs) such as LPS, which are known drive metabolic reprogramming of immune cells to fuel their immune functions such as cytokine output (Mills, Kelly et al. 2016). Triantafilou and colleagues, our lab, showed that sublytic MAC acts as an endogenous trigger of NLRP3 inflammasome activation via calcium flux and mitochondrial membrane potential changes in epithelial cells (Triantafilou, Hughes et al. 2013). However, whether there were any metabolic changes fuelling this MAC-driven inflammasome activation or if this happened in immunological cell types as well, remained obscure. Given these observations have relevance for mitochondrial biology, the purpose of this study was to investigate immunometabolic effects driven by MAC in a primary immunological cell type, MDMs, and

downstream consequences of such alterations to confirm NLRP3 activation, similar to other immune stimuli in myeloid cells.

6.1 Sublytic MAC drives glycolysis-dependant inflammasome activation, reactive oxygen species and lactate production in naïve M-CSF human monocyte-derived macrophages

Naïve MDMs differentiated with M-CSF were initially used for the experiments of this study, using MAC as the pro-inflammatory stimulus to drive NLRP3 activation. Assessment of cytokine secretion of IL-1β, which was dependant on NLRP3 and caspase-1, as well as IL-18 secretion, protein expression of pro-IL-1β and gene expression of NLRP3 and Caspase-1 confirmed NLRP3 inflammasome activation by a sublytic dose of MAC in naïve MDMs, confirming Triantafilou's and Laudisi's findings (Laudisi, Spreafico et al. 2013, Triantafilou, Hughes et al. 2013). Interestingly, a very recent study also showed a MAC-driven NLRP3 activation and IL-1β secretion in the same cell type as here, naïve MDMs, via internalisation of MAC into the cell (Diaz-del-Olmo, Worboys et al. 2021). However, the system used to induce MAC stimulation in that study was using LPS, as priming signal for inflammasome activation, plus purified components of the MAC complex, C5b6-9. Conversely, in this thesis, human serum was used as a more physiological source of complement proteins for MAC stimulation. LPS has been used in many macrophage studies to understand the metabolic mechanisms that modulate inflammation; however, this study aims to understand the immunometabolic changes caused by MAC without the well-known effects of LPS, and understanding endogenous triggers of immunometabolic changes associated with inflammation have more relevance in sterile inflammation scenarios. In addition, C5a has been shown to act as an NLRP3 priming signal (Samstad, Niyonzima et al. 2014, Cao, Wang et al. 2016), therefore, inflammasome activation by complement can happen without external priming stimuli. The present study supports these findings as MDMs treated with control C7-depleted NHS, to block MAC formation, still showed expression of pro-IL-1β, suggesting that other complement components than MAC, potentially C5a, are acting as a priming signal for NLRP3 inflammasome activation.

Importantly, this study demonstrated that sublytic MAC drives an increase in extracellular lactate, viewed here as a by-product of increased glycolysis, and that blockade of glycolysis using inhibitors resulted in inhibition of MAC-mediated NLRP3 priming and activation, by decreased expression and secretion of pro-IL-1β and inflammatory cytokines IL-1β and IL-18, respectively. Studies in macrophages have shown that glycolysis, among other metabolic pathways, are responsible for supporting NLRP3 inflammasome activation and a switch from glycolysis to OXPHOS mediates inhibition of inflammasome activation

(De Nardo and Latz 2011, O'Neill, Kishton et al. 2016). These studies, however, used LPS as a stimulus, but the metabolic changes and modulation of NLRP3 downstream of MAC stimulation were unknown.

Further, the present study also shows that sublytic MAC drives increased expression of genes involved in glucose and amino acid metabolism and ROS production. Increased expression of glucose channel GLUT1 and (Kolev, Dimeloe et al. 2015)– further demonstrated the involvement of MAC as a modulator of glucose metabolism and, interestingly, increased expression of the amino acid channel LAT1, which was dependant on glycolytic enzyme GAPDH, pointed towards MAC-driven changes in amino acid metabolism, which may be subsequent to the observed glycolytic changes, known to generate precursors for the synthesis of amino acids and fatty acids (Kalhan and Hanson 2012). In addition, although the MAC-driven ROS production wasn't tested to be of mitochondrial origin in naïve MDMs, studies in macrophages described that mitochondrial ROS via reverse electron transport was subsequent to increased levels of glycolysis caused by LPS stimulation (Mills, Kelly et al. 2016, O'Neill, Kishton et al. 2016), indicating a potential involvement of mitochondrial biology downstream of MAC, linked to the observed glycolytic changes, which was covered in the following chapters of this thesis with GM-CSF MDMs. Interestingly, complement proteins that have been reported to drive a glycolytic shift to support inflammasome and T cell activation are CD46 and C3b regulation, driving expression of glycolysis-related genes such as GLUT1 and LAMTOR5, which was also observed in this study, and downstream activation of NLRP3 inflammasome (Arbore and Kemper 2016). Similarly, a very recent study showed intracellular C3 and C3aR driving a metabolic shift towards glycolysis that promotes NLRP3 activation and inflammatory tissue priming in synovial fibroblasts from patients with established arthritis (Friščić, Böttcher et al. 2021). Overall, similarly to the studies mentioned above with other complement components, this study pointed towards a novel involvement of glucose metabolism changes driven by MAC in naïve MDMs, which are needed for inflammasome activation. Whether other complement proteins are involved in this process in macrophages, however, hasn't been tested, although results in this study have shown to be MAC-dependant as per the use of C7-depleted NHS or anti-C7 controls in all experiments. In addition, given the different complement proteins involved in this complement-metabolic-inflammasome axis in T cells and synovial fibroblasts from patients (Arbore and Kemper 2016, Friščić, Böttcher et al. 2021), it is apparent that more research is needed to determine whether these changes happen in other immunological cell types, and if other complement proteins are involved.

In addition, the data presented in this study further explored the glycolytic changes driven by MAC in real-time measurement of ECAR and OCR by seahorse assay. However, the lack of changes in ECAR or OCR levels in response to sublytic MAC stimulation in naïve MDMs, which was attributed to the fact that basal OCR levels were below the standard operating parameters for the seahorse, led to question the suitability of M-CSF MDMs as a model for understanding MAC-mediated metabolic changes.

6.2 Sublytic MAC is an immunometabolic regulator of NLRP3 activation and IL-18 secretion in GM-CSF human macrophages

Interestingly, macrophages differentiated with GM-CSF, a growth factor used for generation of classical *in vitro* models of pro-inflammatory macrophages prior to polarisation with, typically, LPS, is known to prime macrophages for pro-inflammatory responses without directly tiggering polarisation and has been shown to dominate in pathogenic inflammatory conditions over M-CSF (Michl, Ohlbaum et al. 1976, Newsholme, Curi et al. 1986, O'Neill and Hardie 2013, Mills, Kelly et al. 2016). In addition, GM-CSF macrophages have higher levels of mitochondrial respiration and aerobic glycolysis (measured by OCR and ECAR by seahorse), as well as higher expression of genes encoding glycolytic enzymes compared to M-CSF MDMs (izquierdo et al 2015), providing energy to the cell needed to support pro-inflammatory functions. This led to test sublytic MAC stimulation in GM-CSF MDMs instead, and investigate the downstream metabolic changes that may modulate NLRP3 activation in this cell type. Indeed, the data presented in this study showed GM-CSF macrophages being more metabolically active than M-CSFs, with higher basal levels of mitochondrial respiration (OCR) and better responsiveness to FCCP, and in response to sublytic MAC stimulation GM-CSF MDMs did show an increase in ECAR levels as measured by seahorse assay, which, to date, hasn't been shown before in other cell types. This was confirmed by measurement of extracellular lactate post sublytic MAC stimulation in GM-CSFs, which showed the lactate concentration being 3-fold higher than M-CSFs, although the trend was similar for both cell types where lactate increase occurred over time starting at 1 hour and peaking at 24 hours.

In this study, the increase in extracellular lactate is suspected to be a product of macrophages undergoing a response to MAC, requiring rapid ATP production via glycolysis and production of pro-inflammatory response elements such as cytokines resulting from inflammasome activation or transcriptional upregulation of HIF1α, a process seen elsewhere in response to other stimuli (Tannahill, Curtis et al. 2013). Conversely,

lactate has also been shown to suppress macrophage pro-inflammatory responses in different disease scenarios, such as tumour microenvironment (Palmieri, Menga et al. 2017, Yang, Xu et al. 2020). In this study, however, understanding how the lactate production would influence other cells in the environment would require a different approach, such as a MAC-stimulated complex co-culture or *in vivo* scenario to have wide-ranging effects beyond that on the macrophage alone, where observations of anti-inflammatory lactate may become more relevant. This could be an interesting incorporation in future studies.

Subsequently, the novel role of sublytic MAC as a trigger of increased glycolysis, was further explored in the present study in GM-CSF MDMs. A shift towards aerobic glycolysis and away from oxidative phosphorylation was confirmed by seahorse measurement of glycolytic proton efflux rate, a more accurate measurement of real-time glycolysis than ECAR, indicating metabolic rewiring of central carbon metabolism which was further explored in metabolomics and proteomics analysis. Furthermore, a MAC-driven collapse in mitochondrial spare respiratory capacity where cells were unable to respond to FCCP was also observed, indicating mitochondrial dysfunction. A likely cause that could explain this phenotype is the limitations in pyruvate uptake into the mitochondria being driven by alterations in pyruvate transport machinery, as observed in this thesis, by a MAC-driven upregulation of PDK4 gene expression which suppresses pyruvate dehydrogenase complex, and actual downregulation of PDHB as seen in proteomics analysis, supporting aberrant preferential activation of glycolysis (Yonashiro, Eguchi et al. 2018). This process may also explain the decrease in intracellular lactate observed in metabolomics analysis and increase in extracellular lactate being generated from glycolysis and quickly exported from the macrophage. Interestingly, it should be mentioned that PDK4 regulation has also been shown to limit pyruvate import and to shift glucose metabolism towards aerobic glycolysis and lactate production, and has been presented as a potential target for sepsis and inflammation (Park and Jeoung 2016) (Van den Bossche, Baardman et al. 2016). It would be interesting to investigate whether this mechanism translates into disease scenarios where where overactivation of complement in macrophages and subsequent inflammation contribute to disease progression, such as RA (Holers and Banda 2018).

Conversely, the MAC-driven metabolic phenotype observed in this study differs from LPS-treated human MDMs, which show no clear changes in oxidative metabolism with a slight decrease in basal glycolysis (Van den Bossche, Baardman et al. 2016). Instead, the phenotype observed here resembles LPS-treated mouse macrophages (BMDMs), which undergo a metabolic switch towards glycolysis (showing higher ECAR and lower OCR values) and inability to respond to FCCP (Mills, Kelly et al. 2016), as well as also

resembling IFN-γ activated human macrophages, which support a classically activated macrophage phenotype inducing a rapid switch to aerobic glycolysis and repurposing of the mitochondria, including ROS production, allowing for HIF-1α and IL-1β production. Importantly, these IFN-γ-driven immunometabolic changes were reported to contribute to atherosclerosis in diabetic patients (Wang, Zhang et al. 2018). Interestingly, a recent study explaining the LPS versus IFN-γ different responses in GM-CSF human macrophages found that IFN-γ suppressed LPS-induced anti-inflammatory and metabolic components of the LPS response, such as IL-10 expression, and superinduced TNF expression supporting macrophage activation (Kang, Bachu et al. 2019). Therefore, it would be interesting to explore other MAC-driven immunometabolic mechanisms that may resemble IFN-γ signalling in macrophages.

In addition, given the altered pyruvate supply to the mitochondria, the present study also shows proteins associated with TCA cycle and electron transport chain being regulated by sublytic MAC in proteomics analysis. For instance, regulation of ATP5IF1, which limits ATP depletion during mitochondrial membrane potential collapse (Campanella, Parker et al. 2009, Weissert, Rieger et al. 2021), as well as modulation of alternative pathways in glutamine, glutamate and nucleotide sugar metabolism as observed from proteomics and metabolomics analysis by regulation of GFPT1, GLUD1 and UDP post MAC stimulation, aligning with phenotypes from glycolytic cancer cells, which use glutamine and glutamate metabolism to supply the TCA cycle. It is worth mentioning that glycolytic enzymes aren't necessarily transcriptionally regulated, instead they are reliant on feedback mechanisms of the metabolites directly, therefore, certain key glycolytic enzymes could be regulated in this mechanism but not observed as regulated proteins in proteomics analysis (DeBerardinis, Mancuso et al. 2007, Tong, Zhao et al. 2009).

Consequently, this study further investigated into the observed mitochondrial dysfunction by exploring mitochondrial physiology, and demonstrated sublytic MAC-driven perturbations in calcium flux by increased mitochondrial calcium, loss of mitochondrial membrane potential, disrupted mitochondrial dynamics and redox biology. These findings study built up on previous findings from our lab which demonstrated that sublytic MAC-treated lung epithelial cells had increased cytosolic calcium leading to calcium transport to the inner mitochondrial membrane via MCU, causing mitochondrial calcium overload and depolarization of the membrane, as was confirmed in this study in macrophages (Triantafilou, Hughes et al. 2013). Observations of mitochondrial fragmentation and mitochondrial ROS production provided further novel insight into the mitochondrial dysfunction mechanism triggered by MAC. Sublytic MAC-driven mitochondrial ROS production was demonstrated in this study not only by direct measurement of intracellular

ROS and extracellular hydrogen peroxide, which was rotenone and glycolysis dependant, but also via oxidation of mitochondrial Prx3, measured initially as a proxy for mtROS production, as well as regulation of SOD2 observed in proteomics analysis, a known regulator of mitochondrial superoxide. Interestingly, these results aligned with previous findings in LPS-treated mouse macrophages, showing a switch to glycolysis with subsequent alteration of the mitochondrial membrane potential, triggering an increase of Reverse Electron Transport-ROS (RET-ROS), which is required to induce an inflammatory response (Mills, Kelly et al. 2016). Given the rotenone-sensitive and glycolysis driven ROS production, as well as S1Q-dependant IL-18 production observed in this study, it is likely that Complex I and an increased NADH/NAD+ ratio fuelling reverse electron transport, are the main cause to the ROS production and downstream inflammatory consequences. The metabolic and functional phenotypes observed in this manuscript resemble those seen in other studies using LPS-stimulated macrophages (Galván-Peña and O'Neill 2014, Mills, Kelly et al. 2016, Meng, Guo et al. 2020, Fan, Pei et al. 2021). This indicates that endogenous triggers such as MAC can also alter the phenotype of macrophages, starting from changes in their bioenergetic profile, similar to well-characterised external stimuli such as LPS.

Importantly, this study demonstrated a sublytic MAC-driven activation of NLRP3 inflammasome, driving released IL-18, ASC speck formation and GSDMD cleavage. This activation is dependant on NLRP3, caspase-1, glycolysis and mtROS, given the complex I and III sensitivity from the superoxide-production site inhibitors S1QE1.1 and S3QEL 2, indicating the need for glycolysis and mitochondrial dysfunction with mtROS production for NLRP3 activation. Importantly, the lack of secreted IL-1β may be explained by the need of a stronger priming inflammasome signal such as LPS that drives pro-IL-1β expression, while IL-18 production is not limited in this way. Although C5a is known to act as a priming signal (Cumpelik, Ankli et al. 2016) and sublytic MAC has been shown to drive transcriptional upregulation of IL-1β in this study, it may still not be sufficient for IL-1β secretion. The molecular mechanisms that explain this controversy, however, remain to be explored. A one-step NLRP3 inflammasome activation, bypassing the requirement of priming and driving IL-18 secretion seems to be the scenario in this thesis for MAC-treated GM-CSF MDMs, as M-CSF MDMs showed secretion of both cytokines downstream of inflammasome activation. However, the reason for this controversy remains to be explored. Importantly, the MAC-induced transcriptional upregulation of HIF1α and PFKFB3 supports a pro-inflammatory metabolic phenotype in macrophages (Kelly and O'neill 2015, O'Neill, Kishton et al. 2016, Shi, Pan et al. 2017).

In addition, there is increasing evidence that MAC may directly be interacting with NLRP3 at later stages (Diaz-Del-Olmo, et al 2021) which has also been observed in this study with MAC and ASC co-localisation after MAC stimulation, leading to question if inflammasome activation is directly through MAC or if it is because of the interplay role of complement and inflammasome pathways. It is believed that MAC deposition on nucleated cells aggregates into packed clusters for elimination from the cell during recovery, can either be shedded from the membrane or internalised into the cell over endocytosis or blebbing (Stratton, Moore et al. 2015, Xie, Jane-Wit et al. 2020), possibly depending on a threshold of the amount of MAC clusters on the membrane. This emerging field of evidence around direct complement-inflammasome interactions is certainly of interest, however, the focus of this study is on the MAC downstream signalling pathway and proposes that the MAC deposition and resulting ion flux, leading to a shift in compensatory glycolytic flux coupled with mitochondrial dysfunction and resulting ROS production, is the primary driver of inflammasome activation, as seen in the sensitivity of IL-18 production to ROS and glycolysis modulators. Therefore, MAC is presented as an endogenous modulator of immunometabolism. Of note, the role of potassium and calcium ion exchange in NLRP3 activation would be worth to examine, by studying the role of potassium efflux to the extracellular space and test whether potassium is essential for this MAC-driven signalling events and downstream NLRP3 activation, as it has been reported that addition of potassium to the cell media to prevent potassium efflux is essential to allow inflammasome activation (Arlehamn, Pétrilli et al. 2010).

Crucially, this present study showed that IL-18 release is facilitated via GSDMD pore formation, without surpassing a threshold for complete pyroptosis activation, possibly by low-level GSDMD pore formation which may be maintained by constitutive activity of caspase-1 (Evavold, Ruan et al. 2018). Avoiding pyroptosis and maintaining cell viability post-sublytic MAC stimulation may be relevant to maintain macrophage function to clear pathogens and effector functions to maintain tissue homeostasis, as well as to possibly trigger IL-18-mediated signalling in other macrophages or target cells (Mazodier, Marin et al. 2005, Yasuda, Nakanishi et al. 2019). Thus, GSDMD inhibitors such as NSA or potentially novel GSDMD inhibitors with better specificity (Pandeya, Li et al. 2019) could be a novel target to effectively block the release of pro-inflammatory cytokines resulting from NLRP3 inflammasome activation, known to contribute to inflammation in many diseases such as RA or sepsis (Pandeya, Li et al. 2019). Importantly, the maintained viability post-sublytic MAC stimulation in this study aligns with other studies showing viability maintenance post MAC-driven NLRP3 activation in epithelial cells and dendritic cells (Laudisi, Spreafico et al. 2013, Triantafilou, Hughes et al. 2013). In addition, in this

study viability has been constantly determined and checked that phenotypes were not the result of perforation or damage of the cell membrane or mitochondrial membrane as per the use of glycine in several metabolic and ROS assays, as well as the unaffected basal OCR rates prior to FCCP injection at early and later time points. Interestingly, however, after 24 hours stimulation of sublytic MAC some elements of metabolic failure do start to appear as measured by proton leak, suggesting macrophages may start to undergo cellular dysfunction and failure. It would be interesting to further investigate these observations between cell death and MAC-driven inflammasome signalling in innate cell death pathways and other immune responses.

Overall, this study shows that sublytic MAC drives metabolic rewiring and mitochondrial dysfunction. This perturbation leads to downstream signalling events which are driven by in the short term by calcium influx, mitochondrial morphology and membrane potential changes, and in the long term by a pro-glycolytic and pro-inflammatory transcriptional response. These changes result in the production of mitochondrial ROS which can directly activate the NLRP3 inflammasome, driving production of IL-18 and cleavage of GSDMD, overall suggesting MAC is an endogenous modulator of immunometabolism. This demonstrates a role for the complement system in cellular metabolic reprogramming linked to inflammasome activation, confirming the involvement of MAC in the complement-metabolism-inflammasome axis of macrophages (Arbore and Kemper 2016). These findings open up a number of therapeutic opportunities for autoimmune diseases such as RA where sublytic MAC and increased glycolysis have been implicated, and contribute to inflammation (Neumann, Barnum et al. 2002, Romero, Fert-Bober et al. 2013, McGarry, Biniecka et al. 2017, Narasimhan, Coras et al. 2018). In addition, MAC deposition caused by glycation of CD59, which was found to be driven by high levels of glucose has been linked with diabetes (Acosta, Hettinga et al. 2000). In these disease scenarios, the novel MAC-driven immunometabolic changes demonstrated in this thesis may have a crucial role in disease progression and therefore should be further investigated as potential novel therapeutic targets.

6.3 Limitations and future directions

In the MAC-NLRP3 inflammasome activation pathway, the exact mechanism of how MAC is directly interacting with NLRP3 is still unknown. Our previous study already indicated that sublytic MAC can activate NLRP3 inflammasome via a signalling cascade involving calcium flux, mitochondrial calcium overload and subsequent changes in mitochondrial membrane potential (Triantafilou, Hughes et al. 2013), in addition to the novel metabolic mechanisms and mitochondrial dysfunction uncovered in this study. However, given the potential direct interaction between MAC and NLRP3 as seen in ASC co-localisation results here and supported by others (Diaz-del-Olmo, Worboys et al. 2021), as well as evidence surrounding MAC internalisation into the cell (Jane-wit, Surovtseva et al. 2015), it is crucial to further characterise if and how does MAC directly interact with the inflammasome and investigate the synergy between this direct interaction and the MAC-immunometabolic pathway in the activation of NLRP3 inflammasome. Potentially, certain components of the MAC signalling pathway will contribute to a direct interaction of internalised MAC with NLRP3, which may happen at a later stage than the immediate ion flux and subsequent metabolic changes, to support inflammasome activation.

Importantly, it would be worth examining the involvement of sublytic MAC deposition in the context of macrophage function, such as phagocytosis and polarisation in disease-relevant settings, given the active inflammasome pathway observed here. Potentially, the subltyic MAC-driven activation of the inflammasome promotes a skewing towards a pro-inflammatory macrophage. The metabolic and functional phenotypes observed in this study resemble those seen in other studies using LPS-stimulated macrophages (Galván-Peña and O'Neill 2014, Mills, Kelly et al. 2016, Meng, Guo et al. 2020, Fan, Pei et al. 2021), suggesting that endogenous triggers such as MAC can also alter the phenotype of macrophages, starting from changes in their bioenergetic profile, similar to that of well-characterised stimuli such as LPS. It would be interesting to explore an in-depth insight into sublytic MAC deposition on classical M1 versus M2-like polarisation and function by cell markers and cytokine production, as well as in follow up studies in complex co-cultures and disease-relevant systems, such as polarised macrophages in inflammation versus tumour, providing a robust and relevant insight that builds on the *in vitro* findings of this study.

It would also be useful to understand the extracellular environmental changes, such as the role of extracellular lactate observed in this study, which is known to have an anti-inflammatory role in different settings (Yang, Xu et al. 2020), and how this influences other macrophage-engaging cell types and external metabolomic landscapes. For instance, to

determine how does MAC influence cell-cell communication via metabolite export, particularly where MAC is not deposited into and acts upon all cells to the same degree. Follow up studies should attempt to understand the relevance of these scenarios in *in vivo* disease models as well as specific complement/inflammasome-KO mice, to have wide-ranging effects of MAC beyond that on the macrophage alone.

Several key limitations in the present study which explored changes in metabolites by a targeted metabolomics analysis need to be noted. Although the proteomics analysis in this study had an anti-C7 control to account for only MAC-dependant responses, in the metabolomics analysis this control wasn't included, therefore the observed metabolite changes were dependant on a sublytic dose of general complement stimulation but can't be associated only with MAC. Future experiments should include an anti-C7 control to confirm that the results observed in metabolomics are MAC-dependant. Moreover, within the top upregulated pathways in metabolomics analysis was caffeine metabolism. Caffeine was supplied externally to the system by direct addition of pooled normal human serum that was gathered from donors with no restriction on diet or caffeine intake. The Caffeine metabolism datapoint is heavily influenced by a high presence of Caffeine/Theobromine in the NHS treated samples only, so this result is believed to be an artefact of the system likely due to exogenous caffeine or caffeine breakdown products. Conversely, however, there was no up- or downregulation of caffeine metabolism associated enzymes in the proteomics data to reflect the metabolomic data, whereas regulation of glucose and mitochondrially-related pathways were reflected in the proteomics dataset. Observing alterations at both the metabolomic and proteomic level give added confidence that these are pathways of interest, as opposed to what looks to be artefactual addition of caffeine and/or its breakdown products. However, future studies should definitely explore untargeted metabolomics and proteomics, to allow overlay of any differentially expressed genes/proteins with any changes in metabolites, downstream of MAC, including an anti-C7 control or using a non-NHS based system for MAC stimulation, such as stimulation with only purified components C5b6-9.

6.4 Concluding remarks

Macrophages are critical innate immune cells with essential roles in host defence in response to pathogens as well as in immunometabolic regulation of innate immune sensors such as inflammasomes, but can also trigger inflammation and contribute to disease in sterile inflammatory scenarios. The complement system, an ancient surveillance network with a crucial role in innate immunity as a sensor of the pattern recognition system, is able to control the NLR-based cellular emergency alarm system, as well as modulating the metabolism of immune cells, bringing attention to a recently discovered complement-metabolism-inflammasome axis, where the involvement of MAC was unknown. The results of this study increased the understanding of the mechanism involving the MAC-NLRP3 inflammasome pathway, previously discovered by our lab, in MDMs and elucidated the involvement of a novel mechanism of cellular metabolic reprogramming with alterations in pyruvate metabolism and mitochondrial dysfunction, that has a crucial role in modulating NLRP3 inflammasome-dependant production of pro-inflammatory cytokine IL-18. Critically, all the results in this thesis are from human primary macrophages, providing highly translatable data, given that most previous studies investigating downstream effects of MAC in inflammation were performed in human cell lines or murine cell/animal models.

As MAC has been involved in progression of several chronic inflammatory, infectious and neurodegenerative diseases contributing to inflammation, including rheumatoid arthritis, Alzheimer's disease, multiple sclerosis, diabetes, sepsis or atherosclerosis, it will be essential to gain a better understanding of how this MAC-driven immunometabolic pathway is regulated in disease settings, as this may identify novel therapeutic targets. Further insights into the MAC-NLRP3 inflammasome axis and the investigating metabolic phenotypes uncovered in this thesis, may shed some light on biomarker options, or even downstream therapeutic targets that may aid to resolve inflammation caused by aberrant complement signalling.

Supplementary figure 1
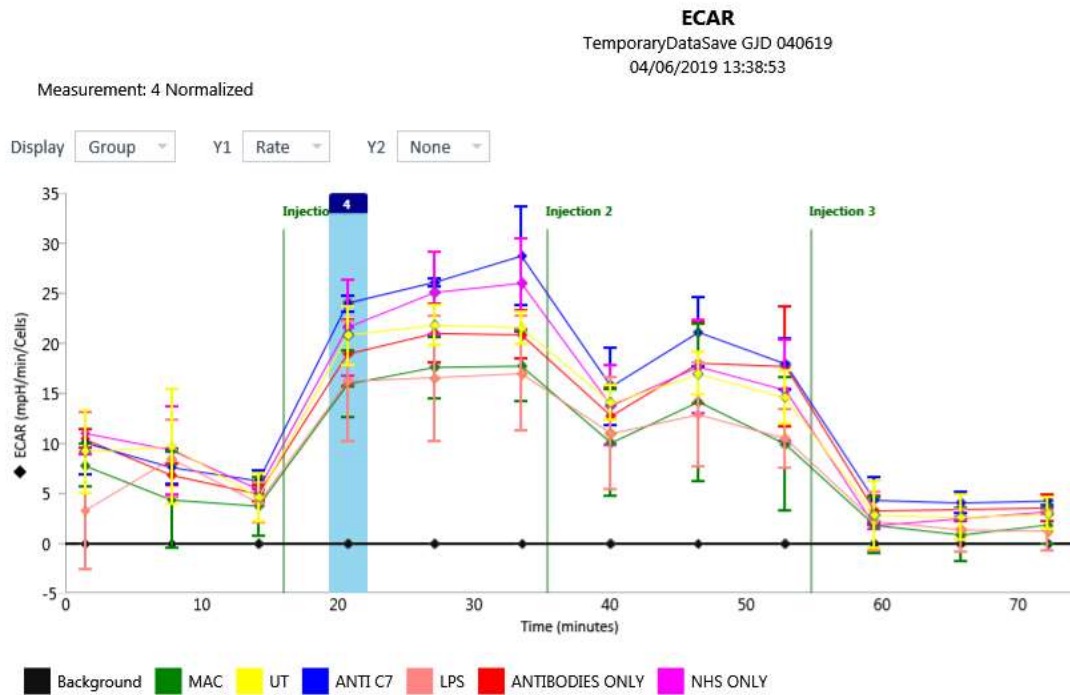
ECAR measurement by seahorse assay post sublytic MAC stimulation in M-CSF macrophages. Seahorse experiments: glycolytic rate (ECAR) measured with standard glycolytic stress test after 1 hour of sublytic MAC stimulation, as well as controls anti-C7 plus MAC, untreated (UT), sensitising antibodies only, a sublytic dose of NHS only, or 3 hours with 100 ng/ml LPS (n=1 donor, n=4 technical replicates). Error bars represent +/- S.E.M

Supplementary figure 2
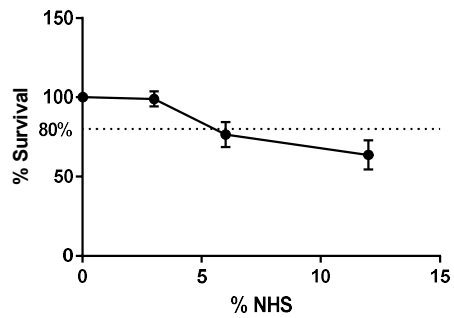
Lytic effect of MAC on GM-CSF MDMs using imaging dishes for fluorescence microscopy.
MDMs treated with antibodies (anti-CD55, CD59, HLA) and increasing concentrations of NHS for 1 hour in fluorescence microscopy imaging dishes before viability measurement by CellTitreGlo. Sublytic doses of MAC were defined as 80% cell survival (n=3). Error bars represent +/- S.E.M.
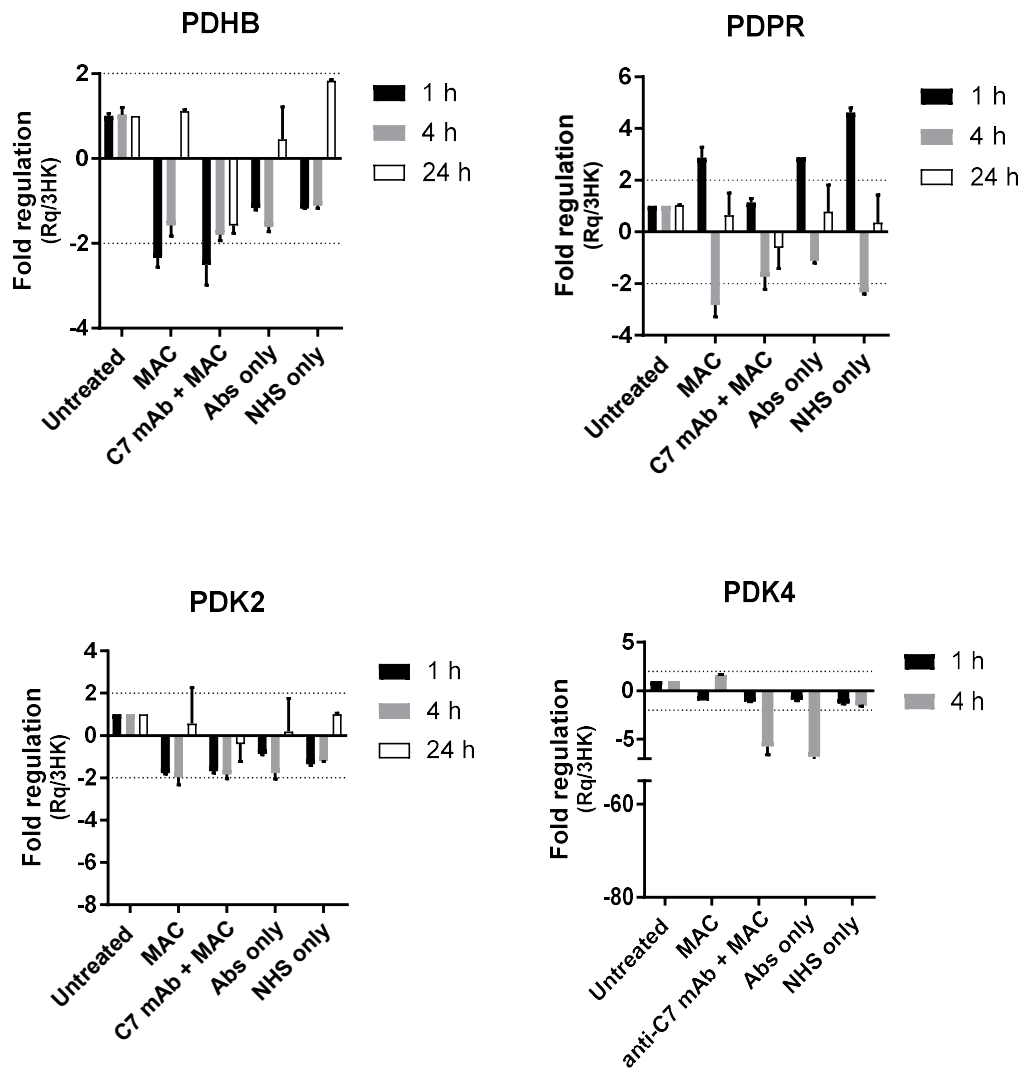
Gene expression of pyruvate metabolic genes upon sublytic MAC stimulation in GM-CSF MDMs. MDMs treated with MAC, anti-C7 plus MAC control. Gene expression of PDHB, PDPR, PDK2 or PDK4 after 1, 4 or 24 hours stimulation with all the conditions (n=5). Gene expression was normalised to housekeeping genes β-actin, HPRT and TBP. ΔΔCt is relative to unstimulated cells. Error bars represent mean +/- S.E.M.

Supplementary Figure 4

IL-1B ELISA
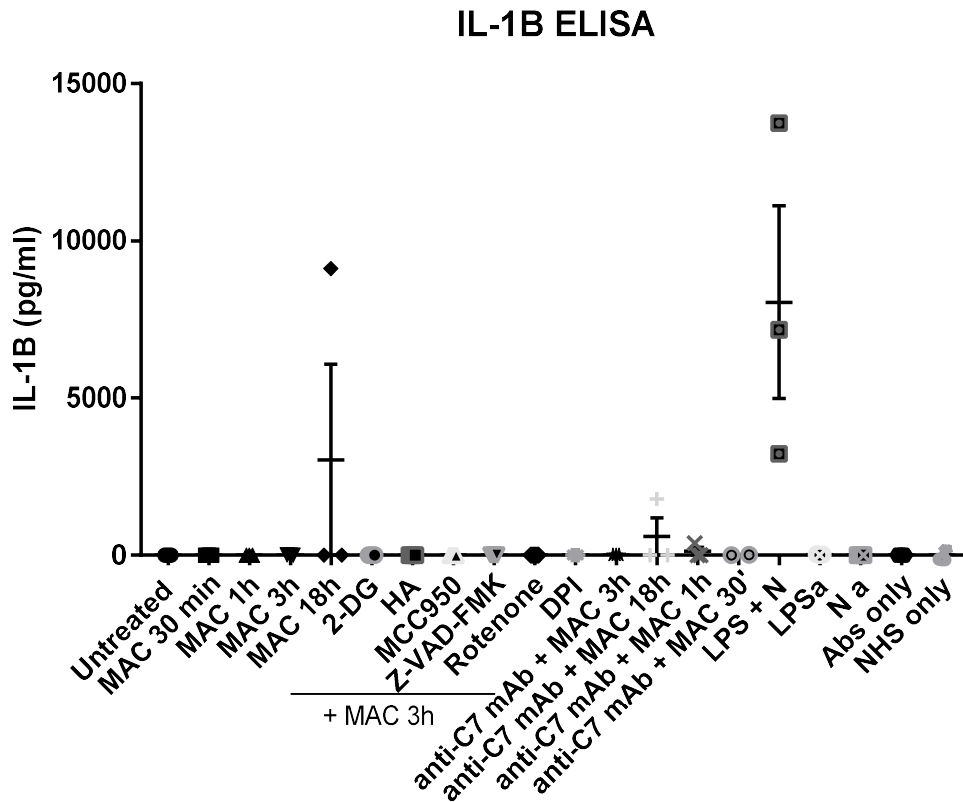
IL-1β production post sublytic MAC stimulation. IL-1B production detected by ELISA in supernatants of MDMs in 1 million cells per condition (24-well plates) stimulated with MAC or controls for select time points: antibodies only (Anti-CD55, CD59 and HLA), NHS only (just NHS without pre-incubation with antibodies), anti-C7 plus MAC or positive control LPS (100 ng/mL for 3h) followed by nigericin (5 μM for 1 h). (n=3). Pre-incubated inhibitors 2-DG (5mM for 2 h), HA (10 μM, 50 min), MCC950 (1 μM), Ac-YVAD-CMK (10 μM) and rotenone (0.5 μM, 50 min) (n=3) were stimulated with MAC for 3 hours (n=3). Error bars represent ± S.E.M.

APPENDIX B

Supplementary table 1: Proteins upregulated by MAC stimulation. Data obtained from proteomics analysis, numbers represent normalized protein intensities (z-score) for significantly MAC-regulated proteins (one-way ANOVA, FDR corrected, with post-hoc Tukey's test $p < 0.05$ significant for MAC vs Untreated and MAC vs anti-C7 + MAC. N= 99 proteins).

Protein ID (Fasta headers)	Untreated	MAC	aC7 + MAC
SERPING1	-0.71255	1.338117	-0.62557
UBR2	-0.73284	1.33567	-0.60283
A1BG	-0.65136	1.309381	-0.65802
HP	-0.85078	1.306739	-0.45596
HPX	-0.81053	1.305941	-0.49541
C5	-0.73911	1.301053	-0.56194
ITIH2	-0.71568	1.300694	-0.58501
SERPINA3	-0.74811	1.29881	-0.5507
APOA1	-0.86949	1.296986	-0.4275
SERPIND1	-0.81375	1.296947	-0.4832
APOB	-0.76986	1.296218	-0.52636
CLU	-0.87726	1.291073	-0.41381
CFB	-0.77141	1.290904	-0.51949
AHSG	-0.8075	1.284994	-0.47749
SERPINA1	-0.80279	1.279609	-0.47682
PPBP	-0.55956	1.276812	-0.71725
PLG	-0.79538	1.272229	-0.47685
RBM25	-0.52358	1.271531	-0.74795
ITIH1	-0.72299	1.262638	-0.53965
PON1	-0.77602	1.259534	-0.48351
CFH	-0.77569	1.249677	-0.47399
SPNS1	-0.69375	1.24736	-0.55361
HBB	-0.71069	1.240967	-0.53028
IGHG4	-0.87111	1.240902	-0.36979
CP	-0.75698	1.238097	-0.48112
A2M	-0.77889	1.228924	-0.45003
ITIH4	-0.85255	1.218072	-0.36552
C1S	-0.93564	1.214084	-0.27844
C3	-0.79324	1.206814	-0.41358
C4B	-0.95619	1.206672	-0.25048
KNG1	-0.73922	1.204148	-0.46493
GC	-0.65353	1.202312	-0.54878
IGHV3-7	-0.64889	1.200161	-0.55127
IGHM	-0.91065	1.194987	-0.28434
ECHS1	-0.74196	1.190987	-0.44903
TNFAIP8	-0.40302	1.176817	-0.7738

ARL3	-0.54583	1.174091	-0.62826
TPM3	-0.61508	1.173412	-0.55834
F2	-0.97608	1.168344	-0.19227
APOA2	-1.02985	1.159158	-0.1293
IGHG2	-0.87977	1.146207	-0.26644
SERPINC1	-0.89485	1.137588	-0.24274
C4A	-0.98477	1.135462	-0.15069
APOC1	-0.97363	1.134989	-0.16136
PAFAH1B2	-0.63681	1.131831	-0.49502
APOC3	-0.8344	1.126326	-0.29193
HBA1	-0.63751	1.114931	-0.47742
IGKC	-0.89884	1.112496	-0.21366
PTPN11	-0.36103	1.109567	-0.74854
APOA4	-1.04336	1.109534	-0.06618
PRKAR1A	-0.40122	1.10773	-0.70651
NDUFB4	-0.69622	1.10625	-0.41003
IGHA1	-0.83461	1.105246	-0.27064
TXNDC12	-0.31087	1.103287	-0.79242
VTN	-0.73897	1.102314	-0.36334
TTR	-0.77598	1.089919	-0.31394
GLUD1	-0.32479	1.089896	-0.7651
IGHG3	-0.95666	1.087918	-0.13126
HRG	-0.76665	1.078019	-0.31137
PSMD11	-0.45692	1.066679	-0.60976
TRIM28	-0.57373	1.06625	-0.49252
OS9	-0.65108	1.064728	-0.41365
SMU1	-0.38585	1.063113	-0.67727
HMGB2	-0.67643	1.060792	-0.38437
GORASP2	-0.30949	1.057231	-0.74774
MTHFD2	-0.22656	1.050459	-0.8239
VPS25	-0.43193	1.044245	-0.61232
DPM1	-0.36463	1.042769	-0.67814
ACTR2	-0.893	1.033825	-0.14083
IGLL5	-0.82442	1.032247	-0.20782
MACF1	-0.42152	1.029411	-0.60789
IGHG1	-0.81882	1.028326	-0.20951
SMC1A	-0.89331	1.01618	-0.12287
STIM1	-0.15589	1.011497	-0.85561
CHMP5	-0.61915	1.010454	-0.3913
RRAGC	-0.49623	1.005379	-0.50915
LAMTOR2	-0.83316	0.994936	-0.16178
TMED10	-0.20135	0.993748	-0.7924
LRCH1	-0.10352	0.987973	-0.88446
PSMD3	-0.39866	0.977633	-0.57898
RPS6KA3	-0.21328	0.973116	-0.75984
DUSP3	-0.31411	0.973027	-0.65892

IGLC3	-0.79193	0.967287	-0.17536
RPA1	-0.32039	0.95364	-0.63325
CD97	-0.39168	0.951541	-0.55986
AKR1C3	-0.35753	0.950579	-0.59305
AUP1	-0.3991	0.947708	-0.54861
EIF3I	-0.35877	0.944758	-0.58599
BAG6	-0.75017	0.944371	-0.1942
DUSP23	-0.7163	0.94184	-0.22554
RARS	-0.5214	0.932948	-0.41155
C1QB	-0.54084	0.924238	-0.3834
SRSF11	-0.44116	0.921527	-0.48036
VPS35L	-0.55743	0.917266	-0.35983
MDH1	-0.40756	0.917197	-0.50964
SRI	-0.46669	0.916254	-0.44956
PSMC6	-0.37077	0.91443	-0.54366
MYDGF	-0.51512	0.914419	-0.3993
CAMSAP1	-0.49145	0.867114	-0.37566

Supplementary table 2: Proteins downregulated by MAC stimulation. Data obtained from proteomics analysis, numbers represent normalized protein intensities (z-score) for significantly MAC-regulated proteins (one-way ANOVA, FDR corrected, with post-hoc Tukey's test $p < 0.05$ significant for MAC vs Untreated and MAC vs anti-C7 + MAC. N= 363 proteins).

Protein (Fasta headers)	Untreated	MAC	aC7 + MAC
CLPTM1	0.41019	-0.85836	0.448172
DHX9	0.421147	-0.86868	0.447537
MAP2K1	0.485653	-0.87155	0.385902
SWAP70	0.384621	-0.87212	0.487497
NT5C2	0.413777	-0.88353	0.469755
ARPC5	0.458051	-0.88551	0.427464
LDHA	0.35808	-0.88683	0.528751
BASP1	0.365377	-0.89077	0.525391
ARRB2	0.559942	-0.89218	0.332236
TGM2	0.453488	-0.89229	0.438807
COX6B1	0.485838	-0.89302	0.407183
CORO1B	0.327894	-0.89303	0.565137
MIEN1	0.356129	-0.89409	0.537965
ACAD9	0.510328	-0.89433	0.384005
GK3P	0.367132	-0.8953	0.528171
UBE2V1	0.348103	-0.89563	0.547527
COPB1	0.598134	-0.89838	0.300245
DNM2	0.513394	-0.90021	0.386811
PSMD8	0.436484	-0.901	0.464518
HSP90AA1	0.322753	-0.90248	0.579724
CD63	0.307394	-0.9049	0.597503
NONO	0.469664	-0.90536	0.435694
SOD2	0.337906	-0.90757	0.569666
ATIC	0.475772	-0.90771	0.431935
CTSA	0.478559	-0.90854	0.429978
COX7C	0.4097	-0.90864	0.498937
ATP6V0D1	0.371056	-0.9099	0.53884
ATP2A2	0.546152	-0.91376	0.367609
NIBAN1	0.611739	-0.91639	0.304653
EEF1E1	0.319473	-0.91656	0.597085
UBE2K	0.565429	-0.91762	0.352195
GYG1	0.455294	-0.91906	0.463768
SEPTIN11	0.289195	-0.9196	0.630409
ACAA1	0.379541	-0.92017	0.540625
SLC25A13	0.444474	-0.92045	0.475973
NAPA	0.403849	-0.92064	0.516795
GRB2	0.244387	-0.92108	0.67669
STOM	0.521715	-0.92443	0.402719

HMGCL	0.275706	-0.92826	0.652554
LMNB1	0.486815	-0.93022	0.443401
DDOST	0.383457	-0.93025	0.546798
IL16	0.414642	-0.93142	0.516773
IDH3A	0.358325	-0.93144	0.573115
SDC2	0.480108	-0.93247	0.452359
FLII	0.556064	-0.93283	0.376769
GFPT1	0.699298	-0.93328	0.233985
COMMD9	0.552278	-0.93352	0.38124
SEC31A	0.371101	-0.93359	0.562491
RDX	0.341887	-0.93418	0.592291
EHD4	0.534113	-0.93682	0.402709
COPS5	0.414584	-0.93698	0.522394
TMA7	0.457998	-0.93849	0.48049
PSMD12	0.191728	-0.93965	0.747926
YWHAQ	0.232763	-0.94356	0.710802
SH3GLB1	0.787504	-0.94374	0.15624
ATP5IF1	0.414002	-0.94589	0.531886
NMT1	0.420713	-0.94804	0.52733
CHMP1A	0.424986	-0.9528	0.527815
SCARB2	0.53267	-0.95286	0.420193
SNRPD2	0.039838	-0.95485	0.915017
RPLP2	0.245535	-0.9554	0.709861
MTPN	0.311485	-0.95563	0.644149
MAGOH	0.391775	-0.95583	0.564059
GOLGB1	0.279951	-0.95675	0.676797
CD14	0.015438	-0.95703	0.941591
PSMB10	0.39909	-0.95896	0.559873
SEPTIN7	0.370236	-0.96029	0.590049
DERA	0.234476	-0.96046	0.725986
CAPRIN1	0.873393	-0.9607	0.087305
GPX1	0.425636	-0.96119	0.535553
S100A6	0.12674	-0.96232	0.835581
PDCD6IP	0.383048	-0.96406	0.581011
RNPEP	0.496114	-0.9652	0.469082
YWHAE	0.148421	-0.96561	0.817194
NUCB2	0.143036	-0.96679	0.823754
PTGR1	0.430937	-0.96749	0.536555
RBBP7	0.543828	-0.9688	0.424967
MAPRE2	0.708279	-0.9696	0.261324
PDCD5	0.187875	-0.97066	0.782785
MOSPD2	0.419879	-0.97068	0.550804
CALM3	-0.04227	-0.97089	1.013161
EPRS	0.53987	-0.97175	0.431876
SYNCRIP	0.324429	-0.97198	0.647551
ECPAS	0.631895	-0.97312	0.34122

AHNAK	0.108581	-0.97356	0.864976
RAP1B	0.797079	-0.97396	0.176878
CARHSP1	0.536537	-0.97511	0.438569
ARL8B	0.420487	-0.97528	0.554794
BSG	0.299224	-0.9761	0.676875
CAB39	0.238143	-0.97774	0.739594
PDXK	0.48233	-0.97833	0.496004
MAT2A	0.495935	-0.98071	0.48478
IPO5	0.674683	-0.98127	0.30659
FCER1G	0.117962	-0.98215	0.86419
RPLP0	0.812724	-0.98294	0.170215
HACD3	0.882775	-0.98341	0.100638
NPC2	0.212605	-0.98352	0.770918
PECAM1	0.639515	-0.98357	0.344058
LYPLA1	0.623819	-0.9836	0.359782
TNPO3	0.491523	-0.98404	0.49252
RBM47	0.282262	-0.98413	0.701873
ASAH1	0.217472	-0.98445	0.766977
COPZ1	0.142011	-0.98476	0.84275
TMED9	0.452915	-0.98568	0.532763
TPI1	-0.011	-0.9864	0.997397
HNRNPDL	0.185537	-0.98676	0.801224
RPS7	0.443002	-0.98756	0.544554
DYNLL1	0.687576	-0.98772	0.300148
PTPRE	0.578776	-0.9883	0.409527
HYOU1	0.667319	-0.98953	0.322209
GLG1	0.746022	-0.98964	0.243618
IARS2	0.22923	-0.98974	0.760506
LRRFIP1	0.203442	-0.99111	0.787672
WASHC5	0.692021	-0.99373	0.301707
ST13	0.119445	-0.99472	0.87527
PRKCD	0.706945	-0.99708	0.290131
ACOX1	0.703793	-0.99716	0.293365
PPP1CB	0.924413	-0.9975	0.073091
SNRPF	0.02904	-0.99754	0.968504
SERBP1	0.192554	-0.99813	0.80558
PABPC4	0.280198	-0.99935	0.719155
LIMS1	0.001825	-0.9994	0.997571
CSRP1	0.401714	-1.00044	0.598728
RHOA	-0.16262	-1.00098	1.163601
EIF3G	0.381594	-1.00223	0.620634
RPL8	0.707964	-1.00272	0.294758
SLC8A1	0.364758	-1.00511	0.640349
MRPL12	0.279662	-1.00608	0.726421
UBE2N	0.613655	-1.00659	0.392934
SARS	0.520637	-1.00745	0.486816

PSMA7	0.238006	-1.00766	0.769657
DNAJC7	0.699951	-1.00817	0.308216
AASDHPPT	0.31844	-1.00842	0.689981
ATG7	0.427036	-1.00864	0.581606
GABARAPL2	0.30433	-1.00878	0.704447
CD84	0.691026	-1.00881	0.31778
EEF1D	0.277812	-1.01092	0.73311
VCP	0.510761	-1.01199	0.501225
PLCB2	0.504676	-1.01392	0.509249
XRCC6	0.443992	-1.01405	0.570053
XPO7	0.884494	-1.01432	0.129823
MAT2B	0.577122	-1.01443	0.437312
PSMA6	0.36092	-1.01699	0.656074
HNRNPD	0.046359	-1.01869	0.972333
XRCC5	0.358418	-1.01882	0.660399
RAD23B	0.328643	-1.02002	0.691374
CANX	0.1716	-1.02124	0.849642
PSMC3	0.642891	-1.0216	0.37871
HERC4	0.912357	-1.02214	0.109779
PSMC4	0.207166	-1.0223	0.815135
ASNA1	0.747502	-1.02278	0.275278
EIF3M	0.006781	-1.02499	1.018207
ARHGAP45	0.771879	-1.02523	0.253351
ARHGAP30	0.778453	-1.02617	0.24772
HYPK	0.224363	-1.02617	0.801811
EIF3H	0.645565	-1.02669	0.381127
EEF1B2	0.190321	-1.02728	0.836963
VAV1	1.028551	-1.02901	0.000462
PSAP	0.248172	-1.03205	0.783874
PRKACA	0.600218	-1.03279	0.432568
CALR	0.294456	-1.03381	0.739358
CDC37	0.07877	-1.03439	0.955624
SAR1A	0.256372	-1.03626	0.77989
CNPY3	0.617823	-1.03639	0.418569
RAB14	0.499145	-1.03681	0.537661
C5AR1	0.371305	-1.03769	0.666386
HNRNPF	0.716899	-1.0391	0.322198
ENSA	0.409574	-1.0404	0.630823
HNRNPUL1	0.443054	-1.04041	0.597353
DOCK8	0.630626	-1.04062	0.409997
CLIC4	0.266166	-1.0413	0.775135
TMEM43	0.602002	-1.04158	0.439574
NDRG1	0.530408	-1.04238	0.511973
CSTB	-0.00483	-1.04252	1.04735
CLTB	0.304718	-1.04368	0.738959
PRPS2	0.540434	-1.04416	0.50373

SUMO3	0.334488	-1.04463	0.710146
ILF2	0.849995	-1.0458	0.19581
RPS15	0.402999	-1.04873	0.645732
MYL6	0.561909	-1.04879	0.48688
RANBP1	0.224651	-1.04897	0.82432
UCHL3	0.27092	-1.05073	0.779813
CLTCL1	0.389523	-1.051	0.661479
TPMT	0.415074	-1.05728	0.642209
CAST	0.211479	-1.05742	0.845938
SUMF2	0.280127	-1.05775	0.77762
PPA1	0.540331	-1.05862	0.518288
EIF3F	0.231252	-1.06087	0.829622
SF3B1	0.621322	-1.06124	0.439922
SNX6	0.648097	-1.06171	0.413616
RPL30	0.817284	-1.0618	0.244514
DARS	0.628788	-1.06218	0.43339
KIF5B	0.678668	-1.06348	0.384814
TXNL1	0.214923	-1.06424	0.849313
PSMB1	0.556783	-1.06432	0.507538
LSP1	0.172491	-1.06514	0.892646
BROX	0.470831	-1.06593	0.595099
UFM1	0.30246	-1.06631	0.763854
GDI2	0.537056	-1.06663	0.529574
SRP9	0.324722	-1.06747	0.74275
PSMA4	0.089094	-1.06901	0.979917
SET	0.164126	-1.06929	0.905165
CSTA	0.347676	-1.06934	0.721663
ALDH3A2	0.492441	-1.06943	0.57699
ARMT1	0.271806	-1.06948	0.797678
SIRPA	0.435267	-1.06986	0.634593
CBR1	0.314085	-1.0706	0.756516
SNAP23	0.320483	-1.07191	0.751426
ANPEP	0.302605	-1.07196	0.769354
STRAP	0.470488	-1.07282	0.602332
MANF	0.403991	-1.07321	0.669219
SUB1	0.12232	-1.07404	0.951719
TRIM25	0.707188	-1.0748	0.367611
STIP1	0.29284	-1.07547	0.782625
TBCB	0.564753	-1.07553	0.510777
SPCS2	0.551356	-1.07642	0.525065
PTPA	0.537846	-1.07875	0.540902
EIF3D	0.60736	-1.07889	0.47153
ARF5	0.57247	-1.08131	0.508844
GGCT	0.462264	-1.08255	0.620288
EIF3B	0.551611	-1.08256	0.530946
PSME3	0.342028	-1.08421	0.74218

ALDH3B1	0.357392	-1.08479	0.727397
PCBP1	0.615402	-1.08554	0.470136
PPP1CA	0.165659	-1.0867	0.921044
CLIC1	0.141116	-1.08751	0.946389
UNC45A	0.708702	-1.08842	0.379717
COMMD7	0.678376	-1.08983	0.411449
DNAJA2	0.596779	-1.09069	0.493913
KCTD12	0.649281	-1.09437	0.445093
ADSL	0.369836	-1.09448	0.724644
YARS	0.327476	-1.09605	0.768571
AK3	0.540709	-1.09623	0.555524
SLC1A4	0.473417	-1.09637	0.622954
OLA1	0.606372	-1.0969	0.490525
COPB2	0.49227	-1.09705	0.604784
ATP1B3	0.455278	-1.09952	0.644245
AP2B1	0.73121	-1.09972	0.368511
CD81	0.374403	-1.10004	0.725635
HSPA4	0.370847	-1.10051	0.729667
JPT1	0.466261	-1.10095	0.634688
EEF1G	0.74887	-1.10168	0.352814
PSMA1	0.289202	-1.10323	0.814031
SLC30A1	0.553537	-1.10361	0.550075
ATOX1	0.240053	-1.10377	0.863714
IQGAP1	0.855377	-1.10443	0.249056
CAP1	0.45661	-1.10567	0.649062
TKT	0.301797	-1.10575	0.803954
PSMA5	-0.06015	-1.10593	1.166083
CRIP1	0.413432	-1.10658	0.693147
RAB10	0.372529	-1.10684	0.734315
HNRNPAB	0.298485	-1.11006	0.811577
ITGB1	0.173361	-1.11016	0.936799
NAA15	0.611674	-1.11081	0.499131
CSK	0.71961	-1.11224	0.392634
LASP1	0.544955	-1.11446	0.569503
ANXA11	0.525823	-1.11582	0.589998
CDS2	0.532589	-1.11599	0.583399
RTN4	0.765684	-1.11719	0.35151
BTF3	0.33832	-1.11728	0.77896
TOR1AIP1	0.327103	-1.11795	0.790845
CAPNS1	0.069497	-1.11888	1.049379
PDAP1	0.360801	-1.11956	0.75876
NDUFA5	0.611642	-1.11962	0.507982
EPB41L3	0.562618	-1.12049	0.557875
GRPEL1	0.284751	-1.12421	0.839454
G3BP1	0.555027	-1.12444	0.56941
CAPZA1	0.36142	-1.12568	0.764257

ATP6V1H	0.502977	-1.12681	0.623832
HNRNPK	0.582447	-1.12891	0.54646
CDV3	0.245218	-1.13024	0.885024
ARF1	0.447917	-1.13124	0.683327
HSPB11	0.558653	-1.13198	0.573322
LCP1	0.429345	-1.13277	0.703422
DNAJB1	0.639762	-1.13447	0.494707
PHB	0.743639	-1.13479	0.391147
S100A11	0.213611	-1.13519	0.921577
CRABP2	0.540283	-1.13625	0.595971
AHCY	0.685087	-1.13758	0.452493
CHMP4B	0.600087	-1.13782	0.537736
TFG	0.311523	-1.13838	0.826854
PPP1R12A	0.149796	-1.14025	0.99045
SGTB	0.347565	-1.14056	0.79299
PDHB	0.52555	-1.14177	0.616219
TFRC	0.953561	-1.14227	0.188704
SLC39A11	0.497139	-1.14246	0.645317
ATP6V1E1	0.614883	-1.14269	0.527804
TBCA	0.313788	-1.14465	0.830863
CCT6A	0.667994	-1.14551	0.477518
EFHD2	0.511722	-1.14552	0.633795
ALCAM	0.49633	-1.14782	0.65149
GBP2	0.470996	-1.14916	0.678162
KLC1	0.560986	-1.14984	0.58885
LPP	0.399825	-1.15076	0.750937
CAND1	0.702859	-1.15122	0.448365
BRK1	0.423172	-1.15499	0.731821
MARCKS	0.40606	-1.15657	0.750508
CMPK1	0.312246	-1.15695	0.844706
WDR11	0.573054	-1.15863	0.585574
EIF1AX	0.463102	-1.15911	0.696011
TMED2	0.569581	-1.1595	0.589921
KHSRP	0.580556	-1.1604	0.579842
SNX5	0.50865	-1.16063	0.651977
PURB	0.496986	-1.16358	0.666593
CBX3	0.449747	-1.1644	0.714658
PTRHD1	0.501413	-1.16441	0.663001
ELOB	0.482243	-1.16468	0.682436
BTF3L4	0.326005	-1.16488	0.838877
RP2	0.443303	-1.16786	0.72456
STAT6	0.812484	-1.16794	0.35546
TMED5	0.481758	-1.16962	0.687862
AARS	0.434878	-1.17183	0.736948
HSPA1B	0.702669	-1.17451	0.47184
FUS	0.488013	-1.17544	0.687423

CCT5	0.595062	-1.17653	0.581472
SLC9A3R1	0.565906	-1.17723	0.611328
UFC1	0.458717	-1.17962	0.720904
NME2	0.382623	-1.18109	0.798468
ISOC1	0.398895	-1.18441	0.785514
CHD4	0.468883	-1.18471	0.715825
SAR1B	0.451921	-1.18513	0.733205
CSE1L	0.635746	-1.18621	0.550463
PSMD14	0.515069	-1.18913	0.674064
ARL8A	0.406843	-1.19083	0.783987
SEC13	0.58594	-1.19172	0.605783
NSFL1C	0.357201	-1.19711	0.839905
DEK	0.601948	-1.19838	0.596432
SCFD1	0.427559	-1.19959	0.772026
ADH5	0.406524	-1.20248	0.795955
WASF2	0.458507	-1.20355	0.745044
CYFIP1	0.61934	-1.2037	0.58436
UBA52	0.481535	-1.20476	0.723228
PPP2R1A	0.678503	-1.20911	0.53061
SSB	0.439882	-1.21053	0.770648
ZYX	0.366826	-1.21338	0.846556
CACYBP	0.639687	-1.21834	0.578657
PITPNB	0.660359	-1.21846	0.558104
REEP5	0.387474	-1.21912	0.831647
GLO1	0.462582	-1.22192	0.759339
SPAG9	0.452051	-1.22338	0.771326
PI4K2A	0.654234	-1.22505	0.570819
CAPN1	0.675083	-1.22717	0.552083
PLAA	0.567759	-1.22841	0.660651
EIF3E	0.37	-1.22861	0.858612
NSUN2	0.510029	-1.22946	0.719433
CD82	0.534568	-1.23374	0.699176
PTPN6	0.595972	-1.23718	0.641207
PPP3R1	0.627218	-1.23799	0.610777
HMGN1	0.650966	-1.24114	0.590176
UBLCP1	0.535318	-1.24301	0.707688
ENOPH1	0.613466	-1.24411	0.63064
EIF2S2	0.417241	-1.24624	0.828997
PAK2	0.6063	-1.2467	0.640403
GMPS	0.738126	-1.24805	0.509928
SEC62	0.491545	-1.25127	0.759724
CCT3	0.743567	-1.26067	0.517099
STT3B	0.731197	-1.26484	0.533641
RAB35	0.432714	-1.26575	0.833037
GPI	0.480027	-1.26678	0.786749
ETF1	0.464872	-1.26893	0.804061

PRDX6	0.64607	-1.27218	0.626109
PTPN1	0.544588	-1.27563	0.731039
TSPO	0.672571	-1.31561	0.643043

REFERENCES

Abramov, A. Y. and M. R. Duchen (2003). "Actions of ionomycin, 4-BrA23187 and a novel electrogenic Ca2+ ionophore on mitochondria in intact cells." Cell calcium **33**(2): 101-112.

Acosta, J., et al. (2000). "Molecular basis for a link between complement and the vascular complications of diabetes." Proceedings of the National Academy of Sciences **97**(10): 5450-5455.

Adler, S., et al. (1986). "Complement membrane attack complex stimulates production of reactive oxygen metabolites by cultured rat mesangial cells." The Journal of clinical investigation **77**(3): 762-767.

Agostini, L., et al. (2004). "NALP3 forms an IL-1β-processing inflammasome with increased activity in Muckle-Wells autoinflammatory disorder." Immunity **20**(3): 319-325.

Akagawa, K. S. (2002). "Functional Heterogeneity of Colony-Stimulating Factor-Induced Human Nonocyte-Derived Macrophages." International journal of hematology **76**(1): 27-34.

Alper, C. A., et al. (1969). "Human C'3: evidence for the liver as the primary site of synthesis." Science **163**(3864): 286-288.

An, L. L., et al. (2014). "Complement C5a potentiates uric acid crystal-induced IL-1β production." European journal of immunology **44**(12): 3669-3679.

Anastasiu, C. V., et al. (2020). "Biomarkers for the noninvasive diagnosis of endometriosis: state of the art and future perspectives." **21**(5): 1750.

Arbore, G. and C. Kemper (2016). "A novel "complement–metabolism–inflammasome axis" as a key regulator of immune cell effector function." European journal of immunology **46**(7): 1563-1573.

Arlehamn, C. S. L., et al. (2010). "The role of potassium in inflammasome activation by bacteria." **285**(14): 10508-10518.

Asgari, E., et al. (2013). "C3a modulates IL-1β secretion in human monocytes by regulating ATP efflux and subsequent NLPR3 inflammasome activation." Blood: blood-2013-2005-502229.

Ashburner, M., et al. (2000). "Gene ontology: tool for the unification of biology." Nature genetics **25**(1): 25-29.

Astier, A. L., et al. (2006). "Alterations in CD46-mediated Tr1 regulatory T cells in patients with multiple sclerosis." The Journal of clinical investigation **116**(12): 3252-3257.

Banda, N. K., et al. (2012). "Role of C3a receptors, C5a receptors, and complement protein C6 deficiency in collagen antibody-induced arthritis in mice." The Journal of Immunology **188**(3): 1469-1478.

Benoit, M. E. and A. J. J. J. o. N. Tenner (2011). "Complement protein C1q-mediated neuroprotection is correlated with regulation of neuronal gene and microRNA expression." **31**(9): 3459-3469.

Beum, P. V., et al. (2008). "Complement activation on B lymphocytes opsonized with rituximab or ofatumumab produces substantial changes in membrane structure preceding cell lysis." The Journal of Immunology **181**(1): 822-832.

Bordbar, A., et al. (2012). "Model-driven multi-omic data analysis elucidates metabolic immunomodulators of macrophage activation." **8**(1): 558.

Brand, M. D., et al. (2016). "Suppressors of superoxide-H2O2 production at site IQ of mitochondrial complex I protect against stem cell hyperplasia and ischemia-reperfusion injury." **24**(4): 582-592.

Brand, M. D., et al. (2016). "Functional Characterization of S1QELs." **100**: S31-S32.

Buchner, H. (1891). "Zur Nomenklatur der schutzenden Eiweisskorper." Centr Bakteriol Parasitenk **10**: 699–701.

Campanella, M., et al. (2009). "IF1: setting the pace of the F1Fo-ATP synthase." Trends in biochemical sciences **34**(7): 343-350.

Campbell, A., et al. (1979). "Rapid increase in intracellular free Ca2+ induced by antibody plus complement." FEBS letters **107**(1): 55-60.

Cao, S., et al. (2016). "CFH Y402H polymorphism and the complement activation product C5a: effects on NF-κB activation and inflammasome gene regulation." British Journal of Ophthalmology: bjophthalmol-2015-307213.

Cardone, J., et al. (2010). "Complement regulator CD46 temporally regulates cytokine production by conventional and unconventional T cells." Nature immunology **11**(9): 862.

Chen, K., et al. (2013). "ATP-P2X4 signaling mediates NLRP3 inflammasome activation: a novel pathway of diabetic nephropathy." The international journal of biochemistry & cell biology **45**(5): 932-943.

Chen, Y., et al. (2007). "Terminal complement complex C5b-9-treated human monocyte-derived dendritic cells undergo maturation and induce Th1 polarization." European journal of immunology **37**(1): 167-176.

Chinetti-Gbaguidi, G., et al. (2015). "Macrophage subsets in atherosclerosis." **12**(1): 10-17.

Cohen, J. J. N. (2002). "The immunopathogenesis of sepsis." **420**(6917): 885-891.

Colten, H. and R. Strunk (1993). Synthesis of complement components in liver and at extrahepatic sites. Complement in health and disease, Springer**:** 127-158.

Conway, B. R., et al. (2007). "Association between haptoglobin gene variants and diabetic nephropathy: haptoglobin polymorphism in nephropathy susceptibility." **105**(3): e75-e79.

Cox, A. G., et al. (2010). "Mitochondrial peroxiredoxin involvement in antioxidant defence and redox signalling." Biochemical Journal **425**(2): 313-325.

Creagh, E. M. and L. A. J. O'Neill (2006). "TLRs, NLRs and RLRs: a trinity of pathogen sensors that co-operate in innate immunity." Trends in Immunology **27**(8): 352-357.

Cumpelik, A., et al. (2015). "Neutrophil microvesicles resolve gout by inhibiting C5a-mediated priming of the inflammasome." Annals of the rheumatic diseases: annrheumdis-2015-207338.

Cumpelik, A., et al. (2016). "Neutrophil microvesicles resolve gout by inhibiting C5a-mediated priming of the inflammasome." Annals of the rheumatic diseases **75**(6): 1236-1245.

Davies, A. and P. J. Lachmann (1993). "Membrane defence against complement lysis: the structure and biological properties of CD59." Immunologic research **12**(3): 258.

De Nardo, D. and E. Latz (2011). "NLRP3 inflammasomes link inflammation and metabolic disease." Trends in immunology **32**(8): 373-379.

DeBerardinis, R. J., et al. (2007). "Beyond aerobic glycolysis: transformed cells can engage in glutamine metabolism that exceeds the requirement for protein and nucleotide synthesis." Proceedings of the National Academy of Sciences **104**(49): 19345-19350.

Diaz-del-Olmo, I., et al. (2021). "Internalization of the Membrane Attack Complex Triggers NLRP3 Inflammasome Activation and IL-1β Secretion in Human Macrophages." **12**.

Dispersyn, G., et al. (1999). "Bcl-2 protects against FCCP-induced apoptosis and mitochondrial membrane potential depolarization in PC12 cells." Biochimica et Biophysica Acta (BBA)-General Subjects **1428**(2-3): 357-371.

Doni, A., et al. (2021). "Serum amyloid P component is an essential element of resistance against Aspergillus fumigatus." **12**(1): 1-15.

Dowling, J. K. and L. A. O'Neill (2012). "Biochemical regulation of the inflammasome." Critical reviews in biochemistry and molecular biology **47**(5): 424-443.

Dunkelberger, J. R. and W.-C. Song (2009). "Complement and its role in innate and adaptive immune responses." Cell Res **20**(1): 34-50.

Duquesnoy, R. J., et al. (2013). "Structural aspects of HLA class I epitopes reacting with human monoclonal antibodies in Ig-binding, C1q-binding and lymphocytotoxicity assays." **74**(10): 1271-1279.

Elimam, H., et al. (2013). "Complement-mediated activation of calcium-independent phospholipase A2γ role of protein kinases and phosphorylation." Journal of Biological Chemistry **288**(6): 3871-3885.

Evavold, C. L., et al. (2018). "The pore-forming protein gasdermin D regulates interleukin-1 secretion from living macrophages." **48**(1): 35-44. e36.

Fan, X. G., et al. (2021). "Melittin ameliorates inflammation in mouse acute liver failure via inhibition of PKM2-mediated Warburg effect." Acta Pharmacol Sin **42**(8): 1256-1266.

Feissner, R. F., et al. (2009). "Crosstalk signaling between mitochondrial Ca2+ and ROS." Frontiers in bioscience: a journal and virtual library **14**: 1197.

Finucane, O. M., et al. (2015). "Monounsaturated fatty acid enriched high fat-diets impede adipose NLRP3 inflammasome mediated IL-1β secretion and insulin resistance despite obesity." Diabetes: db141098.

Fleetwood, A. J., et al. (2005). "Functions of granulocyte-macrophage colony-stimulating factor." **25**(5).

Flyvbjerg, A. J. N. R. N. (2017). "The role of the complement system in diabetic nephropathy." **13**(5): 311-318.

Friščić, J., et al. (2021). "The complement system drives local inflammatory tissue priming by metabolic reprogramming of synovial fibroblasts." **54**(5): 1002-1021. e1010.

Galván-Peña, S. and L. A. O'Neill (2014). "Metabolic reprograming in macrophage polarization." Frontiers in immunology **5**: 420.

Garai, J., et al. (2005). "Ketone bodies affect the enzymatic activity of macrophage migration inhibitory factor." **77**(12): 1375-1380.

Gene Ontology, C. (2021). "The Gene Ontology resource: enriching a GOld mine." Nucleic Acids Research **49**(D1): D325-D334.

Gros, P., et al. (2008). "Complement driven by conformational changes." <u>Nature reviews. Immunology</u> **8**(1): 48.

Guo, H., et al. (2015). "Inflammasomes: mechanism of action, role in disease, and therapeutics." <u>Nature medicine</u> **21**(7): 677-687.

Haeffner-Cavaillon, N., et al. (1987). "C3a (C3adesArg) induces production and release of interleukin 1 by cultured human monocytes." <u>The Journal of Immunology</u> **139**(3): 794-799.

Hamilton, K., et al. (1993). "Interaction between apolipoproteins AI and A-II and the membrane attack complex of complement. Affinity of the apoproteins for polymeric C9." **268**(5): 3632-3638.

Hänsch, G., et al. (1984). "Macrophages release arachidonic acid, prostaglandin E2, and thromboxane in response to late complement components." <u>The Journal of Immunology</u> **133**(4): 2145-2150.

Heneka, M. T., et al. (2013). "NLRP3 is activated in Alzheimer's disease and contributes to pathology in APP/PS1 mice." <u>Nature</u> **493**(7434): 674-678.

Holers, V. M. and N. K. Banda (2018). "Complement in the initiation and evolution of rheumatoid arthritis." <u>Frontiers in immunology</u> **9**: 1057.

Hom, J. R., et al. (2007). "Thapsigargin induces biphasic fragmentation of mitochondria through calcium-mediated mitochondrial fission and apoptosis." <u>Journal of cellular physiology</u> **212**(2): 498-508.

Huang, L. K., Wang M. J. J. (1995). "Image thresholding by minimizing the measures of fuzziness." <u>Pattern recognition</u> **28(1)** 41-51.

Hume, D. A., et al. (2019). "The mononuclear phagocyte system: the relationship between monocytes and macrophages." **40**(2): 98-112.

Ivashkiv, L. B. J. N. R. I. (2018). "IFNγ: signalling, epigenetics and roles in immunity, metabolism, disease and cancer immunotherapy." **18**(9): 545-558.

Izquierdo, E., et al. (2015). "Reshaping of human macrophage polarization through modulation of glucose catabolic pathways." <u>The Journal of Immunology</u> **195**(5): 2442-2451.

Izquierdo, E., et al. (2015). "Reshaping of human macrophage polarization through modulation of glucose catabolic pathways." **195**(5): 2442-2451.

Jane-wit, D., et al. (2015). "Complement membrane attack complexes activate noncanonical NF-κB by forming an Akt+ NIK+ signalosome on Rab5+ endosomes." Proceedings of the National Academy of Sciences **112**(31): 9686-9691.

Jeon, H., et al. (2018). "Activation of the complement system in an osteosarcoma cell line promotes angiogenesis through enhanced production of growth factors." Scientific reports **8**(1): 5415.

Jimenez-Duran, G., et al. (2022). "Complement membrane attack complex is an immunometabolic regulator of NLRP3 activation and IL-18 secretion in human macrophages." **13**.

Jimenez-Duran, G., et al. (2020). "Pharmacological validation of targets regulating CD14 during macrophage differentiation." **61**: 103039.

Jimenez-Duran, G. and M. Triantafilou (2021). "Metabolic regulators of enigmatic inflammasomes in autoimmune diseases and crosstalk with innate immune receptors." Immunology **163**(4): 348-362.

Kalhan, S. C. and R. W. Hanson (2012). "Resurgence of serine: an often neglected but indispensable amino Acid." Journal of Biological Chemistry **287**(24): 19786-19791.

Kang, K., et al. (2019). "IFN-γ selectively suppresses a subset of TLR4-activated genes and enhancers to potentiate macrophage activation." **10**(1): 1-14.

Kanneganti, T.-D. J. N. R. I. (2010). "Central roles of NLRs and inflammasomes in viral infection." **10**(10): 688-698.

Karlsson, K. R., et al. (2008). "Homogeneous monocytes and macrophages from human embryonic stem cells following coculture-free differentiation in M-CSF and IL-3." Experimental hematology **36**(9): 1167-1175.

Kastbom, A., et al. (2008). "Genetic variation in proteins of the cryopyrin inflammasome influences susceptibility and severity of rheumatoid arthritis (the Swedish TIRA project)." Rheumatology **47**(4): 415-417.

Katsiari, C. G., et al. (2010). The pathophysiologic role of monocytes and macrophages in systemic lupus erythematosus: a reappraisal. Seminars in arthritis and rheumatism, Elsevier.

Kaufmann, S. H. (2008). "Immunology's foundation: the 100-year anniversary of the Nobel Prize to Paul Ehrlich and Elie Metchnikoff." Nat Immunol **9**(7): 705-712.

Kelly, B. and L. A. O'neill (2015). "Metabolic reprogramming in macrophages and dendritic cells in innate immunity." Cell research **25**(7): 771-784.

Kim, D. D. and W.-C. Song (2006). "Membrane complement regulatory proteins." Clinical immunology **118**(2): 127-136.

Kim, J., et al. (2009). "The role of apolipoprotein E in Alzheimer's disease." **63**(3): 287-303.

Köhl, J. (2006). "The role of complement in danger sensing and transmission." Immunologic research **34**(2): 157-176.

Kolev, M., et al. (2015). "Complement regulates nutrient influx and metabolic reprogramming during Th1 cell responses." Immunity **42**(6): 1033-1047.

Koopman, J. J., et al. (2021). "Deposition of the membrane attack complex in healthy and diseased human kidneys." **11**: 599974.

Lage, S. L., et al. (2020). Complement-driven inflammasome activation on circulating blood monocytes in immune reconstitution inflammatory syndrome in TB-HIV coinfected patients, The Journal of Immunology. **204:** 225.234.

Lambris, J. D., et al. (2008). "Complement evasion by human pathogens." Nat Rev Micro **6**(2): 132-142.

Latz, E., et al. (2013). "Activation and regulation of the inflammasomes." Nature Reviews Immunology **13**(6): 397-411.

Laudisi, F., et al. (2013). "Cutting edge: the NLRP3 inflammasome links complement-mediated inflammation and IL-1β release." The Journal of Immunology **191**(3): 1006-1010.

Laudisi, F., et al. (2013). "Cutting edge: the NLRP3 inflammasome links complement-mediated inflammation and IL-1β release." The Journal of Immunology: 1300489.

Liang, Y., et al. (2018). "Coagulation cascade and complement system in systemic lupus erythematosus." **9**(19): 14862.

Liu, C.-C., et al. (2017). "ApoE4 accelerates early seeding of amyloid pathology." **96**(5): 1024-1032. e1023.

Liu, W. J., et al. (2017). "Blockage of the lysosome-dependent autophagic pathway contributes to complement membrane attack complex-induced podocyte injury in idiopathic membranous nephropathy." **7**(1): 1-18.

Lueck, K., et al. (2011). "Sub-lytic C5b-9 induces functional changes in retinal pigment epithelial cells consistent with age-related macular degeneration." Eye **25**(8): 1074-1082.

Lusthaus, M., et al. (2018). "Receptor-interacting protein kinases 1 and 3, and mixed lineage kinase domain-like protein are activated by sublytic complement and participate in complement-dependent cytotoxicity." Frontiers in immunology **9**: 306.

Ma, W.-T., et al. (2019). "The role of monocytes and macrophages in autoimmune diseases: a comprehensive review." Frontiers in immunology **10**: 1140.

Martinez, F. O. and S. J. F. r. Gordon (2014). "The M1 and M2 paradigm of macrophage activation: time for reassessment." **6**.

Mayor, A., et al. (2007). "A crucial function of SGT1 and HSP90 in inflammasome activity links mammalian and plant innate immune responses." Nature immunology **8**(5): 497.

Mazodier, K., et al. (2005). "Severe imbalance of IL-18/IL-18BP in patients with secondary hemophagocytic syndrome." **106**(10): 3483-3489.

McGarry, T., et al. (2017). "Resolution of TLR2-induced inflammation through manipulation of metabolic pathways in rheumatoid arthritis." Scientific reports **7**(1): 1-13.

McInnes, I. B., et al. (2016). "Cytokines in rheumatoid arthritis—shaping the immunological landscape." **12**(1): 63-68.

Meng, Q., et al. (2020). "Dexmedetomidine inhibits LPS-induced proinflammatory responses via suppressing HIF1α-dependent glycolysis in macrophages." Aging (Albany NY) **12**(10): 9534.

Merle, N. S., et al. (2015). "Complement System Part II: Role in Immunity." Frontiers in Immunology **6**: 257.

Mevorach, D., et al. (1998). "Complement-dependent clearance of apoptotic cells by human macrophages." Journal of Experimental Medicine **188**(12): 2313-2320.

Meyer, M. M., et al. (2021). "Mitochondrial and Glycolytic Capacity of Peripheral Blood Mononuclear Cells Isolated From Diverse Poultry Genetic Lines: Optimization and Assessment." **8**.

Mi, H., et al. (2019). "PANTHER version 14: more genomes, a new PANTHER GO-slim and improvements in enrichment analysis tools." Nucleic Acids Res **47**(D1): D419-D426.

Michailidou, I., et al. (2018). "Systemic inhibition of the membrane attack complex impedes neuroinflammation in chronic relapsing experimental autoimmune encephalomyelitis." Acta neuropathologica communications **6**(1): 1-17.

Michl, J., et al. (1976). "2-Deoxyglucose selectively inhibits Fc and complement receptor-mediated phagocytosis in mouse peritoneal macrophages. I. Description of the inhibitory effect." The Journal of experimental medicine **144**(6): 1465-1483.

Migneco, G., et al. (2010). "Glycolytic cancer associated fibroblasts promote breast cancer tumor growth, without a measurable increase in angiogenesis: evidence for stromal-epithelial metabolic coupling." Cell cycle **9**(12): 2412-2422.

Mills, E. and L. A. O'Neill (2019). "Not all mitochondrial cristae are the same: Hetero-potential in the inner mitochondrial membrane." Immunometabolism **2**(1).

Mills, E. L., et al. (2016). "Succinate dehydrogenase supports metabolic repurposing of mitochondria to drive inflammatory macrophages." Cell **167**(2): 457-470. e413.

Mills, E. L., et al. (2016). "Succinate Dehydrogenase Supports Metabolic Repurposing of Mitochondria to Drive Inflammatory Macrophages." Cell **167**(2): 457-470 e413.

Moon, J.-S., et al. (2015). "mTORC1-induced HK1-dependent glycolysis regulates NLRP3 inflammasome activation." Cell Reports **12**(1): 102-115.

Moon, J.-S., et al. (2015). "mTORC1-induced HK1-dependent glycolysis regulates NLRP3 inflammasome activation." **12**(1): 102-115.

Moreno-Navarrete, J. M. and J. M. Fernández-Real (2019). The complement system is dysfunctional in metabolic disease: Evidences in plasma and adipose tissue from obese and insulin resistant subjects. Seminars in cell & developmental biology, Elsevier.

Morgan, B. (1990). "The biological effects of complement activation." Complement. Clinical aspects and relevance to disease. Academic Press, London, United Kingdom: 37-55.

Morgan, B. (1992). Effects of the membrane attack complex of complement on nucleated cells. Membrane defenses against attack by complement and perforins, Springer**:** 115-140.

Morgan, B., et al. (1986). "Intracellular Ca2+ and cell injury: a paradoxical role of Ca2+ in complement membrane attack." Cell calcium **7**(5-6): 399-411.

Morgan, B. P. (1989). "Complement membrane attack on nucleated cells: resistance, recovery and non-lethal effects." Biochemical Journal **264**(1): 1.

MORGAN, B. P. (2003). "Beyond lysis: how complement influences cell fate." Clinical science **104**(5): 455-466.

Morgan, B. P. (2016). "The membrane attack complex as an inflammatory trigger." Immunobiology **221**(6): 747-751.

Morgan, B. P. and A. K. Campbell (1985). "The recovery of human polymorphonuclear leucocytes from sublytic complement attack is mediated by changes in intracellular free calcium." Biochemical Journal **231**(1): 205-208.

Murphy, A. J., et al. (2016). "IL-18 production from the NLRP1 inflammasome prevents obesity and metabolic syndrome." Cell metabolism **23**(1): 155-164.

Murray, P. J. J. A. r. o. p. (2017). "Macrophage polarization." **79**: 541-566.

Narasimhan, R., et al. (2018). "Serum metabolomic profiling predicts synovial gene expression in rheumatoid arthritis." Arthritis research & therapy **20**(1): 164.

Neumann, E., et al. (2002). "Local production of complement proteins in rheumatoid arthritis synovium." Arthritis & Rheumatism: Official Journal of the American College of Rheumatology **46**(4): 934-945.

Newsholme, P., et al. (1986). "Metabolism of glucose, glutamine, long-chain fatty acids and ketone bodies by murine macrophages." Biochemical Journal **239**(1): 121-125.

Niculescu, F., et al. (1997). "Activation of Ras and mitogen-activated protein kinase pathway by terminal complement complexes is G protein dependent." The Journal of Immunology **158**(9): 4405-4412.

Noris, M. and G. Remuzzi (2013). Overview of complement activation and regulation. Seminars in nephrology, Elsevier.

O'Neill, L. A. and D. G. Hardie (2013). "Metabolism of inflammation limited by AMPK and pseudo-starvation." Nature **493**(7432): 346.

O'Neill, L. A., et al. (2016). "A guide to immunometabolism for immunologists." Nature Reviews Immunology **16**(9): 553.

Oberbach, A., et al. (2011). "Combined proteomic and metabolomic profiling of serum reveals association of the complement system with obesity and identifies novel markers of body fat mass changes." **10**(10): 4769-4788.

Palmieri, E. M., et al. (2017). "Pharmacologic or genetic targeting of glutamine synthetase skews macrophages toward an M1-like phenotype and inhibits tumor metastasis." **20**(7): 1654-1666.

Palsson-McDermott, E. M., et al. (2015). "Pyruvate kinase M2 regulates Hif-1α activity and IL-1β induction and is a critical determinant of the warburg effect in LPS-activated macrophages." Cell metabolism **21**(1): 65-80.

Pandeya, A., et al. (2019). "Gasdermin D (GSDMD) as a new target for the treatment of infection." **10**(5): 660-667.

Pang, Z., et al. (2021). "MetaboAnalyst 5.0: narrowing the gap between raw spectra and functional insights." Nucleic Acids Research **49**(W1): W388–W396.

Park, H. and N. H. Jeoung (2016). "Inflammation increases pyruvate dehydrogenase kinase 4 (PDK4) expression via the Jun N-Terminal Kinase (JNK) pathway in C2C12 cells." Biochemical and biophysical research communications **469**(4): 1049-1054.

Phieler, J., et al. (2013). The role of the complement system in metabolic organs and metabolic diseases. Seminars in immunology, Elsevier.

Plubell, D. L., et al. (2017). "Extended Multiplexing of Tandem Mass Tags (TMT) Labeling Reveals Age and High Fat Diet Specific Proteome Changes in Mouse Epididymal Adipose Tissue." Mol Cell Proteomics **16**(5): 873-890.

Podack, E. R. and J. Tschopp (1984). "Membrane attack by complement." Mol Immunol **21**(7): 589-603.

Ponard, D., et al. (2020). "SERPING1 mutation update: Mutation spectrum and C1 Inhibitor phenotypes." **41**(1): 38-57.

Pontillo, A., et al. (2010). "Two SNPs in NLRP3 gene are involved in the predisposition to type-1 diabetes and celiac disease in a pediatric population from northeast Brazil." Autoimmunity **43**(8): 583-589.

Porta, C., et al. (2009). "Tolerance and M2 (alternative) macrophage polarization are related processes orchestrated by p50 nuclear factor κB." **106**(35): 14978-14983.

Potter, M., et al. (2016). "The Warburg effect: 80 years on." Biochemical Society Transactions **44**(5): 1499-1505.

Ram, S., et al. (2010). "Infections of people with complement deficiencies and patients who have undergone splenectomy." Clinical microbiology reviews **23**(4): 740-780.

Rambold, A. S. and E. L. Pearce (2018). "Mitochondrial dynamics at the interface of immune cell metabolism and function." Trends in immunology **39**(1): 6-18.

Ramond, E., et al. (2019). "Pivotal role of mitochondria in macrophage response to bacterial pathogens." Frontiers in immunology **10**: 2461.

Reid, E., et al. (2012). Cells, Membranes, and Disease, Including Renal: Including Renal, Springer Science & Business Media.

Ricklin, D., et al. (2010). "Complement: a key system for immune surveillance and homeostasis." Nature immunology **11**(9): 785-797.

Ricklin, D. and J. D. Lambris (2013). "Complement in immune and inflammatory disorders: pathophysiological mechanisms." J Immunol **190**(8): 3831-3838.

Ricklin, D., et al. (2016). "Complement in disease: a defence system turning offensive." Nature Reviews Nephrology **12**(7): 383-401.

Rijkers, M., et al. (2019). "Anti-HLA antibodies with complementary and synergistic interaction geometries promote classical complement activation on platelets." **104**(2): 403.

Robb, E. L., et al. (2015). "Selective superoxide generation within mitochondria by the targeted redox cycler MitoParaquat." Free Radical Biology and Medicine **89**: 883-894.

Romero, V., et al. (2013). "Immune-mediated pore-forming pathways induce cellular hypercitrullination and generate citrullinated autoantigens in rheumatoid arthritis." Science translational medicine **5**(209): 209ra150-209ra150.

Saito, P. K., et al. (2014). "Complement-Dependent Cytotoxicity (CDC) to Detect Anti-HLA Antibodies: Old but Gold." **28**(4): 275-280.

Samstad, E. O., et al. (2014). "Cholesterol crystals induce complement-dependent inflammasome activation and cytokine release." The Journal of Immunology: 1302484.

Schroder, K., et al. (2010). "The NLRP3 inflammasome: a sensor for metabolic danger?" Science **327**(5963): 296-300.

Shi, L., et al. (2017). "Roles of PFKFB3 in cancer." Signal transduction and targeted therapy **2**(1): 1-10.

Shim, K., et al. (2020). "Complement activation in obesity, insulin resistance, and type 2 diabetes mellitus." World J Diabetes **11**(1): 1-12.

Sims, P. J., et al. (1988). "Complement proteins C5b-9 cause release of membrane vesicles from the platelet surface that are enriched in the membrane receptor for coagulation factor Va and express prothrombinase activity." Journal of Biological Chemistry **263**(34): 18205-18212.

Siouti, E. and E. Andreakos (2019). "The many facets of macrophages in rheumatoid arthritis." Biochemical pharmacology **165**: 152-169.

Skattum, L., et al. (2011). "Complement deficiency states and associated infections." Mol Immunol **48**(14): 1643-1655.

Sokolowska, M., et al. (2015). "Prostaglandin E2 inhibits NLRP3 inflammasome activation through EP4 receptor and intracellular cyclic AMP in human macrophages." The Journal of Immunology: 1401343.

Stanley, E. R. and V. J. C. S. H. p. i. b. Chitu (2014). "CSF-1 receptor signaling in myeloid cells." **6**(6): a021857.

Strainic, M. G., et al. (2008). "Locally produced complement fragments C5a and C3a provide both costimulatory and survival signals to naive CD4+ T cells." <u>Immunity</u> **28**(3): 425-435.

Stratton, D., et al. (2015). "Microvesicles released constitutively from prostate cancer cells differ biochemically and functionally to stimulated microvesicles released through sublytic C5b-9." **460**(3): 589-595.

Stremmel, C., et al. (2018). "Yolk sac macrophage progenitors traffic to the embryo during defined stages of development." **9**(1): 1-14.

Tada-Oikawa, S., et al. (2003). "Mechanism for generation of hydrogen peroxide and change of mitochondrial membrane potential during rotenone-induced apoptosis." <u>Life sciences</u> **73**(25): 3277-3288.

Takano, T., et al. (2013). <u>Complement-mediated cellular injury</u>. Seminars in nephrology, Elsevier.

Tannahill, G., et al. (2013). "Succinate is an inflammatory signal that induces IL-1β through HIF-1α." **496**(7444): 238-242.

Tong, X., et al. (2009). "The molecular determinants of de novo nucleotide biosynthesis in cancer cells." <u>Current opinion in genetics & development</u> **19**(1): 32-37.

Triantafilou, K., et al. (2013). "The complement membrane attack complex triggers intracellular Ca2+ fluxes leading to NLRP3 inflammasome activation." <u>J Cell Sci</u>: jcs. 124388.

Triantafilou, K., et al. (2013). "The complement membrane attack complex triggers intracellular Ca2+ fluxes leading to NLRP3 inflammasome activation." <u>J Cell Sci</u> **126**(13): 2903-2913.

Triantafilou, M., et al. (2022). "Human rhinovirus promotes STING trafficking to replication organelles to promote viral replication." **13**(1): 1-16.

Tschopp, J. and K. Schroder (2010). "NLRP3 inflammasome activation: The convergence of multiple signalling pathways on ROS production?" <u>Nature Reviews Immunology</u> **10**(3): 210-215.

Tyanova, S., et al. (2016). "The Perseus computational platform for comprehensive analysis of (prote)omics data." <u>Nature Methods</u> **13**(9): 731-740.

Valente, A. J., et al. (2017). "A simple ImageJ macro tool for analyzing mitochondrial network morphology in mammalian cell culture." <u>Acta histochemica</u> **119**(3): 315-326.

Van den Bossche, J., et al. (2016). "Mitochondrial dysfunction prevents repolarization of inflammatory macrophages." Cell reports **17**(3): 684-696.

Villanueva, E. B., et al. (2021). "Neuronal TNFα, Not α-Syn, Underlies PDD-Like Disease Progression in IFNβ-KO Mice." **90**(5): 789-807.

Walport , M. J. (2001). "Complement." New England Journal of Medicine **344**(14): 1058-1066.

Wang, D. and D. J. G. De Vivo (2018). "Pyruvate carboxylase deficiency."

Wang, F., et al. (2018). "Interferon gamma induces reversible metabolic reprogramming of M1 macrophages to sustain cell viability and pro-inflammatory activity." **30**: 303-316.

Wang, Q., et al. (2011). "Identification of a central role for complement in osteoarthritis." Nature medicine **17**(12): 1674.

Weissert, V., et al. (2021). "Inhibition of the mitochondrial ATPase function by IF1 changes the spatiotemporal organization of ATP synthase." Biochimica et Biophysica Acta (BBA)-Bioenergetics **1862**(1): 148322.

Wicks, I. P. and A. W. J. N. R. R. Roberts (2016). "Targeting GM-CSF in inflammatory diseases." **12**(1): 37-48.

Williams, G. S., et al. (2013). "Mitochondrial calcium uptake." **110**(26): 10479-10486.

Witebsky, E. (1954). "Ehrlich's side-chain theory in the light of present immunology." Ann N Y Acad Sci **59**(2): 168-181.

Xia, J. and D. S. Wishart (2010). "MSEA: a web-based tool to identify biologically meaningful patterns in quantitative metabolomic data." Nucleic Acids Research **38**(Web Server issue): W71-77.

Xia, J. and D. S. J. N. a. r. Wishart (2010). "MSEA: a web-based tool to identify biologically meaningful patterns in quantitative metabolomic data." **38**(suppl_2): W71-W77.

Xie, C. B., et al. (2020). "Complement Membrane Attack Complex: New Roles, Mechanisms of Action, and Therapeutic Targets." Am J Pathol **190**(6): 1138-1150.

Xie, C. B., et al. (2020). "Complement membrane attack complex: new roles, mechanisms of action, and therapeutic targets." **190**(6): 1138-1150.

Xie, C. B., et al. (2019). "Complement Membrane Attack Complexes Assemble NLRP3 Inflammasomes Triggering IL-1 Activation of IFN-γ–Primed Human Endothelium." Circulation research **124**(12): 1747-1759.

Xu, H., et al. (2019). "The N-end rule ubiquitin ligase UBR2 mediates NLRP1B inflammasome activation by anthrax lethal toxin." **38**(13): e101996.

Yan, B., et al. (2021). "SARS-CoV-2 drives JAK1/2-dependent local complement hyperactivation." **6**(58): eabg0833.

Yang, C., et al. (2014). "Soluble complement complex C5b-9 promotes microglia activation." Journal of neuroimmunology **267**(1-2): 16-19.

Yang, K., et al. (2020). "Lactate suppresses macrophage pro-inflammatory response to LPS stimulation by inhibition of YAP and NF-κB activation via GPR81-mediated signaling." **11**: 587913.

Yasuda, K., et al. (2019). "Interleukin-18 in health and disease." **20**(3): 649.

Yen J.C. , C. F. J., Chang S. (1995). "A new criterion for automatic multilevel thresholding " IEEE Transactions on Image Processing **4(3)**: 370-378.

Yin, C., et al. (2019). "ApoE attenuates unresolvable inflammation by complex formation with activated C1q." Nature medicine **25**(3): 496-506.

Yonashiro, R., et al. (2018). "Pyruvate dehydrogenase PDH-E1β controls tumor progression by altering the metabolic status of cancer cells." Cancer research **78**(7): 1592-1603.

Zhang, J., et al. (2014). "Sublytic C5b-9 induces IL-6 and TGF-β1 production by glomerular mesangial cells in rat Thy-1 nephritis through p300-mediated C/EBPβ acetylation." The FASEB Journal **28**(3): 1511-1525.

Zhou, R., et al. (2011). "A role for mitochondria in NLRP3 inflammasome activation." Nature **469**(7329): 221.